Réponses métaboliques des communautés planctoniques marines aux perturbations : apport des mesures à haute fréquence acquises dans les mésocosmes in situ

Tanguy Soulié

▶ **To cite this version:**

Tanguy Soulié. Réponses métaboliques des communautés planctoniques marines aux perturbations : apport des mesures à haute fréquence acquises dans les mésocosmes in situ. Sciences agricoles. Université Montpellier, 2021. Français. NNT : 2021MONTG049 . tel-03558212

HAL Id: tel-03558212
https://theses.hal.science/tel-03558212

Submitted on 4 Feb 2022

HAL is a multi-disciplinary open access archive for the deposit and dissemination of scientific research documents, whether they are published or not. The documents may come from teaching and research institutions in France or abroad, or from public or private research centers.

L'archive ouverte pluridisciplinaire **HAL**, est destinée au dépôt et à la diffusion de documents scientifiques de niveau recherche, publiés ou non, émanant des établissements d'enseignement et de recherche français ou étrangers, des laboratoires publics ou privés.

THÈSE POUR OBTENIR LE GRADE DE DOCTEUR DE L'UNIVERSITÉ DE MONTPELLIER

En Sciences de la Mer

École doctorale GAIA
Biodiversité, Agriculture, Alimentation, Environnement, Terre, Eau

Unité de recherche MARBEC
MARine Biodiversity, Exploitation and Conservation

Réponses métaboliques des communautés planctoniques marines aux perturbations : apport des mesures à haute-fréquence acquises dans les mésocosmes *in situ*

Présentée par Tanguy SOULIÉ
Le 13 décembre 2021

Sous la direction de Behzad MOSTAJIR
et Francesca VIDUSSI

Devant le jury composé de

Pascal CLAQUIN, Professeur, Université Caen Normandie, BOREA, Caen	Rapporteur
Laurent COPPOLA, Chercheur, Sorbonne Université, LOV-IMEV, Villefranche-sur-Mer	Rapporteur
Antoine SCIANDRA, Directeur de recherche, CNRS, LOV-IMEV, Villefranche-sur-Mer	Examinateur
Rutger De WIT, Directeur de recherche, CNRS, MARBEC, Montpellier	Président du Jury
François-Yves BOUGET, Directeur de recherche, CNRS, LOMIC, OOB, Banyuls-sur-Mer	Examinateur
Francesca VIDUSSI, Chargée de recherche, CNRS, MARBEC, Montpellier	Co-encadrante
Behzad MOSTAJIR, Directeur de recherche, CNRS, MARBEC, Montpellier	Directeur de thèse

UNIVERSITÉ DE MONTPELLIER

THÈSE POUR OBTENIR LE GRADE DE DOCTEUR DE L'UNIVERSITÉ DE MONTPELLIER

En Sciences de la Mer

École doctorale GAIA
Biodiversité, Agriculture, Alimentation, Environnement, Terre, Eau

Unité de recherche MARBEC
MARine Biodiversity, Exploitation and Conservation

Réponses métaboliques des communautés planctoniques marines aux perturbations : apport des mesures à haute-fréquence acquises dans les mésocosmes *in situ*

Présentée par Tanguy SOULIÉ
Le 13 décembre 2021

Sous la direction de Behzad MOSTAJIR
et Francesca VIDUSSI

Devant le jury composé de

Pascal CLAQUIN, Professeur, Université Caen Normandie, BOREA, Caen	Rapporteur
Laurent COPPOLA, Chercheur, Sorbonne Université, LOV-IMEV, Villefranche-sur-Mer	Rapporteur
Antoine SCIANDRA, Directeur de recherche, CNRS, LOV-IMEV, Villefranche-sur-Mer	Examinateur
Rutger De WIT, Directeur de recherche, CNRS, MARBEC, Montpellier	Président du Jury
François-Yves BOUGET, Directeur de recherche, CNRS, LOMIC, OOB, Banyuls-sur-Mer	Examinateur
Francesca VIDUSSI, Chargée de recherche, CNRS, MARBEC, Montpellier	Co-encadrante
Behzad MOSTAJIR, Directeur de recherche, CNRS, MARBEC, Montpellier	Directeur de thèse

Résumé

Les processus planctoniques jouant un rôle primordial dans le devenir de la matière et les cycles biogéochimiques globaux, la production primaire brute (PPB), la production communautaire nette (PCN), la respiration (R) et les taux de croissance (μ) et de pertes (*l*) du phytoplancton ont été quantifiés via l'utilisation de données à haute-fréquence (HF) acquises par des capteurs immergés dans des mésocosmes *in situ* lors d'expériences simulant le réchauffement (lagune de Thau) et le brunissement (baie d'Hopavågen, Norvège).

Une nouvelle méthode pour estimer la PPB, la R et la PCN a été établie à partir des données de capteurs mesurant la concentration en O_2 dissout issues d'expériences dans la lagune de Thau. Elle a été comparée avec une méthode utilisant des données HF déjà existante ainsi qu'avec la technique classique des incubations (Winkler). Elle présente l'avantage de prendre en compte la variabilité dans le couplage entre cycles jour-nuit et de l'O_2 dissout et a permis d'estimer une respiration la journée en moyenne 41% plus élevée que celle de la nuit, en accord avec l'effet théorique positif de la lumière sur la respiration. L'application de cette nouvelle méthode lors d'une expérience testant les effets du brunissement sur le fonctionnement des communautés planctoniques de la baie d'Hopavågen a révélé un effet négatif du brunissement d'environ 30% sur la PPB et la R, associé à d'importants changements dans la concentration des pigments phytoplanctoniques liés à une acclimatation physiologique aux faibles conditions de lumières.

Le réchauffement simulant les scénarios pour 2100 en Méditerranée a été testée lors de deux expériences de mésocosmes *in situ* au printemps et à l'automne 2018 à Thau. Ainsi, le réchauffement a augmenté μ et *l* du phytoplancton, estimés avec les données de fluorescence HF. Les estimations de μ et de *l* ont été comparées aux taux de croissance et de prédation obtenus via la technique des dilutions, mettant en évidence une bonne concordance entre les résultats obtenus, confirmant la robustesse des estimations obtenues avec les données HF, ceci malgré certaines différences entre les résultats de deux méthodes employées du fait que *l*, estimé avec les données HF, prend en compte la sédimentation, la mortalité par le broutage du mésozooplancton et par la lyse virale alors que les dilutions ne permettent d'estimer que le broutage du microzooplancton.

Une expérience simulant une vague de chaleur a également été réalisée à Thau au printemps 2019. Les données HF ont mis en lumière un effet positif de la vague de chaleur sur la PPB, la R, μ et *l* qui s'est prolongé plusieurs jours après l'arrêt de la vague de chaleur, sauf pour μ. La vague de chaleur a basculé l'état trophique du système vers l'hétérotrophie et a favorisé les cyanobactéries au détriment des

dinoflagellés, cependant la majorité des processus étudiés ont montré de bonnes résistance et récupération face à la vague de chaleur.

Le réchauffement a induit des réponses contrastées du plancton de la lagune de Thau, basculant le système vers l'autotrophie ou l'hétérotrophie en fonction de la saison investiguée. La communauté de Thau a été plus résistante et a mieux récupéré face à un événement ponctuel du changement climatique que la communauté d'Hopavågen, potentiellement parce que la communauté planctonique de Thau a évolué au sein d'un environnement naturellement soumis aux fortes variations de température et/ou parce que le réchauffement est une perturbation moins drastique que le brunissement.

Les méthodes établies dans la thèse représentent une approche novatrice afin d'obtenir des estimations fiables de processus planctoniques mettant en évidence sur les effets du changement climatique sur le fonctionnement des écosystèmes côtiers. De nombreuses perspectives s'ouvrent quant à la poursuite de ces travaux, en utilisant ces nouvelles méthodes pour étudier d'autres perturbations dans d'autres écosystèmes.

Mots-clés : Données à haute-fréquence, capteurs, mésocosmes *in situ*, perturbation, changement global, processus planctoniques, production primaire brute, respiration, taux de croissance, taux de perte

Abstract

Planktonic processes playing a key role in the fate of matter and global biogeochemical cycles, gross primary production (GPP), net community production (NCP) respiration (R), growth (μ) and loss (*l*) rates of phytoplankton were quantified using high-frequency (HF) data acquired by sensors immersed in *in situ* mesocosms during experiments simulating warming (Thau Lagoon) and brownification (Hopavågen Bay, Norway).

A new method for estimating GPP, R and NCP was established using sensor data measuring dissolved O_2 concentration from experiments in Thau lagoon. It was compared with an existing method using HF data and with the classical incubation technique (Winkler). It has the advantage of considering the variability in the coupling between day-night and dissolved O_2 cycles and allowed to estimate a daytime respiration on average 41% higher than the nighttime one, in agreement with the positive theoretical effect of light on respiration. Application of this new method in an experiment testing the effects of brownification on planktonic community functioning in Hopavågen Bay revealed a negative effect of brownification of about 30% on GPP and R, associated with significant changes in phytoplankton pigment concentration related to physiological acclimation to low light conditions.

The warming scenario for 2100 in the Mediterranean was tested in two *in situ* mesocosm experiments in spring and autumn 2018 in Thau lagoon. Warming increased phytoplankton's μ and *l*, estimated with HF fluorescence data. The estimates of μ and *l* were compared to the growth and grazing rates obtained via the dilution technique, highlighting a good agreement between the two methods, confirming the robustness of the estimates obtained with the HF data, despite some differences between results due to the fact that *l*, estimated with the HF data, considers sedimentation, mesozooplankton grazing mortality and viral lysis while the dilutions only allow the estimation of microzooplankton grazing.

An experiment simulating a heatwave was also carried out in Thau in spring 2019. The HF data showed a positive effect of the heat wave on GPP, R, μ and *l* that lasted for several days after the end of the heatwave, except for μ. The heatwave shifted the trophic state of the system towards heterotrophy and favored cyanobacteria at the expense of dinoflagellates, however most of the studied processes showed good resistance and recovery from the heatwave.

Warming induced contrasting responses in Thau lagoon planktonic community, shifting the system towards autotrophy or heterotrophy depending on the investigated season. The community from Thau lagoon was more resilient and recovered better from a punctual climate change event than the community from Hopavågen, potentially because the planktonic community from Thau evolved in an

environment naturally subject to strong temperature variations and/or because warming is a less drastic disturbance than brownification. The methods established in the thesis represent a novel approach to obtain reliable estimates of planktonic processes highlighting the effects of climate change on the functioning of coastal ecosystems. There are many perspectives to continue this work, using these new methods to study other disturbances in other ecosystems.

Key-words: High-frequency data, sensors, *in situ* mesocosms, disturbance, global change, planktonic processes, gross primary production, respiration, growth rate, loss rate

Remerciements

Je souhaiterai tout d'abord remercier les membres qui composent le jury de thèse, Pr Pascal Claquin, Dr Laurent Coppola, Dr Antoine Sciandra, Pr Rutger de Wit, et Dr François-Yves Bouget, pour avoir accepté d'évaluer ces travaux, je vous en suis profondément reconnaissant.

Bien évidemment, je tiens à vous remercier, Behzad et Francesca, pour m'avoir donné l'opportunité de participer à cette formidable aventure que fût la thèse. Merci pour vos conseils toujours pertinents et éclairés, et surtout, merci de m'avoir apporté sans cesse le soutien et la bienveillance sans lesquels je n'aurais pu avancer, d'avoir toujours été disponibles et à mon écoute, et d'avoir créé une atmosphère de travail chaleureuse et conviviale dans laquelle j'ai pu m'épanouir pleinement. Merci infiniment.

Je tiens à adresser mes remerciements aux membres de mon comité de suivi de thèse : Antoine Sciandra, Hervé Claustre, Benoît Jaillard et Jean-Marc Fromentin. Merci pour vos conseils précieux et avisés et pour votre évaluation de mon travail tout au long de la thèse. Ces réunions m'ont été extrêmement profitables.

Je souhaiterai également remercier les personnes qui ont fait de mon séjour au sein de l'UMR MARBEC une expérience enrichissante, tant sur le plan professionnel qu'humain. Tout d'abord, je voudrai remercier Solange et Sandrine pour leur accueil chaleureux et pour toute l'aide apportée lors des débuts de la thèse. Merci aussi à Delphine pour m'avoir donné la possibilité d'encadrer les TPs Plancton à la SMEL, j'en garde de très bons souvenirs. Merci également à Élise pour les nombreuses heures / journées passées à l'HPLC, à réfléchir à pourquoi tel ou tel module de l'HPLC ne fonctionne plus correctement. Merci également à Fabien pour ta bonne humeur permanente, ton humour à toute épreuve, et les discussions toujours intéressantes (parfois philosophiques, parfois sur les champignons). Merci à Estelle aussi, pour les discussions enrichissantes sur le métier de chercheur et la vie en général, et pour t'être occupée avec attention des gambusies du bureau quand je ne pouvais le faire. Finalement, je tiens à remercier tous les membres de l'UMR, je suis honoré d'en avoir fait partie.

Un grand merci aussi à tous les membres de MEDIMEER et de la SMEL à Sète. Séb, merci infiniment pour ton aide et tes précieux conseils malgré ton emploi du temps extrêmement chargé, et surtout pour ton humour et ton sens de la dérision sans failles. Merci aussi à Rémi, David, Solenn, Camille, et Florian pour tous les bons moments passés à vos côtés lors des expériences et pour votre aide précieuse. Merci également aux participants de l'expérience d'Hopavågen, qui ont rendu ce séjour en Norvège aussi agréable, intéressant et enrichissant. Plus particulièrement, merci à Herwig, Joanna, et Benni pour les soirées pizzas, les films de zombies dans la neige, les randonnées aboutissant aux magnifiques paysages du Trøndelag, et la découverte de sa gastronomie parfois douteuse.

Un grand merci aussi à tous les stagiaires qui ont participé, de près ou d'un peu plus loin, aux travaux de cette thèse. Plus particulièrement, merci à Émilie et à Jean-François pour votre aide inestimable lors des expériences de mésocosmes, ainsi que pour les blind tests survoltés pendant les longues heures de titration.

Je tiens également à adresser mes remerciements à François-Yves Bouget, Olivier Glippa et Jonna Engström-Öst. François-Yves, merci infiniment pour ta confiance lorsque tu m'as proposé un stage au LOMIC. C'est toujours un plaisir d'échanger avec toi. Olivier et Jonna, merci de m'avoir transmis votre passion de l'écologie marine lors de cet été en Finlande qui reste un souvenir exceptionnel.

Ces années de thèse, parfois éprouvantes, ont été constellées de fêtes inoubliables et de merveilleux moments de joie. Simon, Nicoco, Pié, Sex, et tous les autres amis toulousains, merci pour les soirées mémorables se finissant en boîtes de nuit douteuses ou en folles courses de Vélib. Stéphane et Kim, merci pour les bons souvenirs au bar à jeux, en randonnée ou au restaurant, et pour votre incroyable gentillesse. Édouard, Montaine, merci pour votre amitié et votre bienveillance qui durent depuis si longtemps. Thomas, un énorme merci pour ton accueil qui n'aurait pu être plus chaleureux, ta grande gentillesse et pour tes jeux de mots toujours subtils. Thibaut, merci pour les soirées au bar mémorables, les parties de pétanque endiablées, les baignades dans une eau trop froide, les ballons de rugby qui partaient en voyage et l'ajout de sel dans ma tasse de café, on se sera quand même bien amusés. Elsa, Laura et Marie-Charlotte, mes partenaires de début (et de fin pour certaines) de thèse, merci infiniment. Merci pour les bons moments innombrables partagés ensemble, les repas et les soirées autour d'un vin gras et vivace. Valentina, merci pour les discussions passionnantes en franglaispagnol et pour ta bonne humeur permanente, ce fût un réel plaisir de partager le bureau avec toi. Raquel, Mariam, merci pour votre gentillesse et votre bienveillance exceptionnelles, et pour votre rire communicatif. Merci aussi à Lucas et Coline, j'ai beaucoup apprécié les moments passés ensemble.

Un énorme merci aux membres de ma famille pour le soutien et toute l'affection apportés lors de ces trois ans de thèse, c'est toujours agréable de parler d'autre chose que de plancton de temps en temps.

Il serait trop long d'énumérer toutes les raisons pour lesquelles je tiens à te remercier, Justine. Saches simplement que chaque moment passé à tes côtés m'apporte un bonheur inconditionnel, et que je te dois beaucoup dans la réalisation de ces travaux. Merci pour tes encouragements et ton soutien inestimables, ce n'est que le début de folles aventures. Finalement, je tiens à vous remercier, Papa et Maman, Adrian, pour votre soutien inébranlable et votre bienveillance à toute épreuve, même lorsque vous ne compreniez pas forcément mes choix. Je suis extrêmement fier de vous avoir.

« Pour tirer le meilleur parti des connaissances acquises,

Pour en extraire toute la richesse,

Il importe de ne pas s'y habituer trop vite,

De se laisser le temps de la surprise et de l'étonnement »

Hubert Reeves, L'Espace prend la forme de mon regard

« 2 + 2 n'est pas toujours égal à 4 en écologie »

B.M.

Table des matières

Liste des figures

Introduction Générale

Chapitre 1

Chapitre 2

Chapitre 3

Chapitre 4

Discussion Générale

Liste des tableaux

Chapitre 1

Chapitre 2

Chapitre 3

Chapitre 4

Discussion Générale

Introduction Générale

1. Le rôle du plancton dans les cycles biogéochimiques et au sein du réseau trophique

Le plancton comprend des plantes unicellulaires, des bactéries et des protistes flagellés photosynthétiques - le phytoplancton -, des bactéries et des archées non-photosynthétiques – le bactérioplancton -, des virus - le virioplancton - et des animaux généralement de petite taille (millimètres ou moins) - le zooplancton. Tous dérivent au gré des courants. Le phytoplancton est responsable d'environ 45 % de la production primaire annuelle mondiale (environ 50 x 10^{15} g de carbone par an, (Field et al. 1998)) et est brouté par le zooplancton, qui constitue à son tour une source de nourriture pour ses prédateurs, notamment les poissons, dont l'importance commerciale est considérable. Ainsi, le plancton est un élément vital des écosystèmes marins. Il apporte également une contribution majeure aux cycles biogéochimiques mondiaux et atténue l'accumulation de dioxyde de carbone (CO_2) dans l'atmosphère en le séquestrant vers les profondeurs de l'océan. Cependant, l'intégrité de ces rôles est menacée par les impacts liés au changement climatique sur la physiologie des organismes et sur l'organisation et le fonctionnement à grande échelle des communautés planctoniques. En conséquence, il apparaît primordial d'étudier la réponse des communautés planctoniques face au changement climatique, et notamment d'un point de vue fonctionnel.

1.1. La production primaire réalisée par les organismes autotrophes

La photosynthèse est probablement le processus le plus important de la nature. Via ce processus, le phytoplancton, qui comprend donc l'ensemble des organismes planctoniques autotrophes, utilise la lumière pour synthétiser de la matière organique à partir de dioxyde de carbone (CO_2), d'éléments nutritifs, et d'eau. Lors de ce processus, du dioxygène (O_2) est obtenu comme sous-produit de l'oxygénation de l'eau. Cette production d'O_2 est appelée Production Primaire Brute (PPB). L'équation générale de la photosynthèse est la suivante (Equation 1) :

$$Lumière + 6CO_2 + 6H_2O \rightarrow 6O_2 + C_6H_{12}O_6 \qquad \text{Équation 1}$$

Ainsi, la quantité et la disponibilité des nutriments inorganiques, du CO_2 dissout et de la lumière sont les facteurs principaux affectant la production primaire. La température est également un facteur de contrôle important, car elle régule tous les processus enzymatiques et métaboliques selon la loi d'Arrhénius ; le rôle de la température dans le contrôle des processus métaboliques planctoniques est décrit plus en détail dans la **sous-partie 2.2.1** de la présente **Introduction Générale**.

En zone côtière, les nutriments inorganiques proviennent principalement de sources allochtones via des apports d'origine terrigène et depuis les zones plus profondes de l'océan, mais également d'apports autochtones provenant de la reminéralisation des nutriments durant le processus de dégradation de la matière organique par les bactéries hétérotrophes et des excrétions du zooplancton (Butler et al. 1979, Moràn et al. 2002). Ainsi, le phytoplancton fournit une partie de la matière organique utilisée par les bactéries qui la reminéralisent et produisent des nutriments inorganiques utiles au phytoplancton. Cependant, la relation entre phytoplancton et bactéries n'est pas uniquement mutualiste. En effet, les nutriments inorganiques sont également nécessaires aux bactéries, et la compétition entre phytoplancton et bactéries pour l'accès aux nutriments inorganiques régule la production primaire lorsque ces derniers sont présents en faibles concentrations dans le milieu (Joint et al. 2002, Litchman et al. 2004).

L'autre facteur le plus important, la lumière, peut également varier en quantité et en qualité en fonction de plusieurs paramètres physiques, chimiques et biologiques de la colonne d'eau (Kirk 1983). Le phytoplancton possède des pigments dans des combinaisons et quantités spécifiques à chaque taxon, permettant une utilisation optimale de différentes quantités de lumière et longueurs d'onde dans le processus de photosynthèse (Hintz et al. 2021).

On estime que le phytoplancton contribue à plus de 90% de la production primaire marine, et à peu près à la moitié de la production primaire à l'échelle de la planète, alors qu'il représente moins de 1% de la biomasse de tous les organismes photosynthétiques (Pomeroy 1974, Field et al 1998). Cette production primaire conséquente engendre une assimilation du carbone inorganique dissout, utilisé comme substrat de la photosynthèse. Les concentrations en carbone inorganique étant en équilibre entre l'atmosphère et l'océan, le CO_2 atmosphérique en excès implémente les stocks de carbone inorganique dissout océanique. Le phytoplancton est ainsi à l'origine d'une importante assimilation du CO_2 atmosphérique et participe à sa séquestration. Ainsi, on estime qu'environ 40 % de l'ensemble du CO_2 généré par les activités anthropiques a été séquestré dans les océans, ce qui résulte dans le fait que la concentration de CO_2 dans l'atmosphère est inférieure d'environ 200 ppm à ce qu'elle serait sans les océans (Tans et al. 1990, Lal 2008). Cette « pompe biologique à carbone » participe ainsi à la régulation du climat à l'échelle globale de la planète (Raven et Falkowski 1999). De plus, la production primaire contribue au renouvellement de l'O_2 dissout et atmosphérique, permettant ainsi la respiration des organismes au métabolisme aérobie. On considère ainsi le phytoplancton et les océans comme l'un des poumons de la planète. Parmi la grande diversité du phytoplancton, il a été montré que ce sont les grandes diatomées qui sont les contributeurs majeurs de la production primaire (Smetacek 1999, Benoiston et al. 2017). Ainsi, les diatomées sont responsables à elles-seules de la fixation d'au moins un quart du carbone inorganique total dans l'océan chaque année (Granum et al. 2005). Néanmoins, la contribution du pico- et du nanophytoplancton à la production primaire globale a été évaluée à la hausse depuis quelques dizaines d'années (Joint et al. 1993, Uitz et al. 2012).

Le devenir de cette production primaire dépend de nombreuses interactions au sein du réseau trophique planctonique. Ainsi, le zooplancton, en tant que prédateur du phyto- et du bactérioplancton, transfert la matière produite via les biomasses phytoplanctoniques et bactériennes vers les échelons trophiques supérieurs. La lyse virale induite par le virioplancton régule ces biomasses et diminue l'efficacité de transfert de matière vers les échelons trophiques supérieurs en transformant la biomasse en matière dissoute et particulaire.

1.2. La respiration des autotrophes et des hétérotrophes

A l'inverse du processus de photosynthèse, qui produit de l'O_2, la respiration aérobie, ci-après désignée simplement « respiration (R) » , constitue une consommation d'O_2. Ce procédé métabolique est réalisé par les organismes autotrophes et hétérotrophes. Il s'agit du processus physiologique au cours duquel de l'énergie est libérée par l'oxydation de substrats organiques réduits. Dans le cadre de la respiration dite aérobie, c'est l'oxygène qui joue le rôle d'oxydant, et le procédé d'oxydation résulte en la production de CO_2 (del Giorgio et Williams 2005, Robinson 2008). Le glucose est le substrat de la respiration le plus commun. Ainsi, le glucose est oxydé complétement selon la réaction suivante (Equation 2) :

$$C_6H_{12}O_6 + 6O_2 \rightarrow 6H_2O + énergie \quad \text{(Équation 2)}$$

Au sein des écosystèmes aquatiques, ce sont les bactéries hétérotrophes (incluant les procaryotes hétérotrophes et les archées) qui contribuent généralement à la proportion la plus importante de la respiration totale de l'écosystème. Cette contribution varie selon les régions et est comprise entre 23% et 76% (Robinson 2008). Dans certains systèmes, la respiration autotrophe et la respiration du zooplancton contribuent également à une part non négligeable de la respiration totale (Marra et Barber 2004, Hernández-León et Ikeda 2005, Móran et al. 2007).

En plus de la quantité de nutriments inorganiques, la respiration bactérienne dépend aussi de la quantité, de la qualité et de la disponibilité de la matière organique dissoute (MOD) dégradée par les bactéries. Cette matière organique peut avoir plusieurs origines : elle peut provenir du fonctionnement de la communauté actuelle, d'une communauté antérieure ou distante, ou peut provenir de dépôts atmosphériques et d'apports allochtones des rivières et de la côte (Findley et Sinsabaugh 2002). Lorsqu'elle provient de la communauté actuelle, elle est principalement issue de l'exudation du phytoplancton, de l'excrétion et du « sloppy feeding » de proto- et métazoaires, et de la lyse cellulaire d'origine virale (Münster et Chróst 1990, Nagata 2000). La disponibilité de la MOD pour les bactéries dépend de sa composition : certaines sont facilement dégradables, d'autres sont plus récalcitrantes. C'est ainsi que la composition de la MOD peut réguler la respiration bactérienne.

1.3. Le bilan entre production et respiration : indicateur de l'état métabolique du système

Comme vu précédemment, au sein des écosystèmes aquatiques, l'O_2 est produit biologiquement via la production primaire du phytoplancton, et consommé via la respiration de tous les organismes autotrophes et hétérotrophes. La différence entre la quantité d'O_2 produite par photosynthèse et celle consommée par la respiration constitue la quantité d'O_2 nette effectivement produite ou consommée par l'écosystème. Cette quantité, appelée Production Communautaire Nette (PCN), est un indice qui représente l'état métabolique du système et permet d'évaluer la capacité d'un écosystème à produire ou consommer de l'O_2, et, comme vu précédemment, à séquestrer ou non du CO_2 atmosphérique. Ainsi, une PCN positive, correspondant à une production primaire supérieure à la respiration, est représentative d'un système globalement autotrophe, qui produit plus d'O_2 qu'il n'en consomme tandis qu'à l'inverse, une PCN négative est représentative d'un système hétérotrophe, qui consomme de l'O_2 plus qu'il n'en produit.

L'estimation de cet indice est donc primordiale dans la compréhension des cycles biogéochimiques globaux et pour appréhender le fonctionnement actuel et futur des océans. De nombreuses études ont ainsi employé cet indice pour caractériser l'état métabolique de certaines régions de l'océan mondial (Williams et al. 2004, Cottrell et al. 2006, López-Urrutia et al. 2006, Lefèvre et al. 2008). Cependant, d'importantes incertitudes demeurent, et l'évaluation des effets du changement climatique sur l'état métabolique de certaines zones de l'océan global, et notamment des zones côtières, représente encore un challenge pour de futures recherches (del Giorgio et Duarte 2002, Karl et al. 2003, Williams et al. 2013, Serret et al. 2015).

Il faut noter que le métabolisme planctonique de l'O_2 ne constitue pas l'unique facteur impliqué dans les variations de la concentration en O_2 dissout au sein des écosystèmes aquatiques. D'autres facteurs peuvent entrer en jeu : la photosynthèse et la respiration des organismes benthiques, la respiration des organismes non-planctoniques, la nitrification réalisée par certaines bactéries qui consomme de l'O_2 (Ward 2011), et certains phénomènes physiques tels que les échanges d'O_2 entre la surface de l'eau et l'atmosphère (dégazage ou aération). Une représentation schématique et simplifiée des principaux facteurs influençant la concentration en O_2 dissout est présentée dans la figure 1.

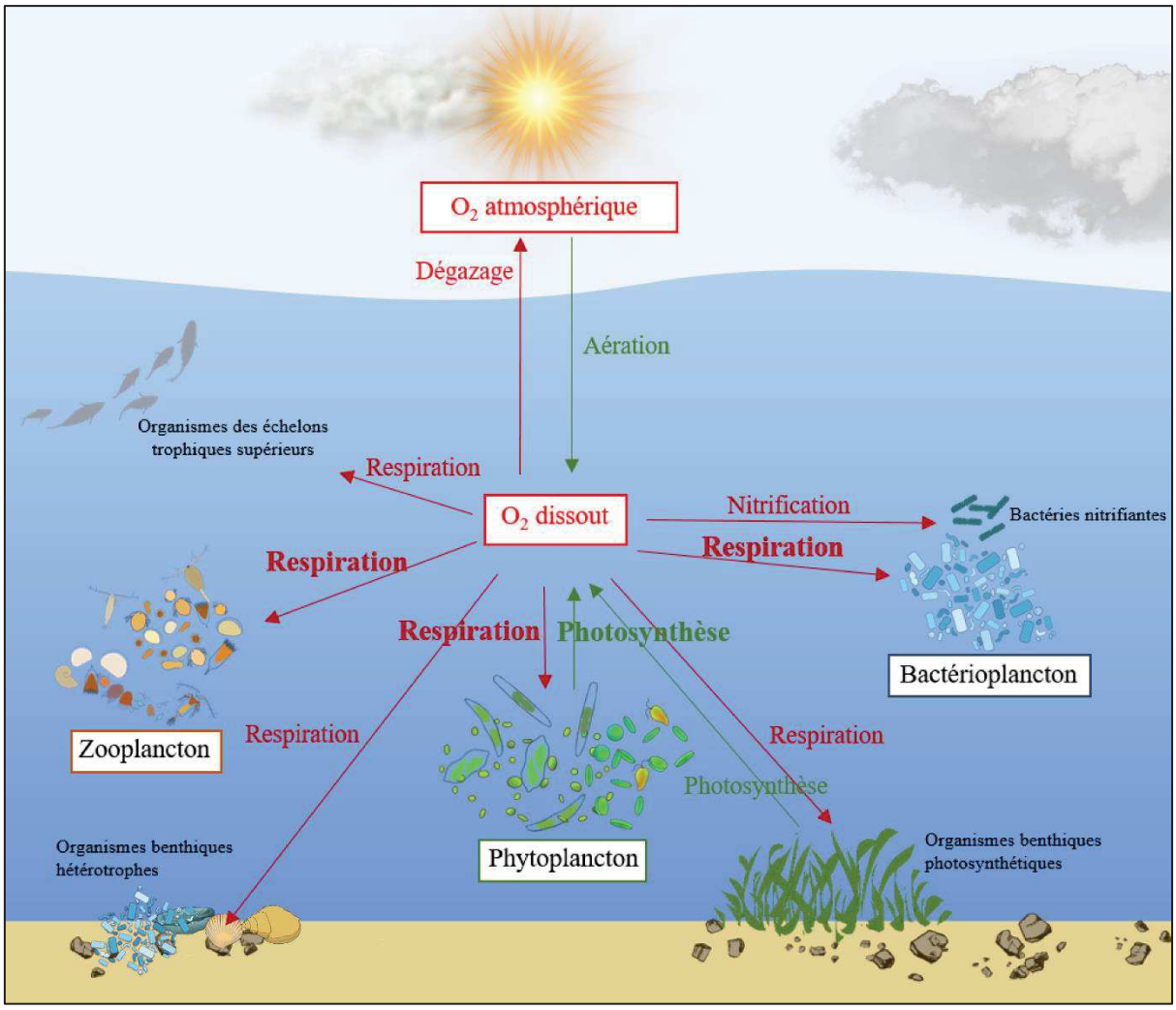

Figure 1. **Représentation schématique des principaux facteurs affectant la concentration en O_2 dissout au sein des écosystèmes aquatiques**. Les flèches en vert représentent les gains d'O_2, et les flèches en rouge représentent les pertes. Le métabolisme du plancton est indiqué en gras. Les illustrations des organismes ont été réalisées par © J.Courboulès.

1.4. Le bilan entre taux de croissance et de perte du phytoplancton : indicateur de la dynamique des producteurs primaires

Comme nous l'avons vu, le phytoplancton est le producteur primaire des océans, et joue donc un rôle primordial dans les cycles biogéochimiques et le réseau trophique. La dynamique des populations de phytoplancton et le devenir de la production primaire sont déterminés par le bilan entre la croissance et les pertes du phytoplancton (Calbet et Landry 2004). Ce bilan permet notamment d'expliquer la formation d'une efflorescence phytoplanctonique ou sa terminaison (Sverdrup 1953, Boyd et al. 1975). Généralement, on considère que le phytoplancton peut être régulé par sa croissance, qui est liée à la disponibilité en ressources, on parle alors de régulation « bottom-up », ou par son taux de perte, on parle alors de régulation « top-down » (Thompson et al. 2008, Mostajir et al. 2015).

La croissance phytoplanctonique représente la division cellulaire et donc la production de biomasse à partir de l'énergie fournie par la photosynthèse. La croissance est donc régulée par les mêmes facteurs que ceux affectant la photosynthèse, à savoir que la température, la quantité et la qualité des nutriments inorganiques et de la lumière sont les plus importants (Baird et al. 2001, López-Sandoval et al. 2021).

Le taux de perte du phytoplancton dépend quant à lui de plusieurs processus. Il est constitué de la mortalité du phytoplancton et de la sédimentation des cellules. On estime que le broutage par des prédateurs en constitue le facteur majeur, le broutage du microzooplancton représentant jusqu'à 67% de la perte de biomasse phytoplanctonique journalière dans l'océan global (Calbet et Landry 2004). Cependant, d'autres facteurs peuvent contribuer à une part non négligeable du taux de perte phytoplanctonique. La lyse virale contribue ainsi de 10 à 50% à ce taux en fonction du système considéré (Bratbak et al. 1993, Suttle et Chan 1994, Fuhrman 1999). Le parasitisme est, dans certains cas, responsable d'une part de la mortalité phytoplanctonique, même si ces cas sont peu étudiés (Park et al. 2004, Skovgaard 2014). Enfin, la sédimentation des cellules de grande taille, notamment les diatomées (Riebesell 1989), et la sénescence naturelle engendrent également d'importantes pertes pour certains systèmes, même si cette dernière contribue généralement faiblement aux pertes totales (Das et Ray 2008).

2. Le plancton face aux perturbations

2.1. Le réchauffement et le brunissement : conséquences du changement climatique

Le plancton est inexorablement soumis aux perturbations et aux pressions qui s'exercent sur l'environnement aquatique. Dans le cadre de la thèse, deux perturbations furent étudiées : le réchauffement (constant ou sous forme de vague de chaleur), et le brunissement. Ces deux perturbations ont pour origine le changement climatique global et l'accroissement des pressions anthropiques. Dans le domaine marin, ce sont les zones côtières qui y sont particulièrement sensibles, de par la faible inertie de leur colonne d'eau ou de par leur proximité avec la terre. En effet, les zones côtières jouent un rôle parmi les plus importants au monde pour les cycles biogéochimiques globaux ainsi que pour les services écosystémiques rendus (Antoine et al. 1996). Ces perturbations diffèrent quant à leurs conséquences sur le métabolisme du plancton : alors que le réchauffement a des effets directs, via l'accélération des réactions enzymatiques, et indirects, le brunissement n'a pas d'effet direct à proprement parler. Cependant, comme le réchauffement, il impacte plusieurs facteurs qui régulent le métabolisme, tels que la quantité de lumière ou de nutriments disponibles. Cette complexité dans leurs effets sur le métabolisme rend leur comparaison intéressante : est-ce que ce sont les effets directs du changement

climatique sur le métabolisme qui ont le plus de conséquences sur le fonctionnement des écosystèmes côtiers, ou bien ses effets indirects ?

2.1.1. Le réchauffement climatique

Depuis l'ère industrielle, les pressions d'origine anthropiques sur les écosystèmes ont gagné en intensité, afin de répondre aux besoins toujours croissants de la population. Ces pressions ont entraîné des changements globaux du climat, parmi lesquels le réchauffement climatique est aujourd'hui le plus médiatisé. Ce phénomène a pour origine l'augmentation de la concentration atmosphérique en gaz à effet de serre, et notamment en CO_2, liée à l'activité humaine. Ainsi, la température à la surface du globe a augmenté d'en moyenne 0,72°C entre 1901 et 2012, et d'en moyenne 0,87 °C entre 2006 et 2015, les trois dernières décennies étant les plus chaudes jamais enregistrées (IPCC 2018). De plus, les scénarios pour les décennies futures prédisent une augmentation encore plus importante de la température, comprise entre 0,8 et 5,4°C d'ici 2080 (IPCC 2013). Cette augmentation de la température atmosphérique est à l'origine d'une augmentation de la température de l'eau de surface des océans, qui est estimée entre 0,7 et 2,6°C d'ici 2100 selon les scenarios le plus optimiste et pessimiste en termes d'émissions de gaz à effet de serre du Groupe d'experts Intergouvernemental sur l'Evolution du Climat (GIEC), le RCP2.6 et le RCP8.5 respectivement (IPCC 2019) (Fig. 2A). Les modèles prévoient également que le réchauffement global et constant s'accompagnera d'une augmentation importante de la fréquence et de l'intensité d'épisodes de températures extrêmes, les vagues de chaleur. Ainsi, les mêmes scénarios du GIEC prédisent une multiplication du nombre de jours de vagues de chaleur d'un facteur de 4 à plus de 10 (Fig. 2B).

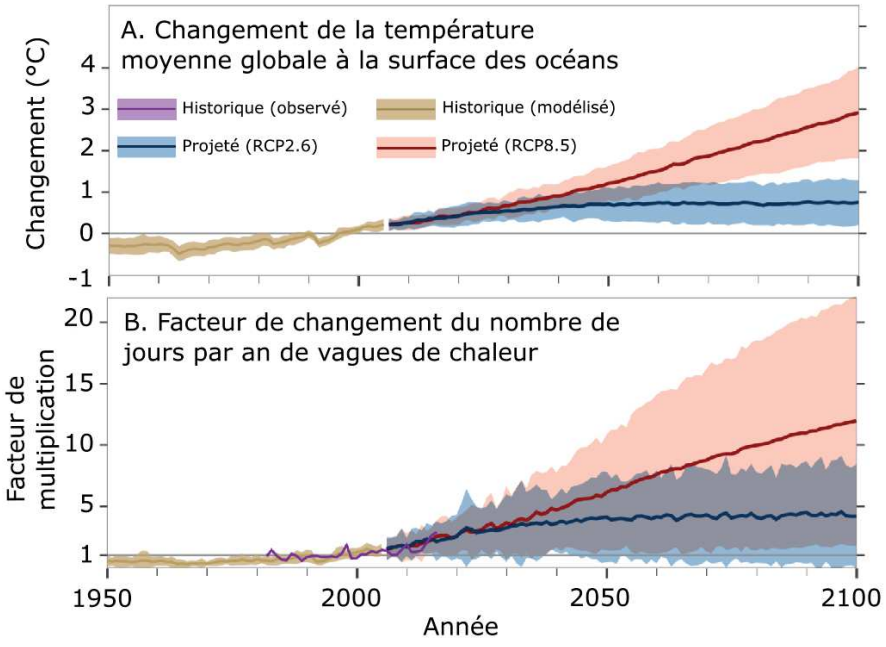

Figure 2. Évolution temporelle du changement moyen de la température globale à la surface des océans (A.) et du facteur de changement du nombre moyen de jours de vagues de chaleur océaniques par an (B.). Les données représentées en violet sont les données historiques d'observations,

celles en doré représentent des données historiques modélisées, et celles en bleu et en rouge représentent les données projetées jusqu'à 2100 selon les scénarios d'émissions de gaz à effet de serre le plus optimiste et pessimiste, RCP2.6 et RCP8.5 respectivement. Figure modifiée d'après le Rapport spécial sur l'Océan et la Cryosphère dans un Climat Changeant du GIEC (IPCC 2019).

Certaines zones et régions sont particulièrement sensibles face au phénomène de réchauffement climatique, même si le réchauffement des eaux de surface affecte l'océan mondial dans sa globalité. Ainsi, la Méditerranée est considérée comme l'une des zones les plus sensibles face à ce phénomène, certains modèles prévoient une augmentation de plus de 3°C de ses eaux de surface d'ici 2099 (Adloff et al. 2015) (Fig. 3). Similairement, d'autres modèles prévoient une augmentation très importante de la fréquence et de la sévérité des vagues de chaleur en Méditerranée suivant les scénarios d'émissions de gaz à effet de serre du GIEC (IPCC 2019, Darmaraki et al. 2019). Enfin, de façon générale, les zones côtières apparaissent plus sensibles que les zones hauturières à cause de leur faible profondeur et donc de la faible inertie thermique de leur colonne d'eau.

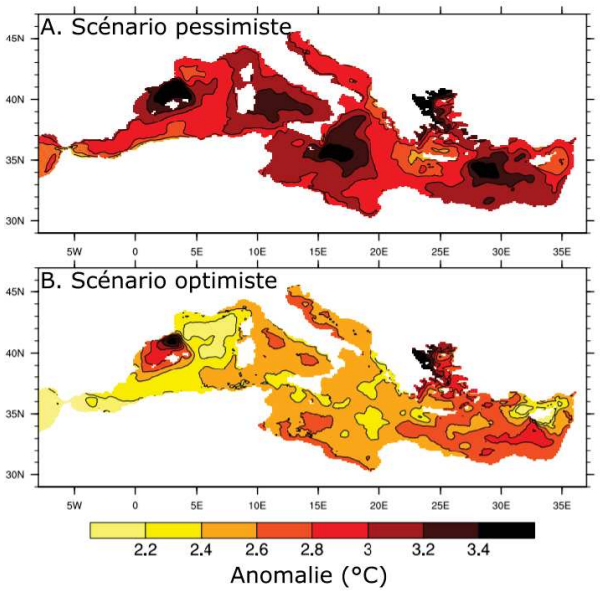

Figure 3. Différence entre la température à la surface modélisée pour la période 2070-2099 et la température mesurée pour la période 1961-1990 pour la mer Méditerranée selon un scénario d'émissions de gaz à effet de serre pessimiste (A.) et optimiste (B.). Les scénarios d'émissions représentés ici sont les minima et maxima d'une comparaison de 21 modèles représentant 21 scénarios différents. Figure modifiée d'après Adloff *et al*. (2015).

2.1.2. Le brunissement des eaux côtières

Le brunissement, un terme qui désigne le changement de la couleur de l'eau vers le brun et le rouge, est un phénomène lié à l'accroissement des apports terrigènes dans les zones côtières septentrionales (Kritzberg et al. 2014). Il a principalement été attribué à l'augmentation des apports en carbone organique dissout (COD), et notamment en matière humique colorée, même si les apports de fer jouent également un rôle important dans certains cas (Roulet et Moore 2006, Monteith et al. 2007, Weyhenmeyer et al. 2014). Le changement climatique, et notamment l'augmentation des précipitations annuelles moyennes et de la fréquence des épisodes de précipitations extrêmes (Fig. 4), a été proposé comme l'une des causes principales de la recrudescence du brunissement dans les écosystèmes

nordiques (Larsen et al. 2011, de Wit et al. 2016). L'augmentation conséquente de la concentration en COD reportée au sein des lacs de Norvège a été directement reliée à l'accroissement des précipitations moyennes dans la région (Hongve et al. 2004). Cependant, d'autres phénomènes sont aussi responsables du brunissement. La diminution des dépôts de souffre atmosphérique depuis la fin des années 1980 semble avoir augmenté la solubilité et le transport de COD depuis les sols jusqu'aux écosystèmes aquatiques (Monteith et al. 2007). Certaines études ont également proposé les changements dans l'utilisation des sols et de la couverture végétale, notamment via l'agriculture, comme facteurs majeurs dans le brunissement de certains écosystèmes aquatiques (Corell et al. 2001, Cluterbuck et Yallop 2010, Kritzberg 2017).

Les zones côtières représentent les zones marines les plus vulnérables face au phénomène de brunissement. En effet, leur proximité directe avec la terre, et donc avec certaines activités humaines d'agriculture et de gestion du territoire, et avec des zones boisées et des tourbières riches en matière organique, ainsi que leur faible profondeur rendant les échanges de masses d'eau moins importants qu'en mer ouverte, les rend sensibles au brunissement. Par exemple, les zones côtières des pays scandinaves sont particulièrement touchées par ce phénomène. Notamment, un brunissement important des eaux côtières norvégiennes a été observé depuis de nombreuses décennies et pour différentes zones (Aksnes et al. 2009, Frigstad et al. 2020).

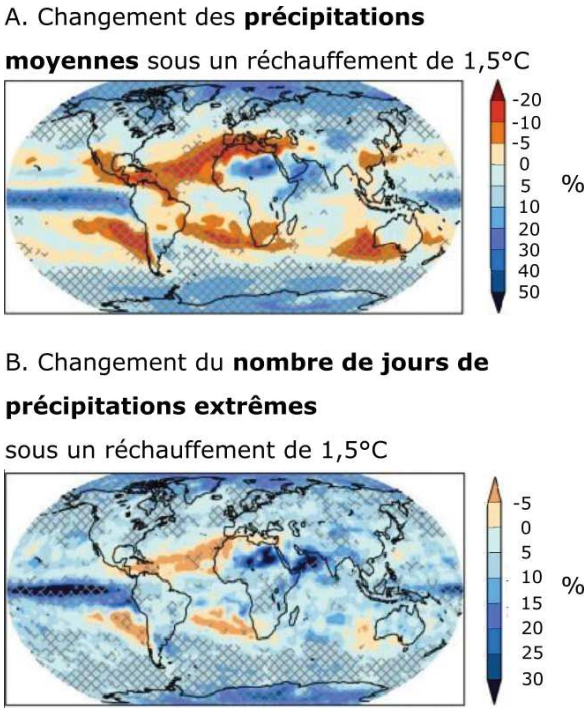

Figure 4. Changements projetés de la quantité de précipitations moyenne (A) et du nombre de jours de précipitations extrêmes (B) selon un scénario de réchauffement global de 1,5°C. Compilation de simulations de plusieurs modèles adaptés de Seneviratme et al. (2016) et Wartenburger et al. (2017). Figure modifiée d'après le Rapport Spécial Impacts d'un Réchauffement Global de 1,5°C sur les Systèmes Naturels et Humains (Hoegh-Guldberg et al. 2018).

2.2. La réponse des communautés planctoniques côtières

2.2.1. Face au réchauffement climatique

La température joue un rôle important dans les processus biologiques et métaboliques. Ce rôle est énoncé par la loi d'Arrhénius qui permet de décrire la vitesse d'une réaction chimique (k) en fonction d'un coefficient de proportionnalité ou facteur de fréquence (A), de la température (T), de la constante des gaz parfaits (R) et d'une énergie d'activation pour la réaction (Ea) (Laidler 1984) (Équation 3).

$$k = A \times e^{\frac{-Ea}{RT}} \qquad \text{(Équation 3)}$$

Ainsi, une augmentation de la température a un effet positif sur le métabolisme du plancton. La Théorie Métabolique de l'Écologie (Metabolic Theory of Ecology, MTE), introduite par Gillooly et al. (2001) et Brown et al. (2004), utilise cette relation fondamentale pour prédire l'effet de la température sur le métabolisme des organismes à l'échelle de l'écosystème, et ainsi comprendre comment les taux métaboliques régulent les procédés écologiques. Appliquée aux écosystèmes aquatiques et au métabolisme du plancton, la MTE prédit un effet positif d'une augmentation de la température sur la production primaire, la respiration, et le taux de croissance des organismes autotrophes et hétérotrophes. Cependant, cet effet positif est plus rapide pour la respiration que pour la production primaire, et pour les processus hétérotrophes que pour ceux autotrophes, à cause d'une énergie d'activation plus importante pour la respiration que pour la photosynthèse liée à un effet antagoniste de la température sur la liaison de l'O_2 et du CO_2 avec l'enzyme principale de la photosynthèse (Gillooly et al. 2001, Brown et al. 2004). En conséquence, sous l'effet du réchauffement, une diminution de la PCN et un basculement vers l'hétérotrophie sont attendus selon la MTE. De nombreuses observations ont vérifié ces prédictions de la MTE, à l'échelle de l'océan global et pour les systèmes estuariens, côtiers et hauturiers (López-Urrutia et al. 2006, Regaudie-de-Gioux et Duarte 2012, Garcia-Corral et al. 2021). La figure 5 présente ainsi les relations générales trouvées entre PPB et température et entre R et température pour les hémisphères nord et sud. López-Urrutia et al. (2006) et Regaudie-de-Gioux et Duarte (2012), utilisant un jeu de données comprenant des mesures de PPB, de R et de température réalisées à l'échelle de l'océan global, ont mis en évidence pour la respiration hétérotrophe et la production primaire brute, respectivement, une énergie d'activation de 0,65 eV (électronvolt) et 0,32 eV (López-Urrutia et al. 2006) et 0,66 ± 0,04 et 0,32 ± 0,05 (Regaudie-de-Gioux et Duarte 2012). Additionnellement, des expériences, *in situ* et au laboratoire, ont permis d'obtenir des résultats similaires (Vásquez-Dominguez et al. 2007, Hoppe et al. 2008, Panigrahi et al. 2013, Vaquer-Sunyer et Duarte 2013). Par exemple, dans des expériences de mésocosmes en eau douce, une augmentation de la température de 3 à 5°C a eu un effet positif plus important sur la respiration que sur la production primaire, avec des mesures d'énergies d'activations proches de celles théorisées par la MTE (Yvon-Durocher et al. 2010).

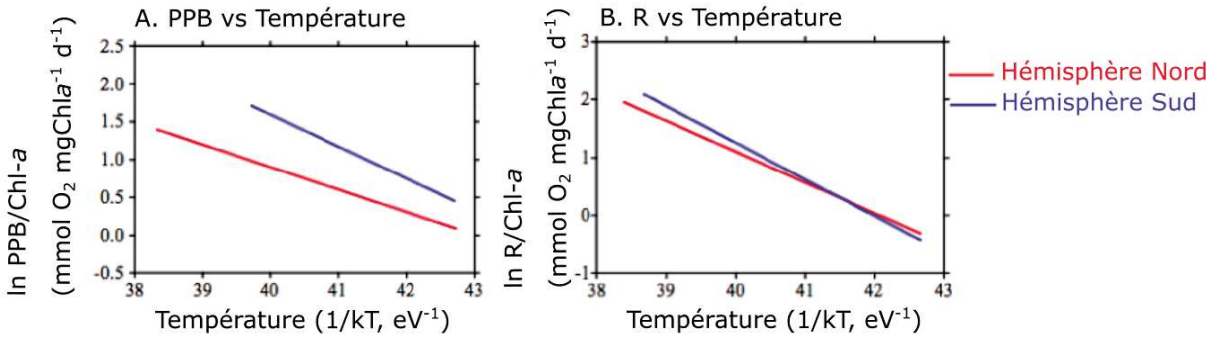

Figure 5. Relations entre PPB et température (A) et entre R et température (B). Régressions linéaires de Type II entre le logarithme de la production primaire brute (PPB) et de la respiration (R) normalisées par la concentration en chlorophylle-*a* et l'inverse de la température pour l'Hémisphère Nord (en rouge) et l'Hémisphère Sud (en bleu). Figure modifiée d'après Regaudie-de-Gioux et Duarte (2012).

Similairement, les prédictions de la MTE quant à l'effet positif d'une augmentation de la température sur le taux de croissance du plancton ont également été vérifiées par des observations à l'échelle globale (Fig. 6). Par exemple, Chen et al. (2012) ont reporté une énergie d'activation de 0,36 ± 0,05 eV pour le taux de croissance du phytoplancton, en compilant un jeu de données représentatif de l'ensemble de l'océan global. Pareillement, Rose et Caron (2007) et Chen et al. (2012) ont mis en évidence la relation positive entre température et taux de croissance des protistes hétérotrophes (bactérivores et herbivores), et entre température et taux de broutage du microzooplancton. De plus, Cabrerizo et Marañon (2021) ont montré un effet positif de la température sur le ratio broutage sur croissance, mais seulement pour les écosystèmes polaires hauturiers (énergie d'activation de ~0,5 eV) et côtiers tropicaux (~0,2 eV), suggérant une grande variabilité saisonnière et géographique dans la dépendance à la température du métabolisme planctonique. Expérimentalement, un effet positif d'une augmentation de la température a également été reporté pour le taux de croissance du phytoplancton (Eppley 1972), du zooplancton (McLaren 1978) et pour celui des protistes hétérotrophes (Rose et Caron 2007).

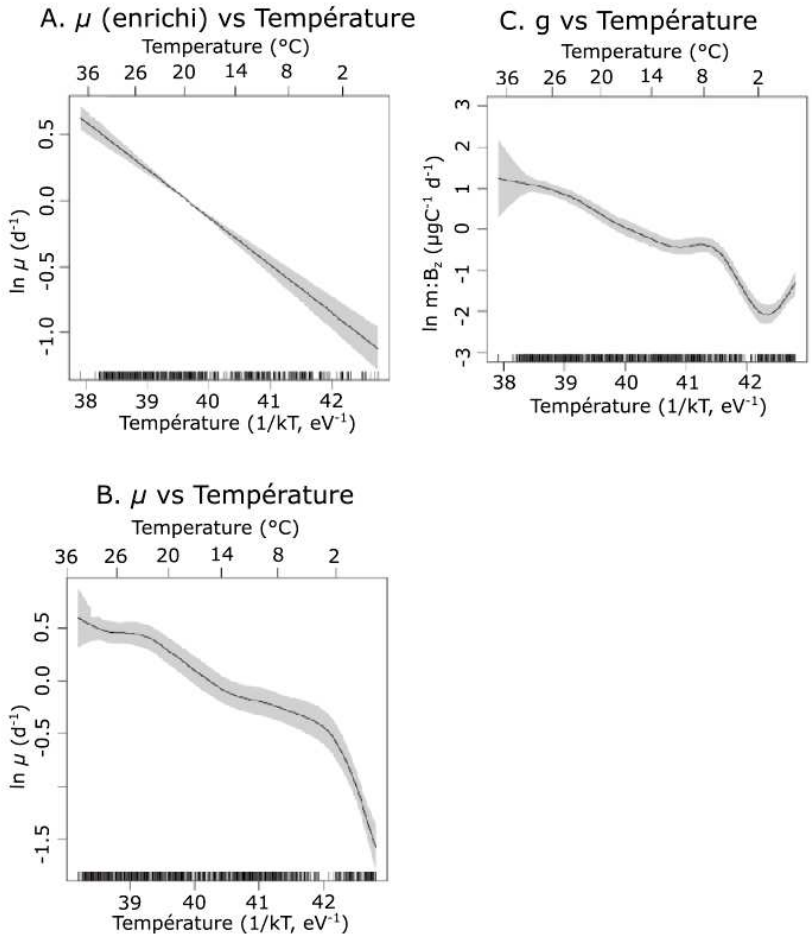

Figure 6. Relations entre taux de croissance (μ) du phytoplancton enrichi en nutriments et température (A), entre taux de croissance du phytoplancton non-enrichi et température (B), et taux de broutage (g) normalisé par la biomasse de microzooplancton (B_z) et température (C). Fonctions obtenues avec des modèles additifs généralisés. La zone grise représente l'intervalle de confiance à 95%. Figure modifiée d'après Chen et al. (2012).

Cependant, dans le milieu naturel, une augmentation de la température est susceptible d'affecter d'autres facteurs que le métabolisme planctonique, comme par exemple la stratification de la colonne d'eau, les interactions entre organismes et la disponibilité en nutriments et en lumière (Winder et Sommer 2012). Le changement de ces facteurs peut jouer un rôle dans la régulation du métabolisme planctoniques. Parmi ces facteurs, il a été montré que la disponibilité en nutriments joue un rôle important dans la réponse des communautés planctoniques face au réchauffement (O'Connor et al. 2009, Lewandowska et al. 2014, Vaquer-Sunyer et al. 2015, Lee et al. 2019, Domingues et al. 2021). Par exemple, les apports très importants de nutriments depuis l'Océan Indien dans la Mer Rouge entraînent une réponse plus rapide du métabolisme phytoplanctonique face à une élévation de la température que celle du métabolisme hétérotrophe (énergie d'activation plus élevée pour la PPB que pour la R), augmentant ainsi la PCN (López-Sandoval et al. 2019). Il est à noter que ces résultats sont

en contradiction avec les prédictions de la MTE. Des études expérimentales ont également reporté un effet contradictoire de la température sur le métabolisme du plancton. Par exemple, Vidussi et al. (2011) ont montré qu'une augmentation de la température de 3°C n'avait aucun effet sur la respiration dans le cadre d'une expérience en mésocosmes *in situ* réalisée en zone côtière Méditerranéenne (lagune de Thau). Les auteurs expliquent cette absence de réponse de la respiration par l'effet positif de l'augmentation de la température sur l'abondance des prédateurs des bactéries hétérotrophes, réduisant *in fine* l'abondance de ces dernières, qui contribuent majoritairement à la respiration. D'autres expériences ont mis en évidence un effet négatif d'une augmentation de la température sur la croissance et le broutage du phytoplancton lagunaire méditerranéen, en contradiction avec les effets théoriques sur le métabolisme du phytoplancton et de ses prédateurs (Courboulès et al. 2021, Domingues et al. 2021). Pour expliquer ces effets inattendus, les auteurs ont proposé plusieurs hypothèses, et notamment une limitation par les nutriments inorganiques, un mécanisme de cascade trophique et une diminution de la qualité nutritionnelle du phytoplancton.

En conclusion, il semblerait que, à l'échelle de l'océan global, les prédictions de la MTE soient vérifiées par les observations, et qu'une augmentation de la température entraîne un basculement de l'écosystème vers l'hétérotrophie. Cependant, l'augmentation de la température affecte également d'autres facteurs que le métabolisme, et ces effets indirects peuvent expliquer les raisons pour lesquelles la réponse métabolique des communautés planctoniques face au réchauffement est souvent plus complexe que la MTE ne le prédit.

2.2.2. Face au brunissement des eaux côtières

Le brunissement est une perturbation plus difficile à caractériser que le réchauffement. Le brunissement affecte les écosystèmes aquatiques selon des mécanismes complexes qui interagissent avec les propriétés physiques, chimiques et biologiques des écosystèmes (Solomon et al. 2015). En fonction des zones géographiques et des saisons, les épisodes de brunissement introduisent une quantité de nutriments organiques et inorganiques différente et induisent un effet sur la quantité et la qualité de la lumière variable. Ainsi, les conséquences du brunissement sur le métabolisme planctonique sont difficiles à prévoir. Par exemple, il est attendu que la réduction de la quantité de lumière induite par le brunissement ait un effet négatif direct sur la photosynthèse du phytoplancton, et donc sur la production primaire. De plus, les apports de matière organique liés au brunissement constituent une source de matière organique pour l'activité des bactéries hétérotrophes, augmentant potentiellement leur respiration. Finalement, la reminéralisation de ces apports de matière organique par les bactéries résulte en une quantité de nutriments inorganiques plus importante disponible pour la production primaire phytoplanctonique (Wikner et Anderson 2012, Creed et al. 2018).

La complexité et la diversité des effets du brunissement rendent les résultats des expérimentations testant ses effets sur les communautés planctoniques souvent différents. De plus, peu d'études se sont portées sur l'effet du brunissement sur des écosystèmes marins, la plupart investiguant des lacs ou des rivières. Ces dernières ont mis en évidence un effet important du brunissement, simulé par l'ajout de matière organique d'origine naturelle ou non, sur la biomasse et la composition de la communauté phytoplanctonique (Nicolle et al. 2012, Urrutia-Cordero et al. 2017). Cependant, la production phytoplanctonique et la respiration ne semblent pas être affectées par le brunissement expérimental (Rasconi et al. 2015, Lebret et al. 2018, Feuchtmayr et al. 2019). Similairement, les études investiguant les effets du brunissement sur les zones côtières ont mis en lumière certains effets considérables sur la composition et le fonctionnement des communautés planctoniques (Deininger et al. 2016, Meunier et al. 2017, Mustaffa et al. 2020). Par exemple, l'ajout de matière organique dans des mésocosmes en Mer du Nord a réduit la biomasse phytoplanctonique et a changé la composition de la communauté en favorisant des espèces adaptées à une quantité de lumière faible comme les dinoflagellés et les cryptophycées (Mustaffa et al. 2020). Cette réduction de la biomasse phytoplanctonique est parfois accompagnée d'un accroissement de la biomasse bactérienne, suggérant un basculement de la communauté planctonique vers l'hétérotrophie (Meunier et al. 2017). Cet accroissement dépend néanmoins de la biodisponibilité de la matière organique simulant le brunissement, matière qui selon sa nature peut être récalcitrante (Lebret et al. 2018). Au contraire, le brunissement peut favoriser le phytoplancton aux dépends des bactéries lorsque le brunissement représente un ajout important de nutriments inorganiques dans un système limité par la disponibilité des nutriments comme cela peut être le cas à certaines périodes de l'année pour les zones côtières méditerranéennes (Liess et al. 2016). En conclusion, les effets du brunissement sur le métabolisme planctonique sont souvent dépendants du type d'apports terrigènes, de la zone étudiée et des conditions biotiques et abiotiques du système au moment de l'étude, et sont encore relativement mal connus.

2.3. Paramètres de stabilité fonctionnelle des communautés planctoniques face à une perturbation

La question de savoir si et à quelle vitesse les communautés planctoniques se rétablissent suite à une perturbation est primordiale pour la compréhension du fonctionnement des communautés planctoniques et la modélisation de leur avenir. Il est donc essentiel d'évaluer la capacité des communautés planctoniques à résister à une perturbation, telle que le réchauffement ou le brunissement, et à revenir à un état stable. Cette évaluation peut se faire via l'estimation de certains paramètres de stabilité : la résistance, la résilience, la récupération et la stabilité temporelle (Fig. 7). La résistance peut être définie comme la capacité des communautés à supporter les changements, la résilience comme étant la vitesse de récupération après la perturbation, la récupération comme l'état final de la communauté et la stabilité

temporelle comme l'inverse de la variabilité autour de la trajectoire de récupération (Hillebrand et al. 2018). Les vagues de chaleur et le brunissement représentent des perturbations épisodiques, c'est-à-dire qu'elles sont de type « pulse », au contraire de pressions constantes de type « presse ». Certaines études ont estimé les paramètres de stabilité des communautés planctoniques face à certaines perturbations pulses et à la combinaison d'une perturbation pulse et d'une perturbation presse, mais ces études sont encore rares (Cabrerizo et al. 2019, Filiz et al. 2020, Urrutia-Cordero et al. 2021).

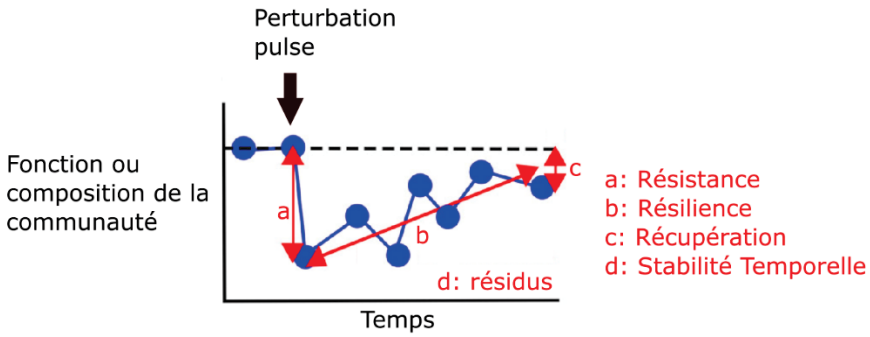

Figure 7. Représentation graphique des paramètres de stabilité d'une fonction ou de la composition de la communauté face à une perturbation « pulse ». La courbe bleue représente l'évolution temporelle de la variable (fonction ou composition) considérée, et les flèches et les lettres rouges représentent les différents paramètres de stabilité : résistance, résilience, récupération et stabilité temporelle. Figure modifiée d'après Hillebrand et al. (2018).

3. Evaluer la réponse du plancton face aux perturbations : l'apport des mésocosmes *in situ* et des mesures à haute-fréquence

3.1. Les mésocosmes in situ : un intermédiaire entre études en laboratoire et observations in situ

3.1.1. Approche et intérêts

La définition du mésocosme par Odum (1984) est « une unité expérimentale extérieure délimitée et partiellement fermée qui simule étroitement l'environnement naturel, et notamment l'environnement aquatique ». Ainsi, les mésocosmes constituent un intermédiaire entre les études en laboratoire et les études directement *in situ*. Leur utilité réside dans la possibilité de tester une ou plusieurs perturbations sur des communautés naturelles dans des conditions contrôlées en se rapprochant fortement de l'environnement naturel, tout en assurant la réplicabilité des traitements. Ils permettent de tester une ou plusieurs perturbations en contrôlant certains paramètres biotiques et abiotiques clés (Dzialowski et al.

2014). Cette approche permet ainsi d'inclure une communauté naturelle comprenant plusieurs niveaux trophiques et d'avoir une vision presque holistique de la réponse des communautés face aux perturbations. De plus, le volume important des mésocosmes permet un échantillonnage soutenu pendant plusieurs semaines, voire même pendant des mois. L'avantage des mésocosmes employés dans la présente thèse est qu'ils sont déployés directement dans le milieu étudié. Les communautés planctoniques de ces mésocosmes *in situ* sont ainsi soumises aux mêmes conditions de température et de lumière que le milieu naturel, rapprochant encore plus les mésocosmes de celui-ci, ce qui n'est pas le cas pour les mésocosmes installés à l'intérieur de bâtiments et laboratoires.

3.1.2. Mésocosmes *in situ* employés dans le cadre de la thèse et sites d'études

Les travaux réalisés et reportés dans la présente thèse sont tous issus de l'utilisation de la même approche expérimentale de mésocosmes *in situ.* Leur utilisation a permis de tester deux perturbations au sein de deux écosystèmes, et aussi de tester la même perturbation au même endroit durant plusieurs saisons. Nous avons pu ainsi évaluer les conséquences de l'augmentation de la température et du brunissement sur les communautés planctoniques côtières au sein de deux sites d'études différents, la lagune de Thau, dans le sud de la France (43°24'N, 3°41'E), et la baie d'Hopavågen, connectée au fjord de Trondheim dans le Trøndelag en Norvège (63°36'N, 9°33'E). Ces deux zones côtières ont pour points communs d'être productives et de rendre de nombreux services écosystémiques aux communautés locales, tels que l'aquaculture ou la conchyliculture. Nous avons élucidé les effets du changement climatique sur les processus planctoniques dans ces deux milieux aux caractéristiques géographiques, climatiques, hydrologiques et écologiques contrastées. Pour la thèse, il était intéressant de comparer comment deux systèmes aux caractéristiques différentes répondent face à des perturbations liées au changement climatique global, cela permet ainsi d'identifier quel système serait le plus vulnérable.

Dans le cadre de cette thèse, trois expériences de mésocosmes *in situ* ont eu lieu dans la lagune de Thau, afin d'étudier les effets du réchauffement sur le métabolisme et le fonctionnement des communautés planctoniques de cette lagune. Il s'agit d'une lagune côtière méditerranéenne typique, d'une profondeur moyenne de 4 m, fortement influencée par les apports marins via trois canaux qui la relient directement à la Mer Méditerranée (Fiandrino et al. 2017). De par sa faible profondeur, la température de l'eau présente une importante variabilité saisonnière (4-30°C environ (Pernet et al. 2012)). Elle est également soumise à une forte pression anthropique et fournit de nombreux services écosystémiques, car elle sert de lieu de récréation, de pêche, et, surtout, de production ostréicole et mytilicole (La Jeunesse et al. 2015). On estime qu'un dixième de la production française d'huître creuse *Crassostrea gigas* est réalisée dans la lagune de Thau, rendant cette dernière indispensable à l'économie de la région. Toutes ces caractéristiques en font un site d'étude dont l'évolution et la réponse face aux pressions humaines et climatiques sont suivies depuis plusieurs décennies (Collos et al. 1997, 2009, La Jeunesse et al. 2002, Bec et al. 2005, Trombetta et al. 2019, 2020, 2021, Derolez et al. 2020, Courboulès et al. 2021). Dans

le cadre de la thèse, les expériences en mésocosmes ont été réalisées via l'infrastructure de MEDIMEER (MEDIterranean platform for Marine Ecosystems Experimental Research), située dans la partie sud-est de la lagune (Fig. 8), à proximité du canal de Sète, qui contribue à plus de 90% des échanges avec la Mer Méditerranée (Fiandrino et al. 2017).

Une autre expérience de mésocosmes *in situ* faisant partie de la thèse a été réalisée à Hopavågen, cette fois-ci pour identifier les effets du brunissement sur le métabolisme et le fonctionnement des communautés planctoniques de cette baie. Il s'agit d'une baie semi-fermée située au centre de la Norvège, dans le comté de Trøndelag, directement reliée au fjord de Trondheim. Sa profondeur moyenne est de 18 m, et ses conditions hydrologiques sont très proches de celles du fjord de Trondheim, car en moyenne 14% du volume total de la baie est échangé quotidiennement avec le fjord (van Marion 1996). L'impact des activités humaines est limité, car la baie est située dans une zone assez isolée et très peu urbanisée, les pressions anthropiques les plus importantes étant la pêche de loisir, l'aquaculture dans le fjord de Trondheim adjacent, et une activité agricole limitée (van Marion 1996, Öztürk et al. 2003, Stibor et al. 2004). Dans le cadre de la présente thèse, l'expérience en mésocosme a été réalisée via les infrastructures de la station de Sletvik de l'Université Norvégienne de Sciences et Technologies (NTNU), et les mésocosmes ont été placés dans l'une des parties les plus profondes de la baie, au centre (Fig. 8).

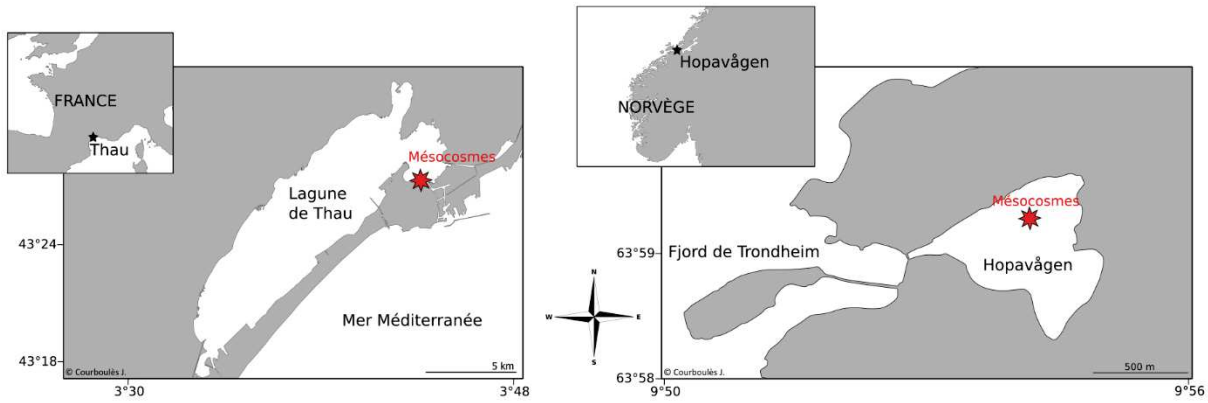

Figure 8. **Sites d'études de la thèse** où les expériences de mésocosmes in situ ont été réalisées. La lagune de Thau est représentée à gauche, et la baie d'Hopavågen à droite. Les étoiles rouges représentent la position des mésocosmes *in situ* au sein du site d'étude.

3.2. L'utilisation de capteurs automatisés et des mesures à haute fréquence

3.2.1. Dans le cadre des programmes d'observation et des études expérimentales

Depuis quelques décennies, le développement de capteurs automatisés et submersibles a permis le suivi de variables biotiques et abiotiques et l'acquisition de données à haute-fréquence (HF, de toutes les

minutes à toutes les heures) dans de nombreux écosystèmes aquatiques. Ces capteurs, installés sur des stations fixes, des bouées, des flotteurs, des véhicules autonomes et des gliders, ont fourni des séries de données permettant de suivre l'évolution temporelle et spatiale de paramètres clés, tels que la fluorescence de la chlorophylle-*a* (chl-*a*), la concentration et la saturation en O_2 dissout, la salinité ou la température. Ces données ont été utilisées pour comprendre les tendances des variables biologiques et physiques et le fonctionnement de divers écosystèmes aquatiques, notamment quant à l'évolution de la biomasse phytoplanctonique dans le temps et l'espace et sa relation avec divers paramètres environnementaux (Alkire et al. 2012, Beaulieu et al. 2013, Mignot et al. 2014, Coppola et al. 2018, Trombetta et al. 2019, Serre-Fredj et al. 2021). Ces données jouent également un rôle de plus en plus important dans le management des écosystèmes aquatiques (Jankowski et al. 2021). Parmi toutes ces données, le suivi de la concentration en O_2 dissout permet l'estimation de la PPB, de la R et de la PCN, qui sont des paramètres fondamentaux dans le suivi de l'état de santé des écosystèmes aquatiques (Staehr et al. 2010, Welti et al. 2017) et interviennent de plus en plus dans les programmes de surveillance et de management des écosystèmes aquatiques (Arroita et al. 2019, Chowanski et al. 2020, Jankowski et al. 2021).

L'utilisation de capteurs automatisés HF dans le cadre d'études expérimentales, et notamment d'expériences en mésocosmes, présentent de nombreux avantages (Mostajir et al. 2012, 2013). Auparavant, l'échantillonnage des mésocosmes se faisait généralement de manière discrète, certaines contraintes techniques et humaines limitant fortement la fréquence de mesure. Cependant, de nombreux processus planctoniques et microbiens ont une échelle de temps beaucoup plus courte, de l'ordre de quelques heures, et l'échantillonnage discret réalisé peut manquer beaucoup de ces processus à courte échelle de temps. Ainsi, le principal intérêt de l'utilisation de capteurs réside dans la possibilité de suivre à HF les paramètres physiques, chimiques et biologiques dans les mésocosmes et d'identifier les processus biologiques à courte échelle de temps. La quantité de données engendrée permet également une robustesse statistique impossible avec un échantillonnage manuel. L'utilisation des capteurs présente un autre avantage par rapport aux méthodes classiques : ils permettent une acquisition des données quelques que soient les conditions météorologiques et l'accessibilité aux mésocosmes, et sont ainsi particulièrement indiqués dans le cadre d'expériences ayant lieu dans des endroits difficiles d'accès. L'aspect non-invasif des capteurs représente également un avantage pour leur utilisation, en comparaison des méthodes classiques souvent très invasives pour les organismes. Enfin, méthodologiquement, les capteurs permettent la réalisation de traitements expérimentaux fins et régulés (par exemple, une augmentation de la température de l'eau dans les mésocosmes ou de la quantité du rayonnement ultraviolet reçue qui suit les variations naturelles *in situ,* (Nouguier et al. 2007).

3.2.2. L'estimation du métabolisme planctonique via l'utilisation des capteurs à haute-fréquence : théorie, avantages et limites méthodologiques

La concentration d'O_2 dissout suit généralement un cycle journalier : elle augmente durant la journée via la photosynthèse, et elle diminue pendant la nuit à cause de la respiration qui n'est plus contrebalancée par la photosynthèse. En suivant ce cycle nycthéméral, il est possible d'estimer la PPB, la R et la PCN au sein d'écosystèmes aquatiques, c'est la méthode des changements journaliers d'O_2 (Staehr et al. 2010). L'équation fondamentale, proposée par les frères Howard et Eugène Odum en 1955, provient d'un bilan de masse classique et est présenté via l'Équation 4 (Odum et Odum 1955) :

$$\frac{\Delta O_2}{\Delta t} = PPB - R - F - A \qquad \text{(Équation 4)}$$

Ainsi, la variation de la concentration en O_2 au cours du temps, $\frac{\Delta O_2}{\Delta t}$, est due à la photosynthèse (PPB), à la respiration (R), à l'échange physique d'O_2 entre la surface de l'eau et l'atmosphère (*F*), et aux autres phénomènes physiques et chimiques pouvant influer sur la concentration en O_2 dissout, très souvent négligés et regroupés dans le terme (*A*). À partir de cette équation, de nombreux modèles ont été développés afin d'estimer les paramètres métaboliques. Ces modèles diffèrent dans leur approche ou dans le contexte dans lequel ils peuvent être appliqués. On distingue deux grands types de modèles généralement utilisés : les modèles qui se basent sur l'utilisation de certaines tranches horaires dans une période de 24 heures pour estimer les paramètres métaboliques (Cole et al. 2000, Staehr et al. 2010, Mostajir et al. 2013, Herrera et Nadaoka 2021), et ceux qui sont basés sur une modélisation inversée des cycles d'O_2 dissout via l'utilisation d'équations fondamentales décrivant la relation entre paramètres métaboliques et température et lumière (Grace et al. 2015, Winslow et al. 2016, Appling et al. 2018).

A l'époque des frères Odum, à cause de la relative difficulté et pénibilité de la mesure de la concentration d'O_2, la méthode se basait sur des mesures peu nombreuses, par exemple au lever et au coucher de soleil. Depuis, la fréquence des données a augmenté au fil du temps et la méthode a été utilisée pour estimer les paramètres métaboliques de lacs, de rivières et de zones marines (Odum 1956, Oviatt et al. 1986, Staehr et al. 2010, Kritzberg et al. 2014). Depuis quelques dizaines d'années, des capteurs optiques (optodes) mesurant la concentration et la saturation en O_2 dissout de façon fiable et précise ont été développés et conséquemment utilisés pour l'étude des systèmes aquatiques. Ainsi, la technique des changements dans le cycle nycthéméral d'O_2 a pu être adaptée afin d'estimer le métabolisme *in situ* des communautés aquatiques à une fréquence toujours plus importante et dans divers écosystèmes aquatiques (Van de Bogert et al. 2007, Hanson et al. 2008, Staehr et al. 2010, Laas et al. 2012).

Classiquement, pour estimer le métabolisme planctonique de l'O_2, la technique de Winkler (Winkler 1888) est employée pour mesurer la concentration en O_2 dissout dans des bouteilles dans lesquelles une petite partie de la communauté planctonique est incubée au noir ou à la lumière pendant plusieurs heures (Vidussi et al. 2011, Liess et al. 2016). La méthode des incubations et de Winkler nécessite le

confinement d'une petite partie de la communauté planctonique (généralement quelques centaines de mL d'eau) dans des bouteilles, ce qui introduit potentiellement plusieurs biais : la communauté enfermée dans la bouteille n'est pas forcément représentative de la communauté totale étudiée, et les organismes adaptent peut-être leur métabolisme aux nouvelles conditions dans lesquelles ils évoluent. Ainsi, cet « effet bouteille » a été documenté depuis plusieurs décennies (Williams et Purdie 1991). A l'inverse, utiliser des capteurs immergés directement *in situ* ou dans des mésocosmes permet de s'affranchir de cet effet.

L'utilisation des capteurs HF présente donc de nombreux avantages par rapport aux méthodes d'incubation de Winkler. Cependant, quelques questionnements méthodologiques persistent, soit inhérents à la méthode des changements journaliers d'O_2 en elle-même, ou bien à son application en mésocosmes *in situ*. Les trois principaux sont la variabilité dans le couplage entre les cycles jour-nuit et de l'O_2 dissout (Soulié et al. 2021), l'estimation de la respiration planctonique ayant lieu la journée (Staehr et al. 2010), et l'estimation de l'échange physique d'O_2 entre la surface et l'atmosphère (Staehr et al. 2010). La variabilité dans le couplage entre les cycles jour-nuit et de l'O_2 dissout, induisant un potentiel biais dans les estimations des paramètres métaboliques, n'est généralement pas prise en compte dans les applications de la méthode (Cole et al. 2000, Staehr et al. 2010, Mostajir et al. 2013). C'est pourquoi la méthode établie dans le cadre du Chapitre 1 de la présente thèse considère cette variabilité et permet de s'affranchir des potentiels biais liés à celle-ci. Similairement, les applications déjà existantes de la méthode considèrent que la respiration la journée est égale à celle la nuit afin de simplifier les calculs, malgré de nombreuses preuves suggérant que la respiration la journée est significativement plus élevée que celle la nuit car la respiration à la lumière est accrue via l'utilisation directe des produits de la photosynthèse comme substrat pour la respiration (Xue et al. 1996, Carignan et al. 2000, Pringault et al. 2007, Mantikci et al. 2017). Ainsi, cette simplification entraîne un biais significatif dans les estimations de R et de PCN. La nouvelle méthode établie dans le Chapitre 1 propose également une façon d'estimer une respiration la journée différente et plus élevée que celle la nuit. Finalement, la dernière incertitude, qui concerne l'estimation de l'échange physique d'O_2 entre la surface et l'atmosphère, est spécifique à l'application de la méthode aux mésocosmes. Elle est due au fait que mesurer le coefficient de vitesse d'échange demeure un challenge important à cause de la difficulté de le mesurer directement ou indirectement dans une enceinte fermée telle qu'un mésocosme (Dugan et al. 2016, Winslow et al. 2016, Hall et Ulseth 2020). L'erreur sur la valeur du coefficient se propage de façon importante aux estimations de R et de PCN (Staehr et al. 2010). La nouvelle méthode présentée dans le Chapitre 1, et l'Encadré à ce propos, permettent de prendre en compte la variabilité importante dans l'estimation du coefficient d'échange liée à la température et à la salinité, même s'ils ne résolvent pas entièrement la problématique de l'estimation de l'échange physique entre la surface et l'atmosphère.

3.2.3. L'estimation des taux de croissance et de perte du phytoplancton via l'utilisation des capteurs à haute-fréquence

Comme vu auparavant, estimer les taux de croissance et de perte du phytoplancton est indispensable pour apprécier le fonctionnement d'un système aquatique. Il est possible d'estimer ces taux en utilisant les données de capteurs de fluorescence de la chl-*a* HF. En effet, du fait que la fluorescence de la chl-*a* suit un cycle journalier naturel lié principalement à la croissance du phytoplancton la journée et à sa perte la nuit, l'application d'un modèle exponentiel sur les données de fluorescence de la chl-*a* durant la journée permet d'estimer la croissance de la communauté phytoplanctonique, tandis que cette application sur les données de la nuit permet d'estimer la perte (Neveux et al. 2003, Neveux et al. 2010). Classiquement, les taux de croissance et de mortalité par prédation du phytoplancton sont estimés via la technique dite des « dilutions » (Landry et Hassett 1982), qui consiste à incuber une communauté naturelle planctonique et à la diluer à différents niveaux de dilutions afin de diminuer les rencontres proies-prédateurs. Cette technique nécessite généralement un travail d'échantillonnage, des incubations et un travail de laboratoire longs qui ne permettent toutefois pas une grande résolution temporelle. Au contraire, l'utilisation des capteurs permet la récolte de données en continu et de façon robuste, tout en ne nécessitant qu'une intervention humaine limitée (Carberry et al. 2019). Dans le Chapitre 3, nous avons présenté la méthode, l'avons appliqué à deux expériences de mésocosmes, et avons réalisé l'interprétation écologique des données issues. Néanmoins, certaines incertitudes demeurent quant à l'utilisation des mesures de fluorescence de la chl-*a* HF pour estimer les taux de croissance et de perte du phytoplancton. Ces incertitudes sont liées au fait que la quantité de chl-*a* contenue dans les cellules phytoplanctoniques peut varier en fonction de la taxonomie, de la photoacclimation et de la phase de croissance (Kruskopf et Flynn 2006, Moore et al. 2006, Kasprzak et al. 2008). Une autre incertitude concerne la prise en compte du « quenching » non-photochimique de la fluorescence de la chl-*a*. Ce mécanisme intracellulaire permet au phytoplancton de se protéger d'une trop forte quantité de lumière via le retour à leur état d'origine de molécules de chl-*a* excitées par la lumière reçue sans passer par le mécanisme de production de photon habituel, et donc sans fluorescence (Carberry et al. 2019). Dans le cadre de la méthode développée dans le Chapitre 3, ce phénomène est pris en compte via l'interpolation des données de fluorescence entre le lever et le coucher du soleil (Li et al. 2008). La validité de cette prise en compte est évaluée via une analyse présentée en Annexe I.

4. Les objectifs et l'organisation du manuscrit de la thèse

Le métabolisme planctonique jouant un rôle important dans le fonctionnement des écosystèmes aquatiques et dans les cycles biogéochimiques, il apparaît crucial d'estimer précisément sa réponse face à différents forçages liés au changement climatique afin de comprendre et de modéliser le futur des écosystèmes marins. Dans ce cadre, **l'objectif principal** de la thèse est de caractériser la réponse

métabolique de communautés planctoniques côtières face à diverses perturbations liées au changement global via l'utilisation de mesures HF acquises lors d'expériences en mésocosmes *in situ*.

L'objectif principal de la thèse est décliné en plusieurs sous-objectifs, qui correspondent aux chapitres de la thèse, listés ci-dessous.

Sous-objectif 1 : Établir une méthode permettant d'estimer les paramètres métaboliques de l'O_2 à partir de mesures de concentration en O_2 dissout HF et qui prend en compte la variabilité dans la respiration la journée et la nuit et dans le couplage entre cycle de l'O_2 et cycle jour-nuit.

Sous-objectif 2 : Évaluer les effets d'un épisode de brunissement sur les paramètres métaboliques et la composition d'une communauté planctonique côtière septentrionale (baie d'Hopavågen).

Sous-objectif 3 : Évaluer les effets d'une augmentation constante de la température sur les taux de croissance et de perte phytoplanctoniques lors de deux périodes productives contrastée en zone côtière méditerranéenne (lagune de Thau).

Sous-objectif 4 : Évaluer la stabilité fonctionnelle et compositionnelle d'une communauté planctonique côtière méditerranéenne (lagune de Thau) face à un épisode de vague de chaleur.

Les quatre sous-objectifs décrits précédemment sont déclinés sous la forme de quatre chapitres. Ces chapitres sont structurés sous la forme de quatre articles scientifiques rédigés en anglais, soit publiés, en révision, soumis, ou en préparation, et ont pour but de répondre aux sous-objectifs énoncés plus haut. Avant chaque chapitre, un Avant-Propos, écrit en français, introduit le contexte et les principaux objectifs de l'étude faisant l'objet du chapitre. De plus, certains chapitres sont suivis d'un encadré présentant des résultats non-inclus dans l'article mais nécessaire pour la Discussion Générale de la thèse. Cette dernière suit les chapitres et a pour objectif de mettre en relation les différents travaux de la thèse, de les confronter avec la littérature existante sur le sujet, et de proposer des perspectives générales pour la continuation de ces travaux. Il faut noter que les références de chaque section se trouvent regroupées dans la section Bibliographie de la thèse.

Le Chapitre 1 est intitulé « **Etablissement d'une nouvelle méthode pour estimer le métabolisme planctonique de l'oxygène et qui prend en compte les variabilités dans la respiration la journée et la nuit et dans le couplage entre cycles de l'oxygène et jour-nuit** ». Le manuscrit correspondant, intitulé « A new method to estimate planktonic oxygen metabolism using high-frequency sensor measurements in in situ mesocosm experiments and considering daytime and nighttime respirations », écrit par Tanguy Soulié, Sébastien Mas, David Parin, Francesca Vidussi, et Behzad Mostajir, a été publié dans la revue *Limnology and Oceanography: Methods* le 18 février 2021. La version publiée de l'article et des données complémentaires associées à l'article est présentée en Annexe III.

Le Chapitre 2 est intitulé « **Effets du brunissement sur le métabolisme de l'oxygène et la composition d'une communauté planctonique d'une zone côtière septentrionale : une expérience de mésocosmes *in situ* combinée aux mesures à haute-fréquence** ». Le manuscrit correspondant, intitulé « Brownification reduces oxygen gross primary production and community respiration and changes the phytoplankton community composition: an *in situ* mesocosm experiment with high-frequency measurements in a North Atlantic bay », par Tanguy Soulié, Herwig Stibor, Sébastien Mas, Benjamin Braun, Johanna Knechtel, Jens C. Nejstgaard, Ulrich Sommer, Francesca Vidussi et Behzad Mostajir, est en révision dans la revue *Limnology and Oceanography* depuis le 15 juin 2021. Ces travaux ont été présentés lors de congrès scientifiques, dont le détail est fourni en Annexe II.

Le Chapitre 3 est intitulé « **Effets du réchauffement sur les taux de croissance et de perte du phytoplancton durant deux périodes productives en zone côtière Méditerranéenne : apports des mesures de fluorescence de la chlorophylle-*a* à haute-fréquence** ». Le manuscrit correspondant, intitulé « Warming enhanced phytoplankton growth and mortality rates during two contrasted productive seasons in Mediterranean coastal waters : evidences from *in situ* mesocosm experiments and high-frequency measurements », écrit par Tanguy Soulié, Francesca Vidussi, Justine Courboulès, Sébastien Mas, et Behzad Mostajir sera soumis dans une revue spécialisée très prochainement.

Le Chapitre 4 est intitulé « **Stabilité fonctionnelle d'une communauté planctonique côtière Méditerranéenne face à une vague de chaleur : une expérience de mésocosmes *in situ* combinée aux mesures à haute-fréquence** ». Le manuscrit correspondant, intitulé « Low functional stability of a coastal Mediterranean plankton community during an *in situ* mesocosm experiment simulating a marine heatwave and combined with high-frequency measurements », écrit par Tanguy Soulié, Francesca Vidussi, Sébastien Mas et Behzad Mostajir sera soumis dans une revue spécialisée très prochainement.

Il faut noter que les travaux de la présente thèse s'inscrivent dans les objectifs du projet AQUACOSM, financé par le programme de recherche et d'innovation Horizon 2020 de l'Union Européenne. Parce que les écosystèmes aquatiques, à la fois marins et d'eau douce, sont connectés, il est primordial de coordonner la recherche expérimentale en écologie aquatique. Cette coordination est l'objectif d'AQUACOSM, qui vise à rassembler les infrastructures expérimentales européennes en un réseau unique, afin d'uniformiser les bonnes pratiques et les protocoles dans le but de pouvoir comparer la réponse de systèmes différents, à la fois spatialement et temporellement, face à des perturbations similaires ou non. L'objectif est ainsi de comprendre les processus derrière les réponses observées à différentes échelles, de locales à globales. Plus précisément, les travaux de cette thèse s'inscrivent en partie dans les objectifs du Work Package 8, qui vise à développer les bonnes pratiques quant à l'acquisition automatique ou semi-automatique des données dans le cadre d'expériences en mésocosmes et l'instrumentation permettant des observations HF permettant la description de la

réponse des écosystèmes face au changement global. Des informations complémentaires sont accessibles à l'adresse suivante : https://www.aquacosm.eu/project-information/aquacosm/.

Finalement, l'Annexe I présente une évaluation de la correction des données de fluorescence pour le quenching non-photochimique réalisée dans les Chapitres 3 et 4, l'Annexe II présente les formations auxquelles j'ai eu l'opportunité de participer au cours de la thèse, ainsi que mes activités d'enseignement et qu'un récapitulatif des publications scientifiques dans les revues spécialisées à comité de lecture et des présentations orales lors de congrès scientifiques internationaux. Les Annexes III et IV présentent les versions publiées de l'article faisant l'objet du Chapitre 1 ainsi que d'un article dont je suis co-auteur, respectivement.

Chapitre 1

Etablissement d'une nouvelle méthode pour estimer le métabolisme planctonique de l'oxygène et qui prend en compte les variabilités dans la respiration la journée et la nuit et dans le couplage entre cycles de l'oxygène et jour-nuit

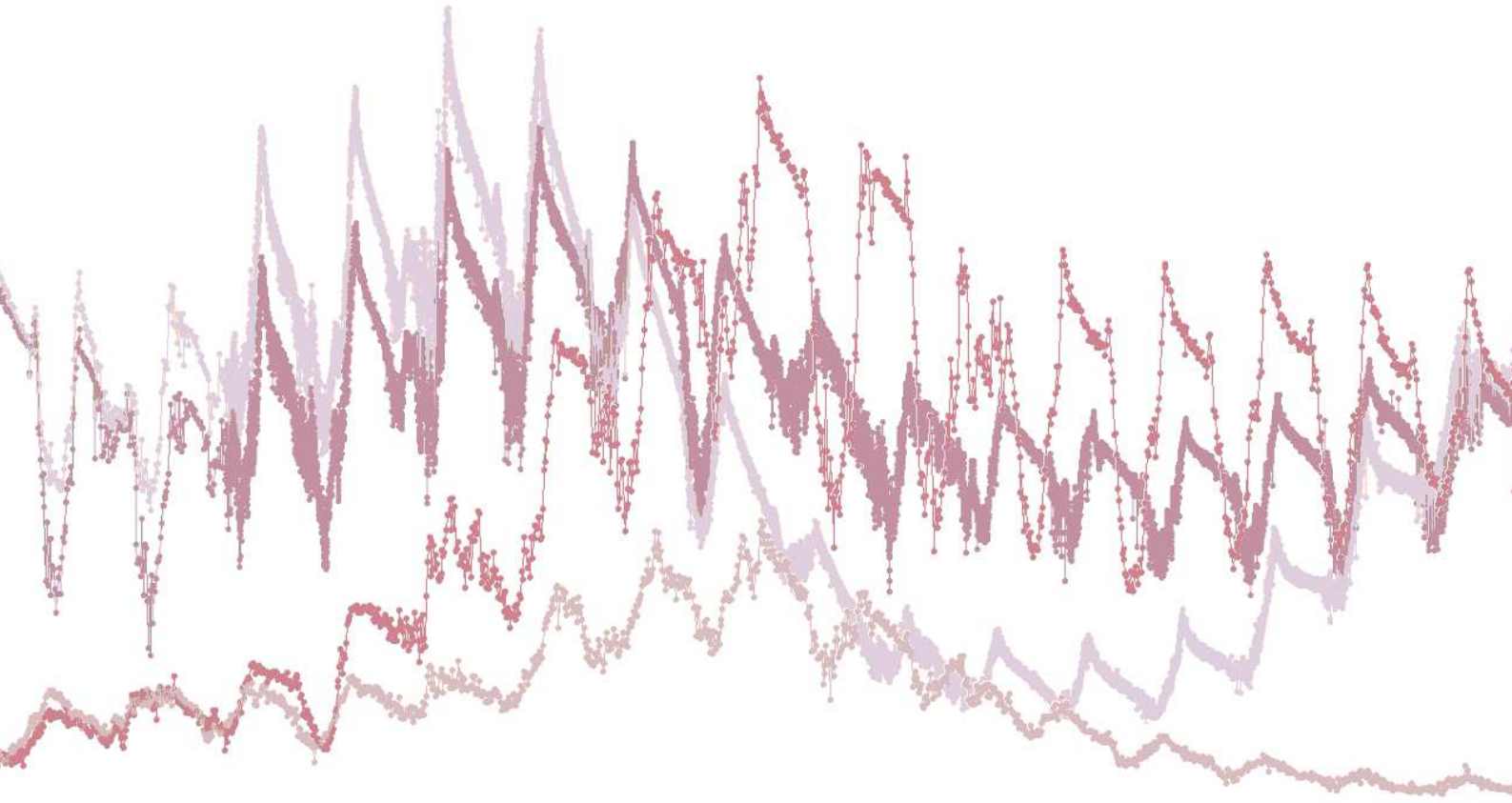

Avant-Propos

En mesurant la concentration et la saturation en O_2 dissout durant un cycle complet de 24h, il est possible, via la méthode dite des changements dans le cycle nycthéméral de l'O_2, d'estimer certains paramètres métaboliques de la communauté planctonique : la Production Primaire Brute (PPB), la Production Communautaire Nette (PCN) et la respiration (R) communautaire. Cette méthode a été employée pour de nombreux écosystèmes différents (lacs, rivières, zones côtières et océans) et via différentes applications (bouées, gliders, campagnes océanographiques et expériences en mésocosmes) (Cole et al. 2000, Staehr et al. 2010, Herrera et Nadaoka 2021). Cependant, certaines limites de la méthode persistent, notamment quant à l'estimation de la respiration qui a lieu durant la journée.

Une nouvelle méthode pour estimer la respiration la journée, et ainsi la PPB, la PCN et la R, à partir de données de concentration d'O_2 dissout à haute-fréquence (HF) a été établie dans ce chapitre, présenté sous la forme de l'article Soulié et al. (2021), publié dans la revue *Limnology and Oceanography : Methods*. Cette nouvelle méthode permet également de prendre en compte la variabilité dans le couplage entre les cycles jour-nuit et de l'O_2 dissout, cette variabilité n'étant pas prise en compte par les méthodes déjà existantes. Afin d'évaluer la nouvelle méthode, les données de 6 mésocosmes contrôles (i.e., dans lesquels aucune perturbation n'a été appliquée) ont été utilisées, provenant de 2 expériences différentes, réalisées en Octobre 2018 et en Mai et Juin 2019 dans la lagune de Thau dans le cadre du projet européen AQUACOSM (Network of Leading European AQUAtic MesoCOSM Facilities Connecting Mountains to Oceans from the Arctic to the Mediterranean). Dans chaque mésocosme, un jeu de capteurs a été immergé à 1 m de profondeur. Chaque jeu est notamment composé d'une optode mesurant la concentration et la saturation en O_2 dissout, d'un conductimètre mesurant la salinité, et de trois sondes de température placées à des profondeurs différentes. Les données de ces capteurs ont permis de tester la nouvelle méthode pour estimer la respiration la journée, et de la comparer avec une méthode déjà publiée (Mostajir et al. 2013). De plus, tous les 2 jours lors des 2 expériences de mésocosmes, des incubations furent réalisées afin de mesurer la PPB, la PCN et la R via la méthode de Winkler (1888) modifiée par Carritt et Carpenter (1966), afin de comparer ces paramètres métaboliques obtenus avec les incubations avec ceux estimés avec la méthode nouvellement établie pour estimer la respiration la journée. L'estimation de la valeur de coefficient d'échange d'O_2 entre la surface et l'atmosphère constitue une des limites les plus importantes de l'application de la méthode, surtout dans le cadre de mésocosmes *in situ* testant l'effet d'une augmentation de la température. Puisque la méthode est appliquée dans le cadre d'expériences testant l'effet du réchauffement (Encadré Chapitre 3, Chapitre 4), un encadré est associé au présent chapitre afin de présenter les équations pour prendre en compte la variabilité dans la valeur du coefficient d'échange lié à la température et à la salinité. Une comparaison entre PPB, PCN et R obtenues avec un coefficient constant et avec un coefficient variable en fonction

de la température et de la salinité est également présentée. Les résultats de cet encadré seront discutés dans la Discussion Générale de la thèse (p 174).

Lors des 2 expériences de mésocosmes dont les données ont été utilisées pour ce chapitre, j'ai participé, avec de nombreux chercheurs, étudiants, techniciens et ingénieurs, à la mise en place des mésocosmes et des capteurs, à l'échantillonnage journalier et j'ai réalisé les expériences d'incubation. J'ai traité et analysé l'ensemble des données issues des capteurs. De plus, j'ai analysé des échantillons de pigments phytoplanctoniques par chromatographie liquide à haute performance (HPLC), qui font l'objet d'une partie des chapitres 3 et 4 de la thèse. De plus, une partie de ces données a servie dans le cadre d'un article, pour lequel je suis co-auteur, présenté dans l'Annexe IV et publié dans la revue ***Aquatic Ecology***, (doi : 10.1007/s10452-021-09852-7). Comme annoncé précédemment, le présent chapitre est présenté sous la forme d'un article rédigé en anglais. Cet article est publié depuis le 18 février 2021 sous le titre « **A new method to estimate planktonic oxygen metabolism using high-frequency sensor measurements in mesocosm experiments and considering daytime and nighttime respirations** » écrit par Tanguy Soulié, Sébastien Mas, David Parin, Francesca Vidussi, et Behzad Mostajir, dans la revue ***Limnology and Oceanography : Methods*** (doi : 10.1002/lom3.10424). La version publiée de l'article et les données complémentaires associées à l'article sont présentées en Annexe III.

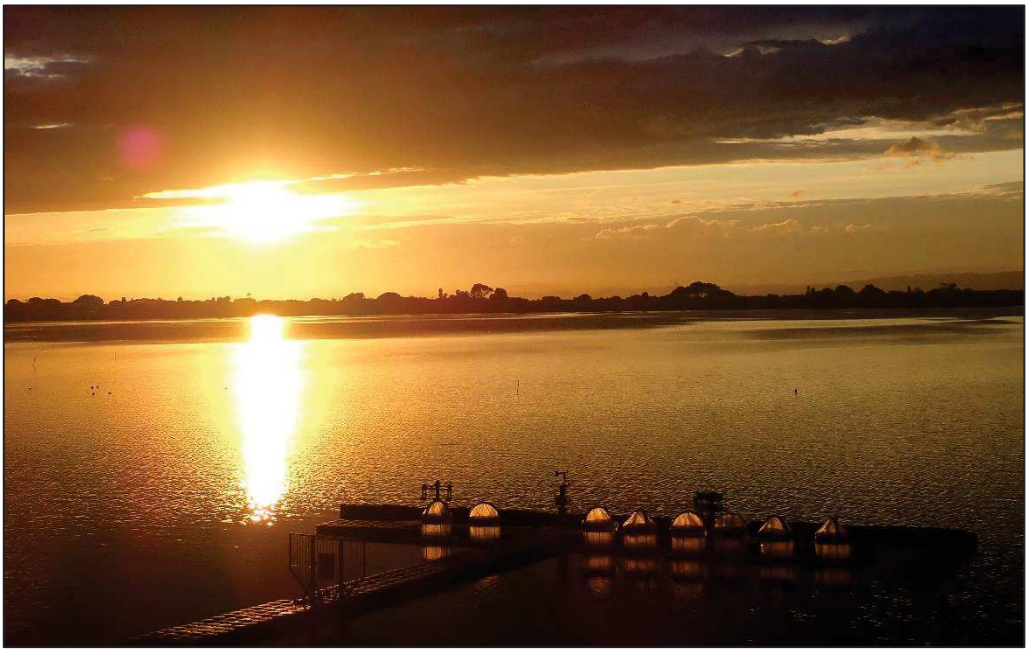

Les mésocosmes dans la lagune de Thau. Photo © J.Courboulès

A new method to estimate planktonic oxygen metabolism using high-frequency sensor measurements in mesocosm experiments and considering daytime and nighttime respirations

Tanguy Soulié [1*], Sébastien Mas [2], David Parin [2], Francesca Vidussi [1], Behzad Mostajir [1]

[1] MARBEC (MARine Biodiversity, Exploitation and Conservation), Univ Montpellier, CNRS, Ifremer, IRD, Montpellier, France

[2] MEDIMEER (Mediterranean Platform for Marine Ecosystems Experimental Research), OSU OREME, CNRS, Univ Montpellier, IRD, IRSTEA, Sète, France

* corresponding author: Tanguy Soulié, Email: tanguy.soulie@umontpellier.fr

Keywords: planktonic oxygen metabolism, high-frequency, mesocosm, production, respiration, diel oxygen cycle

Running head: Plankton metabolism using O_2 sensors

Citation: Soulié, T., Mas, S., Parin, D., Vidussi, F. and Mostajir, B. (2021), A new method to estimate planktonic oxygen metabolism using high-frequency sensor measurements in mesocosm experiments and considering daytime and nighttime respirations. *Limnol Oceanogr Methods*, **19**: 303-316. https://doi.org/10.1002/lom3.10424

Abstract

Understanding how aquatic ecosystems respond to perturbations has emerged as a crucial way to predict the future of these ecosystems and to assess their capacity to produce oxygen and store atmospheric carbon. In this context, in situ mesocosm experiments are a useful approach for simulating disturbances and observing changes in planktonic communities over time and under controlled conditions. Within mesocosm experiments, the estimation of fundamental parameters such as gross primary production (GPP), net community production (NCP) and respiration (R) allows the evaluation of planktonic metabolic responses to a perturbation. The continuous estimation of these metabolic parameters in real time and at high frequency is made possible by employing noninvasive automated sensors in the water column. However, some uncertainties and methodological questions about the estimation of daytime respiration remain to be addressed for this method, and notably to address the fact that respiration could be significantly higher during the day than during the night. In this study, data from two in situ mesocosm experiments performed in fall and spring in a coastal Mediterranean area were used to develop a new method of estimating daytime respiration, and in turn daily GPP, R and NCP, by considering the maximum instantaneous R, and that takes into account the variability of the coupling between day-night and dissolved oxygen cycles. This new method was compared with the Winkler incubation technique and with another existing method. Results showed that using this existing method, daytime R was significantly underestimated relative to estimates obtained with the newly proposed method.

1 Introduction

Aquatic ecosystems undergo many perturbations at different temporal and spatial scales due to natural and anthropogenic factors. Understanding how these perturbations affect these ecosystems is crucial for predicting their future status. Due to their importance in global biogeochemical cycles and in aquatic ecosystem functioning, assessing the response of planktonic communities to various environmental disturbances is therefore of great importance and interest. To do so, mesocosm experiments are experimental units that can be used to simulate disturbances and observe changes in the studied community over time and under controlled conditions while ensuring the reproducibility of the tested perturbations (Stewart et al. 2013; Dzialowski et al. 2014). They closely simulate the natural environment and therefore constitute a link between laboratory and field observations (Odum 1984; Crossland and Point 1992).

Changes in the metabolic processes associated with planktonic communities indicate the response of these communities to disturbances; therefore, measuring metabolic parameters during mesocosm experiments is essential, and there is a need to obtain reliable estimates of these parameters. Some of these metabolic parameters that are related to oxygen, such as gross primary production (GPP), which is the autotrophic production of oxygen through the conversion of inorganic carbon to organic carbon, and aerobic respiration (R), which is the consumption of oxygen through the oxidation of organic carbon to inorganic carbon by both autotrophic and heterotrophic organisms, are of great importance in understanding and managing aquatic ecosystems (Hanson et al. 2008). Indeed, the net community production (NCP), which is the difference between GPP and R, represents the balance between anabolic and catabolic processes and thus between autotrophy and heterotrophy (Staehr et al. 2012).

Due to their importance in understanding the functioning of aquatic ecosystems, these metabolic parameters have been estimated for more than half a century using various methods. The Winkler incubation method, which is the reference method, consists of light and dark incubations of natural samples in small glass bottles for a certain interval of time. The production of dissolved oxygen (DO) in the light bottles and its consumption in the dark bottles is determined by titration with the Winkler technique (Winkler 1888). Another technique used to estimate metabolic parameters is measuring the diel free-water changes in the DO concentration over a certain period of time (Odum 1956). Oviatt et al. (1986) proposed estimating the net production from dawn to dusk and the respiration from dusk to the following dawn. More recently, Kritzberg et al. (2014) obtained GPP, R and NCP with four DO measurements over a 24 h period.

Additionally, submersible automated DO sensors, that provide high-frequency DO measurement data allowing for real-time observations at intervals of every minute to every hour, can be used to assess

metabolic parameters. These sensors can be deployed for a long period and in remote locations and are traditionally used on buoys and gliders to monitor key environmental parameters, at various time scales and for different aquatic systems. They have enabled a better understanding of the trends in the physical and biological variables in these systems and have even provided new insights into ecosystem functioning (de Eyto et al. 2019; Trombetta et al. 2019). Within the framework of mesocosm experiment, using sensor data to estimate metabolic parameters has several advantages compared to the traditional incubation technique, as the sensors are noninvasive and their use does not introduce bottle or container effects into the measurement, thus avoiding the error propagation associated with incubations (Staehr et al. 2010a). Moreover, ecologically important short-timescale temporal changes in the DO can easily be monitored with sensors but are not detected by the Winkler incubation method.

Despite its advantages, only a few studies have used the free-water method of estimating metabolic parameters in mesocosm experiments, and even fewer studies have used high-frequency sensors to assess metabolic parameters in mesocosm experiments (Oviatt et al. 1984, 1986; Brinkman et al. 1995; Leclercq et al. 1999; Whitledge and Rabeni 2000; Mostajir et al. 2013; Reijo et al. 2018; Hensley and Cohen 2020). Because of the substantial technical constraints, estimating oxygen-related metabolic parameters using high-frequency sensors in mesocosm experiments is still not widespread in the scientific community. However, high-frequency sensors have been commonly used to estimate oxygen metabolic parameters in the field, especially in lake studies (Van de Bogert et al. 2007; Hanson et al. 2008; Staehr et al. 2010b; Alkire et al. 2012; Wikner et al. 2013; Briggs et al. 2018; Demars et al. 2018).

Due to the limited number of studies that have used high-frequency DO data to estimate metabolic parameters in mesocosm experiments, there are still some methodological questions regarding the use of this technique and the reliability of the metabolic estimates derived from it. The main uncertainty is related to the estimation of respiration occurring during the day (Rdaytime). For simplicity, Rdaytime has been assumed to be equal to the R that occurs at night (Rnight) in most field studies using sensor data to derive planktonic respiration rate (Hanson et al. 2003; Lauster et al. 2006; Staehr et al. 2010a), despite increasing evidence that Rdaytime is significantly greater than Rnight, e.g., up to 640% higher at the beginning of the night than that at the end of it (Markager et al. 1992; Xue et al. 1996; Pringault et al. 2007; Carvalho and Eyre 2012). Indeed, previous studies have reported that respiration is enhanced by photosynthesis and the resultant photosynthetic products (Markager and Sand-Jensen 1989; Markager et al. 1992; Mantikci et al. 2017), with postillumination rates 50 to 340% higher than dark respiration levels (Beardall et al. 1994; Hotchkiss and Hall 2014). The calculation of Rdaytime has been proposed to be done just after sunset, when autotrophic respiration still relies on the photosynthetic products accumulated during the daylight period (Mostajir et al. 2013). Nevertheless, the method of Mostajir et al. (2013) does not consider the fact that the DO cycle does not strictly follow the day-night cycle. Indeed, this method assumes that the DO concentration starts to decrease at sunset; however, this decrease can start earlier if respiration is stronger than production even when there is still daylight. This

mismatch can be caused by various environmental factors, including the amount of light available for photosynthesis and the water temperature, which affects metabolic processes. Hence, it seems clear that considering a period starting at sunset for the calculation of Rdaytime may yield very different estimates for days when the cycle of oxygen matches the light cycle and days when the cycles do not match. Therefore, there is a need to establish a method that considers this variability in the calculation of Rdaytime.

Accordingly, a new method to estimate Rdaytime using high-frequency DO data from enclosed mesocosm experiments that takes into account the potential variability between DO and day-night cycles is provided in this investigation. In addition, the metabolic estimates obtained with this new method were compared with those obtained with the method of Mostajir et al. (2013) and with the Winkler incubation technique. Moreover, a comparison was performed between two time periods used for the daily integration of daytime and night respiration estimates. Overall, this new method is based on data obtained during two in situ enclosed mesocosm experiments conducted in a Mediterranean coastal shallow lagoon in fall 2018 and spring 2019.

2 Materials & Procedures

2.1 Experimental setup

2.1.1 Mesocosm experiments

Two mesocosm experiments were carried out in Thau Lagoon, which is a productive shallow (4 m mean depth) coastal lagoon located in the western Mediterranean in southern France. The experiments lasted 15 days in October 2018 (Exp. 1) and 17 days in May and June 2019 (Exp. 2). In this paper, data from three mesocosms in Exp. 1 (Oct-1, Oct-2 and Oct-3) and three mesocosms in Exp. 2 (Jun-1, Jun-2 and Jun-3) were used. As an example, Oct-1 refers to the dataset obtained for the mesocosm n°1 of the three replicates mesocosms of the Exp 1 which took place in October 2018.

The mesocosms were established at the Mediterranean platform for Marine Ecosystem Experimental Research (MEDIMEER) pontoon (43°24’53” N, 3°41’16” E) located on the east side of the lagoon. The mesocosm bags were 280 cm high, with a diameter of 120 cm and an additional 50 cm long sediment trap located at the bottom of the bag. They were made of a transparent nylon-reinforced 200 µm thick vinylacetate polyethylene film (Insinööritoimisto Haikonen Ky). The emerged part of each mesocosm was covered with a transparent plastic dome to avoid contamination by rain and waves (Fig. 1), making the total structure 300 cm high. The main use of the dome is to prevent precipitations and other external

inputs into the mesocosm, however it allows gas exchange with the atmosphere. The mesocosms were filled with 2200 L of lagoon water.

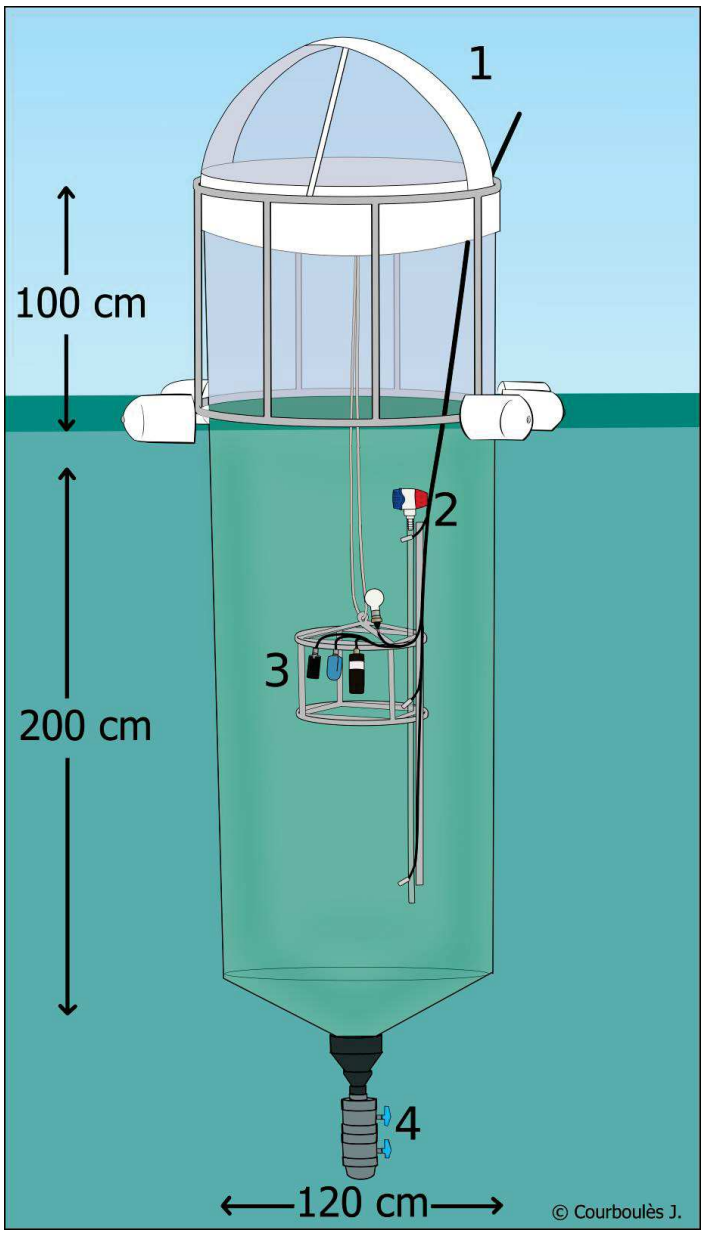

Figure 1. A single mesocosm unit equipped with a dome to cover the structure (1), a pump (2), a sensor system (3), and a sediment trap at the bottom (4) (Illustration courtesy of Justine Courboulès).

The water column was gently mixed with a pump (Rule, Model 360), leading to a turnover rate of approximately 3.5 d^{-1}. Each mesocosm unit was equipped with a set of high-frequency automated sensors positioned 1 m deep to measure the DO concentration with an oxygen optode (Oxygen optode 3835, Aanderaa), the conductivity with an electromagnetic induction conductivity sensor (Conductivity sensor 4319, Aanderaa), and the incident photosynthetically active radiation (PAR) with a spherical underwater quantum sensor (LI-193, Li-Cor). Additionally, the water temperature was measured by

three temperature sensors (Campbell Scientific Ltd. Thermistor probe 107) placed at three different depths (0.5, 1 and 1.5 m). For the present study, only the data measured by the oxygen optode and the conductivity, temperature and incident PAR sensors were used.

2.2 Estimating metabolic parameters with light and dark incubations using the Winkler method

To compare the metabolic sensor data with data obtained with a classical reference method, Winkler incubations were performed every two days. To do so, mesocosm water was sampled using a 5 L Niskin water sampler. Nine borosilicate bottles of 120 mL were directly filled with water from the Niskin bottle for each mesocosm. The DO contained in three bottles (the t0 bottles) was immediately fixed by adding Winkler reagents as described by Carrit (1966). Three other bottles were carefully wrapped in aluminum foil (the dark bottles) to prevent photosynthesis. These bottles were then incubated in incubation mesocosms along with the three remaining bottles (the light bottles) from 10:00 to 18:00. The two incubation mesocosms were established to incubate light and dark incubation bottles following the Winkler technique as described above. Incubation mesocosms were used to avoid potential contamination and changes in the light environment of the main mesocosms. For the October and June experiments, the incubation mesocosms were located directly adjacent to the other mesocosms and were therefore subject to the same environmental conditions as the control mesocosms. After incubation, the dissolved oxygen in the incubated bottles was fixed as described above. The oxygen concentration in the bottles was measured by using an automated Winkler titrator with a potentiometric titration method (Crisson titrator and Methrom 916-Ti-touch titrator in the October and June experiments, respectively) (Carpenter 1965).

NCP (in $gO_2\ m^{-3}\ d^{-1}$) was then calculated as in Equation 1:

$$NCP = \left(\frac{mean\left(O_{2_{Light}}\right) - mean\left(O_{2_{t0}}\right)}{Incubation\ time} \right) * dayfraction * 24 \qquad \text{Eq. 1}$$

where the *mean (O_{2Light})* is the mean value from the triplicate bottles incubated in the light (in $gO_2\ m^{-3}$), the *mean (O_{2t0})* is the mean value from the triplicate bottles directly fixed after sampling (in $gO_2\ m^{-3}$), and the day fraction is $dayfraction = {lightperiod}/{24}$, where the light period refers to the duration from sunrise to sunset in hours.

Respiration (R) (in $gO_2\ m^{-3}\ d^{-1}$) was then calculated as in Equation 2:

$$R = \left(\frac{mean\left(O_{2_{t0}}\right) - mean\left(O_{2_{Dark}}\right)}{Incubation\ time} \right) * 24 \qquad \text{Eq. 2}$$

where the *mean (O_{2Dark})* is the mean value from the triplicate dark bottles (in $gO_2\ m^{-3}$).

Then, GPP (in $gO_2\ m^{-3}\ d^{-1}$) was obtained as: $GPP = NCP + R.$ Eq. 3

2.3 Free-water diel oxygen method for metabolic parameter measurements using sensors

2.3.1 Sensor data acquisition and correction

Sensor data were acquired every 1 min in all the mesocosms. The choice of the sampling frequency is very important as useful information to get reliable metabolic estimates could be missed with a slow frequency while a rapid frequency could lead to high amount of data not necessarily needed. This question was addressed and a power analysis assessing the required duration of sensor deployment with sampling frequencies ranging from 1 to 60 min was performed, suggesting that sampling frequencies up to 10 min were sufficient for the 15 days lasting October experiment. This analysis is presented in appendix (Supp. Data, Appendix 1.).

Oxygen sensors were calibrated before and after each deployment using three saturation points (0, 50, and 100%) and at three different temperatures (17, 20, and 22°C), according to a calibration procedure described in Bittig et al. (2018). The 100% saturation point was reached by bubbling air into the water, and the 0 and 50% saturation points were reached by adding potassium metabisulfite. The raw DO data measured during the mesocosm experiments were then corrected with the obtained calibration coefficient. Then, the DO data were corrected with the salinity and water temperature data obtained from the conductivity sensors and the temperature probe positioned at 1 m deep, respectively; salinity and temperature correction is required for oxygen optodes in order to take into account variations in O_2 solubility (Bittig et al. 2018). The DO-corrected data were then smoothed using a 9-point moving average. To estimate planktonic metabolism, the smoothed data were then separated into different periods according to the minima and the maxima of the DO curve. Periods between a minimum and the following maximum, indicating that DO was increasing and thus the instantaneous NCP of O_2 was positive, were considered Positive NCP periods. Periods between a maximum and the following minimum, when DO was decreasing and thus the instantaneous NCP was negative, were considered Negative NCP periods. An example of the separation of the data into periods is given for the Oct-1 DO dataset in Fig. 2a.

A five-parameter sigmoidal model was built to fit the DO data for each Positive NCP period and each Negative NCP period to reduce short-timescale noise (Mostajir et al. 2013) (SigmaPlot software version 12.3). The initial raw data calibrated and corrected for salinity and temperature, the data smoothed by

a 9-point moving average followed by a locally estimated scatterplot smoothing (LOESS) regression and the data modeled with the five-parameter sigmoidal model are presented in Fig. 2.b, c, and d, respectively. Outliers in the raw sensor dataset were defined as values 20% higher or lower than their direct neighbors and were removed. Consequently, between 0 (Oct-1) and 1.49% (Oct-2) of the initial DO data was removed. Missing values were extrapolated using a linear regression in the local neighborhood of the missing value.

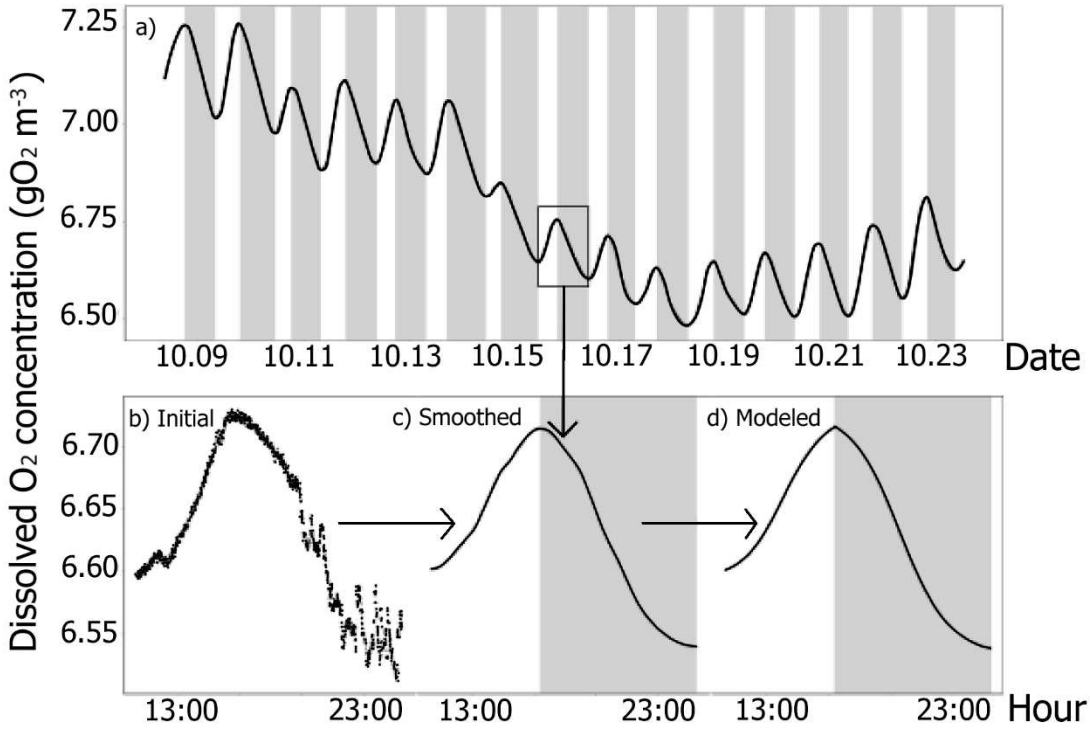

Figure 2. (a) Oct-1 smoothed DO data. Shading separates Positive NCP periods (white background) and Negative NCP periods (gray background). The parts in which DO is increasing are considered Positive NCP periods, and the parts in which DO is decreasing are considered Negative NCP periods. The same separation was applied to the data from all the mesocosms. The black rectangle shown in Fig. 2a is shown in the bottom figure as Fig. 2 b, c, and d, corresponding to the initial data (raw data calibrated and corrected for salinity and temperature) **(b), the smoothed data with a 9-point moving average followed by a LOESS regression (c) and the data modeled using a 5-parameter sigmoidal model (d)**

2.3.2 Metabolic parameter calculation

Instantaneous net community production

The governing equation comes from (Odum & Odum, 1955), the first application of the method:

$$\frac{\Delta O_2}{\Delta t} = GPP - R - F - A \qquad \text{Eq. 4}$$

where $\frac{\Delta O_2}{\Delta t}$ is the change in DO concentration during a time interval Δt, GPP is the gross primary production, R is the respiration, F is the exchange of O_2 between the water and the atmosphere, and A is a combined parameter that includes all other phenomena responsible for changes in the DO concentration in the considered system. In this paper, A was considered to be negligible.

The exchange between the water surface and the atmosphere, F, was calculated as:

$$F = (k * (O_2 - O_{2_{Sat}}))/Z_{mix} \quad \text{Eq. 5}$$

where O_2 is the concentration in DO, O_{2sat} is the oxygen saturation, *k* is the piston velocity coefficient and Z_{mix} is the mixing depth of the water column, i.e., in the present study, the depth of the mesocosms. In this study, k was set to 0.000156 $m.min^{-1}$. This value was chosen as it was experimentally measured in open-top laboratory microcosm (Alcaraz et al. 2001) in salinity and temperature conditions close to the conditions of both of the mesocosm experiments used in the present investigation. Moreover, this k value was chosen because it was the lowest value obtained with nonnull conditions as our in situ mesocosms naturally experience turbulence due to marine waves. To test eventual differences on metabolic estimates induced by the choice of the k value, a sensitivity analysis using the lowest and the highest value of k measured in similar experimental conditions as in our in situ mesocosms (Alcaraz et al. 2001) was performed and is presented in appendix (Supp. Data Appendix 2.). It appeared that GPP estimates were not significantly sensitive to the choice of the k value. In contrast, significantly higher estimates of R were obtained with the lower k, pointing out that the choice of the k value is more critical for the estimation of R.

For each time step of 1 minute, the instantaneous NCP was calculated as:

$$NCP = \Delta O_2 - F \quad \text{Eq. 6}$$

where NCP is the instantaneous net community production of O_2 per minute, ΔO_2 is the difference between two successive DO concentration values, and F is the exchange between the water surface and the atmosphere as previously described.

Instantaneous metabolism values can be integrated over certain periods of the day and the night to obtain daily estimates of GPP, NCP, and R. However, it is still unclear how daily metabolic parameters, notably Rdaytime, should be calculated. Various methods are selected, compared and presented in the following sections.

2.4 Statistical analyses

Analyses of variance (ANOVAs) were used to assess the differences between sensor-based metabolic estimates such as Rdaytime, Rnight and R24h and to test the effects of the sampling period and the piston velocity coefficient variations on these sensor-based metabolic estimates. A p-value less than or

equal to 0.05 was considered statistically significant. These analyses were also used to compare the sensor-based metabolic estimates with the estimates obtained with the Winkler method. When the assumptions of ANOVA could not be met even through data transformation (logarithmic, exponential or square-root transformation), a nonparametric Kruskal-Wallis test was used instead. Following the ANOVAs, Tukey honest significant difference (Tukey HSD) tests were used to perform multiple comparisons of means and to test the differences among estimates. Following the Kruskal-Wallis tests, a post hoc nonparametric Dunn test was performed. All statistical analyses were performed using R software (version 3.4.2, R Core Team, 2017).

2.5 Estimation of R during the day (Rdaytime), at night (Rnight), and daily R (R24h), using sensor data

In the present study, as shown in Table 1, Rdaytime, Rnight and R24h were estimated using sensor data and certain periods of the instantaneous NCP data and were integrated either from sunrise to sunset or only over the production period (e.g., only when the instantaneous NCP was positive). Means of instantaneous NCP over certain time periods were used as in previous studies, including Staehr et al. (2010), Laas et al. (2012); Idrizag et al. (2016); Richardson et al. (2017); and Chiu et al. (2020) . More precisely, Rdaytime was estimated either with the mean of the instantaneous NCP during a 1-h period centered on the maximum of the instantaneous Negative NCP (hereafter referred to as the "Max" method) or with the mean of the instantaneous NCP during a 1-h period following sunset, as in Mostajir et al. (2013) (hereafter referred to as the "Most" method). As the Winkler method is still considered the reference method for estimating planktonic metabolism, the R obtained from sensor data by applying the Max and Most methods were then compared with the R obtained using the Winkler method.

Table 1. Presentation of the 2 methods for estimating Rdaytime and Rnight compared in the present work using certain periods of the instantaneous NCP data.

Data and methods	Rdaytime calculation	Rnight calculation
Sensor data and "Max" method (present study)	Mean of instantaneous NCP during a 1-h period centered on the maximum instantaneous Negative NCP	Mean of instantaneous NCP for the entire Negative NCP period
Sensor data and "Most" method (Mostajir et al. 2013)	Mean of instantaneous NCP during a 1-h period following sunset	Mean of instantaneous NCP for the entire Negative NCP period, apart from the period considered in the Rdaytime calculation

Once the instantaneous Rdaytime and Rnight were calculated as described in Table 1, they were integrated to provide daily values. Two methods of integration were compared. Rdaytime was integrated either over the whole day (e.g., from sunrise to sunset, hereafter referred to as SS) or over the production period (e.g., when instantaneous NCP was positive, hereafter referred to as PP).

When Rdaytime was integrated from sunrise to sunset, Rnight was integrated over the whole night (e.g., from sunset to the following sunrise). When Rdaytime was integrated over the production period, Rnight was integrated over the Negative NCP period.

Therefore, Rdaytime and Rnight were calculated with the following equation:

$$R = (Mean\ of instantaneous\ NCP\ during\ the\ considered\ period) * 60 * integration\ period \quad \text{Eq. 7}$$

where R corresponds to either Rdaytime or Rnight ($gO_2\ m^{-3}\ d^{-1}$), the mean of instantaneous NCP is measured in $gO_2\ m^{-3}\ min^{-1}$, and the integration period either to the period from sunrise to sunset (hours) or to the production period (the Positive NCP period, in hours) for Rdaytime calculation, or to the period from sunset to the following sunrise (hours) or to the Negative NCP period (hours) for Rnight calculation. It should be noted that the units of Rdaytime (or Rnight) are indifferently $gO_2\ m^{-3}$ integration $period^{-1}$ or $gO_2\ m^{-3}\ d^{-1}$ because during a given 24h period, Rdaytime (or Rnight) only occurs during the period in which it is integrated, so its value per 24h is equal to its value per integration period.

Then, the daily R (R24h) was calculated as the sum of Rdaytime and Rnight. A summary of all the parameters compared in the present work and their designations is presented in Table 2. For the Winkler estimates, the instantaneous Winkler-R was integrated over the Positive NCP period (Rdaytime-Winkler-PP) or from sunrise to sunset (Rdaytime-Winkler-SS) to obtain the daytime R, and it was integrated over the Negative NCP period (Rnight-Winkler-PP) or from sunset to sunrise (Rnight-Winkler-SS) to obtain the night R.

Table 2. **Presentation of all daily integrated parameters** that are compared in the present study.

Parameter	Method	Integrated from sunrise to sunset (SS)	Integrated over the production period (PP)
Rdaytime	Max	Rdaytime-Max-SS	Rdaytime-Max-PP
	Most	Rdaytime-Most-SS	Rdaytime-Most-PP
	Winkler	Rdaytime-Winkler-SS	Rdaytime-Winkler-PP
Rnight	Max	Rnight-Max-SS	Rnight-Max-PP
	Most	Rnight-Most-SS	Rnight-Most-PP
	Winkler	Rnight-Winkler-SS	Rnight-Winkler-PP
R24h	Max	R24h-Max-SS	R24h-Max-PP
	Most	R24h-Most-SS	R24h-Most-PP
	Winkler	R24h-Winkler	R24h-Winkler

3 Assessment

3.1 Comparison of Rdaytime, Rnight and R24h estimations from the three different methods and two integration periods

For all mesocosms, the Rdaytime, Rnight and R24h estimates integrated from sunrise to sunset (SS) and over the PP are presented in Fig. 3. Regardless of their integration period, the Rdaytime estimates were significantly different depending on the method used for their estimation (ANOVA, $p < 10^{-4}$ for all mesocosms and for the two integration periods, Supp. Data Table 1). Rnight estimates were significantly different for 3 mesocosms out of 6 (Oct-2, Jun-1 and Jun-3) (ANOVA or Kruskal-Wallis test, $p < 0.05$, Supp. Data Table 1). Consequently, R24h estimates were significantly different for all mesocosms when they were integrated from sunrise to sunset and over the production period. The only exception was in the Oct-1 mesocosm when the estimates were integrated over the production period; these estimates were not significantly different.

Post hoc tests were performed to assess multiple comparisons between estimates and to determine which estimates were significantly different. For all mesocosms, and regardless of the integration period considered, Rdaytime-Max was significantly higher than Rdaytime-Most (between 75 and 198% higher, depending on the period of integration and on the mesocosm). For both integration periods, Rdaytime-Winkler was significantly higher than Rdaytime-Most for the October mesocosms (on average 150.2%) and significantly lower than Rdaytime-Max for the June mesocosms (on average -

61.6%). However, for Rnight, the Max, Most and Winkler methods gave similar estimates, with only one exception (Rnight-Max-PP was significantly different from Rnight-Winkler-PP for Oct-2). As a result of the differences in Rdaytime and Rnight, R24h-Max was generally significantly higher than R24h-Most. The only exceptions were for Jun-3 integrated over the production period and for Oct-2 and Oct-3 integrated from sunrise to sunset. In contrast, R24h-Winkler was systematically lower than R24h-Max and R24h-Most for all June mesocosms, whereas it was significantly higher than R24h-Most for the Oct-2 and Oct-3 mesocosms. Notably, R24h-Most-PP was on average 1.43, 1.47 and 1.58 times higher than R24h-Winkler for Jun-1, Jun-2 and Jun-3, respectively.

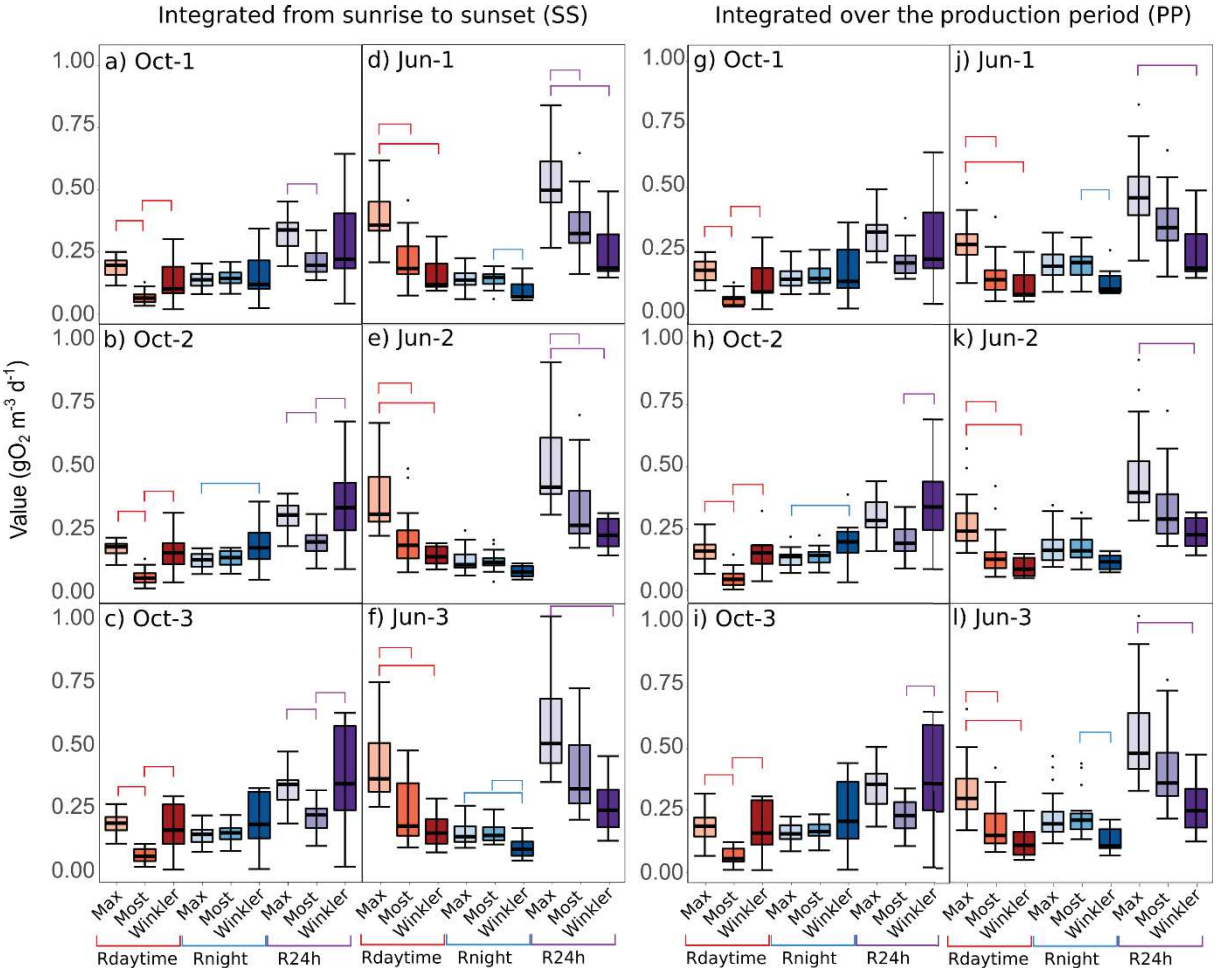

Figure 3. **Estimates of Rdaytime** (the 3 leftmost boxplots in orange), **Rnight** (the 3 boxplots in blue in the middle) **and R** (the 3 rightmost boxplots in purple) **obtained from sensor data using the Max and Most methods and from Winkler incubation data integrated from sunrise to sunset or over the production period** for Oct-1 (a, g), Oct-2 (b, h), Oct-3 (c, i), Jun-1 (d, j), Jun-2 (e, k) and Jun-3 (f, l). For each box, the lower quartile, median, and upper quartile values are displayed with horizontal lines. Whiskers show the range of the data, from the minimum to the maximum, excluding outliers. Brackets represent the comparisons between estimates that were found to be significantly different ($p<0.05$, Tukey HSD or Dunn test). Oct-1, Oct-2 and Oct-3 refer to the mesocosms n°1, n°2 and n°3 of the October 2018 experiment, and similarly Jun-1, Jun-2 and Jun-3 refer to the mesocosms n°1, n°2 and n°3 of the May and June 2019 experiment.

The comparisons reported earlier were performed for the entire experiments. In addition, day-by-day comparisons were also performed and are presented in the supplementary information (Supp. Data Table 2). Generally, the day-by-day comparisons had the same results as reported for the entire experiment. However, occasionally, the difference between Rdaytime-Max and Rdaytime-Most was not significant, as the periods considered for the Max and the Most methods were almost the same. An example is given in Fig. 4: on day 11 in Jun-1, Rdaytime-Max was only 48.9% higher than Rdaytime-Most (Fig 4.b), unlike on day 4 in Oct-1, when Rdaytime-Max was 100.6% higher than Rdaytime-Most (Fig 4.a). The greatest discrepancy between Rdaytime-Max and Rdaytime-Most was found on day 14 of Oct-2 (485.4%), while the smallest difference was on day 14 of Jun-2 (34.8%).

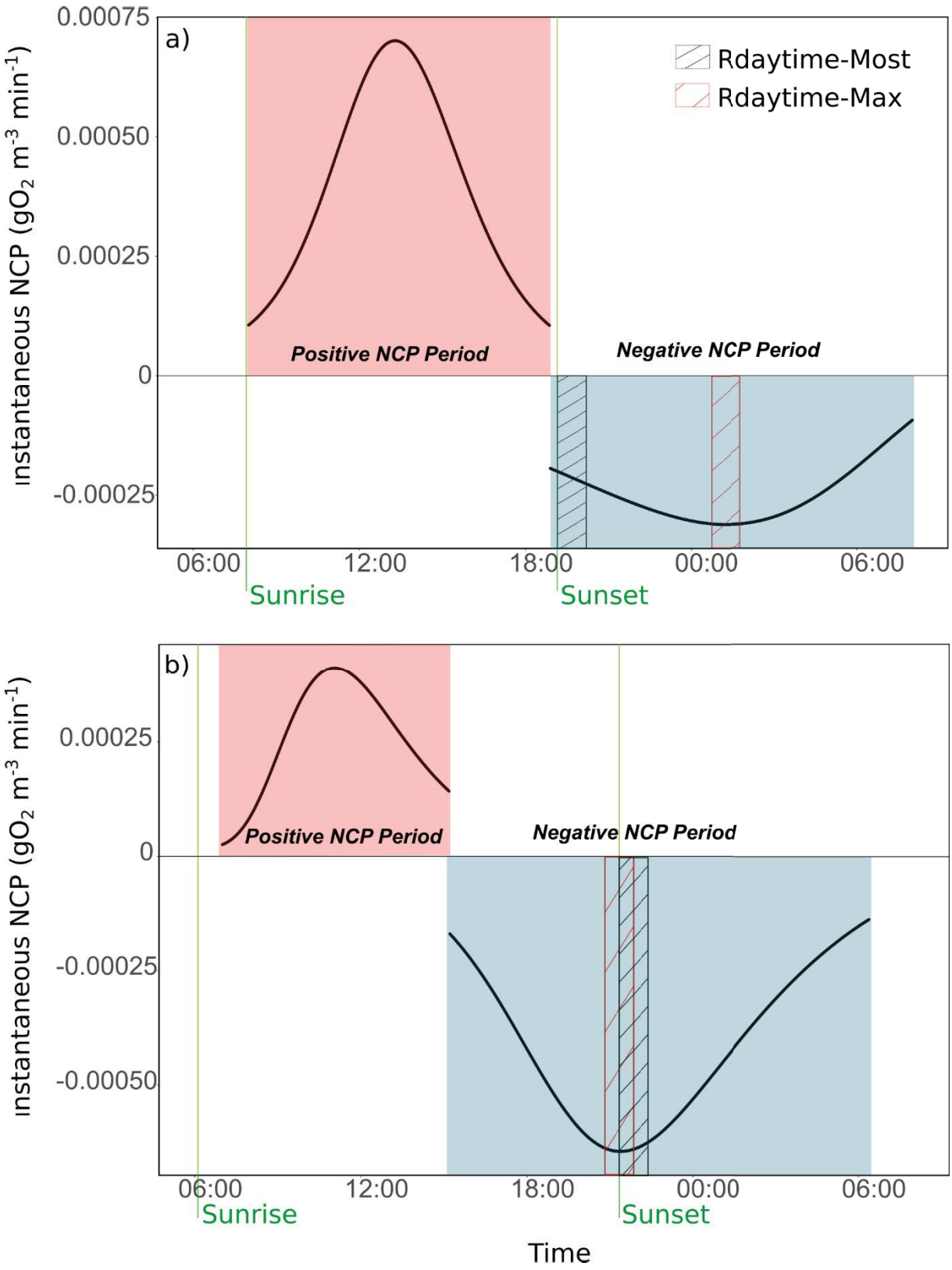

Figure 4. **Instantaneous NCP during the Positive and the Negative NCP periods on (a) Day 4 (2018-10-11) in Oct-1 and (b) Day 11 (2019-06-05) in Jun-1.** The sunrise and sunset times are shown as vertical green lines. The Positive NCP period is represented by a red rectangle, and the Negative NCP period is represented by a blue rectangle. The periods considered for the Rdaytime-Most and Rdaytime-Max calculations are shown as black and red striped rectangles, respectively. The gap

between the instantaneous NCP during the Positive NCP Period and during the Negative NCP Period is a consequence of modeling the DO curve separately for each Positive NCP Period and for each Negative NCP Period.

To assess whether the integration period significantly affected the results for Rdaytime, Rnight and R24h, comparisons were also performed between integration periods (e.g., from sunrise to sunset or over the production period) (Table 3). The ANOVA and Kruskal-Wallis test results showed nonsignificant differences in October, while the values of Rdaytime and Rnight were significantly different in June (Table 3). More precisely, Rdaytime-Max-SS was between 4% and 36% higher than Rdaytime-Max-PP. The observed differences were similar when the Most method was used.

Table 3. **Summary table of the p-values obtained for the one-way ANOVA comparisons between Rdaytime, Rnight and R24h obtained with the Max and Most methods integrated from sunrise to sunset or over the production period**. When the assumptions for a parametric test were not met, a Kruskal-Wallis test was used instead. p-values lower than 0.05 were considered significant and are presented in bold ($p < 0.05$ *, $p < 0.01$ **).

Estimate	Test	Oct-1	Oct-2	Oct-3	Jun-1	Jun-2	Jun-3
Rdaytime	Max-SS x Max-PP	0.43	0.51	0.76	**0.01***	**0.02***	**0.03***
	Most-SS x Most-PP	0.61	0.68	0.82	0.09	0.12	0.15
Rnight	Max-SS x Max-PP	0.53	0.64	0.70	**0.006****	**0.02***	**0.03***
	Most-SS x Most-PP	0.53	0.63	0.67	**0.001****	**0.009****	**0.008****
R24h	Max-SS x Max-PP	0.92	0.86	0.99	0.49	0.33	0.52
	Most-SS x Most-PP	0.81	0.87	0.78	0.92	0.88	0.71

3.2 A new method of estimating Rdaytime, Rnight, R24h, GPP and NCP using sensor data

Regardless of the integration period, Rdaytime-Max was significantly higher than Rdaytime-Most, as demonstrated above. As numerous studies have shown that light respiration is substantially higher than dark respiration (Markager et al. 1992; Tobias et al. 2007; Pringault et al. 2007), we suggest using the

new method presented in this investigation, called the "Max method", to estimate Rdaytime, Rnight and therefore R24h.

Moreover, as demonstrated above, major discrepancies were introduced into the respiration estimates for the Jun experiment by the integration period (SS vs PP). Thus, we also suggest integrating Rdaytime over the production period, as this method enables us to consider only the period in which production is higher than respiration and therefore is representative of the most productive period of the day. In the same way, we suggest that Rnight be integrated over the Negative NCP period (e.g., when the DO concentration is decreasing).

Hence, based on the sensor data, we suggest calculating Rdaytime, Rnight, R24h, GPP and NCP as presented in Equations 8, 9, 10, 11 and 12 respectively:

$$\boldsymbol{Rdaytime} = (mean\ instantaneous\ NCP\ during\ Max\ period) * 60 * duration\ of\ Production\ Period \quad \text{Eq. 8}$$

where Rdaytime is measured in $gO_2\ m^{-3}\ d^{-1}$, the Max period is a 1-h period centered on the maximum instantaneous Negative NCP, the mean instantaneous NCP is measured in $gO_2\ m^{-3}\ min^{-1}$, and the duration of the production period is the duration of the Positive NCP period in hours.

$$\boldsymbol{Rnight} = (mean\ instantaneous\ NCP\ during\ Night\ period) * 60 * duration\ of\ Night\ Period \quad \text{Eq. 9}$$

where Rnight is measured in $gO_2\ m^{-3}\ d^{-1}$, the Night period refers to the Negative NCP period, the mean instantaneous NCP is measured in $gO_2\ m^{-3}\ min^{-1}$, and the duration of the night period is the duration of the Negative NCP period in hours.

R24h is calculated as:

$$\boldsymbol{R24h} = Rdaytime + Rnight \quad \text{Eq. 10}$$

Hence, GPP is calculated as follows:

$$\boldsymbol{GPP} = mean\ of\ instantaneous\ NCP\ during\ the\ Positive\ NCP\ period * 60 * duration\ of\ Production\ Period + Rdaytime \quad \text{Eq. 11}$$

where GPP and Rdaytime are measured in $gO_2\ m^{-3}\ d^{-1}$, and the duration of the production period is the duration of the Positive NCP period in hours.

Finally, NCP is calculated as follows:

$$\boldsymbol{NCP} = \boldsymbol{GPP} - \boldsymbol{R24h} \quad \text{Eq. 12}$$

4 Discussion

4.1 A computation of daytime respiration that takes into account variations in the coupling of the day-night and O2 cycles

As discussed before, it has been shown that planktonic daytime respiration is significantly higher than night respiration. Therefore, in the present work, Rdaytime is proposed to be estimated with the maximum instantaneous respiration th at can be measured at night. With this method, an average Rdaytime ranging from 23 to 58% higher than Rnight was obtained; this range is consistent those in with previous studies calculated using other methods, as previously noted.

In the present study, the Rdaytime estimated with this new method, using the maximal respiration at night (i.e., the Max method) was compared with the method proposed by Mostajir et al. (2013) (i.e., the Most method). For all mesocosms and regardless of the integration period considered, the Rdaytime obtained with the Max method was generally significantly higher than the Rdaytime obtained with the Most method. This means that respiration directly after sunset had not reached its maximum value yet in most cases. However, on some long, warm days (in the present work, in June, when days were more than 15 h long), the DO cycle does not perfectly match the day-night cycle (e.g., the DO concentration starts to increase sometime after sunrise and/or starts to decrease some time before sunset, Fig. 4.b), resulting in Rdaytime-Most and Rdaytime-Max being equivalent. In these cases, the mismatch observed between the DO and the day-night cycles occurred because more DO was consumed through respiration than was produced through photosynthesis, even though the irradiance was still strong in the middle of the afternoon. This phenomenon can be explained by several factors, including a decrease in O_2 production from photosynthesis due to photoinhibition induced by the high irradiance level (Powles 1984) or an increase in bacterial and phytoplankton respiration due to warmer conditions (Jones 1977; Robinson 2008). These variations in the coupling of the day-night and O_2 cycles were not taken into account in previous methods of estimating Rdaytime, whereas the Max method proposed in this paper considers them.

As Rdaytime is used to calculate GPP estimates, they were significantly different when estimated with the Max and the Most methods, and are presented in Supp. Data Table 4. The Max method resulted in GPP estimates between 32.6 and 50.5% higher in average than those estimated with the Most method, depending on the mesocosm and the integration period considered. As Rdaytime is also used for the R24h calculation (the total daily respiration), the R24h estimates obtained with the Max method were, similarly to GPP, between 48.2 and 55.8% compared to those obtained with the Most method. As a consequence, daily NCP estimates, which represent the balance between GPP and R24h, were not significantly different using the Max or the Most methods. Therefore, even if one method is

underestimating both GPP and R24h comparing to the other, because it is to the same extent, the global oxygen balance is not significantly different.

4.2 Patterns in the nighttime data

Dark, or night, respiration by phytoplankton can be basically separated into three distinct phases (Markager and Sand-Jensen 1989; Markager et al. 1992; Mantikci et al. 2017). The first phase corresponds to the direct enhancement of respiration by photosynthesis and lasts for only a few minutes after the onset of darkness. This period is followed by a second phase in which respiration is still higher than basal maintenance respiration due to the intracellular substrate pool created during the previous light exposure (Mantikci et al. 2017, 2019) and lasts for several hours (from 2.5 to 3.6 hours (Falkowski et al. 1985; Sadro et al. 2011)). Moreover, the duration of this light-enhanced respiration period is season-dependent, with longer durations in the months with longer daylengths (Sadro et al. 2011). This phase is also dependent on the substrate pool available for phytoplankton and must be differentiated from the final phase, which represents basal maintenance respiration (Mantikci et al. 2017). However, in the present study, the durations of the second phase (e.g., between the start of the Negative NCP period, when respiration starts to be higher than O_2 production, and the point of maximum instantaneous respiration) in October and June were similar (Supp. Data Table 3). This phase includes a period in which production is still occurring but is lower than respiration (between the start of the Negative NCP period and sunset, see Fig 4.b.). The latter phase was several hours longer in June than in October because the DO concentration started to decrease well before sunset in June. Consequently, the period in which only respiration occurs (e.g., from sunset to the point of maximum respiration) was longer in October than in June, and its duration is in line with those measured in previous studies (Falkowski et al. 1985; Markager and Sand-Jensen 1989; Sadro et al. 2011).

Moreover, the respiration pattern observed in the present investigation encompasses also heterotrophic respiration, and not only phytoplanktonic one. Bacterial respiration depends on other types of substrates, and does not necessarily vary throughout day and night the same way phytoplanktonic respiration does. An increasing respiration rate during dark conditions was found for a planktonic population dominated by bacteria (for example, a planktonic community after a phytoplankton bloom). This increase in respiration during a dark period was proposed to be related to an increase in bacteria biomass and production. (Briand et al. 2004). Overall, the nighttime respiration pattern gives information about the dominant respiratory processes in the studied system (Mantikci et al. 2019). Indeed, the nighttime respiration pattern varies accordingly to the quality and the quantity of organic substrates available, as well as the distribution of the global respiration between heterotrophic and autotrophic organisms. In a

system with different characteristics than that of the present study, respiration patterns may be very different from the ones observed in the present investigation.

4.3 Comparison between sensor data and Winkler data

The values of Rdaytime, Rnight and R24h estimated by the Winkler method, which were normalized on the same period as those obtained with the Max and the Most methods, were sometimes significantly different from those obtained using sensor data. These discrepancies are in accordance with Mostajir et al. (2013), who obtained Winkler respiration rates that were 3 times lower than sensor respiration rates. These discrepancies may be due to several fundamental differences between the two methods. First, the Winkler method requires the confinement of the plankton community in small, closed bottles (several hundred milliliters). As a result, the metabolism estimated in the glass bottles might not be representative of the mesocosm (several m^3). Additionally, the plankton community must acclimate to its new confined environment, leading to potential differences between the metabolism of the community in the incubation glass bottles and that of the natural or mesocosm waters. This so-called "bottle effect" has long been noted as a potential bias in metabolism estimation using the Winkler technique (Bender et al. 1987). Moreover, to measure respiration, Winkler incubations are typically performed during the day or under light exposure, with bottles covered to prevent light and thus photosynthesis (Smith and Kemp 1995; Liess et al. 2016; Mesa et al. 2017). Therefore, Winkler respiration values are obtained from a community that is acclimated to natural light conditions and is suddenly put in the dark. Thus, the organisms must instantaneously change their metabolism without an acclimation period, which creates a source of bias in respiration measurements. In contrast, the sensors installed in the mesocosms allow us to measure the plankton community's metabolic parameters in a noninvasive way, directly in their quasi-natural environment, with natural light conditions during the day and at night.

4.4 Comparison of two integration periods for the sensor data

The discrepancies between the daily Rdaytime estimates integrated from sunrise to sunset and those integrated over the production period were greater when the daylength was longer (i.e., in June in the present study). This is because, even if the daylength varies, the production period is still comparable across seasons (Supp. Data Table 3). This characteristic of the production period may be explained by the fact that metabolic processes are controlled by various mechanisms, such as temperature variations, throughout the seasons and not only by the daylength and the amount of light received (Solomon et al.

2013; Alfonso et al. 2018; Lopez Sandoval et al. 2019). As a result, during long days, the actual production period is considerably shorter than the daylength, and hence Rdaytime integrated over the production period is in fact integrated over a significantly shorter period than that integrated from sunrise to sunset. Rnight estimates were also significantly different between the two integration periods but in the opposite way as Rdaytime estimates; the Rnight estimates integrated from sunset to the following sunrise are integrated over a shorter period than those integrated over the entire Negative NCP period. Consequently, R24h was not significantly affected by the integration period, as the differences induced in both Rdaytime and Rnight were equal to each other. Hence, when comparing Rdaytime estimates obtained in different seasons, the estimates should be integrated over comparable time periods, but the integration time period is less important in studies focusing only on R24h.

5 Comments & Recommendations

In situ mesocosm experiments are a useful approach in aquatic ecology because they allow the assessment and quantification of the responses of planktonic and microbial communities to various perturbations within a controlled environment under in situ conditions. The ability of these experiments to effectively mirror in situ conditions has been investigated often; although there are some discrepancies between the biotic and abiotic parameters of mesocosms and those of the ecosystem they are deployed in, mesocosms still represent one of the best experimental ways to address certain fundamental questions in aquatic ecology (Dzialowski et al. 2014). However, mesocosm experiments often require a meticulous, time-consuming and labor-intensive sampling effort to obtain enough data to be able to monitor several key parameters, such as oxygen concentrations. High-frequency automated sensors can be used to monitor these parameters in a more efficient and easier way, as they need only to be deployed at the beginning of the experiment and retrieved at the end. Data generated via these sensors can be used to obtain valuable insights into the responses of the system to the tested perturbation(s), notably by assessing the metabolism of the system. As mentioned before, this method has many advantages compared to classical methods; however, it also has a few limitations and uncertainties. One of the limitations is the dependence of the method on a reliable estimate of the air-water exchange coefficient. This is combined with the fact that physical phenomena and their contributions to DO variability may vary greatly depending on both the tested ecosystem and the mesocosm structure. These physical aspects should be the focus of future research. Nevertheless, the goal of mesocosm experiments is to compare control mesocosms with mesocosms in which one or more disturbance(s) were applied. In this context, an over- or underestimated piston velocity coefficient will not have a substantial impact on the measured responses of the treatment compared to control mesocosms as long as the same piston velocity coefficient is used for all mesocosms.

Another limitation of this method is that it relies on strong daily DO cycles in order to be applicable. Therefore, this method is fully applicable in locations with pronounced day-night cycles, and it might be challenging to apply in low-production systems, like turbid rivers and estuaries. However, this method becomes more challenging to apply at latitudes where the cycle is less marked and impossible to apply when DO does not have a daily cycle. This means that the method can be used to calculate instantaneous NCP during only certain months of the year in polar ecosystems, as it is not possible to estimate both GPP and R without DO cycles.

To conclude, in the present study, we presented a reliable method of estimating daytime respiration developed using automated sensors in in situ mesocosms. This method takes into account the variability of the coupling between day-night and O_2 cycles and therefore provides a better assessment of planktonic metabolic parameters than other methods. We also provide recommendations about various aspects of the technique, such as the SP to use and the physical air-water exchange of oxygen.

Mesocosm studies investigating the responses of aquatic communities to environmental stress should move toward the use of devices that are more autonomous and less costly in terms of time, work, and price than classical methods. The use of high-frequency sensors in mesocosms is one way to achieve this goal. By addressing certain methodological questions regarding the use of the free-water diel oxygen technique for in situ enclosed mesocosm experiments, this work improves our ability to assess high-frequency instantaneous metabolism and consequently the metabolic responses of communities to disturbance and establishes a common protocol for data analysis.

6 Author contributions

Behzad Mostajir and Francesca Vidussi conceived the study. Behzad Mostajir, Francesca Vidussi and Sébastien Mas designed and managed the mesocosm experiments. David Parin set up the sensor system and retrieved the sensor data. Tanguy Soulié and Sébastien Mas calibrated the sensors. Tanguy Soulié processed the sensor data, performed all the analyses, and wrote the original draft of the article, with the input of Behzad Mostajir, Francesca Vidussi and Sébastien Mas.

7 References

(Voir la section Bibliographie de la thèse)

8 Acknowledgments

We would like to thank Rémi Valdès, Solenn Soriano, Kevin Mestre and Camille Suarez-Bazille, the staff of the Sète Marine Station, for helping with setting up the mesocosms and with daily sampling. We also thank Thomas Trombetta, Emilie Eveque and Jean-François Thevenot for assistance with the daily sampling and with the oxygen sample analyses. Furthermore, we would like to thank Emilie le Floc'h for commenting the model construction and Justine Courboulès for providing the illustration of the mesocosm system. The research leading to these results and a part of the PhD scholarship awarded to TS were funded under the European Union Horizon 2020 Program (H2020/2017-2020), grant agreement n°731065-AQUACOSM: Network of Leading European AQUAtic MesoCOSM Facilities Connecting Mountains to Oceans from the Arctic to the Mediterranean. We would like to acknowledge Robert Ptacnik and Herwig Stibor for their helpful comments on the previous version of the manuscript, as well as other participants of the AQUACOSM European project for the constructive discussions during workshops and meetings.

Encadré – Chapitre 1

Effets de la température et de la salinité sur la valeur de coefficient d'échange avec l'atmosphère *k*

Comme vu précédemment dans le Chapitre 1, l'estimation de la valeur du coefficient d'échange avec l'atmosphère *k* est l'une des limitations les plus importantes à l'estimation des paramètres métaboliques de l'oxygène via l'utilisation de mesures HF dans le cadre d'expériences en mésocosmes. Une sur- ou une sous-estimation de *k* entraîne un biais dans les estimations de R et de PCN, mais pas de PPB qui ne semble pas affectée par la valeur de *k* (voir les données complémentaires de l'article faisant l'objet du Chapitre 1, Annexe III). La valeur de *k* dépend notamment de la température et de la salinité de l'eau. Ainsi, dans le cadre d'expériences en mésocosmes testant l'effet d'une augmentation de la température, l'échange avec l'atmosphère est accéléré dans les mésocosmes chauffés par rapport aux mésocosmes contrôles, l'augmentation de la température diminuant la solubilité des gaz dans l'eau. Afin d'estimer ce phénomène et son influence sur les paramètres métaboliques de l'oxygène, la valeur de *k* a été considérée variable en fonction de la température et de la salinité de l'eau, et les paramètres métaboliques calculés avec cette valeur variable ont été estimés pour les mésocosmes contrôles et chauffés de l'expérience d'Octobre 2018 (Chapitre 1 & Chapitre 3). Cette analyse ne fait pas partie du Chapitre 1 mais sera discutée en détails dans la Discussion Générale de la présente thèse. L'effet de la température et de la salinité a été implémenté dans la valeur du *k* de référence utilisé dans la méthode décrite auparavant dans le Chapitre 1 (k_{ref} = 0.000156 m min^{-1}, Soulié et al. 2021) en suivant la méthode décrite dans Holtgrieve et al. (2010). Premièrement, le nombre de Schmidt (Sc), un nombre sans dimensions caractérisant les écoulements de fluide dans lesquels interviennent viscosité et transfert de matière, pour l'oxygène (O_2) dans l'eau douce (FW) en fonction de la température (T) est calculé avec la formule suivante (Éq. 1) :

$$Sc_{O_2FW}(T) = -120.1 \times T + 3.7818 \times T^2 - 0.047608 \times T^3 + 1800.6 \quad \text{(Éq. 1)}$$

Puis, le coefficient m est calculé comme (Éq. 2) :

$$m = 3.286 \times 10^{-5} \times T + 2.474 \times 10^{-3} \quad \text{(Éq.2)}$$

Ensuite, ce coefficient est utilisé pour introduire la variabilité liée à la salinité (S) dans le nombre de Schmidt via l'équation suivante (Éq. 3) :

$$Sc_{O_2}(T,S) = Sc_{O_2FW} \times (1 + S \times m) \quad \text{(Éq. 3)}$$

Finalement, le k est calculé via l'équation suivante (Éq. 4) :

$$k(T,S) = k_{ref} \times \left(\frac{Sc_{O_2}(T,S)}{Sc_{O_2}(ref)}\right)^{-0.5} \quad \text{(Éq. 4)}$$

avec $Sc_{O2}(ref)$ le nombre de Schmidt pour les conditions d'obtention de k_{ref} (T = 16°C, S = 37.5), égal à 675,58.

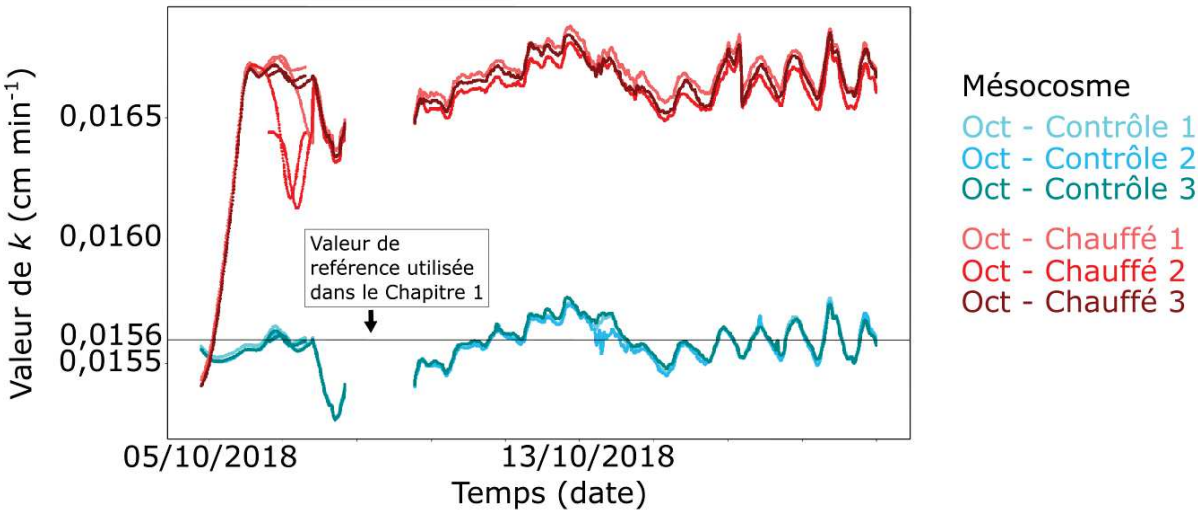

Figure E1.1. **Evolution temporelle de la valeur du coefficient d'échange avec l'atmosphère *k*** lorsqu'il est considéré variable en fonction de la température et de la salinité, pour les mésocosmes contrôles (nuances de bleu) et les mésocosmes chauffés (nuances de rouge) de l'expérience d'Octobre 2018 (dénommée Exp 1 dans le Chapitre 1). La ligne verticale représente la valeur de référence utilisée dans le Chapitre 1.

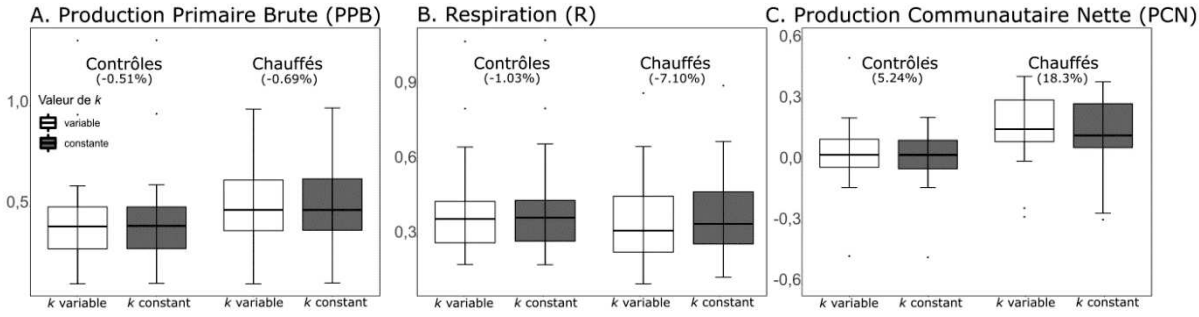

Figure E1.2. **Diagrammes en boîte représentant les valeurs de Production Primaire Brute (PPB, A.), la Respiration (R, B.) et la Production Communautaire Nette (PCN, C.)**, obtenues avec une valeur de coefficient d'échange avec l'atmosphère k variable en fonction de la température et de la salinité (en blanc) ou constante (en gris) et pour les mésocosmes contrôles (à gauche de chaque panneau) et les mésocosmes chauffés (à droite de chaque panneau) de l'expérience d'Octobre 2018 (dénommée Exp 1 dans le Chapitre 1). Les valeurs entre parenthèses correspondent à la différence entre la moyenne des valeurs obtenues avec un k variable et la moyenne des valeurs obtenues avec un k constant.

La valeur de *k* considérée variable est plus élevée d'en moyenne 6,23% dans les mésocosmes chauffés à +3°C que dans les mésocosmes contrôles (Fig E1.1), et d'en moyenne 4,61% par rapport à la valeur de référence. Dans les mésocosmes contrôles, la valeur de *k* considérée variable est plus faible d'en moyenne 0,23% par rapport à la valeur de référence.

Concernant la PPB, les estimations obtenues avec un *k* variable sont plus faibles d'en moyenne 0,51 et 0,69% que celles obtenues avec un *k* constant pour les mésocosmes contrôles et chauffés, respectivement (Fig E1.2A). Par contre, concernant la R, les différences sont plus importantes, avec des estimations obtenues avec un *k* variable plus faibles d'en moyenne 1,03 et 7,1% pour les mésocosmes contrôles et chauffés, respectivement (Fig E1.2B). En conséquence, les estimations de PCN sont plus fortes d'en moyenne 5,24 et 18,3% pour les mésocosmes contrôles et chauffés, respectivement, quand le *k* est considéré variable (Fig E1.2C).

Les résultats de cet encadré sont discutés dans la Discussion Générale de la thèse (p 174).

Chapitre 2

Effets du brunissement sur le métabolisme de l'oxygène et sur la composition d'une communauté planctonique d'une zone côtière septentrionale : une expérience de mésocosmes *in situ* combinée aux mesures à haute fréquence

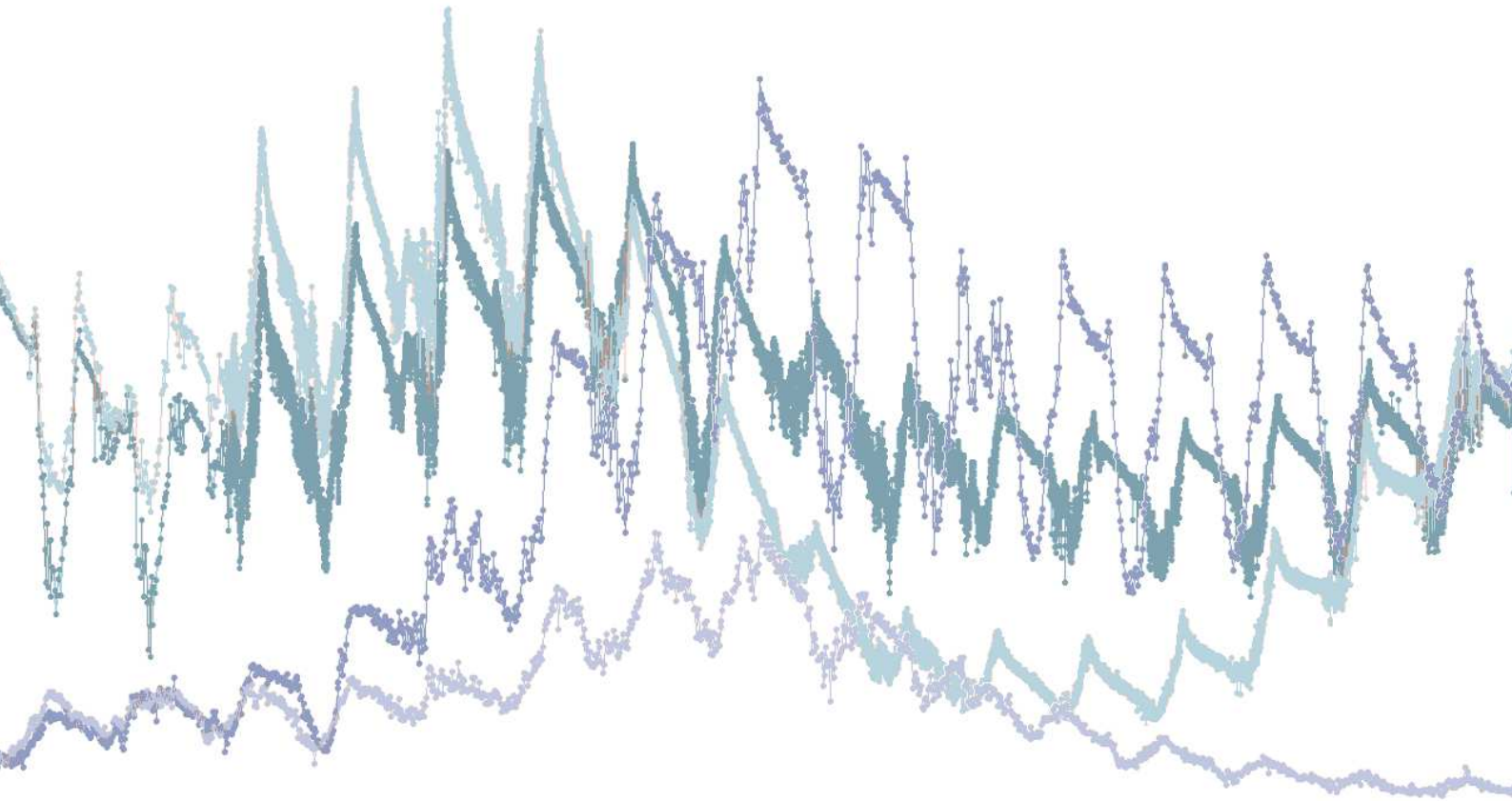

Avant-Propos

Depuis plusieurs décennies, les zones côtières des latitudes septentrionales sont sujettes à une augmentation des apports de carbone organique d'origine terrigène. Cet accroissement des apports est à l'origine d'un brunissement de la couleur de l'eau. L'augmentation des précipitations moyennes et des épisodes de précipitations extrêmes dans ces régions, liée au changement climatique global, et la modification de l'utilisation des sols, liée aux activités humaines, en sont les principales causes.

Dans ce contexte, l'objectif de ce chapitre est d'étudier les effets du brunissement sur le métabolisme et la composition d'une communauté planctonique d'une zone côtière septentrionale. Une expérience de mésocosmes *in situ* a été réalisée dans ce but pendant 14 jours au mois d'Août 2019 à Hopavågen, une baie située dans le comté du Trøndelag et connectée au fjord de Trondheim, au centre de la Norvège. Cette expérience a été effectuée dans le cadre du projet européen AQUACOSM (Network of Leading European AQUAtic MesoCOSM Facilities Connecting Mountains to Oceans from the Arctic to the Mediterranean) et en collaboration avec des équipes de recherche allemandes de l'Université Ludwig-Maximilians de Munich, du Leibniz-Institute of Freshwater Ecology and Inland Fisheries, et du GEOMAR Helmholtz-Zentrum für Ozeanforschung Kiel. Des expériences au protocole expérimental similaire ont été réalisées en Finlande et au Danemark durant le même été, et en Crète à l'été 2020, dans le cadre de ce projet européen. Afin de simuler le brunissement, une substance humique extrêmement colorée, HuminFeed®, a été ajouté dans 3 mésocosmes afin d'obtenir une concentration finale de 2 mg L^{-1}, tandis qu'un autre triplicat de mésocosmes, dans lesquels aucune substance a été ajoutée, a servi de contrôle. Dans chaque mésocosme, un jeu de capteurs, comme ceux présentés dans le chapitre précédent, a été immergé à 1 m de profondeur, afin de suivre certains paramètres clés, tels que la concentration et la saturation en O_2 dissout ou la quantité de radiation photosynthétique active (Photosynthetically Active Radiation, PAR). Ces données de capteurs ont servi à estimer le métabolisme planctonique de l'O_2, en appliquant pour la première fois la méthode présentée et établie dans le chapitre précédent. De surcroît, la composition pigmentaire de la communauté phytoplanctonique, la composition de la communauté zooplanctonique et la concentration en nutriments inorganiques dissouts ont été mesurées via un échantillonnage manuel des mésocosmes. À partir des données obtenues lors de l'expérience, il est également possible d'évaluer la stabilité fonctionnelle et compositionnelle des communautés planctoniques face au brunissement. Cette analyse est présentée dans un encadré associé au chapitre. Les valeurs de résistance, de résilience, de récupération et de stabilité temporelle seront comparées à celles obtenues pour une expérience ayant eu lieu dans la lagune de Thau dans la Discussion Générale de la thèse (p 189).

Lors de cette expérience, j'ai participé à la mise en place des mésocosmes et des jeux de capteurs et à l'échantillonnage journalier. De plus, j'ai réalisé des incubations afin de mesurer les paramètres métaboliques du plancton avec la technique de Winkler (données ne faisant pas partie du chapitre), j'ai analysé les échantillons pigmentaires de phytoplancton par chromatographie liquide à haute

performance (HPLC), et j'ai traité et analysé l'ensemble des données issues des capteurs. Les résultats de cette expérience sont présentés dans le chapitre sous la forme d'un article rédigé en anglais, « **Brownification reduces gross oxygen primary production and community respiration and changes phytoplankton community composition : an in situ mesocosm experiment combined with high-frequency sensor measurements of oxygen metabolism** », par Tanguy Soulié, Herwig Stibor, Sébastien Mas, Benjamin Braun, Johanna Knechtel, Jens C. Nejstgaard, Ulrich Sommer, Francesca Vidussi et Behzad Mostajir, actuellement en révision par la revue ***Limnology and Oceanography*** depuis le 15 juin 2021. De plus, ces résultats ont été présentés lors du Symposium AQUACOSM (2nd International Aquatic Mesocosm Research Symposium, 12-16 Avril 2021, en ligne), lors du congrès ASLO 2021 Aquatic Sciences (Aquatic Sciences for a Sustainable Future : Nurturing Cooperation, 22-27 Juin 2021, en ligne), et lors du colloque ILICO-EVOLECO (Évolution à long terme des écosystèmes côtiers) en novembre 2021 à La Rochelle.

Les mésocosmes déployés dans la baie d'Hopavågen en Norvège. Photo ©T. Soulié

Brownification reduces oxygen gross primary production and community respiration and changes the phytoplankton community composition: an in situ mesocosm experiment with high-frequency sensor measurements in a North Atlantic bay.

Tanguy Soulié[1*], Herwig Stibor[2], Sébastien Mas[3], Benjamin Braun[2], Johanna Knechtel[2], Jens C. Nejstgaard[4], Ulrich Sommer[5], Francesca Vidussi[1], Behzad Mostajir[1*]

[1]MARBEC (MARine Biodiversity, Exploitation and Conservation), Univ Montpellier, CNRS, Ifremer, IRD, Montpellier, France

[2]Department Biologie, Aquatic Ecology, Ludwig-Maximilians-Universität München, Martinsried-Planegg, Germany

[3]MEDIMEER (Mediterranean Platform for Marine Ecosystems Experimental Research), OSU OREME, CNRS, Univ Montpellier, IRD, IRSTEA, Sète, France

[4]Dep. 3, Experimental Limnology, Leibniz-Institute of Freshwater Ecology and Inland Fisheries (IGB), Zur alten Fischerhuette 2, Stechlin, Germany

[5]GEOMAR Helmholtz-Zentrum für Ozeanforschung Kiel, Wischofstraße 1-3, Kiel, Germany

*corresponding authors: Tanguy Soulié: tanguy.soulie@gmail.com, Orcid ID: 0000-0002-6761-9196; Behzad Mostajir: behzad.monstajir@umontpellier.fr, Orcid ID: 0000-0003-4911-794X

Running head: O_2 metabolism under brownification

Keywords: brownification, gross primary production, respiration, phytoplankton community composition, HPLC, phytoplankton pigments, in situ mesocosm, high-frequency sensor, LAMP sensor system

Abstract

In recent decades, the increase in terrestrial inputs to freshwater and coastal ecosystems, especially occurring at northern latitudes, has led to a process of water color darkening known as 'brownification'. To assess how brownification affects plankton community composition and functioning in northern coastal areas, an in situ mesocosm experiment using a highly colored humic substance to simulate a brownification event was performed in a North Atlantic bay (Hopavågen, Norway) in August 2019. Manual sampling for analyses of nutrient concentrations, phytoplankton pigments and zooplankton abundances was combined with high-frequency (every 15 min) monitoring of key environmental variables to investigate the response of the plankton community in terms of oxygen metabolism and community composition. In response to brownification, the oxygen gross primary production (GPP) and community respiration (R) slowed down significantly, by almost one-third. However, GPP and R both decreased to the same extent; thus, the oxygen metabolic balance was not affected. Moreover, the chlorophyll-*a* concentration significantly decreased under brownification, by 9% on average, and the chemotaxonomic pigment composition of the phytoplankton changed, indicating their acclimation to the reduced light availability. In addition, brownification seemed to favor appendicularians, the dominant mesozooplankton group in the mesocosms, which potentially contributed to lowering the phytoplankton biomass. In conclusion, the results of this in situ mesocosm experiment suggest that brownification could induce significant changes in phytoplankton and zooplankton community composition and significantly alter the overall oxygen metabolism of plankton communities in a northern Atlantic bay.

1 Introduction

Both freshwater and marine ecosystems are naturally subject to terrestrial inputs bringing humic organic substances and inorganic nutrients during natural rainfall events (Roulet and Moore 2006; Monteith et al. 2007). However, an increase in terrestrial inputs has been observed in freshwater and coastal ecosystems in recent decades (Roulet and Moore 2006; SanClements et al. 2012). This increase is related to changes in land cover and uses (Correll et al. 2001; Clutterbuck and Yallop 2010) and to the intensification and higher frequency of extreme rainfall events due to global climate change (Førland and Hanssen-Bauer 2000; Arhonditsis et al. 2002; Hyvärinen 2003; Hongve et al. 2004; Larsen et al. 2011; Westra et al. 2013; de Wit et al. 2016). The increase in inputs has led to the darkening of the water color, also known as water 'brownification'. Brownification is observed most often in northern latitudes (Haaland et al. 2010; Sepp et al. 2018), notably in Scandinavian countries (Solomon et al. 2015), and is predicted to become more common in the upcoming centuries (Larsen et al. 2011; de Wit et al. 2016). Brownification, by increasing humic organic substance concentrations in the water column, alters not only the light conditions but also the availability of organic and inorganic matter (Karlsson et al. 2009; Kritzberg et al. 2020). These changes may affect planktonic communities (Ejankowski and Lenard 2015; Williamson et al. 2015) and therefore the functioning of aquatic ecosystems. For instance, several studies have reported changes in plankton community composition and primary production and therefore in the overall ecosystem functioning of lakes due to brownification (Seekell et al. 2015; Williamson et al. 2015; Lenard and Ejankowski 2017).

Despite the growing interest in studying the effects of humic substance inputs on aquatic ecosystems, because brownification affects mainly freshwater systems, only a few studies have focused on such effects in coastal marine ecosystems (Grytaas 2020; Mustaffa et al. 2020; Paczkowska et al. 2020). Thus, knowledge about the effect of humic substances on marine plankton communities is particularly lacking, though coastal waters are highly exposed to human activities and changes in freshwater runoff and are therefore particularly sensitive to brownification (Mustaffa et al. 2020). This is the case for Norwegian coastal waters, which have already darkened over the past decades (Aksnes et al. 2009). Moreover, shallow coastal areas of Northern latitude greatly contribute to ecosystem services such as fisheries and aquaculture (Albretsen et al. 2012). It is therefore of great importance to assess how brownification affects coastal waters and their ecosystem functioning.

HuminFeed® (HuminTech, Germany), a well-characterized, Leonardite-derived, highly colored humic substance (Meinelt et al. 2007), has typically been used under laboratory and in situ conditions to experimentally test the effects of brownification on planktonic metabolism and community composition, especially in lakes and rivers in the Northern Hemisphere (Ratcovich 2014; Rasconi et al. 2015; Urrutia-Cordero et al. 2016; Urrutia-Cordero et al. 2017; Lebret et al. 2018; Birk et al. 2020).

After the addition of HuminFeed® to lakes, some studies reported no changes in planktonic metabolism or phytoplankton biomass (Ratcovich 2014; Rasconi et al. 2015; Lebret et al. 2018). Other studies, however, noted changes in the phytoplankton community composition; the addition of HuminFeed® favored low-light-adapted phytoplankton species (Lebret et al. 2018) and toxic cyanobacteria when combined with warming (Urrutia-Cordero et al. 2016). These modifications in the phytoplankton community composition could also lead to reductions in diversity (Urrutia-Cordero et al. 2017).

One of the key parameters used to study the functioning of plankton communities is the oxygen metabolic balance, which provides insights into the metabolic status of an aquatic ecosystem (Robinson and Williams 1999). The metabolic balance can be measured by assessing the balance between the oxygen produced by autotrophs via photosynthesis (gross primary production (GPP)) and the oxygen consumed through the entire community (aerobic respiration (R)). Therefore, net community oxygen production (NCP), which corresponds to the difference between GPP and R, is of great importance in understanding and managing aquatic ecosystems (Staehr et al. 2012).

On the one hand, inputs of humic substances to aquatic systems, by reducing the amount of light available for photosynthesis and by changing the light spectrum (Meinelt et al. 2007, Lenard and Ejankowski 2017), can potentially directly or indirectly alter GPP by affecting the phytoplankton biomass and/or community composition. On the other hand, these inputs, by increasing the dissolved organic carbon (DOC) concentration, could potentially enhance the activity and thus the respiration of heterotrophic bacteria. Finally, the addition of humic substances to aquatic systems could potentially affect their metabolic oxygen balance by favoring heterotrophic bacterial respiration while reducing phytoplankton oxygen production, leading to an imbalance between heterotrophic and autotrophic processes.

To study the effects of the addition of HuminFeed® on the functioning of the marine plankton community of a North Atlantic bay (Hopavågen, Norway), six in situ mesocosms were established and sampled according to two sampling procedures during the 15 days of the experiment. The first sampling procedure involved low-frequency sampling in order to measure nutrient concentrations, zooplankton abundances and phytoplanktonic pigment biomarkers (Vidussi et al. 2000) to evaluate the changes in nutrient concentrations, zooplankton community composition, and especially the phytoplanktonic community composition and acclimation to potentially altered light conditions. The second sampling procedure involved high-frequency sampling (one measurement every 15 min) to measure the dissolved oxygen (DO) concentration, chlorophyll-a fluorescence, water temperature, salinity, and photosynthetically active radiation (PAR). This procedure was carried out by deploying a set of automated sensors in every in situ mesocosm. High-frequency DO concentration measurements were then used to estimate GPP, NCP and R following a new method that considers the variability in the

coupling between day-night and DO cycles (Soulié et al. 2021) in order to evaluate the metabolic oxygen balance of this marine system following the addition of humic substances.

2 Material and Methods

2.1 Study site and *in situ* mesocosm setup

An in situ mesocosm experiment was performed in August 2019 in Hopavågen, a landlocked coastal bay in Norway (63°36'N, 9°33'E). This embayment has a mean depth of 18 m and a maximum depth of 31 m, and it is subject to limited human activity, with discharges of sewage and nutrients only from a nearby farm (van Marion 1996). It exchanges approximately 14% of its water with the adjacent Trondheim fjord every day, and the variations in its water temperature and salinity follow those of the surface layer of the Trondheim fjord, making it a good outdoor laboratory for hydrographic and biological studies of the coastal waters of central Norway (van Marion 1996).

Six in situ mesocosm enclosures were deployed in Hopavågen Bay for 15 days. The enclosures were cylinders made from 200 µm low density polyethylene (LDPE) at Ludwig-Maximilians-Universität Munich and measured 3.6 m in length and 1m in diameter, resulting in a 3 m long water column when the enclosures were suspended in water. The mesocosms were moored on a raft located at the center of the bay and were filled on the evening of August 5th by lifting the enclosures from ca. 7 m deep to the surface. Three mesocosms were used as controls. HuminFeed® (HuminTech, Germany) was added to the other three mesocosms (hereafter referred to as +HF mesocosms). The HuminFeed® was diluted in distilled water before being added to the mesocosms on August 6th (hereafter called d 0) to reach a concentration of 2 mg L-1 (corresponding to the addition of 0.8 mg L-1 of DOC (Meinelt et al. 2007)). HuminFeed® is a well-characterized substance derived from Leonardite that has been used in several studies to study the impact of increased water coloration on aquatic systems (Meinelt et al. 2007; Rasconi et al. 2015; Lebret et al. 2018).

2.2 Sensor setup in the in situ mesocosms and high-frequency data acquisition

Each mesocosm was equipped with a set of automated sensors immersed at 1 m depth. The sensors measured biotic and abiotic parameters at high frequency (one measurement every 15 min) during all 15 days of the experiment. The automated sensors that provided the data used in the present investigation were i) an oxygen optode (Model 3835, Aanderaa) to measure the DO concentration and oxygen saturation, ii) an electromagnetic induction conductivity sensor (Model 4319, Aanderaa) to measure the conductivity (and therefore the salinity) and water temperature, and iii) a spherical underwater quantum sensor (Li-193, Li-Cor) to measure the incident PAR.

To ensure the accuracy of the sensor data and to avoid any potential drift, every sensor was calibrated before and after deployment. The oxygen optodes were calibrated using three different saturation points (0, 50 and 100%) and at two different temperatures (10 and 18°C). The 100% saturation level was reached by bubbling air into a 1 L beaker filled with distilled water, while 0 and 50% saturation were reached by adding potassium metabisulfite. The DO data were also corrected for salinity and temperature, as explained in Bittig et al. (2018). The conductivity sensors were calibrated to three levels of salinity (0, 20 and 35 mg L-1) using sodium chloride in distilled water at two temperatures (10 and 18°C).

2.3 Nutrient sampling and analyses

Water samples were taken for ammonium (NH4+), phosphate (PO43-), nitrate (NO3- + NO2-) and silicate (SiO44-) analyses at d 0, d 8 and d 14. For this purpose, depth-integrated water samples were taken with a 2 m tube sampler (KC Denmark). Then, they were filtered through a combusted, acid-washed filter (Whatman GF/F, 25 mm diameter) before being frozen (-28°C) until further analyses. The dissolved inorganic nutrients were analyzed according to Grasshoff et al. (1999).

2.4 Zooplankton sampling and analyses

Zooplankton samples were taken at the beginning (d 0) and the end of the experiment (d 14) using a 250 µm mesh size net (Hydrobios, 25 cm diameter). On d 0, in situ water (707 L) was sampled directly from the bay, just before filling the mesocosms and by lifting the zooplankton net on the same water column as used for filling the mesocosms, from ca. 7 m deep to the surface. At the end of the experiment, after gently mixing each mesocosm to ensure a homogenous distribution of zooplankton organisms, each mesocosm was sampled (442 L) for zooplankton analyses using the net immersed at the middle of the enclosure's water column. Directly after sampling, the samples were fixed with ethanol (50% final concentration) and counted within the next few days. Zooplankton organisms were identified at the genus level and counted using a dissecting microscope (Leica MZ8 binocular, Leica Microsystems, Wetzlar, Germany).

2.5 Phytoplankton pigment and community composition sampling and analyses

Samples for phytoplankton pigments were taken daily in every mesocosm at 1 m deep using a 5 L Niskin water sampler. The algae in each sample (800 to 1200 mL) were collected on a glass-fiber filter (Whatman GF/F 25 mm, nominal pore size 0.7 µm) using a low-vacuum pump and under low-light conditions. The filters were then stored at -80°C until analyses. The pigments were extracted in 2 mL of 95% methanol for 1 h at -20°C. Then, after a sonication step, the pigments were extracted for an additional hour at -4°C. The extracts were then clarified on glass-fiber filters (Whatman GF/F) and

analyzed by high-performance liquid chromatography (HPLC, Waters) directly after extraction following the method of Zapata et al. (2000) and the protocol detailed in Vidussi et al. (2011).

Phytoplankton pigment concentrations were used as taxonomic and acclimation biomarkers (Vidussi et al. 2000; Deininger et al. 2016). Though accessory pigments are not always restricted to one taxonomic group, they are generally the major accessory pigments of a specific group and secondary or less ubiquitous pigments of a second or several groups; thus, they can be used to characterize the group in which the pigment is dominant. More specifically, in the present study, fucoxanthin and chlorophyll-*c2* (Chl-*c2*) were associated with Bacillariophyceae (diatoms); chlorophyll-*b* (Chl-*b*) was associated with Chlorophyceae and Euglenophyceae; zeaxanthin was associated with Cyanophyceae (cyanobacteria); and 19'-hexanoyloxyfucoxanthin (19'-HF) was associated with dinoflagellates, mainly Type II and Prymnesiophyceae. It should be noted that Prymnsiophytes were probably present in our experiment but were not identified by inverted microscopy due to their small size. Finally, chlorophyll-*c3* (Chl-*c3*) was assigned mainly to Bacillariophyceae (Roy et al. 2011). Peridinin, which is the major pigment of peridinial dinoflagellates, was not detected during this study, suggesting that peridinial dinoflagellates were absent or present at very low abundances and preventing the identification of peridinial dinoflagellates using their specific pigment biomarker. Furthermore, other accessory pigments are indicators of the photoacclimation process; thus, the beta-beta-carotene (ββc):Chl-*a* and diadinoxanthin:Chl-*a* ratios were used to indicate the acclimation of the phytoplankton community to high-light and low-light conditions, respectively (Deininger et al. 2016).

Furthermore, phytoplankton community composition was assessed five times during the experiment (d 0, d 5, d 9, d 11 and d 14). To do so, samples were taken using a 2 m tube sampler (KC Denmark). Samples were stored in 250 mL brown glass bottles, preserved in 1% lugol and counted via light inverted microscopy (Leica DMIL) using Utermöhl settling chambers (Utermöhl 1958). Identified species were regrouped into five taxa: Bacillariophyceae (*Pseudonitzschia* sp., *Nitzschia longissima*, *Thalassionema* sp., *Dactyliosolen* sp., *Corataulina* sp., *Skeletonema* sp., *Phaeodactylum* sp.), Prasinophyceae (*Pyramimonas* sp.), Euglenophyceae (*Eutreptiella* sp.), Cryptophyceae (*Teleaulax* sp., *Plagioselmis* sp.) and dinoflagellates (*Ceratium tripos*, *C. fusus*, *C. lineatum*, *Scrippsiella* sp., *Heterocapsa triquetra*, *Dinophysis* sp., *Prorocentrum micans*). Cell volume was calculated for 30 to 50 individuals and cell abundances were converted into carbon biomass by using specific volumetric conversion factors following Sommer et al. (2017).

2.6 Daily light integral calculation using high-frequency PAR measurements

High-frequency PAR data measured at 1 m deep were used to calculate the daily light integral (DLI), which corresponds to the quantity of photosynthetically active photons that are received by a one square

meter surface over a 24 h period (Faust and Logan 2018). The DLI (mol m^{-2} d^{-1}) was calculated using the mean PAR (µmol m^{-2} s^{-1}) between sunrise and sunset as follows:

$$DLI = \frac{Mean\ PAR * day\ length * 3600}{1 * 10^6} \quad \text{Eq. 1}$$

2.7 GPP, R and NCP estimations using high-frequency DO data

High-frequency DO data were used to estimate the daily GPP, R during the day (Rdaytime), R at night (Rnight), daily R and NCP, following a new method developed and described in Soulié et al. (2021); this method was applied for the first time in the present study. The method is derived from the free-water diel oxygen method first described by Odum and Odum (1955), and it takes into account variations in the coupling between the day-night and DO cycles. The method involves several steps. First, the calibrated and corrected DO data were smoothed using a 9-point moving average and a 5-parameter sigmoid model (Soulié et al., 2021). Then, community metabolism was estimated based on the fundamental equation (Odum and Odum 1955; Odum 1956) as follows:

$$\frac{\Delta O_2}{\Delta t} = GPP - R - F - A \quad \text{Eq. 2}$$

where $\frac{\Delta O_2}{\Delta t}$ is the instantaneous change in DO, F is the physical exchange of oxygen between the water surface and the atmosphere, and A is a term including all other phenomena (chemical and physical phenomena) that affect DO in the considered system. These other phenomena include nonaerobic DO consumption and horizontal and vertical advection; A is considered negligible in the present study and most other studies (Staehr et al. 2010 ; Mostajir et al. 2013).

The atmosphere-water exchange term F can be calculated as follows:

$$F = (k * (O_2 - O_{2_{Sat}}))/Z_{mix} \quad \text{Eq. 3}$$

where O_2 is the DO, O_{2sat} is the oxygen saturation, *k* is an air-water constant coefficient and Z_{mix} is the mixing depth of the mesocosm enclosures. In the present work, we used a value of *k* equal to 0.000387 m min^{-1}, which corresponds to a high value measured as a function of turbulence in mesocosms (Alcaraz et al. 2001) and as proposed in Soulié et al. (2021).

Then, the instantaneous NCP can be calculated as follows:

$$NCP = \Delta O_2 - F \quad \text{Eq. 4}$$

For each DO cycle, the DO and instantaneous NCP data were separated into two periods: one period in which the DO concentration increases (i.e., the NCP was positive), called ‘positive NCP periods’, and one period in which the DO concentration decreases (i.e., the NCP was negative), called ‘negative NCP

periods'. Then, the positive and negative NCP periods were used to calculate the daily GPP, Rdaytime, Rnight, daily R and daily NCP.

First, Rdaytime, corresponding to the respiration rate occurring during the day, can be calculated as:

$$Rdaytime = (mean\ of\ instantaneous\ NCP\ during\ Max) * 60 * duration\ of\ positive\ NCP\ period \quad \text{Eq. 5}$$

where Rdaytime is expressed in $gO_2\ m^{-3}\ d^{-1}$, Max refers to a 1 h period centered on the maximum instantaneous NCP during the negative NCP period, the mean instantaneous NCP is expressed in $gO_2\ m^{-3}\ min^{-1}$, and the duration of the positive NCP period is expressed in hours.

Rnight, corresponding to the respiration rate occurring at night, can be calculated as:

$$Rnight = (mean\ of\ instantaneous\ NCP\ during\ the\ Negative\ NCP\ period) * 60 * duration\ of\ Negative\ NCP\ Period \quad \text{Eq. 6}$$

where Rnight is expressed in $gO_2\ m^{-3}\ d^{-1}$, the mean instantaneous NCP is expressed in $gO_2\ m^{-3}\ min^{-1}$, and the duration of the negative NCP period is expressed in hours.

The daily R (R24h) can simply be calculated as:

$$R24h = Rdaytime + Rnight \quad \text{Eq. 7}$$

The daily GPP (in $gO_2\ m^{-3}\ d^{-1}$) can then be calculated with the following equation:

$$Daily\ GPP = mean\ of\ instantaneous\ NCP\ during\ the\ positive\ NCP\ period * 60 * duration\ of\ positive\ NCP\ Period + Rdaytime \quad \text{Eq. 8}$$

At a result, the daily NCP (in $gO_2\ m^{-3}\ d^{-1}$) can be calculated as:

$$Daily\ NCP = Daily\ GPP - R24h \quad \text{Eq. 9}$$

This method is based entirely on the fact that the DO concentration displayed sufficiently noticeable daily cycles. In the present study, it was possible to estimate these daily metabolic parameters for d 1 to d 12. The data from d 0, d 13 and d 14 could not be used to reliably estimate the metabolic parameters.

2.8 Statistical analyses

We used repeated measures analysis of variance (RM-ANOVA) with treatment as fixed factor and time as random factor (linear mixed-effects models, lme(Response~Treatment, random = ~1|Time), *nlme* package, R software) to test the effects of HuminFeed® addition during the entire experiment on physical parameters (water temperature, salinity, DLI, nutrient concentrations), metabolic parameters (GPP, R), the Chl-*a* concentration, and pigment concentrations and ratios. The significance level was set at 0.05. When the assumptions of the RM-ANOVA could not be met even after transforming the

data (logarithmic, square-root or exponential transformations), a nonparametric Kruskal-Wallis test was performed instead. For the abundance of each zooplankton genus obtained on the last day of the experiment, an unpaired *t*-test comparing the mean abundance in the control and in the +HF treatment was performed. To assess the environmental drivers and pigment contributors of the metabolic response to HuminFeed® addition, ordinary least squares linear relationships were assessed between log response ratios (LRR) of metabolic parameters, environmental variables and pigment concentrations. Moreover, Spearman's correlations were performed between dissolved nutrient and Chl-*a* concentrations. All statistical analyses were performed using R software (R-Project, version 4.0.1).

3 Results

3.1 Effects of brownification on the physical and chemical parameters

Overall, the water temperature decreased during the experimental period, ranging from 14.3 ± 0.1°C on d 0 to 13.1 ± 0.1°C on d 14 in the control (Fig. 1a). The water temperature was similar between the +HF treatment and the control (RM-ANOVA, p=0.67, $F_{1,14}$=0.19). The salinity ranged from 31.09 ± 0.02 (d 13) to 31.19 ± 0.02 (d 6) in the +HF treatment and from 31.10 ± 0.02 (d 12) to 31.17 ± 0.01 (d 6) in the control (Fig. 1b), with a significant but very small treatment effect (RM-ANOVA, p = 0.02, $F_{1,14}$ = 7). Similarly to water temperature, the DO concentration decreased during the experimental period, and ranged from 291.1 ± 0.1 µmol O_2 L^{-1} to 251.4 ± 1.4 µmol O_2 L^{-1} in the control (Fig. 1c). When considering the entire period, it was not significantly different between treatments (Kruskal-Wallis, p = 0.96).

In the control, the DLI was generally above 10 mol m^{-2} d^{-1}, with the highest value on d 0 (17.87 ± 1.43 mol m^{-2} d^{-1}), and the lowest values on d 2 (3.52 ± 0.83 mol m^{-2} d^{-1}) and d 6 (2.68 ± 0.46 mol m^{-2} d^{-1}). As expected, the DLI was significantly lower in the +HF treatment than in the control (RM-ANOVA, $p = 2.4 \times 10^{-3}$, $F_{1,14}$ = 13.69), by an average of 23%. The difference in DLI between the +HF treatment and the control varied from 6% (d 8) to 48% (d 11) (Fig. 1d) over the course of the experiment.

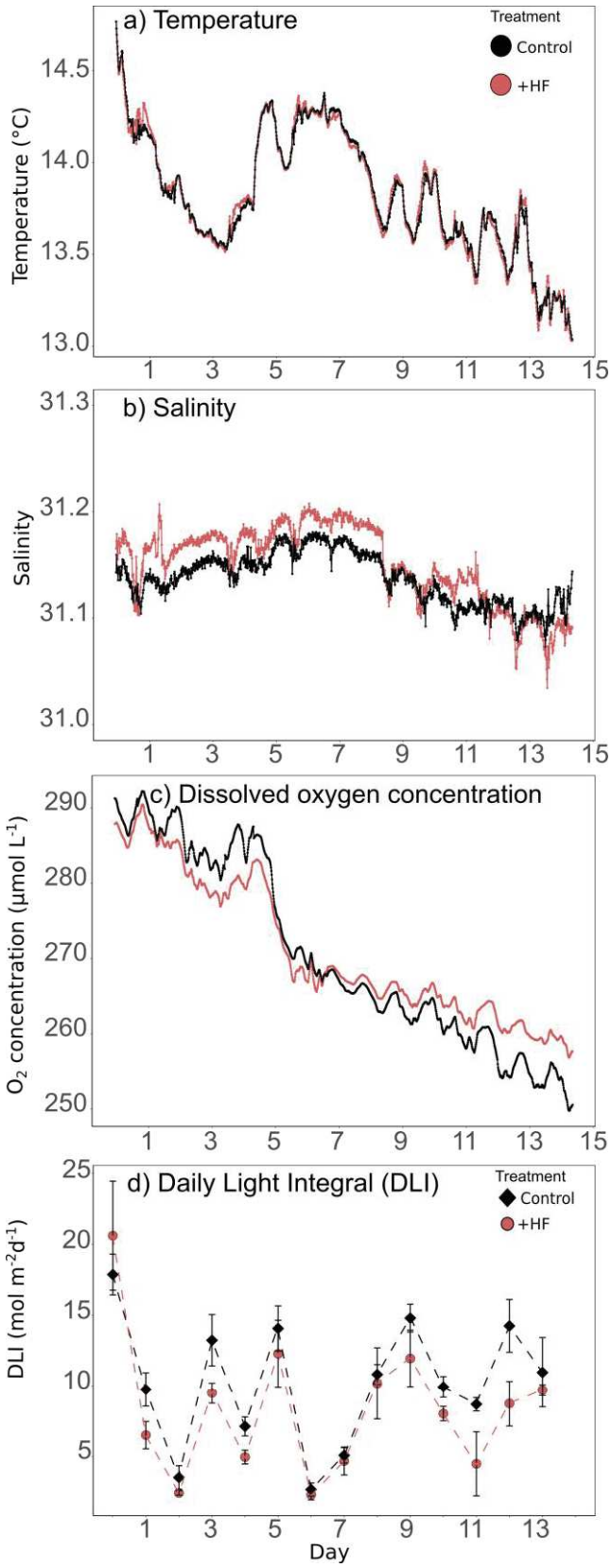

Figure 1. Parameters based on high-frequency measurements in the control (black) and in the +HF (red) treatment over the course of the experiment. A) Water temperature, b) salinity, c) dissolved oxygen concentration, and d) mean daily light integral (DLI) with standard deviation (error bars).

Overall, the nutrient concentrations were low in both the control and the +HF treatment (Table 1). Moreover, the ammonium (NH_4^+), phosphate (PO_4^{3-}), nitrate (NO_3^- + NO_2^-) and silicate (SiO_4^{4-}) concentrations were not significantly different between the +HF and control treatments (Table 1). The ammonium concentration increased over the course of the experiment, reaching 5.1 ± 2.4 µg L^{-1} in the control and 4.3 ± 2.5 µg L^{-1} in the +HF treatment on d 14. Similarly, the nitrate concentration increased during the experiment, reaching 3.6 ± 0.1 µg L^{-1} in the control and 4.2 ± 0.3 µg L^{-1} in the +HF treatment on d 14. Additionally, the phosphate concentration peaked on d 8 in both treatments, reaching 1.2 ± 0.4 µg L^{-1} in the control and 1.5 ± 0.4 µg L^{-1} in +HF. In contrast, the silicate concentration decreased during the entire experiment, from 6.0 (d 0) to 1.7 ± 0.6 µg L^{-1} (d 14) in the control and from 6.0 (d 0) to 1.3 ± 0.6 µg L^{-1} (d 14) in the +HF treatment.

Significant correlations were found in the control and the +HF treatments between ammonium and silicate concentrations (Spearman, ρ = -0.94 and ρ = -0.89), between nitrate and silicate (Spearman, ρ = -0.68 and ρ = -0.78) and between ammonium and nitrate only in the +HF treatment (Spearman, ρ = -0.68).

Table 1. **Mean dissolved inorganic nutrient concentrations expressed in µg L^{-1} (± standard deviations) in the control and in the +HF treatment** at d 0, d 8 and d 14 and repeated measures analyses of variance (RM-ANOVA) *p*-values for the effect of the treatment on nutrient concentrations. The values in brackets are the F-values, when applicable. When homoscedasticity and normality assumptions could not be met even after transforming the data, a nonparametric Kruskal-Wallis (KW) test was used instead (as indicated in the table). On d 0, samples were taken directly from Hopavågen bay. A value of 0 indicates that the concentration was below the detection limit. The * symbol indicates that samples were not taken in triplicates, thus no standard deviation could be calculated for d 0.

		Control	+HF	*p*-value
NH_4^+	d 0	0*	0*	*p* = 0.29 (KW)
	d 8	2.39 ± 1.72	0 ± 0.68	
	d 14	5.09 ± 2.4	4.32 ± 2.5	
NO_3^- + NO_2^-	d 0	3*	3*	*p* = 0.28 ($F_{1,14}$ = 1.29)
	d 8	3.74 ± 0.3	3.56 ± 0.26	
	d 14	3.57 ± 0.11	4.24 ± 0.35	
PO_4^{3-}	d 0	1*	1*	*p* = 0.21 ($F_{1,14}$ = 1.73)
	d 8	1.23 ± 0.38	1.48 ± 0.36	
	d 14	0.85 ± 0.44	0.90 ± 0.17	
SiO_4^{4-}	d 0	6*	6*	*p* = 0.82 (KW)
	d 8	4.67 ± 0.58	5.33 ± 0.58	
	d 14	1.67 ± 0.58	1.33 0.58	

3.2 Effects of brownification on gross oxygen primary production, community respiration and net oxygen community production

3.2.1 Oxygen gross primary production (GPP)

The oxygen GPP ranged from 0.11 ± 0.04 (d 2) to 0.63 ± 0.16 gO_2 m^{-3} d^{-1} (d 11) in the control treatment and peaked on d 3, d 9 and d 11 (Fig. 2a). Moreover, GPP was significantly lower in the +HF treatment than in the control (p =1.2 × 10−3, $F_{1,11}$= 18.52), by an average of 31%. GPP was lower in the +HF treatment than in the control on 11 out of 12 days, with the minimum difference between treatments on d 4 (8%) and the maximum difference on d 3 (62%). The GPP: Chl-*a* ratio, used as proxy of photosynthetic efficiency, followed a similar trend as GPP during the first part of the experiment, with significantly lower values in the +HF treatment than in the control from d 1 to d 3 (Kruskal-Wallis, p = 0.04), by an average of 53% (Fig. 2d). However, in contrast to GPP, no significant differences were reported between treatments during the second part of the experiment (from d 4 to d 10, Kruskal-Wallis, p = 0.66).

3.2.2 Community respiration (R)

The community respiration (R) ranged from 0.13 ± 0.03 (d 2) to 0.73 ± 0.12 gO_2 m^{-3} d^{-1} (d 4) in the control treatment (Fig. 2b). It was significantly lower in the +HF treatment than in the control (p = 1.6 × 10−3, $F_{1,11}$ = 17.22), by an average of 27%. The difference between the +HF and control treatments varied over the course of the experiment, with the minimum difference between treatments on d 4 (6%) and the maximum difference on d 3 (75%).

3.2.3 Net community oxygen production (NCP)

The NCP, which corresponds to GPP minus R (Fig. 2c), was negative on 11 out of 12 days, with an average value of -0.08 ± 0.12 gO_2 m^{-3} d^{-1}, indicating a globally heterotrophic system (NCP < 0, GPP: R < 1). The NCP was higher in the +HF treatment than in the control by 12% on average, but the difference was not significant (p = 0.36, Kruskall-Wallis).

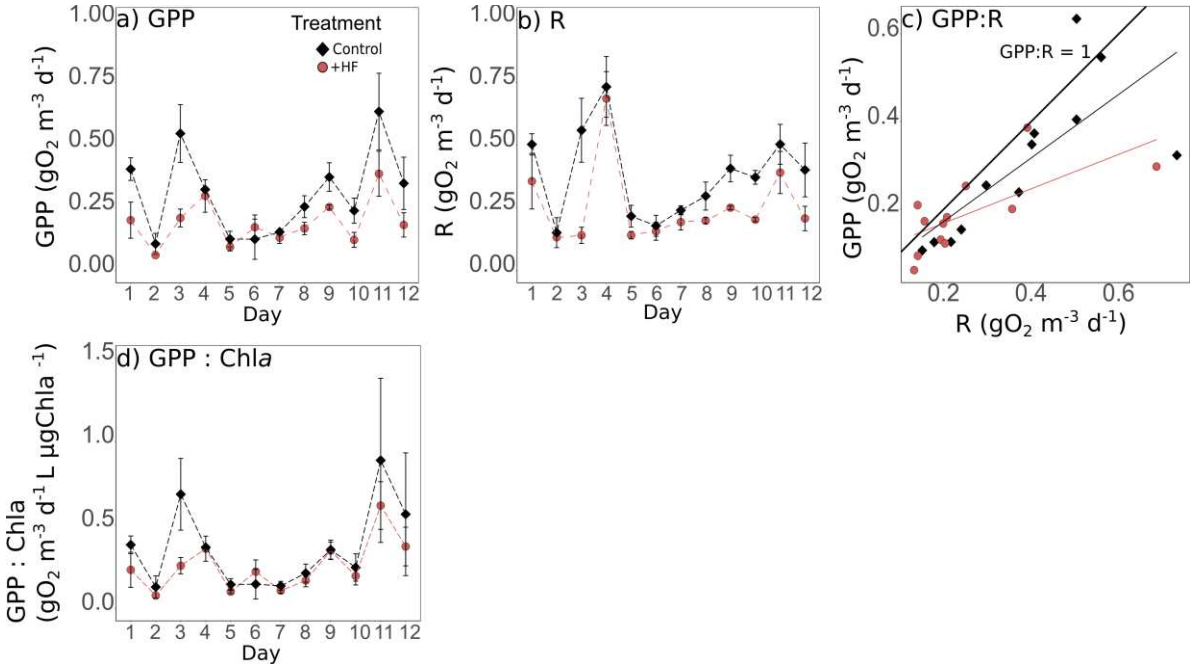

Figure 2. **(a) Mean gross primary production (GPP) and b) mean community respiration (R)** with standard deviations (error bars) over time in the control (black diamonds) and the +HF treatment (red circles); **(c) gross primary production (GPP): respiration (R) ratio** in the control (black diamonds) and the +HF treatment (red circles). GPP: R > 1 indicates an autotrophic system, while GPP: R < 1 indicates a heterotrophic system; d) Mean photosynthetic efficiency (expressed as GPP : Chlorophyll-*a* ratio) with standard deviations (error bars) over time in the control (black diamonds) and the +HF treatment (red circles).

3 3 Effects of brownification on the phytoplankton community: Chl-*a* concentration, pigment composition and light acclimation

3.3.1 Phytoplankton Chl-*a* concentration

In both the control and the +HF treatments, the Chl-*a* concentration decreased during the first 3 days of the experiment (from d 0 to d 2), stabilized during next 4 days (from d 3 to d 6), and then increased in the middle of the experiment (from d 7 to d 8 in the control) before decreasing again until the end of the experiment (Fig. 3). The highest Chl-*a* concentration was observed at the beginning of the experiment, at 1.59 ± 0.13 µg L^{-1} (d 0) in the control, while the lowest value was measured at the end of the experiment, at 0.29 ± 0.09 µg L^{-1} (d 14) in the control. The addition of HuminFeed® significantly reduced the Chl-*a* concentration, by an average of 9%, over the entire experimental period (Table 2). However, the effect of HuminFeed® addition was greater after d 8 and until the end of the experiment (Fig. 3), with the highest difference between treatments occurring on d 9 (30%).

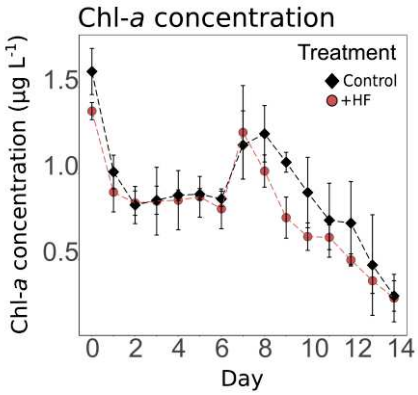

Figure 3. Mean chlorophyll-*a* concentration (Chl-*a,* µg L^{-1} ± standard deviation in error bars) over time in the control (black diamonds) and the +HF (red circles) treatments.

3.3.2 Phytoplankton pigment and community composition

The phytoplankton pigment concentrations showed different trends (Fig. 4). In the control and +HF treatment, the dominant pigments were the Bacillariophyceae-associated pigments fucoxanthin and chlorophyll-*c*2 (Chl-*c*2) (Fig. 4a, b), whereas the concentration of remaining pigments were generally lower (Fig. 4c-f).

The fucoxanthin and Chl-*c2* concentrations showed a strong decreasing trend during the experiment in the control (by 1446% and 307%, respectively) as well as in the +HF treatment (by 533% and by 382%, respectively, Fig. 4a, b). Similarly, the zeaxanthin concentration decreased by 718% in the control and by 346% in the +HF treatment (Fig. 4c). In contrast, the Chl-*b*, Chl-c*3* and 19'-HF concentrations peaked in the middle of the experiment, on d 7 or d 8 depending on the pigment and treatment, in both the control and +HF treatments (Fig. 4d, e, f).

The results of the RM-ANOVAs testing the effect of HuminFeed® addition and the percentage changes of the pigment concentrations during the entire experiment and during the last half of the experimental period (d 9 to d 14) are presented in Table 2.

The concentrations of both pigments associated with Bacillariophyceae (fucoxanthin and Chl-*c2*) as well as of those associated with Cyanophyceae (zeaxanthin) and type-2 Prymnesiophyceae (19'-HF) were not significantly different between the +HF treatment and the control over the entire experimental period. In contrast, the Chl-*b* and Chl-*c3* concentrations were significantly higher in the +HF treatment than in the control (Table 2).

Other pigments, such as β-β-carotene (ββc), chlorophyll-*c2* monogalactosyldiacylglyceride ester (Chl-*c2* MGDG), alloxanthin and diadinoxanthin, were present at much lower concentrations, and their

concentrations were not significantly different between the +HF treatment and the control over the entire experimental period (Table 2).

Interestingly, during the second half of the experimental period (from d 9 to d 14), there were strong, clear differences in almost all pigment concentrations between the +HF treatment and the control. Indeed, except for the Chl-*c2*, ββc and 19'-HF concentrations, all pigment concentrations were significantly higher in the +HF treatment than in the control (Table 2). More specifically, the strongest effect was observed on the Chl-*c3* concentration. Finally, the differences between treatments found on d 0 for the chl-c3 and the 19'-HF concentrations might be due to rare phytoplanktonic organisms heterogeneously distributed during the filling procedure.

Table 2. Repeated measures analyses of variance (RM-ANOVA) *p*-values for the effect of HuminFeed® addition and percentage changes on pigment concentrations over the entire experimental period (d 0 to d 14) and during the last half of the experimental period (d 9 to d 14). The values in brackets are the F-values. Bold values indicate significant p-values ($p < 0.05$). When homoscedasticity and normality assumptions could not be met despite transforming the data, a nonparametric Kruskal-Wallis (KW) test was used instead.

Pigment or ratio	The entire experiment		From d 9 to d 14	
	p RM-ANOVA	% change	*p* RM-ANOVA	% change
Chl-*a*	**4.5×10^{-2} ($F_{1,74}$=8.57)**	-9	**7.9×10^{-2} ($F_{1,29}$=8.13)**	-24
Chl-*c2*	0.06 ($F_{1,74}$ = 3.51)	5	0.13 ($F_{1,29}$ = 4.46)	7
Fucoxanthin	0.09 ($F_{1,74}$ = 2.99)	4	**5×10^{-4} ($F_{1,29}$ = 15.09)**	54
Zeaxanthin	0.71 (KW)	1	**6.3×10^{-3} ($F_{1,29}$ = 8.68)**	30
Chl-*b*	**1×10^{-4} ($F_{1,74}$ = 16.22)**	25	**$< 1 \times 10^{-4}$ ($F_{1,29}$ = 25.29)**	57
Chl-*c3*	**0.04 ($F_{1,74}$ = 5.22)**	23	**$< 1 \times 10^{-4}$ ($F_{1,29}$ = 77.60)**	131
19'-HF	0.41 ($F_{1,74}$ = 0.68)	-4	0.77 ($F_{1,29}$ = 0.09)	-5
ββc	0.78 (KW)	1	**0.04 ($F_{1,29}$ = 4.84)**	-15
Chl-*c2* MGDG	0.05 ($F_{1,74}$ = 4.52)	-6	**1.4×10^{-3} ($F_{1,29}$ = 12.46)**	-21
Alloxanthin	0.58 (KW)	31	n.d.	n.d.
Diadinoxanthin	0.36 ($F_{1,74}$ = 0.86)	-2	**1.4×10^{-3} (KW)**	66
Chl-c2:Chl-*a*	**7×10^{-4} ($F_{1,74}$=12.63)**	24	**7×10^{-4} ($F_{1,29}$=14.30)**	42
Fucoxanthin:Chl-*a*	**9×10^{-4} ($F_{1,74}$=11.93)**	27	**$< 1 \times 10^{-5}$ ($F_{1,29}$=100.89)**	111
Zeaxanthin:Chl-*a*	**0.01 ($F_{1,74}$=6.52)**	21	**8×10^{-4} ($F_{1,29}$=13.85)**	69
Chl-*b:*Chl-*a*	**9×10^{-4} ($F_{1,74}$=15.24)**	47	**$< 1 \times 10^{-5}$ ($F_{1,29}$=38.45)**	96
Chl-*c3*:Chl-*a*	**0.01 ($F_{1,74}$=6.78)**	61	**8.7×10^{-5} (KW)**	171
19'-HF:Chl-*a*	0.66 ($F_{1,74}$ = 0.19)	19	0.52 ($F_{1,29}$ = 0.42)	46
ββc:Chl-*a*	0.07 (KW)	16	**0.02 ($F_{1,29}$=5.48)**	11
Chl-*c2* MGDG:Chl-*a*	0.79 ($F_{1,74}$ = 0.08)	3	0.58 ($F_{1,29}$ = 0.32)	-4
Alloxanthin:Chl-*a*	0.43 (KW)	41	n.d.	n.d.
Diadinoxanthin:Chl-*a*	0.20 (KW)	26	**1×10^{-4} ($F_{1,29}$ = 20.39)**	133

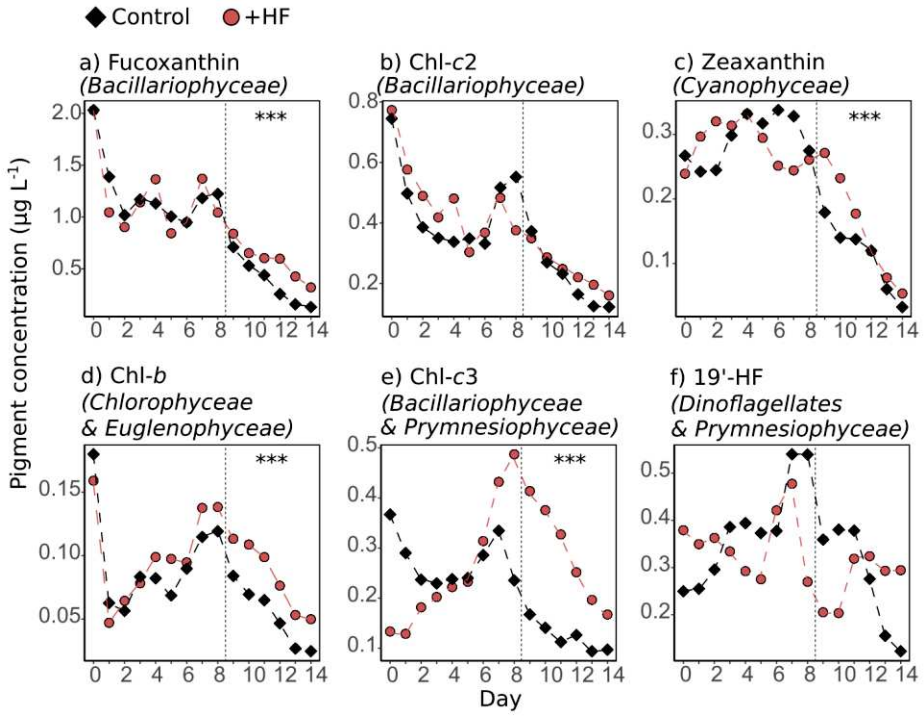

Figure 4. **Mean phytoplankton pigment concentrations** (µg L^{-1}) over time in the control (black diamonds) and +HF treatments (red circles). The dashed black vertical line highlights the d 9 to d 14 period, during which a stronger treatment effect was observed. The * symbols represent the result of an RM-ANOVA testing the effect of the +HF treatment at the end of the experiment (from d 9 to d 14; *** $p < 0.001$). Note that the scales of the y-axes are different. a) Fucoxanthin; b) chlorophyll-*c2* (Chl-*c2*); c) zeaxanthin; d) chlorophyll-*b* (Chl-*b*); e) chlorophyll-*c3* (Chl-*c3*); f) 19'-hexanoyloxyfucoxanthin (19'-HF).

In both treatments, the Bacillariophyceae were the dominant phytoplankton taxon, for which the biomass strongly decreased over time (Fig. 5a), while other groups were present with a lower biomass. Bacillariophyceae biomass was significantly lower in the +HF treatment compared to the control from d 5 to d 11, by an average of 42% (Kruskal-Wallis, $p = 0.04$), while it was more than 20 times higher in the +HF treatment compared to the control on d 14. The biomasses of Prasinophyceae and dinoflagellates were significantly higher in the +HF treatment, by an average of 142 and 61% respectively between d 5 and d 14 (Kruskal-Wallis, $p = 0.04$ and $p = 0.02$, respectively). The biomasses of other groups were generally higher but not significantly (Kruskal-Wallis, $p > 0.05$).

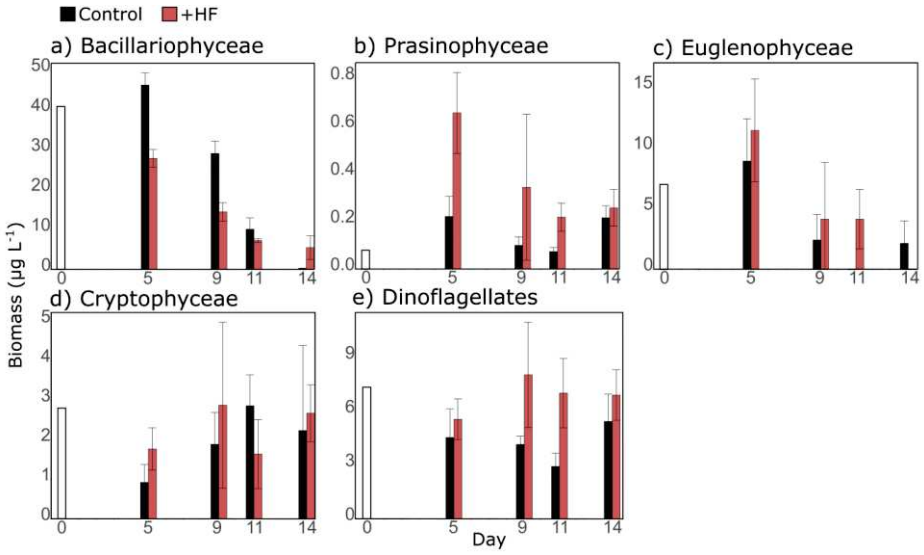

Figure 5. **Mean biomass (µg L^{-1}) for major phytoplankton taxa** with standard deviations (error bars) during five days of the experiment (d 0, d 5, d 9, d 11, and d 14) in the control (black) and +HF (red) treatments. The sample on d 0 was taken directly into the bay few minutes before filling the mesocosms and is represented in white. Note that the scales of the y-axes are different. a) Bacillariophyceae; b) Prasinophyceae; c) Euglenophyceae; d) Cryptophyceae; e) Dinoflagellates.

3.3.3 Phytoplankton pigment ratios

The addition of HuminFeed® significantly increased some pigment ratios during the second half of the experimental period (Fig. 6, Table 2). This trend was observed for the Chl-*c*2:Chl-*a* and the fucoxanthin:Chl-*a* ratios, which increased significantly between d 9 and d 14 (42% and 111% higher, on average, in the +HF treatment than in the control, respectively). Similarly, the zeaxanthin:Chl-*a*, Chl-*b*:Chl-*a*, Chl-*c*3:Chl-*a* and ββc:Chl-*a* ratios were significantly higher by 69%, 96%, 171% and 11% in the +HF treatment, respectively. The 19'-HF:Chl-*a* ratio was also higher in the +HF treatment than in the control, but not significantly.

Furthermore, the diadinoxanthin:Chl-*a* ratio, which is an indicator of low-light acclimation, was significantly higher in the +HF treatment than in the control during the last half of the experiment by an average of 133%, indicating that phytoplankton had to acclimate to the low-light conditions that developed at the end of the experiment in the +HF treatment (Fig. 6g). Moreover, the ββc:Chl-*a* ratio decreased strongly but was not significantly different between the two treatments over the entire experimental period (Fig. 6h). However, it was significantly higher in the +HF treatment from d 9 to d 14, but only by an average of 11% (Table 2).

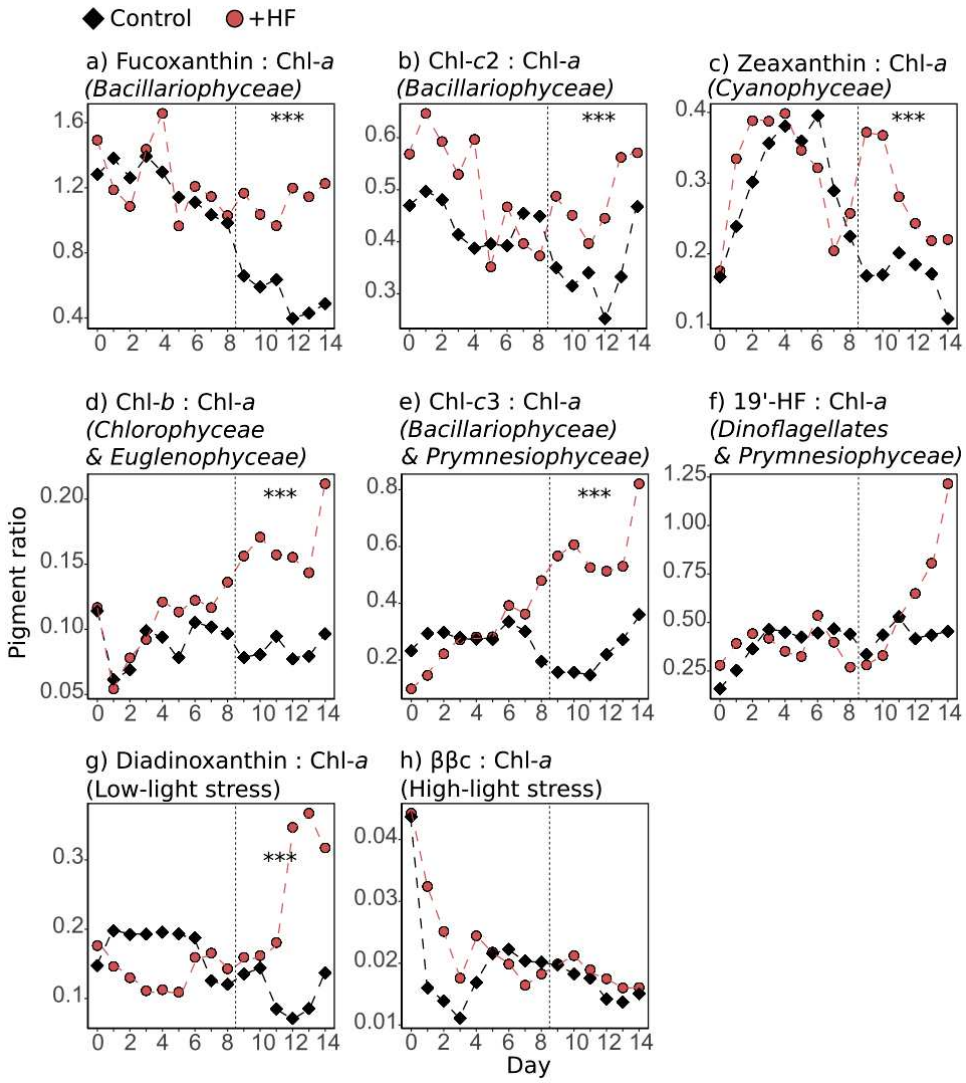

Figure 6. **Mean phytoplankton pigment ratios** over time in the control (black diamonds) and +HF treatments (red circles). The dashed black vertical line highlights the d 9 to d 14 period, during which a stronger treatment effect was observed. The * symbols represent the result of an RM-ANOVA testing the effect of the +HF treatment at the end of the experiment (from d 9 to d 14; *** $p < 0.001$). Note that the scales of the y-axes are different. a) Fucoxanthin: Chl-*a*, b) Chl-*c2*: Chl-*a*, c) zeaxanthin: Chl-*a*; d) Chl-*b*: Chl-*a*; e) Chl-*c3*: Chl-*a*; f) 19'-HF: Chl-*a*; g) diadinoxanthin: Chl-*a* (dark acclimation); h) ββc: Chl-*a* (light acclimation).

3 4 Effects of brownification on zooplankton community composition

At the beginning of the experiment (d 0), the zooplankton abundances in the bay were very low, and the zooplankton community was dominated by the appendicularian genus *Oikopleura*, the copepod genus *Acartia* and the cladoceran genus *Evadne,* with abundances of 93, 34 and 21 ind m^{-3}, respectively. Over the course of the experiment (from d 0 to d 14), the abundances of both *Oikopleura* and *Acartia* increased, by 2678% and 1785%, respectively, in the control and by 3431% and 1076%, respectively,

in the +HF treatment (Table 3). The *Oikopleura* abundance was significantly higher in the +HF than in the control treatment, while the *Acartia* abundance was significantly lower in the +HF than in the control treatment (Table 3). In contrast, the abundance of *Evadne* decreased by 76% in the control and increased by 4% in the +HF treatment from d 0 to d 14. Other genera were present at very low abundances, and the effects of the +HF treatment on these genera were therefore not significant and limited.

Table 3. **Mean abundances (± standard deviations), expressed as ind m^{-3}, of the main zooplankton genera** at the beginning of the experiment sampled directly from the bay and at the end of the experiment (d 14) sampled from the control and +HF treatments and the results of an unpaired *t*-test comparing the means of the control and +HF treatments on d 14; significance is indicated by * ($p < 0.05$).

Zooplankton genus	In situ d 0 (ind m^{-3})	Control d 14 (ind m^{-3})	+HF d 14 (ind m^{-3})	*t*-test *p* value for d 14
Oikopleura	93	2584 ± 463	3284 ± 220	0.04*
Acartia	34	641 ± 49	400 ± 102	0.02*
Evadne	21	5 ± 3	22 ± 20	0.4
Podon	1	5 ± 3	19 ± 8	0.07
Obelia	8	9 ± 2	7 ± 6	0.57

3 5 Environmental and pigment drivers of GPP and R in response to brownification

To assess the potential correlations between biological and environmental variables, ordinary least square linear relationships were assessed between the log response ratios (LRR) of GPP, R, DLI, and pigment concentrations (Fig. 7). A positive significant relationship was found between GPP and R (Fig. 7a). In addition, responses of GPP and DLI were positively related (Fig. 7b), as well as responses of R and Chl-*a* concentration (Fig. 7e). The only significant relationship with pigments responses was found between GPP and zeaxanthin (Fig. 7h). In addition, on days when the nutrient concentrations were measured, in both treatments, the Chl-*a* concentration was significantly and positively correlated with the silicate concentration (Spearman's rho = 0.92 and 0.95 in the control and the +HF treatment, respectively). However, the Chl-*a* concentration was significantly negatively correlated with the ammonium concentration (Spearman's rho = -0.90 and -0.80 in the control and the +HF treatment, respectively) and with the nitrate concentration only of the +HF treatment (Spearman's rho = -0.88). Finally, the Chl-a concentration was not significantly correlated with DLI, as well as with other variables (temperature, salinity) (data not shown).

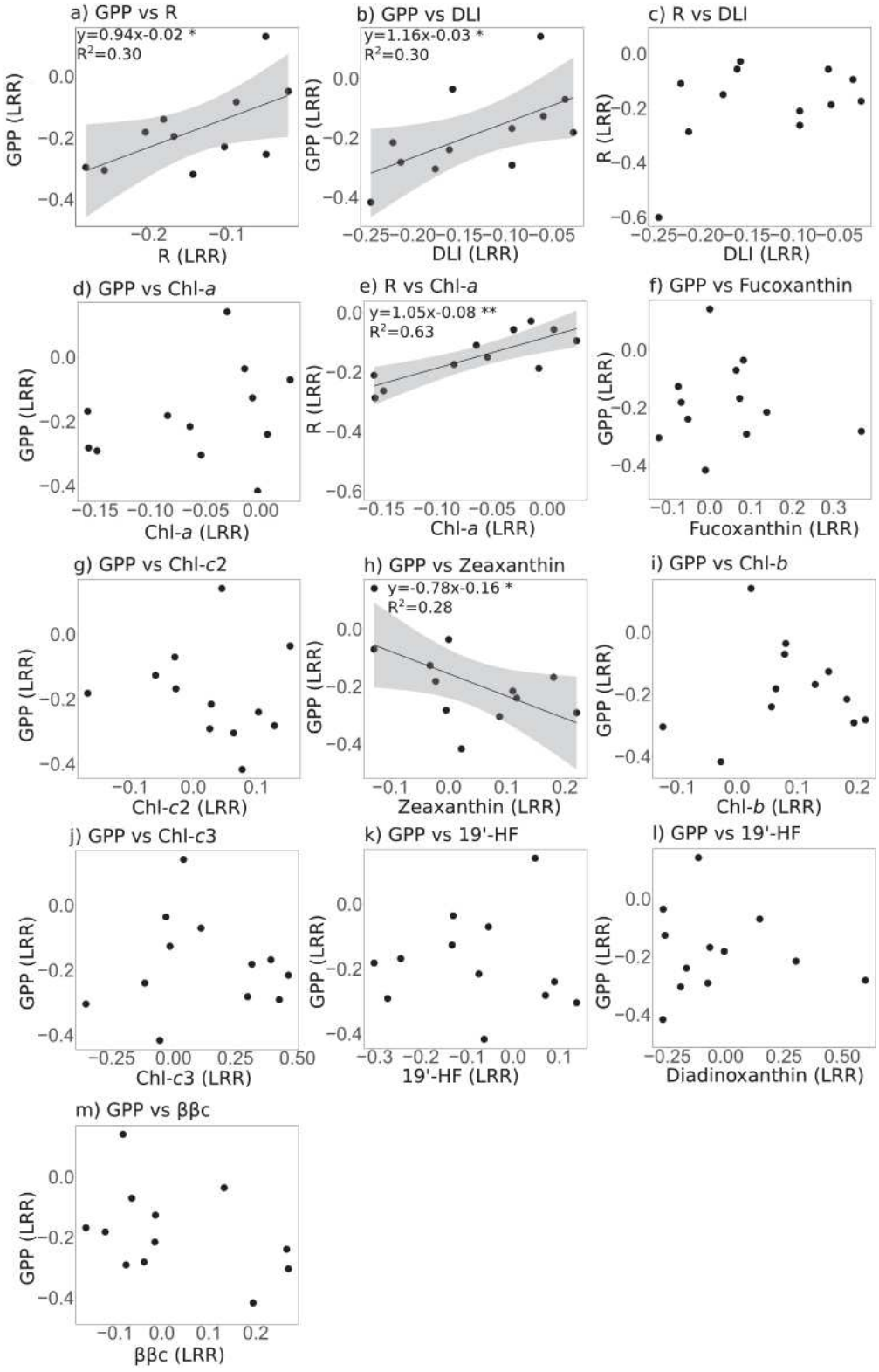

Figure 7. Ordinary least squares linear relationships between the log response ratios (LRR) of GPP, R, DLI, and pigment concentrations. For significant relationships (p <0.05), the solid black line represents the least square fit, and the grey area represents the 95% confidence limits. a) GPP vs R; b) GPP vs DLI; c) R vs DLI; d) GPP vs Chl-*a*; e) R vs Chl-a; f) GPP vs Fucoxanthin; g) GPP vs Chl-*c*2; h) GPP vs Zeaxanthin; i) GPP vs Chl-*b*; j) GPP vs Chl-*c*3; k) GPP vs 19'-HF; l) GPP vs

Diadinoxanthin; and m) GPP vs ββc. Note that one extremely low point (-0.49 x -0.61) was removed from GPP vs R to avoid a biased relationship.

4 Discussion

4.1 Brownification significantly slowed down both gross primary production and community respiration

High-frequency sensor measurements allowed us to detect a significant effect of brownification, simulated via HuminFeed® addition, on oxygen metabolism. High-frequency sensors have rarely been used to estimate biological processes in the context of in situ mesocosm experiments (Soulié et al. 2021). However, this technique has many advantages over traditional sampling methods, as it is a noninvasive, less time-consuming way to estimate plankton oxygen metabolism that produces a large amount of data providing details on oxygen dynamics (Staehr et al. 2010).

Brownification resulted in significant reductions in GPP and R. To our knowledge, this is the first time that a significant slowing down of both GPP and R was induced by brownification in a coastal marine plankton community. The reduction in DLI (23%) due to the simulated brownification is one of the factors that altered the GPP, as the effects of the HuminFeed® addition on GPP and on DLI were linearly related (Fig. 6b). The fact that the light availability was the main factor controlling the GPP response to brownification was expected as it has been shown that phytoplankton primary production responds quickly to light fluctuations (Talling 1971; Kirk 1983; Morison et al. 2020). Additionally, the photosynthetic efficiency, assessed as GPP normalized by Chl-*a* concentration, was depressed by brownification during the first part of the experiment, before joining the control level during most of the second part of the experiment, in contrast to GPP alone. This tends to imply that the observed decrease of GPP under brownification was certainly due to reduced light availability during the first part of the experiment, while it was mainly related to lower phytoplankton biomass in the second part of the experiment. Other physical, chemical and biological factors combined with light reduction may also have played a role. Indeed, it has been established that brownification could have multiple cascading effects that influence phytoplankton primary production (Solomon et al. 2015). This is especially true in coastal areas, as coastal plankton metabolism can be driven by various factors, among which allochthonous inputs from river loads can play an important role (Duarte et al. 2004).

In addition to a decrease in GPP, brownification resulted in a decrease in community R to a similar extent. This result was unexpected, as the input of humic substances constitutes an input of DOC that becomes available to heterotrophic bacteria (Robinson 2008); this input was expected to increase bacterial respiration and, in turn, the community R. Nevertheless, the lower R reported here is in line with the results of Lebret et al. (2018), in which the addition of HuminFeed® did not enhance total

community R in lakes. The addition of 2 mg L^{-1} HuminFeed® corresponded to a small DOC input (0.8 mg L^{-1}), which is lower compared to the DOC concentrations that are naturally present in Hopavågen Bay (around 1.5 mg L^{-1}, Olsen et al. 2006); this may explain why HuminFeed® addition did not considerably increase bacterial respiration. Moreover, bacteria could potentially preferentially use other sources of carbon, suggesting that HuminFeed® represents a DOC source of poor bioavailability for bacteria. Taken together, these results indicate that R was likely controlled by factors other than the DOC concentration alone.

The decrease in R was positively and significantly correlated with the decrease in GPP and in Chl-a concentration (Fig 6.). This suggests a strong coupling between GPP and R and therefore a strong coupling between phytoplanktonic and bacterial communities. Indeed, in coastal ecosystems, bacterial respiration can contribute up to 76% of the whole community R, and bacterial respiration likely depends mainly on phytoplankton exudates rather than on other carbon sources (Robinson 2008). This is in line with the literature, which states that autotrophic production strongly affects both autotrophic and heterotrophic respiration, particularly in coastal ecosystems (Larsson and Hagtsröm 1979; Sampou and Kemp 1994; Pringault et al. 2009).

As the decreases in GPP and R were similar in extent (31% and 27%, respectively), the simulated brownification resulted in an NCP that was not significantly different from that in the control. The NCP, which represents the net oxygen balance, was negative throughout almost the entire experiment in both treatments, reflecting a globally heterotrophic system. Regarding the drivers of plankton metabolism, the effects of the simulated brownification on GPP and R were not positively correlated with its effect on the concentration of a particular phytoplankton pigment, suggesting that these GPP and R reductions were not due to the response of one or certain phytoplankton groups but were rather related to the response of the whole phytoplankton community and might occur in other planktonic assemblages. Taking into account that reductions in plankton community metabolism are expected to have cascading consequences on the entire food web as it relates to its fundamental functions (Agusti et al. 2017), the results described in the present study suggest that the entire pelagic ecosystem of Hopavågen Bay could be affected by brownification.

4 2 Brownification reduced the chlorophyll-*a* concentration and modified the zooplankton community composition

Brownification significantly reduced the Chl-*a* concentration mostly during the second half of the experiment, in contrast to the rapid decrease in GPP and R. This decrease in Chl-*a* concentration is in line with Nicolle et al. (2012) and Mustaffa et al. (2020), who found similarly lower Chl-*a* concentrations under brownification, but differs from Rasconi et al. (2015) and Lebret et al. (2018), who did not find any significant effect of the addition of HuminFeed® on Chl-*a* concentrations in

lacustrine plankton communities. The decrease in Chl-*a* observed in the present investigation seems not to be driven directly by light availability, as the Chl-*a* concentration was not correlated with DLI. Instead, as the Chl-*a* concentration was negatively correlated with the ammonium and nitrate concentrations, especially in the brownification treatment, bottom-up controls related to the availability of ammonium and nitrate may have driven the decrease in Chl-*a*. However, these negative relationships could be assessed only at three days during the present experiment and may not reflect the dynamics between nutrients and Chl-*a* concentrations during the whole period of the experiment. The reduction in the Chl-a concentration caused by brownification could also be due to grazers and their grazing activity.

The main zooplankton group observed during the experiment, the appendicularian *Oikopleura* sp., as well as all other zooplankton species, had very low abundances at the beginning of the experiment. The unusual high temperatures of the weeks before the experiment resulted in a strong stratification with high surface temperatures. We suggest that the low initial zooplankton abundances were due avoidance of the upper part of the water column where the mesocosms were filled. Additionally, the Hopavågen bay and its surroundings are known to host large abundances of jellyfishes (Tiller et al. 2014), resulting in a high grazing pressure on meso- and microzooplankton. However, as the abundance of jellyfish was very low in the enclosures, the loss of grazing pressure by large jellyfish may also have contributed to the generally rapid increase of appendicularians and copepods observed across the experiment. Thus, even if zooplankton was not sampled at the middle of the experiment, we can hypothesize that zooplankton abundances had increased by the middle of the experiment, which could have significantly contributed to the decrease in Chl-*a* concentration observed from d 8 in both treatments. In addition, at the end of the experiment, the abundance of the appendicularian *Oikopleura* sp., was significantly higher under brownification than in the control; while it was the opposite for the copepod *Acartia* sp., suggesting a different grazing pressure on phytoplankton between treatments, which could result in the lower Chl-*a* concentration reported. The positive effect of brownification on *Oikopleura* sp. corroborates the results of Kammerlander et al. (2016) and Minguez et al. (2020), who showed that some grazers performed better under low-light, high DOC conditions and that intensified water color coupled with warming could lead to stronger top-down control of the Chl-*a* concentration by grazers (Nicolle et al., 2012). Moreover, the effect of brownification on the zooplankton community structure reported at the end of the experiment might explain the higher Bacillariophyceae and the lower Euglenophyceae found under brownification on d 14, as it has been shown that *Oikopleura* sp. can feed mostly on small-sized organisms (Troedsson et al. 2007), as Euglenophyceae, while *Acartia* feed more efficiently upon larger prey such as Bacillariophyceae (Berggreen et al. 1988).

4 3 Brownification changed the phytoplankton pigment and community composition, resulting in light acclimation

It should be noted that the timing of the experiment might have already excluded some phytoplankton groups, as the extreme heatwave that occurred a few weeks before the experiment could have affected the phytoplankton community composition. For example, Katechakis and Stibor (2004) reported some Prymnesiophyceae and Chrysophyceae in Summer at Hopavågen that were not identified in our experiment. Brownification induced a change in the composition of the phytoplankton community, by depressing Bacillariophyceae biomass in the middle of the experiment and increasing it at the end, and by promoting Prasinophyceae, Cryptophyceae, and dinoflagellates during the second part of the experiment. Brownification also triggered a change in the concentration of pigment-based taxonomic markers, especially during the second half of the experiment, from d 9 to d 14, when the specific biomarker pigments of Bacillariophyceae, Cyanophyceae, Chlorophyceae and Euglenophyceae as well as their respective ratios to Chl-*a* increased in the HuminFeed® treatment compared with those in the control treatment. As pigment concentrations and ratios to Chl-*a* can depict changes in both the community composition and light acclimation, a comparison between phytoplankton biomasses estimated using microscopy and associated pigment concentrations can help disentangle the physiological and the compositional effects of brownification. For example, the higher biomass of Bacillariophyceae at the end of the experiment in the brownified treatment (d 14) is congruent with the increase in fucoxanthin concentration on the same day, suggesting that the latter is related to phytoplankton community composition changes. Conversely, the lower Bacillariophyceae biomass on d 9 and d 11 under brownification was concomitant with higher fucoxanthin concentrations, suggesting a physiological acclimation rather than a change in the community composition. Similarly, the higher Chl-*b* concentration and ratio to Chl-*a* from d 9 to d 14 in the +HF treatment compared to the control do not match with the lower Euglenophyceae biomass on d 14, potentially reflecting a physiological acclimation rather than a community composition change. Hence, the phytoplankton biomass data tend to indicate that Bacillariophyceae were disadvantaged by brownification during most of the experiment, maybe because they were outcompeted by other phytoplankton such as Prasinophyceae, Euglenophyceae and dinoflagellates for which biomass was enhanced in the +HF treatment, thus departing from a study in a freshwater system reporting higher relative abundances of Bacillariophyceae with the addition of HuminFeed® (Lebret et al. 2018). Additionally, the phytoplankton pigment data reported in the present study highlights a potential physiological acclimation to the lower light conditions of most investigated phytoplankton groups.

Another hypothesis to explain the observed increase in the pigment concentrations and ratios relates to the quality of the available light, not only to its quantity, as discussed previously. Indeed, HuminFeed® has been shown to absorb more light in the UV and blue wavelengths (Meinelt et al. 2007). In a parallel experiment performed at the same time and location as the present work, the addition of different concentrations of HuminFeed® strongly shifted the light spectrum toward red wavelengths (Herwig Stibor, pers. comm.). Therefore, the addition of HuminFeed® likely led to a change in the light

spectrum available for phytoplankton photosynthesis, which in turn could have shifted the competition within the phytoplankton communities toward groups that are more adapted to red light, such as cyanobacteria (Luimstra et al. 2020) leading to the reported increase in their pigment biomarker. It should be noted that both the light quantity and the light quality hypotheses mentioned above could have occurred synergistically.

Among other ratios, the addition of HuminFeed® significantly enhanced the diadinoxanthin:Chl-*a* ratio during the second half of the experiment. The diadinoxanthin:Chl-*a* ratio is a good indicator of low-light stress, as the diadinoxanthin cycle is the major xanthophyll cycle notably in Bacillariophyceae (Demers et al. 1991; Goss and Jakob 2010; Deininger et al. 2016; Kuczynska et al. 2020). Therefore, the increase in the diadinoxanthin:Chl-*a* ratio further indicate that the phytoplankton in these taxa acclimated to the low-light conditions during the second half of the experiment. The concomitant increase in the fucoxanthin:Chl-*a* ratio observed during the second half of the experiment is also in agreement with previous studies reporting an increase in this ratio under low-light conditions (Schlüter et al. 2000). Surprisingly, while phytoplankton are known to adapt quickly to changes in light conditions (Goss and Jakob 2010), it appears that the light acclimation of the phytoplankton community occurred only during the second half of the experiment, 9 days after the addition of HuminFeed®, conversely to changes in the phytoplankton community that were already noticeable on d 5. This delay in the response of pigment ratios might be explained by the fact that pigment ratios can depend on other parameters rather than on only direct immediate responses to the light availability and spectrum. They can also be due to changes in phytoplankton composition, some ratios varying greatly among species of the same taxon (Mackey et al. 1996), growth phases, some ratios being up to 10-fold higher during the stationary growth phase than during the exponential growth phase (Ruivo et al. 2011), and nutrient conditions, as nutrient depletion can change multiple pigment:Chl-*a* ratios (Goericke and Montoya 1998, Henricksen et al. 2002). Therefore, the fact that pigment ratios seemed to respond to the addition of HuminFeed® only after 9 days of the experiment could be due to several factors that concomitantly affected the pigment ratios and not only to a direct immediate response to the reduction in light availability.

In conclusion, the results presented here, showing the slowing down of plankton metabolic rates and the shift in phytoplankton community and pigment composition in a natural northern-latitude coastal system under simulated brownification, call into question the whole-ecosystem implications of brownification. Although these results come from a single mesocosm experiment and any resultant generalizations must be considered carefully, they stress the importance of considering the brownification-induced modification of these metabolic processes in future modeling projections. If the results of the present experiment can be scaled up to the ecosystem level, they highlight the fact that brownification may affect the capacity of coastal Norwegian waters to both produce oxygen and to release it to the atmosphere. However, as both oxygen production and community consumption were reduced to the same extent under brownification, the net oxygen balance was not significantly altered,

suggesting that brownification might not affect the balance between the capacity to consume and to produce oxygen from the water column. In the context of the expected increase in water column deoxygenation in coastal waters as a physical consequence of the increased temperatures caused by global warming, the concomitant slowing down of plankton metabolic rates due to brownification could potentially interact with and alter the oxygen cycle in coastal areas, particularly at those northern latitudes.

5 Acknowledgments

We would like to thank David Parin for his participation in the mesocosm experiment and for setting up the sensors and performing data acquisition. We would like to thank Kiersti Andresen for nutrient analyses and Tore and Katja Alstad for logistical support at the Sletvik field station of the Norwegian University of Science and Technology (NTNU). Furthermore, we thank Robert Ptacnik for his helpful comments on the previous version of the manuscript. This work and a part of the PhD grant of TS were funded under the AQUACOSM project, which have received funding from the European Union's Horizon 2020 research and innovation program (H2020/2017-2020) under grant agreement n°731065.

6 Authors' contributions

B.M., H.S. and F.V. conceived the study and designed the mesocosm experiment. T.S. and S.M. calibrated the sensors used in the study. T.S., H.S., S.M., B.B., J.K. and U.S. participated in the daily manual sampling of the mesocosms. H.S., B.B. and J.K. counted the zooplankton samples and analyzed the zooplankton data. T.S. and F.V. performed the HPLC analyses and the related data processing. T.S. processed the sensor data, performed the analyses and wrote the original draft of the manuscript with inputs from H.S., S.M., J.C. N., U. S., F.V. and B.M.

7 References

Voir la section Bibliographie de la thèse

Encadré – Chapitre 2

Paramètres de stabilité fonctionnelle et compositionnelle de la communauté planctonique en réponse au brunissement

Il est important d'estimer les paramètres de stabilité de la communauté planctonique, à savoir la résistance, la résilience, la récupération et la stabilité temporelle, afin de comprendre comment la communauté réagit pendant et après une perturbation donnée. Ces paramètres ont été estimés avec les données qui font l'objet du présent Chapitre, et selon la méthode décrite ci-après et dans le Chapitre 4 (p 153). Ces paramètres ne sont pas inclus dans le Chapitre 2, mais, dans le but de comparer les travaux concernant différentes perturbations et en discuter dans la Discussion Générale de la présente thèse, ils font l'objet de cet encadré.

La résistance, la résilience, la récupération et la stabilité temporelle ont été calculées pour la PPB, la R, la PCN, et les concentrations en fucoxanthine, chlorophylle-*c*2, zéaxanthine, chlorophylle-*b*, chlorophylle-*c*3 et 19'-hexanoyloxyfucoxanthine en utilisant les formules décrites dans Hillebrand et al. (2018) et récapitulées dans le tableau suivant (Tableau E2.1). Brièvement, la résistance est calculée comme le logarithme du ratio de réponse le jour où la perturbation est appliquée (dans le cas de l'expérience décrite dans ce chapitre, le jour 0), la résilience est calculée comme la pente de la courbe représentant le logarithme du ratio de réponse par rapport au temps durant la période qui suit la perturbation (ici, jour 1 à 14 pour les concentrations pigmentaires et 1 à 12 pour la PPB, la R et la PCN), la récupération est calculée comme le logarithme du ratio de réponse le dernier jour de l'expérience (jour 14 pour les concentrations pigmentaires et jour 12 pour la PPB, la R et la PCN), et la stabilité temporelle est calculée comme l'inverse de l'écart-type des résidus autour de la résilience.

Tableau E2.1. **Les paramètres de stabilité** lors de l'expérience de brunissement à Hopavågen, et la période expérimentale pour laquelle ils sont estimés, la formule mathématique de leur estimation, et leur interprétation, d'après Hillebrand et al. (2018). * X_{HF} and X_C représentent la valeur du paramètre d'intérêt dans les traitements +HF et control respectivement. ** sd : écart-type, res_b : résidus autour de la résilience.

Paramètre	Période	Estimation	Interprétation
Resistance (a)	d0	$a = \ln\left(\frac{X_{HF}}{X_C}\right)$ *	$a = 0$ → résistance maximale $a > 0$ → surperformance $a < 0$ → sous-performance
Résilience (b)	d11-d20	$\ln\left(\frac{X_{HF}}{X_C}\right) = b * t + i$	$b = 0$ → pas de récupération $b > 0$ → récupération plus rapide (si $i <$ 0) $b < 0$ → déviation supplémentaire par rapport au control (si $i < 0$)
Récupération (c)	d20	$c = \ln\left(\frac{X_{HF}}{X_C}\right)$	$c = 0$ → récupération maximale $c > 0$ → surcompensation $c < 0$ → récupération incomplète
Stabilité temporelle (d)	d11-d20	$d = \frac{1}{(sd(res_b)}$ **	Plus d est grand et moins les fluctuations sont importantes

Tableau E2.2. **Résistance, résilience, récupération et stabilité temporelle** pour certaines fonctions et concentrations pigmentaires.

Paramètre	Résistance	Résilience	Récupération	Stabilité temporelle
Fonctions				
PPB	-0,70	-0,10	-0,65	2,85
R	-0,35	0,01	-0,66	2,62
PCN	0,45	0,01	-0,73	3,52
Pigments				
Fucoxanthine	$-5{,}7 \times 10^{-4}$	0,04	0,39	9,07
Chl-*c*2	0,05	$1{,}4 \times 10^{-3}$	0,12	8,18
Zeaxanthine	-0,15	$2{,}5 \times 10^{-3}$	0,22	7,25
Chl-*b*	0,09	0,03	0,31	20,63
Chl-*c*3	-0,55	0,05	0,24	6,68
19'-HF	0,30	$5{,}5 \times 10^{-3}$	0,38	4,81

Pour les paramètres métaboliques de l'oxygène, la PPB et la R ont montré une faible résistance, avec une valeur négative indiquant une sous-performance du système en réponse au brunissement (Tableau E2.2). En conséquence, la résistance de la PCN était également faible, car loin de la valeur de référence, mais positive, indiquant une surperformance du système. Ces valeurs de résistance sont accompagnées de valeurs de résilience négative pour la PPB et la R, suggérant un écart encore plus important entre mésocosmes brunifiés et contrôles au cours du temps. Finalement, tous les paramètres métaboliques ont présenté une récupération largement incomplète, et une stabilité temporelle assez faible également.

La résistance des **concentrations pigmentaires** a varié fortement en fonction du pigment concerné. La fucoxanthine, la chlorophylle-*c*2 (chl-*c*2) et la chlorophylle-*b* (chl-*b*) ont montré une résistance importante, alors que la zeaxanthine et la chlorophylle-*c*3 (chl-*c*3) étaient moins résistants et ont sous-performés, et que le 19'-hexanoyloxyfucoxanthine (19'-HF) a surperformé. Toutes les valeurs de résilience associées aux concentrations pigmentaires étaient positives, et représentatives d'un retour progressif aux conditions de départ, résultant ultimement en une surcompensation pour tous les pigments. La plus forte stabilité temporelle était celle de la chl-*b*, alors que le 19'-HF a montré la plus faible.

Ces résultats sont comparés à ceux obtenus lors d'une expérience dans la lagune de Thau dans la Discussion Générale de la thèse (p 153).

Chapitre 3

Effets du réchauffement sur la croissance et la mortalité du phytoplancton durant deux périodes productives en zone côtière Méditerranéenne : apports des mesures de fluorescence de chlorophylle-*a* à haute fréquence

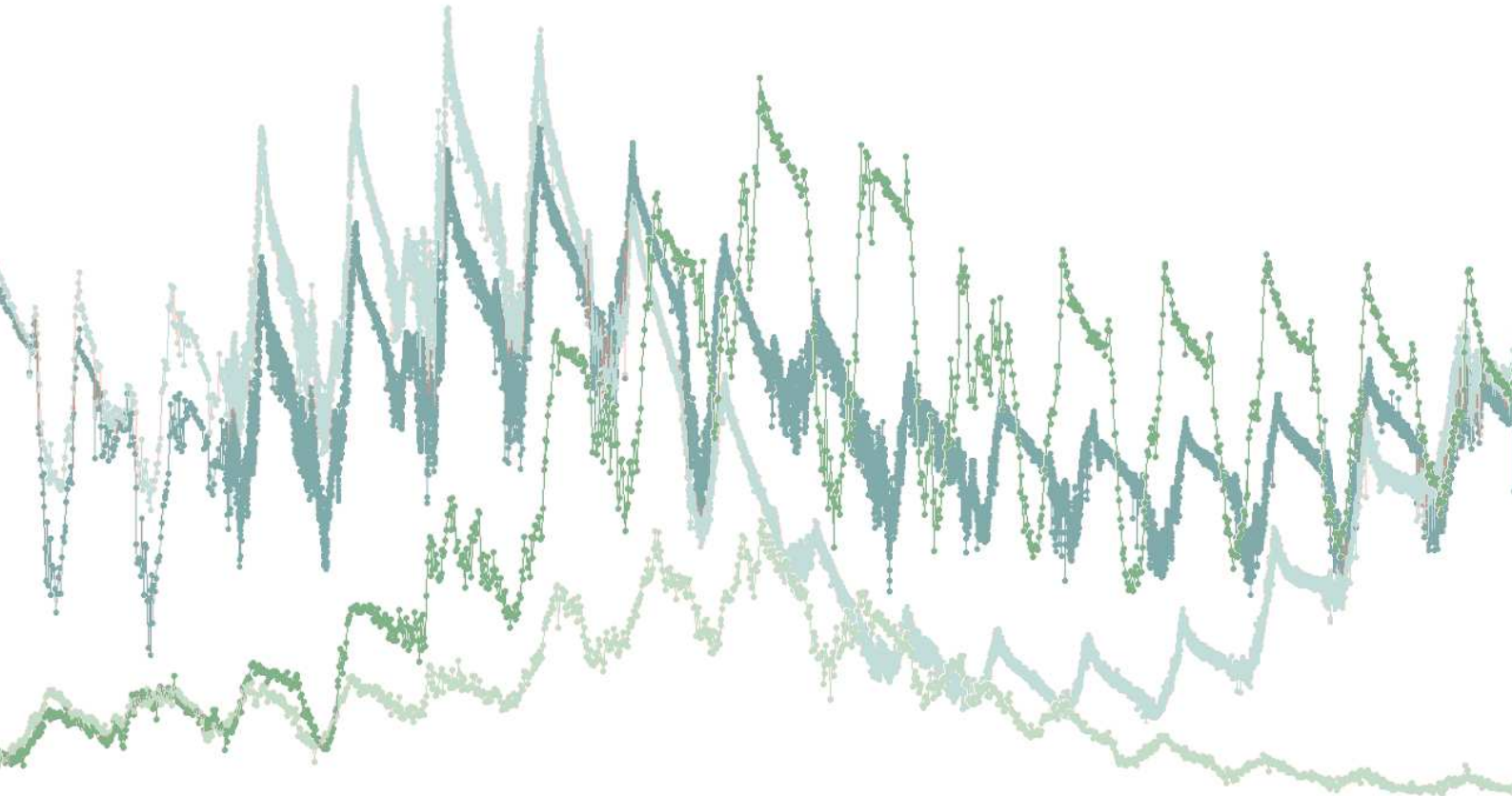

Avant-Propos

Les taux de croissance et de perte du phytoplancton sont des paramètres importants qui permettent d'évaluer et de prédire la dynamique des producteurs primaires au sein des écosystèmes aquatiques. Ainsi, il apparaît essentiel de comprendre l'effet du réchauffement climatique sur ces paramètres, et notamment lors du printemps et de l'automne, les deux saisons les plus productives en Méditerranée.

L'objectif du présent chapitre est donc d'évaluer l'effet d'un réchauffement de 3°C, simulant les scénarios du GIEC pour la fin du siècle en Méditerranée, sur les taux de croissance, de perte et sur la composition de la communauté du phytoplancton côtier méditerranéen et de comparer la réponse obtenue au printemps et en automne. Pour cela, deux expériences de mésocosmes ont été réalisées dans la lagune de Thau au printemps (Avril 2018) et en automne (Octobre 2018), dans le cadre des projets PHOTOPHYTO (Effet du réchauffement climatique sur le déclenchement du bloom phytoplanctonique : photopériodisme, composition et adaptation, financé par l'Agence Nationale de la Recherche) et AQUACOSM (Network of Leading European AQUAtic MesoCOSM Facilities Connecting Mountains to Oceans from the Arctic to the Mediterranean, financé par l'Union Européenne). Le même protocole expérimental a été utilisé lors des deux expériences : un triplicat de mésocosmes a été chauffé à +3°C par rapport à la température naturelle d'un triplicat de mésocosmes contrôles. Les données issues de capteurs de fluorescence de la chlorophylle-*a* immergés à 1 m de profondeur dans les mésocosmes ont permis d'estimer les taux de croissance et de perte du phytoplancton, via l'application d'une méthode employée pour la première fois dans le cadre d'expériences en mésocosmes. Un échantillonnage journalier et manuel des mésocosmes a permis d'évaluer la composition de la communauté phytoplanctonique via la mesure de pigments biomarqueurs taxonomiques et de suivre la concentration en nutriments inorganiques dissouts. Finalement, les taux de croissance et de perte estimés avec les données des capteurs ont été comparés aux taux de croissance et de broutage obtenus avec la technique des dilutions, et le taux de variation net quotidien de fluorescence de la chlorophylle-*a* a été comparé à celui de la concentration en chlorophylle-*a* obtenues avec la chromatographie liquide à haute-performance (HPLC). La production primaire brute, la respiration communautaire et la production communautaire nette ont également été calculées à partir des données HF d'O_2 dissout. Ces paramètres ne font pas partie de l'article faisant l'objet du chapitre, mais sont présentés dans l'Encadré associé à ce chapitre, car ils seront comparés à ceux obtenus pour une autre expérience dans la lagune de Thau dans la Discussion Générale de la thèse (p 176). Le quenching non-photochimique de la fluorescence de la chlorophylle constitue le principal biais dans l'estimation de la concentration en chlorophylle-*a* à partir de de sa fluorescence. Dans ce chapitre, ce phénomène a été pris en compte en interpolant linéairement les données de fluorescence entre le lever et le coucher du soleil. Cette technique n'ayant jamais été utilisée dans le cadre d'expériences en mésocosmes, sa validité est évaluée en comparant les valeurs de taux de croissance et de ratio croissance sur pertes obtenues avec les fluorescences corrigées et non-

corrigées pour le quenching. Cette évaluation est présentée dans l'Annexe I de la thèse, et sera discutée dans la Discussion Générale de la thèse (p 175).

J'ai participé à l'expérience d'Avril 2018 lors de mon stage de fin d'étude en école d'ingénieur, et j'ai pris part à l'installation et à l'échantillonnage journalier des mésocosmes, ainsi qu'à la filtration pour le dosage de certaines vitamines et pour du métabarcoding (données ne faisant pas partie de la thèse). Lors de ma thèse, j'ai également traité et analysé l'ensemble des données issues des capteurs de cette expérience et j'ai participé à l'expérience d'Octobre 2018. J'ai pris part à l'installation et à l'échantillonnage des mésocosmes, j'ai traité et analysé les données issues des capteurs de cette expérience, j'ai réalisé des incubations afin de mesurer les paramètres métaboliques du plancton (données faisant partie du chapitre 1) et j'ai analysé la composition pigmentaire du phytoplancton via l'HPLC.

Le chapitre est présenté sous la forme d'un article rédigé en anglais et intitulé « **Warming enhanced phytoplankton growth and loss rates during two contrasted productive seasons in Mediterranean coastal waters : evidences from in situ mesocosm experiments and high-frequency measurements** », écrit par Tanguy Soulié, Francesca Vidussi, Justine Courboulès, Sébastien Mas, et Behzad Mostajir, et qui sera soumis très prochainement dans une revue spécialisée.

Participants lors des expériences au printemps et à l'automne 2018. Photos ©B. Mostajir

Warming enhanced phytoplankton growth and loss rates during two contrasted productive seasons in Mediterranean coastal waters: evidences from *in situ* mesocosm experiments and high-frequency sensor measurements

Tanguy Soulié[1]*, Francesca Vidussi[1], Justine Courboulès[1], Sébastien Mas[2], Behzad Mostajir[1*]

[1]MARBEC (MARine Biodiversity, Exploitation and Conservation), Univ Montpellier, CNRS, Ifremer, IRD, Montpellier, France

[2]MEDIMEER (Mediterranean Platform for Marine Ecosystems Experimental Research), OSU OREME, CNRS, Univ Montpellier, IRD, IRSTEA, Sète, France

*corresponding authors: Tanguy Soulié, tanguy.soulie@umontpellier.fr

Behzad Mostajir, behzad.mostajir@umontpellier.fr

Key words: Phytoplankton growth, loss, in situ mesocosms, fluorescence sensors, warming

Running head: Phytoplankton growth and loss responses to warming

Abstract

Warming is expected to have complex consequences on phytoplankton, notably because effects on its growth (μ) and loss (*l*) rates can differ, finally controlling the fate of the marine primary production. We conducted two in situ mesocosm experiments in shallow coastal waters of the Mediterranean Sea (Thau lagoon) in autumn and spring during 18 days in order to assess μ and *l* responses to an experimental warming. Using automated high-frequency chlorophyll-*a* fluorescence sensors, phytoplankton biomass, μ and *l* were estimated and compared to those found using the conventional dilution method. A joint daily manual sampling for nutrient concentrations and pigment composition was performed. The effects of warming were investigated on μ and *l* as well as on pigment composition. Warming enhanced μ by 18.3% in spring and 28.1% in fall. In addition, warming enhanced strongly *l* by 37.1% during the spring experiment. As a result, warming lowered the μ : *l* ratio in spring and increased it in fall. Moreover, warming induced contrasted changes in the phytoplankton community composition, by enhancing dinoflagellates in spring and diatoms in fall, while depressing prymnesiophytes, diatoms and cyanobacteria in spring and green algae in fall. Moreover, ammonium, nitrate and nitrite concentrations appeared to be the major factors controlling μ, and diatoms were found to be its main contributors, but only in fall. Finally, we compared μ and *l* obtained with the high-frequency sensors with those estimated with the traditional dilution method, and no significant differences between methods were found. Finally, our experiments tend to indicate that warming could induce important changes in phytoplankton processes and community composition during productive seasons, potentially having drastic consequences on the entire Mediterranean coastal ecosystem functioning.

1 Introduction

The world's oceans surface temperature has increased since the last decades (IPCC 2019). Warming is expected to greatly affect plankton communities and their metabolic processes (Doney 2006). Indeed, an increase in temperature is known to have direct effects on plankton growth rates, as biological processes and enzyme activities are directly related to temperature following the Arrhenius' law. Hence, warming was shown to increase the growth rate of phytoplankton (Eppley 1972; Barton and Yvon-Durocher 2019) and bacteria (Rivkin et al. 1996). However, an increase in temperature is known to have indirect effects on phytoplankton as it also increases the abundance and activity of their grazers (Aberle et al. 2007; Rose and Caron 2007; Lewandowska et al. 2014), potentially resulting in a higher grazing pressure on primary and secondary producers. Moreover, warming can modify physical parameters of the water column, and thus alter the resource availability, which in turn controls plankton growth rates. It can change the composition of the plankton communities by favoring more adapted groups at the expense of others and by modifying the interactions among the organisms (Trombetta et al. 2020; Courboulès et al. 2021), leading to complex trophic cascades within the plankton food web (Vidussi et al. 2011).

Even if the ocean warming is occurring worldwide, it is not homogenous and some areas are more sensitive than others. Among these hot-spots, the Mediterranean Sea is considered as very sensitive to global warming (Lejeusne et al. 2010; Cramer et al. 2020), with a predicted increase of 3°C in sea surface temperature by the end of the century (Pörtner et al. 2019). In the Mediterranean Sea, it is known that warming can have important consequences on the planktonic community, and notably during the highly productive spring blooms (Vidussi et al. 2011; Pulina et al. 2016), but little is known about its effect during the other most productive season, fall. Notably, it is yet unsure if warming will have similar effects on the plankton communities as the ones identified during a spring bloom.

In a natural environment, the growth and the losses due to grazing, viral lysis and sedimentation are the main factors driving the fate of phytoplankton, and therefore of primary production (Calbet and Landry 2004). Therefore, it seems clear that estimating growth and loss rates is of prime interest when assessing the responses of phytoplankton to experimental warming, and in a broader scale to predict the effect of global warming on the ocean primary production. Traditional methods estimate growth and grazing rates using dilution experiments and are often tedious, time-consuming and labor-intensive, and might not be appropriate to apply in in situ experiments taking place in remote locations, as they rely on manual sampling. Moreover, they often only estimate microzooplankton grazing and are not used commonly to measure the total phytoplankton loss rate, while other factors than zooplankton grazing can be responsible of an important part in phytoplankton losses in certain systems (Fahnenstiel et al. 1995, Brussaard 2004).

On the other side, the use of high-frequency automated sensors to measure chlorophyll-*a* (chl-*a*) fluorescence, a proxy of phytoplankton biomass, its accumulation and losses over time, and finally, to estimate phytoplankton growth and loss rates, offers several advantages, especially as part of in situ mesocosm experiments. Data can be obtained in a non-invasive way for the organisms and for a long period of time, even if the mesocosms are not easily accessible. Moreover, sensors can monitor changes with a small timescale of less than a minute, which is not doable with manual sampling (Mills and Fones 2012). Nonetheless, estimating growth and mortality rates from sensor chl-*a* fluorescence measurement was rarely done (Neveux et al. 2003, 2010), and never in the frame of in situ mesocosm experiments to our knowledge.

We conducted two in-situ mesocosm experiments in the coastal Thau lagoon (Northwestern Mediterranean in the Southern coast of France) at two different seasons (spring and fall) of the same year (2018) to (1) assess how automated sensors can help to unravel the effects of warming on phytoplankton growth (μ) and losses (*l*) rates in the context of in situ mesocosm experiments, and (2) compare the responses toward warming of a coastal Mediterranean phytoplankton community during the productive seasons of spring and fall. In both in situ mesocosm experiments, replicate mesocosms were heated at +3°C above the natural ambient lagoon temperature and compared to other replicate mesocosms let at ambient natural lagoon temperature that served as controls. A new method based on high-frequency chl-*a* fluorescence data obtained with a set of sensors immersed at 1m depth in the mesocosms was implemented to estimate μ and *l*. These rates were compared to growth and grazing rates estimated multiple times during the spring experiment by performing dilution experiments, and to daily net changes of chl-*a* concentrations obtained with high performance liquid chromatography (HPLC). Moreover, the high-frequency sensor monitoring was combined to daily manual sampling to assess potential environmental drivers (such as nutrient availabilities) and phytoplanktonic major contributors (with the community composition assessed through pigment biomarkers) of the response of μ and *l* to warming.

2 Material and methods

2 1 *In situ* mesocosm experiments

Two in situ mesocosm experiments were carried out in 2018 in the Mediterranean coastal Thau Lagoon on the Mediterranean platform for Marine Ecosystem Experimental Research facilities (MEDIMEER: 43°24’53’’N, 3°41’16’’E). The first experiment was performed during 18 days in April 2018 and is referred as the Spring experiment hereafter, and the second experiment was performed during 18 days in October 2018 and is referred as the Fall experiment hereafter. Mesocosms consisted of 280 cm high and 120 cm wide cylindrical bags made of 200 μm-thick transparent vinyl acetate polyethylene film reinforced with nylon (Insinööritoimisto Haikonen Ky). They were covered by a transparent dome made of polyvinyl chloride and were moored individually to a floating pontoon. All the mesocosms were

simultaneously filled with 2200L of lagoon water screened through a 1000-µM mesh to remove large particles and organisms, resulting in a mesocosm water column of approx. 2 m. A more precise description of the mesocosm filling procedure is given in Courboulès et al. (2021). A pump (Rule, Model 360) was immersed at 1 m depth in the mesocosms to gently mix the water column, resulting in a turn-over rate of approximatively 3.5 d^{-1}, in order to prevent stratification.

The mesocosms were equipped with a set of automated sensors immersed at 1 m depth to measure at a high-frequency (one measurement every 15 min for the Spring experiment and one measurement every 1 min for the Fall experiment). Each set was composed of a fluorometer (ECO-FLNTU, Wetlabs) for chl-*a* fluorescence, an oxygen optode (Oxygen optode 3835, Aanderaa) for dissolved oxygen (DO) concentration, an electromagnetic induction conductivity sensor (Conductivity sensor 4319, Aanderaa) for conductivity, and three temperature probes (Thermistor probe 107, Campbell Scientific) for water temperature at three different depths (0.5, 1 and 1.5 m). Data from the chl-*a* fluorometer, the quantum sensor and from temperature probes were used in the present work.

2 2 Water temperature control in the mesocosms

In the Spring experiment, three mesocosms served as controls, but only two of them were equipped with sensors and were used for the present study (hereafter referred as C1-Spring and C2-Spring), and followed the same temperature as the lagoon, while three other mesocosms were warmed at +3°C compared to the in situ lagoon temperature and to the controls, but similarly only two of them were equipped with sensors and were used for the present study (hereafter referred as T1-Spring and T2-Spring). In the Fall experiment, three mesocosms were used as controls and equipped with sensors (hereafter referred as C1-Fall, C2-Fall, C3-Fall) and three mesocosms were warmed at +3°C and equipped with sensors (T1-Fall, T2-Fall, T3-Fall). The heating procedure enabled to constantly adjust a 3°C increase in temperature in the warmed mesocosms to precisely follow the natural temperature variations of the lagoon and of the controls, as described precisely and in details in previous studies (Nouguier et al. 2007; Vidussi et al. 2011).

2 3 Daily Light Integral (DLI) from high-frequency PAR measurements

The Daily Light Integral, which is the quantity of photons available for photosynthesis received in a 1 m^2 surface over a 1d period, was estimated using high-frequency PAR measurements measured at 2 m above the surface with a Quantum SKP 215 PAR sensor (Skye Instruments) placed next to the mesocosms on the pontoon, with the following equation (Eq. 1):

$$DLI = \frac{mean\ PAR * day\ length * 3600}{1 * 10^6} \qquad \text{Eq 1.}$$

with the DLI expressed in mol m^{-2} d^{-1}, the mean PAR between sunrise and sunset expressed as µmol m^{-2} s^{-1}, and the day length, which is the duration between sunrise and sunset, expressed in hr.

2 4 Nutrient analyses

Dissolved nutrient concentrations were measured daily with the same protocol for both experiments. In this regard, water was sampled from each mesocosm at 1 m depth every morning using a 5 L Niskin water sampler. The samples (50 mL) were then taken from the Niskin water sampler and put in acid-washed polycarbonate bottles. Directly after, they were filtered with 0.45 µm filters (Gelman) and using a low-vacuum pump, before being stored at -20°C until further analyses. Dissolved nutrients (ammonium (NH_4^+), nitrate (NO_3^-), nitrite (NO_2^-), orthophosphate (PO_4^{3-}) and silicate (SiO_2)) concentrations were then determined using a colorimeter (Skalar Analytical).

2 5 Phytoplankton pigment composition

The phytoplankton pigment composition was assessed every day for both experiments. To do so, samples were taken from each mesocosm at 1 m depth every morning using a 5 L Niskin water sampler. Every sample (from 800 to 1500 mL of water) was then directly filtered at low ambient light on a glass-fiber filter (Whatman GF/F, 25 mm diameter, 0.7 µm nominal pore size) using a low-vacuum pump, and then frozen at -80°C until further analyses. The pigment extraction consisted in two steps. First, the filters were put in 2 mL of 95% ethanol and stored at -20°C for 1 h. Then, filters were sonicated and stored at -4°C for 1 h. Finally, the extracts were clarified on a glass-fiber filter (Whatman GF/F). The extracts were then directly analyzed through HPLC (Waters), following the method of Zapata et al. (2000) and the detailed protocol in Vidussi et al. (2011).

Some pigments can be used as taxonomic biomarkers, as they are representative of particular phytoplankton groups (Vidussi et al. 2000; Vidussi et al. 2001). In the present study, the pigment biomarkers and their taxonomic attribution, from the literature, are presented in the following table (Table 1). Other pigments were also identified, but as there are ubiquitous and present in multiple groups, they were not assigned to one specific phytoplankton group.

Table 1. **Summary table of the main pigment used as taxonomic biomarkers in the present study**, and their taxonomic attribution following Vidussi et al. (2001) and Roy et al. (2011).

Pigment	Taxonomic attribution
Chlorophyll-*b* (Chl-*b*)	Green algae
Prasinoxanthin	Prasinophytes
Fucoxanthin	Diatoms
Zeaxanthin	Cyanobacteria
19'-hexanoyloxyfucoxanthin (19'-HF)	Prymnesiophytes
Peridinin	Dinoflagellates

2 6 High-frequency chl-*a* fluorescence data acquisition, calibration and correction

First, the raw fluorescence data were systematically transformed into µg chl-*a* L^{-1} (hereafter referred as to µg L^{-1}) following the manufacturer's recommendations. Each chl-*a* fluorometers was calibrated using an algae monoculture for which the chl-*a* concentrations were measured with high performance liquid chromatography (HPLC). More precisely, for the Spring experiment, the calibration was performed with *Dunaliella tertiolecta* (Dunaliellaceae), with 6 chl-*a* concentration points, ranging from 0 to 10 µg L^{-1}. For the Fall experiment, the fluorometers were calibrated with a culture of *Tetraselmis chui* (Chlorodendraceae) and with 5 chl-*a* concentration points, ranging from 0 to 12.7 µg L^{-1}. After the raw chl-*a* fluorescence data were corrected with the calibration coefficients, then they were additionally corrected using the daily chl-*a* concentration measured by HPLC from samples taken in every mesocosms once a day at 09:00. Finally, the chl-*a* fluorescence data was corrected for non-photochemical quenching (NPQ), as a strong decrease in chl-*a* fluorescence was found to occur in almost all daily chl-*a* cycles during sunlight hours. To account for NPQ, chl-*a* fluorescence data was linearly interpolated between sunrise and sunset (Li et al. 2008). This interpolation could be done because the assumption of spatial homogeneity in the phytoplankton community inside each mesocosm was made due to the use of a pump gently mixing the water column of each mesocosm (Carberry et al. 2019).

2 7 Phytoplankton growth and loss rates estimations using high-frequency sensor data

The phytoplankton growth (µ) and loss (l) rates were estimated using the corrected chl-*a* fluorescence data, and with a method following similar principles as in Neveux et al. (2003, 2010). To do so, each daily chl-*a* cycle was separated in two different parts: the first period, which starts from sunrise until when the fluorescence maximum is attained (generally a few hours after sunset) and which is called hereafter the "increasing period", and the second period, from when the fluorescence maximum is attained until the following sunrise. This latter period called hereafter the "decreasing period" is a part of the night as the maximum chl-*a* fluorescence always occurred several minutes to a few hours after sunset. For each period, an exponential regression was performed using the chl-*a* fluorescence as y and the time as x, and following the formula (Eq. 2):

$$F_{chla} = a * e^{bt} \qquad \text{Eq 2.}$$

with F_{chla} the chl-*a* fluorescence (µg L^{-1}), a (µg L^{-1}) and b (min^{-1}) some constants, and t the time (min). Following Siegel et al. (1989) and Neveux et al. (2003), as there is no growth during the night, and as mesocosms are enclosed systems continuously mixed, the changes in F_{chla} are assumed to be only due to l at night, and so during the "decreasing period". Therefore, during the "decreasing periods", $b = l$, with l in min^{-1}, and during the "increasing periods", $b = \mu - l$. Then, µ (min^{-1}) was calculated as (Equation 3):

$$\mu = (\mu - l) + l \qquad \text{Eq 3.}$$

Finally, l and μ were converted into hr^{-1} by multiplying by 60, to get hourly rates. Then, hourly l rates were multiplied by 24 to get daily rates (d^{-1}) as we assumed that losses occurred during the entire 24-hr period, and hourly μ rates were multiplied by the duration of the increasing period, in hours, as growth only occurred during the increasing period (Neveux et al. 2003).

Moreover, the daily net chl-*a* fluorescence change was calculated in order to be compared with the daily net chl-*a* concentration change obtained with HPLC values. As HPLC samples were obtained every day from 09:00 to 10:00, the daily net chl-*a* fluorescence change was calculated using the high-frequency chl-*a* fluorescence data only from 09:00 to 10:00. For each day, it was calculated as Eq. 4:

$$r_n = \frac{1}{t} * \log\left(\frac{F^{sensor} chla_n}{F^{sensor} chla_{n-1}}\right) \qquad \text{Eq 4.}$$

with r_d, the daily net chl-*a* fluorescence change (d^{-1}) on day n, t the time (in d, which was equal to 1 day most of the time), $F^{sensor} chla_n$ the mean chl-a fluorescence from 09:00 to 10:00 (μg L^{-1}) on day n, and $F^{sensor} chla_{n-1}$ the mean chl-*a* fluorescence from 09:00 to 10:00 (μg L^{-1}) on day n-1. Similarly, the daily net chl-*a* concentration change obtained with the HPLC values was calculated as Eq. 5:

$$r_n^* = \frac{1}{t} * \log\left(\frac{C^{HPLC} chla_n}{C^{HPLC} chla_{n-1}}\right) \qquad \text{Eq 5.}$$

with r_d^*, the daily net chl-*a* concentration change (d^{-1}) on day n, t the time (in d, which was equal to 1 day most of the time), $C^{HPLC} chla_n$ the mean chl-*a* concentration obtained with HPLC (μg L^{-1}) on day n, and $C^{HPLC} chla_{n-1}$ the mean chl-*a* concentration obtained with HPLC (μg L^{-1}) on day n-1.

2 8 Phytoplankton growth and grazing rates estimations using the dilution method

To compare growth and mortality rates obtained with the chl-*a* fluorescence data, growth and grazing rates were assessed 5 times during the Spring experiment on d5, d7, d9, d11 and d13 in the C3-Spring and T1-Spring mesocosms, and 2 times during the Fall experiment (d2, d8) in all six mesocosms. Growth and grazing rates were measured using the two-points modified version of the original dilution method of Landry and Hassett (1982). This method consists of two levels of dilution: 100% and 10% (Worden and Binder 2003; Chen 2015). Mesocosm water (20 L) was sampled using a low-vacuum pump and screened on a 200 μm mesh. Triplicate Whirlpack bags (2 L) were then filled with this sampled water and constituted the 100% dilution level. Another triplicate of Whirlpack bags (2 L) were filled with the same sample water but were enriched with inorganic nutrients (final concentrations of 4 μM N, 0.25 μM P, and 4 μM Si), constituted the 100%+Nut dilution level, and were used to evaluate a

potential nutrient limitation in the dilution bags. Finally, another part of the sampled water was filtered on 0.8 and then on 0.2 µm (Whatman Polycap TC filter capsule, 0.8/0.2 µm). This 0.2 µm filtered water was mixed with the 200 µm screened water with a proportion of 90:10 to reach the 10% dilution level. Triplicate Whirlpack bags (2 L) were then filled with this 10% diluted water. Then, all the bags were incubated for 24 h in incubation mesocosms, which consisted of two additional mesocosms (one control and one warmed: Incubation mesocosms) which were located next to the main mesocosms. For each mesocosm, 1 L of the 200 µm screened water was sampled before the incubation and constituted the T0, and 500 to 1800 mL were sampled from every bag after the 24 h incubation, constituting the T24. These samples were then filtered through a glass-fiber filter (Whatman GF/F, 25 mm diameter, 0.7 µm nominal pore size) using a low-vacuum pump, and then frozen in liquid nitrogen before being kept at -80°C until further analyses. The chl-*a* concentration was then measured for each T0 and each T24 samples with HPLC and following the protocol detailed in the previous section. For the 100% and 10% level bags, instantaneous growth was calculated with the following equation (Landry and Hassett 1982) (Eq. 6):

$$k = \frac{1}{t} * \log(\frac{Cchla_{T24}}{Cchla_{T0}}) \qquad \text{Eq 6.}$$

with k the instantaneous growth rate (d^{-1}), t the time (d), $Cchla_{T24}$ and $Cchla_{T0}$ the chl-*a* concentration at T24 and T0 ($\mu g\ L^{-1}$), respectively. Then, the growth rate was considered equal to the instantaneous growth rate in the 10% bags, and the grazing rate equal to the growth rate in the 10% bags minus the growth rate in the 100% bags (Worden and Binder 2003; Chen 2015; Courboulès et al. 2021).

2 9 Statistical analyses

To test the effect of warming on daily time series of DLI, nutrient concentrations, pigment concentrations, and µ and *l*, one-way variance analyses of repeated measures (RM-ANOVA) were performed with treatment as fixed factor and time as repeated random factor. *P*-values below or equal to 0.05 were considered as representative of a significant effect of the treatment. RM-ANOVAs were performed on the entire experiments time series, as well as on shorter periods when a specific trend for certain variables was observed and explained in the text. When the normality and the homoscedasticity assumptions of the RM-ANOVA were not met, even after logarithmic, exponential or square-root data transformation, a non-parametric Kruskal-Wallis test was performed instead. To compare the warming effect magnitude between the Spring and the Fall experiments, Cohen's *d* effect sizes were calculated using the mean values of certain parameters. The Cohen's *d* effect size (Cohen 1977) was calculated as the difference between the mean values in the warmed and in the control treatments, divided by a pooled standard deviation. The effect of warming was considered as very small if the Cohen's *d* was higher than |0.01|, small if it was higher than |0.2|, medium if it was higher than |0.50|, large if it was higher

than |0.80|, and very large if it was higher than |1.2| (Cohen 1977). Moreover, to assess the principal drivers of the nutrient concentrations, DLI, pigment concentrations, and μ and *l* responses to warming, ordinary least squares linear relationships were assessed using the effect of warming expressed as the log response ratio (LRR). Ordinary least squares linear relationships and one-way ANOVA were also performed to test the linear relationship and to compare the daily net chl-*a* fluorescence change obtained using the sensors data with the daily net chl-*a* concentration change obtained using HPLC data, the growth rate obtained using the sensor with that obtained with dilution experiments, and the loss rate obtained using the sensor with the grazing rate obtained with dilution experiments. When the normality and the homoscedasticity assumptions of the ANOVA were not met, a non-parametric Kruskal-Wallis test was performed instead. All the data management and the statistical analyses were performed using the R software (R-Project, version 4.0.1).

3 Results

3 1 Physical and chemical conditions

As expected, the experimental warming procedure enabled to significantly enhance the water temperature in the warmed compared to the control treatment by in average 2.87 ± 0.20 °C in the Spring experiment and by in average 3.04 ± 0.08 °C in the Fall experiment (Fig 1, Table 2). The average temperature in the control treatment was 14.84 ± 0.03 °C and 19.01 ± 0.02 °C in the Spring and Fall experiments, respectively. It increased from d10 until the end of the experiment in the Spring experiment, while it stayed relatively constant during the Fall experiment.

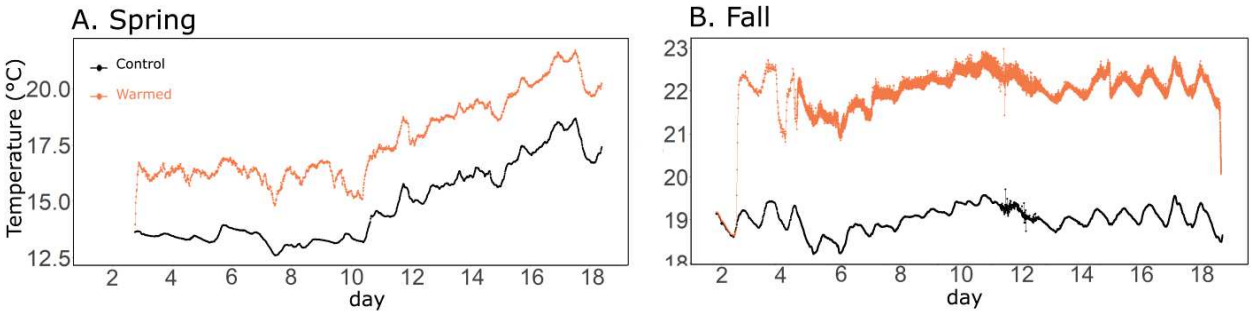

Figure 1: **High-frequency water temperature in the control (black) and warmed (orange) treatments during the Spring (A) and Fall (B) experiments**. In the Spring experiment, water temperature was measured every 15 min and, in the Fall experiment, every 1 min. Data from d1 and d2 are missing in the Spring experiment due to technical difficulties.

The Daily Light Integral (DLI) was relatively similar during the Spring and the Fall experiments, with average values of 25.26 ± 9.84 and 26.04 ± 10.44 mol m^{-2} d^{-1}, respectively (Fig 2). During the Spring experiment, the highest (40.84) and the lowest (7.34) values were attained on d0 and d9, respectively.

During the Fall experiment, the highest (35.54) and the lowest (3.98) values were attained on d12 and d6, respectively.

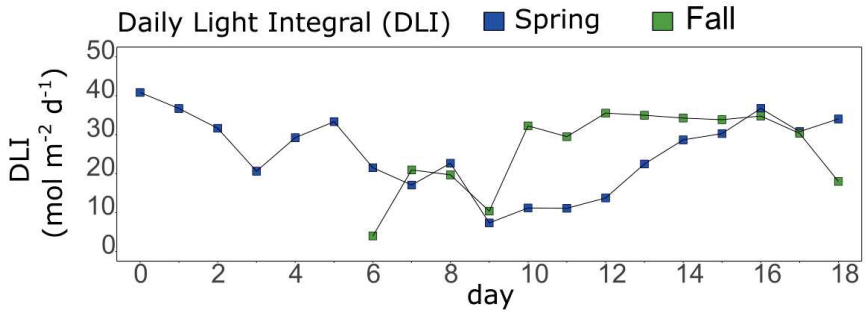

Figure 2: **Daily Light Integral (DLI) obtained from high-frequency photosynthetically active radiation measurements during the Spring (blue) and Fall (green) experiments**. Data from d0 to d5 are missing in the Fall experiment due to technical difficulties.

Nutrient concentrations were measured daily in all mesocosms (Fig 3A, B, Table 2). In the controls, ammonium (NH_4^+) concentrations were higher in the Spring than in the Fall experiment (0.45 ± 0.08 µM, and 0.41 ± 0.05 µM, respectively). The only statistically significant difference between ammonium concentrations in the control and warmed mesocosms was found at the end of the Fall experiment, with ammonium concentrations reaching 0.58 ± 0.23 µM on average between d11 and d17 in the warmed mesocosms, while staying rather low (0.21 ± 0.09 µM, d11 – d17) in the control mesocosms. In contrast, ammonium concentrations were not significantly different between control and warmed mesocosms for the Spring experiment (Table 2). Overall, concerning ammonium concentrations, Cohen's *d* effect size was larger during the Fall experiment.

Generally, the nitrates + nitrites (NO_3^- + NO_2^-) concentrations were higher during the Spring experiment compared to the Fall experiment (0.71 ± 0.08 µM and 0.23 ± 0.02 µM on average in the controls, respectively). Moreover, warming had a different effect depending on the experiment. In Spring, nitrates + nitrites concentrations were significantly higher in the warmed mesocosms from d8 until the end of the experiment (Fig 3C, D, Table 2), with an average difference of 540.5% between warmed and control mesocosms, which corresponds to a very large effect of warming. In contrast, nitrates + nitrites concentrations were significantly lower in the warmed compared to the control mesocosms for the entire Fall experiment, with an average 20.4% difference and a medium effect size.

Similarly to nitrate + nitrite concentrations, orthophosphate (PO_4^{3-}) concentrations (Fig 3E, F, Table 2) were higher during the Spring than during the Fall experiment (0.55 ± 0.07 µM and 0.17 ± 0.01 µM on average in the controls, respectively). They were negatively affected by warming during the entire Spring experiment, by an average of 9.3%. However, the largest negative effect of warming was found at the end of the Fall experiment, with a decrease by an average of 16.7% between d15 and d17.

In contrast to the other nutrient concentrations, the silicate (SiO_2) concentrations (Fig 3G, H, Table 2) were on average lower during the Spring experiment compared to the Fall experiment (3.31 ± 0.18 µM and 10.42 ± 0.15 µM on average in the controls, respectively). Warming had a very large positive significant effect during the second part of the Spring experiment (from d10 to d17), with concentrations being in average 27.8% higher in the warmed than in the control mesocosms. On the contrary, the strongest effect of warming on silicate concentrations was found at the end of the Fall experiment, when silicate concentrations were significantly lower in the warmed mesocosms by an average of 10.8% from d15 to d17.

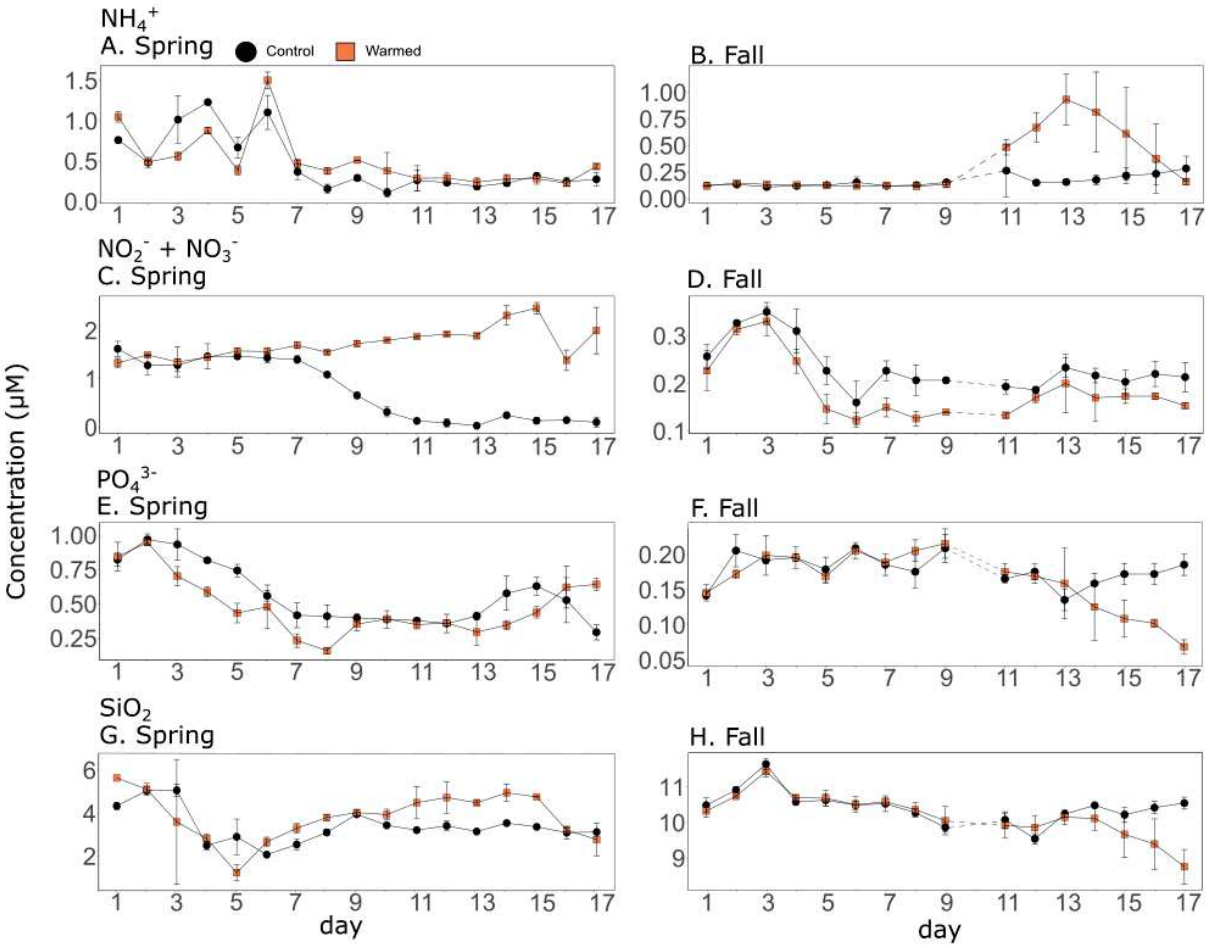

Figure 3. **Ammonium (NH_4^+, A.), nitrates (NO_3^-+NO_2^-, B.), silicate (SiO_2, C.) and orthophosphate (PO_4^{3-}, D.) concentrations over the course of the Spring (A., C., E., G.) and the Fall (B., D., F., H.) experiments** in the control (black) and the warmed (orange) treatments. Dotted lines represent the missing data on d10 in the Fall experiment due to bad weather conditions. For the Spring experiment, figures start at d2 to match with growth and mortality rates which could only be estimated from d2 to d17.

Table 2. **Summary table of the *p*-values obtained with the RM-ANOVA comparing physical parameters and nutrient concentrations in the warmed and in the control mesocosms**. When the assumptions for a parametric test were not met, despite transforming the data, a Kruskal-Wallis test was used instead. *P*-values lower than 0.05 were considered as significant and are indicated in bold in the table. Large and very large Cohen's d effect sizes were also indicated in bold. Tests were performed only from d2 for the Spring experiment as warming reached +3°C at d2.

Experiment	Variable	Period	*P*-value	Cohen's d
Spring	Temperature	2-17	**$<1.0 \times 10^{-4}$** ($F_{1,16}$=3180)	**1.62**
	NH_4^+	2-17	0.29 (KW)	0.07
	NO_3^-+NO_2^-	2-17	**2.1×10^{-5}** (KW)	**2.06**
		8-17	**1.6×10^{-5}** (KW)	**4.91**
	PO_4^{3-}	2-17	**0.04** ($F_{1,14}$=5.1)	-0.47
		2-10	**4.4×10^{-3}** ($F_{1,8}$=15.3)	-0.62
	SiO_2	2-17	0.19 ($F_{1,14}$=1.9)	0.36
		10-17	**0.03** (KW)	**1.53**
Fall	Temperature	1-17	**1.8×10^{-7}** (KW)	**4.66**
	NH4+	1-17	0.55 (KW)	0.78
		11-17	**0.01** (KW)	**1.93**
	NO_3^-+NO_2^-	1-17	**8.0×10^{-3}** (KW)	**-0.82**
	PO_4^{3-}	1-17	0.37 (KW)	-0.47
		15-17	**0.04** (KW)	**-5.18**
	SiO_2	1-17	0.09 ($F_{1,15}$=3.1)	-0.42
		15-17	**0.04** (KW)	**-3.21**

3 2 Effects of warming on phytoplankton: chlorophyll-*a* fluorescence, μ and *l* rates derived from sensor data, and pigment composition

In the Spring experiment, the daily chl-*a* fluorescence was on average 5.28 ± 0.21 µg L^{-1} in the control mesocosms (Fig 4A, B). It displayed a bloom-like dynamic: it increased from d2 to d10, attaining its maximum value on d10 (8.62 ± 0.15 µg L^{-1}), before decreasing until the end of the experiment. In the Fall experiment, the average daily chl-*a* fluorescence was on average lower than in the Spring experiment (4.30 ± 0.59 µg L^{-1}) (Fig 4C, D), and displayed a relatively flat dynamic during the entire experiment, with a maximum value on d8 (5.53 ± 0.58 µg L^{-1}).

Warming significantly reduced the chl-*a* fluorescence in both experiments (Table 3), by an average of 69.5% from d5 until the end of the Spring experiment, and by an average of 31.7% from d8 until d15 in the Fall experiment. Conversely, warming significantly enhanced it at the beginning of the Fall experiment, by an average of 19.4% between d2 and d6. Generally, the effect magnitude was larger in Spring than in Fall experiment (Table 3).

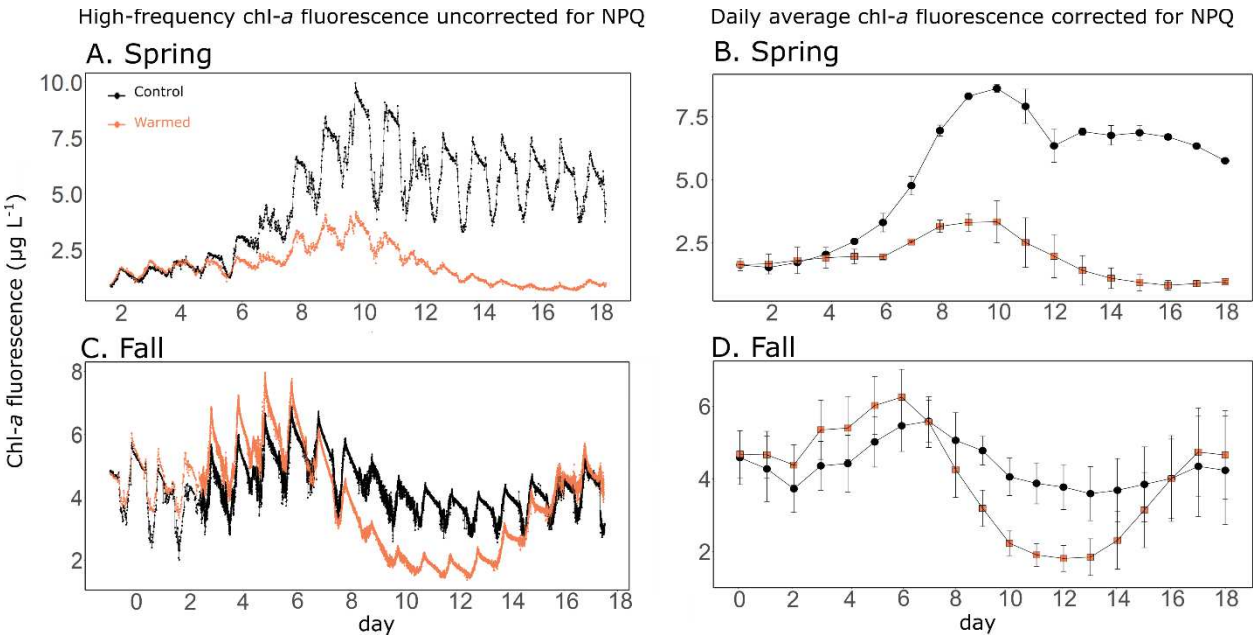

Figure 4. **High-frequency chlorophyll-*a* fluorescence data, uncorrected for NPQ**, measured with the sensors during the Spring (A.) and the Fall (C.) experiments, and **daily average chlorophyll-*a* fluorescence** during the Spring (B.) and Fall (D.) experiments, in the control (black) and warmed (orange) treatments.

In the control treatment, µ was higher in the Spring than in the Fall experiments, with average values of 0.44 ± 0.04 d^{-1} and 0.32 ± 0.05 d^{-1} respectively (Fig 5A, B). During both experiments, the maximum µ was attained during the first half of the experiment, on d7 (0.99 ± 0.01 d^{-1}) in the Spring and on d4 (0.61 ± 0.03 d^{-1}) in the Fall experiment. Moreover, for both experiments, warming enhanced µ by an average of 18.3% and 28.1% over the entire Spring and Fall experiments, respectively, and by an average of 56.8% and 50.9% from d8 until the end (Table 3). The effect size was larger for the Fall experiment compared to Spring (Table 3). In addition, during the Spring experiment, warming significantly reduced µ during the first part of the experiment (d2-d7), with a 18.8% difference on average between treatments.

In contrast to µ, *l* was on average almost similar in the Spring experiment compared to Fall, with average values of 0.39 ± 0.04 d^{-1} and 0.40 ± 0.07 d^{-1} in the controls of the Spring and the Fall experiments, respectively (Fig 4C, D). During the Spring experiment, warming had a positive effect on *l* with an average difference of 37.1% and 59.1% between treatments over the entire experiment and from d8 to d17, respectively. This positive effect was larger than the positive effect found for µ. During the Fall experiment, the effect size of warming was not as large, and *l* was significantly higher in the warmed treatment only at the middle of the experiment, by 20.4% on average from d7 to d11.

In the control treatment in Spring, µ was higher than *l* during the first part of the experiment (d2-d9), before being lower for the rest of the experiment (d10-d17). Warming significantly lowered the µ : *l*

ratio by an average of 28.9% during the first half (d3- d8) of the experiment (Fig 4E, Table 3), while no significant effect was found for the rest of the experiment. In the control treatment in Fall, the μ : *l* ratio was generally lower than in Spring (Fig 5B). In this experiment, warming increased significantly this ratio by an average of 92.9% during the second half of the experiment (d11-d17, Table 3).

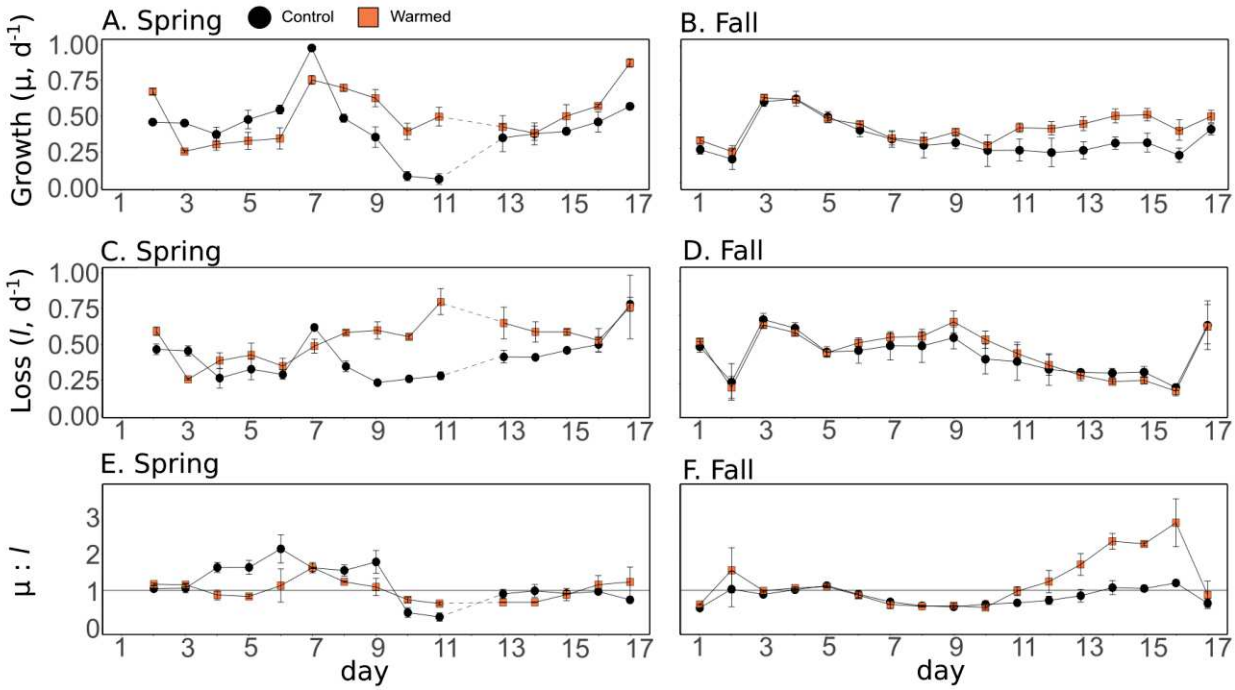

Figure 5. **Growth rate (μ, A, B), loss rate (*l*, C, D) and μ : *l* ratio (E, F)** estimated using the sensor data over the course of the Spring (A, C, E) and the Fall (B, D, F) experiments in the control (black) and the warmed (orange) treatments. In the Spring experiment, μ and *l* could not be estimated on d1 and d12 and, for the later, the missing data are represented in dotted lines.

Table 3. **Summary table of the *p*-values and the F-values obtained with the RM-ANOVA comparing the chl-*a* fluorescence, μ and *l* in the warmed and in the control treatments** over the entire Spring and Fall experiments or over specific periods defined after trends observed in the data. Associated Cohen's *d* effect sizes are also indicated. When the assumptions for a parametric test were not met, despite transforming the data, a Kruskal-Wallis test was used instead and indicated by KW in brackets. *P*-values lower than 0.05 were considered as significant and are indicated in bold in the table. Large and very large Cohen's *s* d effect sizes were also displayed in bold.

Experiment	Variable	Period	*P*-value	Cohen's *d* effect size
Spring	chl-*a*	2-17	**$< 1 \times 10^{-4}$** ($F_{1,17}$=29.4)	**-1.84**
		5-17	**$< 1 \times 10^{-4}$** ($F_{1,17}$=51.5)	**-3.03**
	μ	2-17	0.17 ($F_{1,14}$=2.1)	0.41
		2-7	0.2 (KW)	-0.49
		8-17	**2.3×10^{-3}** ($F_{1,8}$=19.3)	**1.22**
	l	2-17	**0.01** ($F_{1,14}$=8.3)	**0.92**
		8-17	**4.1×10^{-3}** (KW)	**1.62**
	μ : *l*	2-17	0.19 ($F_{1,14}$=1.9)	-0.39
		3-8	**0.046** ($F_{1,5}$=6.1)	**-1.46**
Fall	chl-*a*	2-18	0.15 ($F_{1,15}$=2.3)	-0.37
		2-6	**2×10^{-4}** ($F_{1,4}$=163.6)	**1.27**
		8-15	**1×10^{-4}** ($F_{1,7}$=72.1)	**-2.07**
	μ	2-17	**3×10^{-4}** ($F_{1,15}$=22.2)	0.78
		11-17	**2.7×10^{-3}** (KW)	**3.01**
	l	2-17	0.55 ($F_{1,15}$=0.38)	0.05
		7-11	**0.01** ($F_{1,4}$=32.7)	**1.15**
	μ : *l*	2-17	0.1 (KW)	0.78
		11-17	**1.6×10^{-3}** ($F_{1,6}$=29.9)	**1.55**

The phytoplankton pigment composition was found to be different between the Spring and the Fall experiments (Fig 6). In the Spring experiment, the main pigments were the Prymnesiophyte-associated pigment 19'-HF and the diatom-associated pigment fucoxanthin (with a mean concentration in the controls of 2.91 ± 0.14 μg L^{-1} and 1.14 ± 0.10 μg L^{-1}, respectively). Additionally, other pigments were present in rather high concentrations, such as the dinoflagellate-associated pigment peridinin (0.18 ± 0.01 μg L^{-1}), the green algae-associated pigment Chl-*b* (0.14 ± 0.01 μg L^{-1}), the cyanobacteria-associated pigment zeaxanthin (0.08 ± 0.01 μg L^{-1}), and the Prasinophyte-associated pigment prasinoxanthin (0.06 ± 0.01 μg L^{-1}).

In the Fall experiment, the dominant pigments were the cyanobacteria-associated pigment zeaxanthin (with an average concentration in the controls of 1.78 ± 0.22 μg L^{-1}), the diatom-associated pigment fucoxanthin (1.07 ± 0.27 μg L^{-1}), the green algae-associated pigments Chl-*b* (0.69 ± 0.14 μg L^{-1}), and the Prymnesiophyte-associated pigment 19'-HF (0.68 ± 0.16 μg L^{-1}). Among the main pigments found during the Spring experiments, peridinin, and prasinoxanthin were not found or found in negligible concentrations during the Fall experiment, while lutein was found during the Fall experiment but not during the Spring experiment.

Warming had a different effect on the pigment concentrations regarding the experiment and the pigment considered (Table 4). In the Spring experiment, warming had a large and significant negative effect on 19'-HF and zeaxanthin concentrations, which concentrations were decreased by on average 75.4% and 75.2%, respectively. Conversely, warming had a medium significant positive effect on the peridinin concentration which was enhanced by in average 101%.

In the Fall experiment, warming had a large significant positive effect, especially during the second part of the experiment, on the fucoxanthin concentration, which was increased by in average 210.7% between d13 and the end of the experiment. On the contrary, Chl-*b* concentration was significantly lowered by in average 19.5%. In addition, the zeaxanthin concentration was also significantly lowered at the middle of the experiment by an average of 43.4% from d11 to d15.

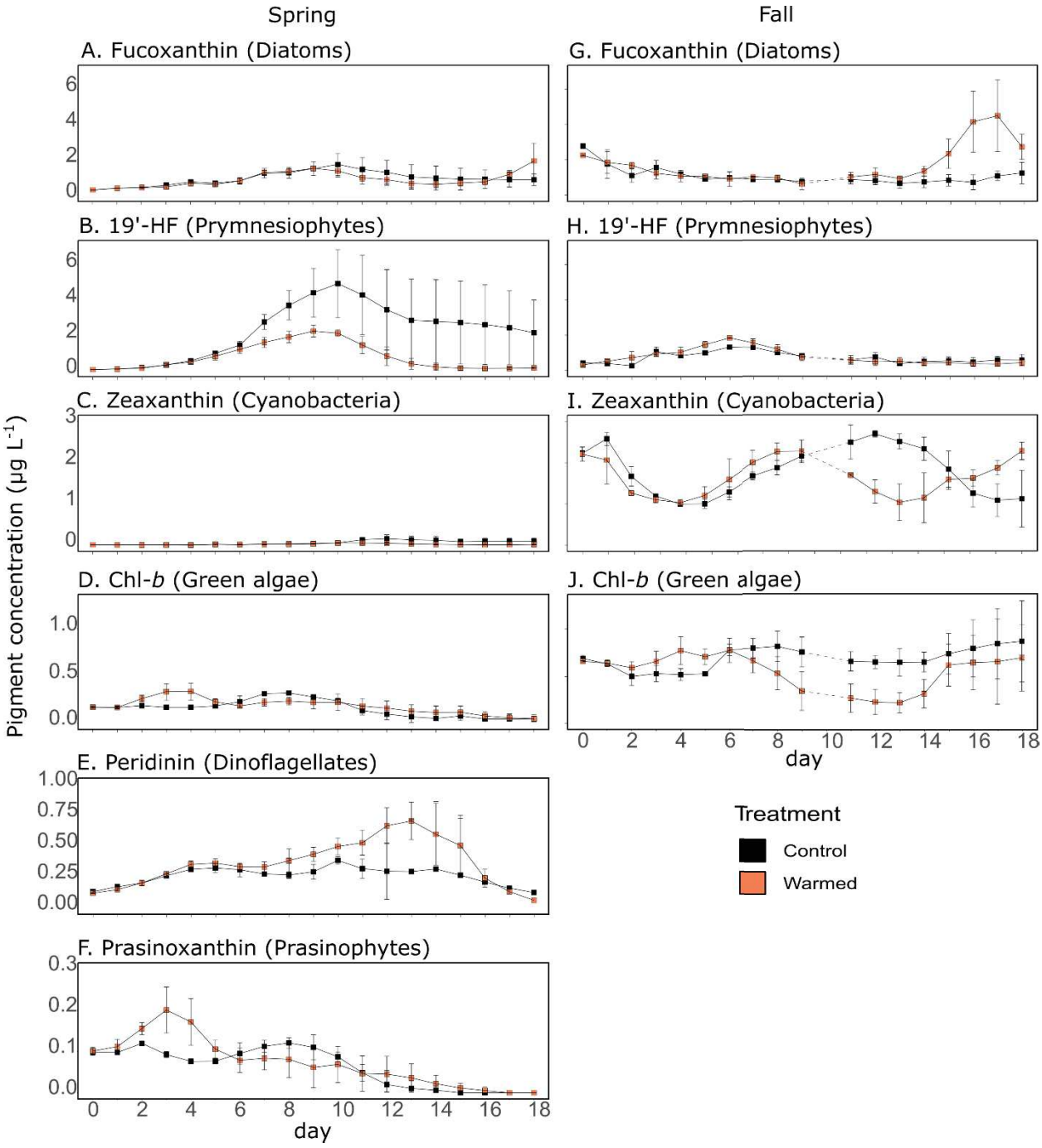

Figure 6. **Daily pigment concentrations (µg L^{-1}) in the control (black) and warmed (orange) treatments for the Spring (A-F) and the Fall (G-J) experiments**. Dotted lines represent the missing data on d10 in the Fall experiment due to bad weather conditions. A,G: Fucoxanthin; B,H: 19'-Hexanoyloxyfucoxanthin; C,I: Zeaxanthin; D,J: Chlorophyll-*b*; E: Peridinin, and F: Prasinoxanthin.

Table 4. **Summary table of the *p*-values and the F-values obtained with the RM-ANOVA comparing the chl-*a* fluorescence, the growth and mortality rates in the warmed and in the control treatments** over the entire Spring and Fall experiments or over specific periods defined after trends observed in the data. Associated Cohen's *d* effect sizes are also indicated. When the assumptions for a parametric test were not met, despite transforming the data, a Kruskal-Wallis test was used instead and indicated by KW in brackets. *P*-values lower than 0.05 were considered as significant and are indicated in bold in the table. Large and very large Cohen's *s* d effect sizes were also displayed in bold. Tests were performed only from d2 to d18 for the Spring experiment as warming reached +3°C from d2.

Experiment	Pigment	Period	*P*-Value	Cohen's *d* effect size
Spring	19'-HF	2-18	**4.1×10^{-4}** (KW)	**-1.45**
	Fucoxanthin	2-18	0.45 ($F_{1,16}$=0.59)	-0.17
	Zeaxanthin	2-18	**0.01** (KW)	**-1.2**
	Chl-*b*	2-18	0.13 ($F_{1,16}$=2.5)	0.31
	Peridinin	2-18	**4.3×10^{-3}** ($F_{1,16}$=11.2)	**0.87**
	Prasinoxanthin	2-18	0.35 ($F_{1,16}$=0.9)	0.16
	19'-HF	1-18	0.82 ($F_{1,17}$=0.05)	0.15
	Fucoxanthin	1-18	**0.01** (KW)	0.72
		13-18	**5.6×10^{-3}** ($F_{1,5}$=21.7)	**1.73**
	Zeaxanthin	1-18	0.52 (KW)	-0.25
		11-15	**0.01** ($F_{1,5}$=19.6)	**-3.35**
		15-18	0.17 ($F_{1,5}$=3.1)	**1.54**
	Chl-*b*	1-18	**0.04** (KW)	**-0.85**

To highlight potential relations between phytoplankton processes, environmental variables and phytoplankton community composition, ordinary least squares linear relationships were assessed between the effect of warming, expressed as the logarithmic response ratio, on μ and the effect on *l*, nutrient concentrations and pigment concentrations. Only significant relationships for at least one experiment are displayed on Fig 7. A significant positive linear relationship was found between the effects of warming on μ and *l*. Moreover, the effect on μ was positively and linearly related to the effect on temperature, on ammonium, nitrate and nitrite concentrations. A positive relationship was also found with the effect on nitrate + nitrite concentrations but only for the Fall experiment.

In the Spring experiment, the effect on μ was not significantly related to the effect on any pigment concentrations. In the Fall experiment, the effect on μ was significantly and positively linearly related with the effect on the diatom-associated pigment fucoxanthin, while significant negative relationships were found with the green algae-associated pigment Chl-*b* and the cyanobacteria-associated pigment zeaxanthin.

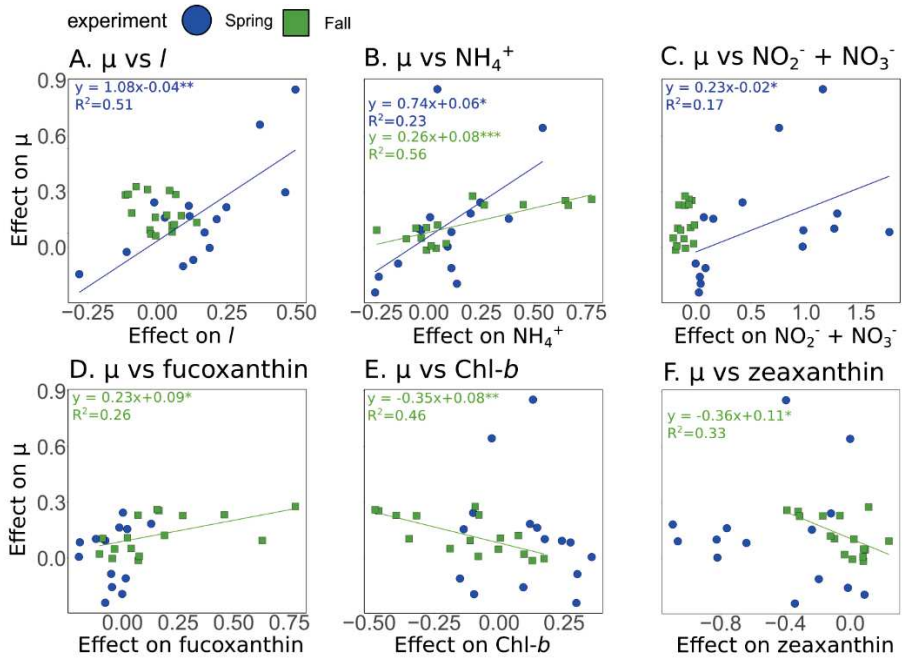

Figure 7. **Ordinary least squares linear relationships between the effect of warming, expressed as the log response ratio, on μ and the effect of warming on *I* (A), nutrient concentrations (B, C), and pigment concentrations (D-G.) for the Spring (blue circles) and Fall (green squares) experiments**. Relationships were assessed for each experiment individually: when the relationship was significant ($p<0.05$), solid blue lines represent the linear least square fit for the Spring experiment, and solid green lines represent the linear least square fit for the Fall experiment.

3 3 Comparisons between μ and *I* estimated using the chl-*a* fluorescence sensor data and those obtained using traditional techniques

Sensor-obtained μ and *I* were compared with growth and grazing obtained with the dilution method during the Spring and the Fall experiments (Fig 8A-D). A significant linear relationship ($R^2 = 0.19$, $p = 0.04$) was found between sensor-obtained and dilution-obtained growth estimates (Fig 8A). Sensor-obtained μ were on average 20% higher than dilution-obtained growth estimates, however this difference was not statistically significant (Kruskal-Wallis, $p = 0.44$) (Fig 8B). Conversely, no significant linear relationship was found between sensor-obtained *I* and dilution-obtained grazing rates (Fig 8C). The sensor-obtained *I* was not significantly lower by an average of 2% than dilution-obtained grazing (Kruskal-Wallis, $p = 0.98$) (Fig 8C). Finally, the daily net change in chl-*a* fluorescence obtained with the sensors was compared with the daily net change of chl-*a* concentration measured by HPLC from daily sampling (Fig 8E, F). A significant linear relationship ($R^2 = 0.37$, $p = 3.8 \times 10^{-15}$) was found between sensor-obtained daily net change and HPLC-obtained daily net change (Fig 8E). Sensor-obtained daily net change was not significantly different from the HPLC-obtained one (ANOVA, $p = 0.71$, $F_{1,135} = 0.135$) (Fig 8F).

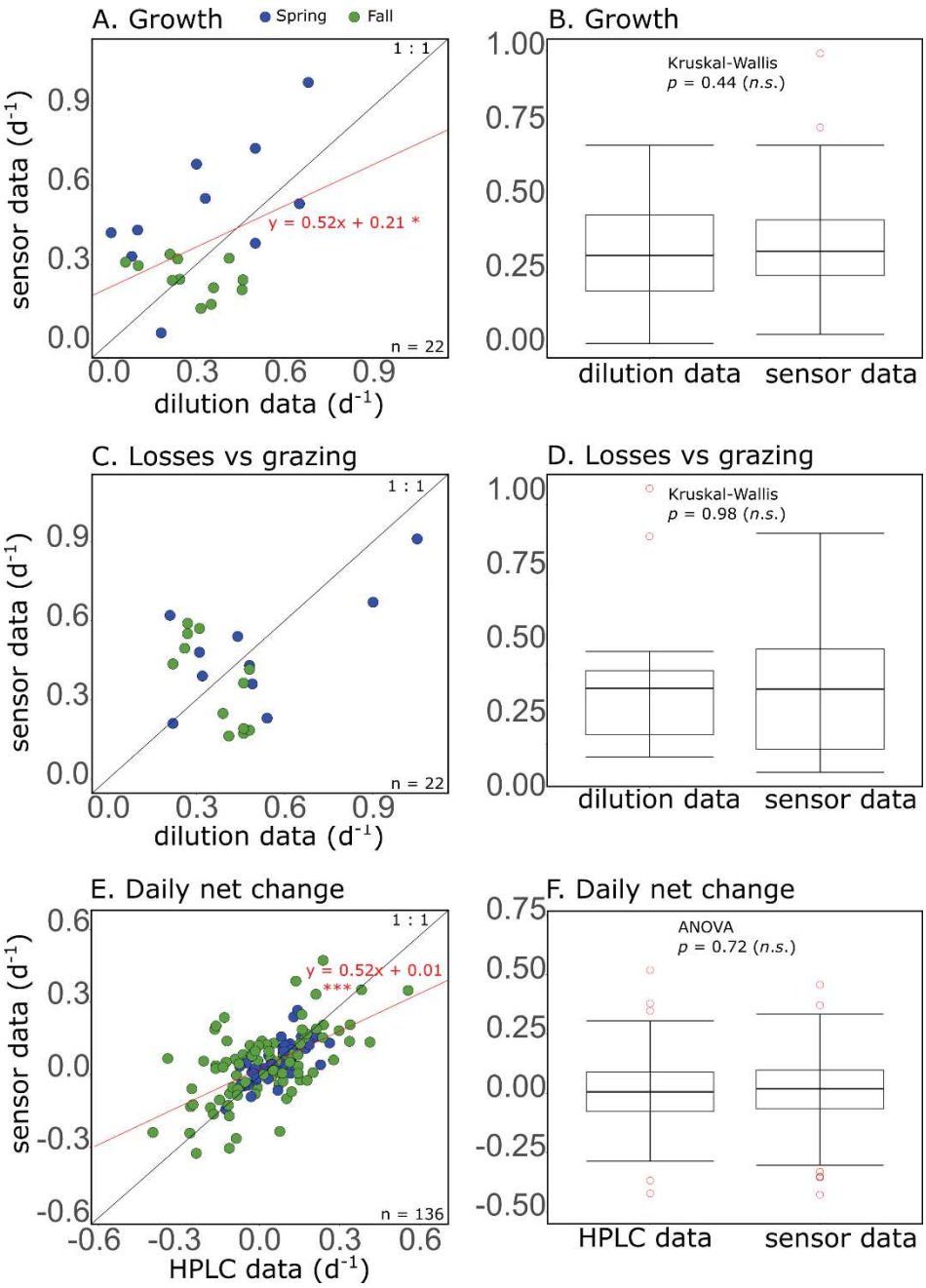

Figure 8. **Comparisons between sensor-obtained growth (μ) and dilution-obtained growth rate (A, B), between sensor-obtained loss (*l*) and dilution-obtained grazing rate (C, D), and between daily net change of chlorophyll-*a* (chl-*a*) fluorescence obtained from sensor data and daily net change of chl-a concentration obtained from HPLC (E, F).** In the left panels, the black line represents the 1:1 relationship. When a significant ($p < 0.05$, *) relationship was found, it is represented by a red line and its equation is indicated in red. The result of a statistical analysis comparing the estimates obtained with both methods are indicated in each right panel (*n.s*: not significant).

4 Discussion

4 1 Warming enhanced both μ and *l*

There are increasing evidences that phytoplankton processes responses to warming are often complex and depend on multiple factors (Lewandowska et al. 2014). Surprisingly, in the present study, even if the system was different in spring and fall, it responded quite similarly to warming in terms of μ and *l* based on chl-*a* fluorescence sensor measurements. Indeed, in both experiments, warming significantly enhanced μ, and especially during the second half of the experiments. This positive effect of warming joins the predictions of the Metabolic Theory of Ecology (MTE, Brown et al. 2004) and confirms the direct positive effect of warming on μ (Eppley 1972). This result is also congruent with another mesocosm experiment from coastal waters in which experimental warming increased μ (Bénard et al. 2018).

Among all the variables that could control μ, only the ammonium, the nitrate and the nitrite concentrations were positively related with μ response to warming, while the quantity of light and the water temperature seemed to not be the main controlling factors. More precisely, the positive effect of warming, expressed as the logarithmic response ratio, on ammonium concentration was linearly related with the positive effect on μ for both experiments, while it was only the case in spring for nitrate and nitrite concentrations. Altogether, these results suggest that the nitrogen availability was a key parameter in regulating μ response to warming at both seasons, joining previous studies which have shown that nitrogen is generally limiting in Thau lagoon (Collos et al. 1997; Souchu et al. 1998) and that resource availability generally overtakes the effect of warming on μ (Marañon et al. 2014). Hence, in our work, the greater effect of warming on μ in spring compared to fall is likely related to the higher nutrient availabilities and, in this regard, the fact that the lagoon trophic status is currently going toward oligotrophication (Derolez et al. 2020) might mitigate the effect of warming on μ in the future. Similarly, the negative effect of warming on μ reported at the beginning of the Spring experiment is probably due to low orthophosphate concentrations which could have triggered a more important competition with bacteria in the warmed mesocosms (von Scheibner et al. 2013).

In addition to enhancing μ during both experiments, warming also increased significantly *l*, in congruence with the MTE predictions (Brown et al. 2004) and with previous experimental studies (Rose et al. 2009). However, the magnitude of the warming effect on *l* was different between seasons: *l* was increased by a large extent during the entire Spring experiment, and by a lower extent only at the middle of the Fall experiment. To explain this seasonal difference, one hypothesis is that spring communities might be more sensible to high temperature than fall ones, as fall communities experienced high summer temperatures few weeks before, while spring communities were coming out of cold winter months (Courboulès 2020). Moreover, it must be stressed that, in a natural environment, *l* could be due to several factors: grazing by predators, viral lysis, natural death and sedimentation (Brussaard 2004;

Calbet and Landry 2004). Among these factors, it is known that warming can enhance grazing by boosting the metabolism of phytoplankton predators (Aberle et al. 2007; Rose et al. 2009), and viral abundances, potentially increasing viral lysis (Lara et al. 2013). Hence, the lower effect of warming on *l* in fall compared to spring might be the consequence of multiple cascading effects and complex interactions among grazers. For example, Lewandowska et al. (2014) showed that zooplankton switched from grazing on phytoplankton to grazing on ciliates under warming and low nutrient conditions, thus releasing the grazing pressure on phytoplankton. This switch could have occurred in fall as nutrient concentrations were lower than in spring, except for silicate.

In natural environments, the μ : *l* ratio drives the phytoplankton dynamics (Calbet and Landry 2004). Warming is suggested to increase this ratio at low chl-*a* levels and to decrease it at high chl-*a* levels (Chen et al. 2012). In the present study, contrary to what is suggested by the literature, even if the average chl-*a* level was rather similar in the control treatment of both experiments, warming had a different effect on the ratio: in spring, warming significantly depressed it, while it significantly enhanced it in fall. Therefore, results of our experiments suggest that warming could lead to a phytoplankton biomass stock decrease during spring bloom and a stock increase during fall, making spring less productive and fall an even more productive season than what it currently is. It was reported from the literature that warming can decrease phytoplankton biomass during blooms, and notably in a northern environment during spring (Sommer and Lengfellner 2008). However, the estimations of μ and *l* and of the related ratio performed in the present study can help to unravel the reasons behind this negative effect, as the positive effect of warming on μ is exceeded by the positive effect of warming on *l*. In contrast to spring, the effect of warming on μ and *l* in fall is not well-documented in the literature, and our work is the first one, to our knowledge, to show that warming enhanced μ more than *l* in a Mediterranean coastal lagoon at this season.

4 2 Warming changed the phytoplankton pigment composition differently depending on the season

In the present study, the phytoplankton community composition was assessed through pigment biomarker concentrations measured by HPLC in order to highlight the main phytoplanktonic contributors to μ response to warming estimated with the sensors. We showed that diatoms, represented by fucoxanthin, were the main contributors to μ response to warming in fall, in accordance with the literature reporting that diatoms can be major components of natural phytoplankton assemblages and thus contribute greatly to μ (Landry et al. 2011). Conversely, no specific phytoplankton group seemed to be positively correlated with μ in spring, suggesting that μ response to warming was representative of a global response of the community rather than related to one or some particular groups.

This difference in the pigment contributors to µ response to warming in spring and in fall is due to the fact that warming had a different effect on phytoplankton community composition, assessed through pigment biomarkers, depending on the experiment: diatoms were negatively affected by warming in spring, while they were positively affected in fall; green algae were not significantly affected in spring while they were depressed in fall. Conversely, prymnesiophytes were depressed in spring but unaffected in fall. It is important to note that the results are representative of two extremely different phytoplankton communities from the start. Indeed, the spring community was dominated by Prymnesiophytes and diatoms, which are well-representative of spring communities in Thau lagoon (Trombetta et al. 2019), while the fall community displayed extremely high abundances of cyanobacteria and green algae for the season, the latter being attributed to *Picochlorum sp.*, which have massively bloomed in the weeks following our experiment and was responsible of an ecological and economic crisis known as the "green waters" (Courboulès et al. 2021). Hence, diatoms could likely develop in the warmed treatment in fall only because green algae were significantly depressed by warming, thus potentially releasing competitive pressure and nutrient availabilities for diatoms. Generally, our study tends to indicate that the phytoplankton community composition is not a parameter that will strongly drive µ response to warming, as the effect of warming on µ was similar in seasons with different phytoplankton community composition. However, this hypothesis should be confirmed at other seasons and with other phytoplankton assemblages.

4 3 Using *in situ* mesocosms and automated high-frequency measurements to assess the effect of warming on µ and *l*

Assessing µ and *l* responses toward a given disturbance is of prime interest to better understand phytoplankton fate under future climate scenario, and hence to predict ocean's primary production in the future. However, traditional methods such as the dilution technique often require a time-consuming and labor-intensive effort, making it challenging to obtain data with high temporal and/or spatial distributions. The present study highlights the high potential of assessing µ and *m* responses to warming by using automated high-frequency sensors and in situ mesocosm experiments. The data generated by automated sensors can provide a reliable way to estimate these key parameters with a high-frequency and in an efficient way. The method displays many advantages: the data acquisition does not rely on mesocosm sampling, meaning that mesocosms can be deployed in remote locations and that data can be acquired in a non-invasive way for organisms and even in case of bad weather conditions.

As high-frequency chl-*a* fluorescence data are not commonly used to estimate µ and *l* in in situ mesocosms, we compared these sensor-obtained rates with the traditional dilution method (Landry and Hassett 1982). No significant differences were found as a result of these comparisons, suggesting that high-frequency fluorescence data can produce reliable estimates of µ and *l*. However, a significant linear relationship was found between sensor-obtained and dilution-obtained growth estimates, while no linear

relationship was found between sensor-obtained *l* and dilution-obtained grazing. This discrepancy can be due to the fact that the two methods were not applied on exactly the same communities. The sensors-obtained rates take into account the whole communities from the entire mesocosms, as the sensors are directly immerged in the mesocosms. On the contrary, dilutions were performed in 2 L bags filled with mesocosm water screened through a 200 µm mesh potentially excluding large phytoplankton (e.g. chain forming diatoms) and expressly large grazers (e.g. mesozooplankton) as this approach is designed for microzooplankton grazing estimations. Hence, the contribution of microzooplankton grazing to global *l* has certainly changed over the experiments, leading to the lack of linear relationship found between *l* and microzooplankton grazing. Finally, the concomitant use of sensors and dilution experiments could help to unravel the effects of warming on the ecosystem food web as it can disentangle the contributions of microzooplankton grazing from the total phytoplankton losses.

In addition, the sensor method is based on measurements of chl-*a* fluorescence, while the dilution technique is based on measurements of chl-*a* concentration. This could be seen as a limitation of the sensor-method as it has been shown that the chl-*a* fluorescence to chl-*a* concentration ratio can vary depending on species, nutrient conditions, photoacclimation and growth phase (Falkowksi and Kiefer 1985, Chekalyuk and Hafez 2011, Roesler et al. 2017), making chl-*a* fluorescence not always an accurate proxy of phytoplankton biomass in all cases and conditions. However, we calibrated the fluorescence sensors before the experiment and corrected the sensor-data after the experiment with HPLC-derived chl-*a* concentration measured in the mesocosms, and daily net chl-*a* fluorescence changes obtained from the sensors were found to not be significantly different from daily net chl-*a* concentration changes from HPLC, suggesting that chl-*a* fluorescence was a good proxy of chl-*a* concentration in our system.

In conclusion, using automated chl-*a* fluorescence sensors in in situ mesocosms is a promising way to evaluate and quantify the effects of a disturbance on µ and *l* in a non-invasive way and in conditions as close as possible to the natural environment. Future research should focus on making in situ mesocosms more autonomous, less time-consuming and labor-requiring, and therefore using high-frequency sensors seems to be a good way to achieve this goal. The present work is the first, to our knowledge, that highlighted the ability of in situ mesocosms and high-frequency chl-*a* fluorescence sensors to efficiently estimate the effects of warming on µ and *l*, and it contributes to broader our understanding of the complex effects of warming on coastal Mediterranean plankton assemblages during two contrasted seasons. Finally, it highlights the fact that studies need to be performed at various seasons in order to get a global view of the response of a system to a given disturbance.

5 Acknowledgements

The authors would like to thank the MEDIMEER crew for assistance during the mesocosm experiments, and especially: David Parin for setting up the sensor system and for retrieving sensor data, Remy Valdès, Solenn Soriano, and Camille Suarez-Bazille for their help with the daily sampling of the mesocosms and for the analyzes of the nutrient samples. Moreover, we want to acknowledge Julien Dupont, Thomas Trombetta and Jean-François Thévenot for their assistance in the mesocosm experiments and with the HPLC data analysis, and Maria Protopapa for her help with the dilution experiments. The Spring experiment was part of the Photo-Phyto project funded by the French National Research Agency (ANR-14-CE02-0018). The Fall experiment was a part of the AQUACOSM project, which funded also a part of the PhD grant of TS. AQUACOSM has received funding from the European Union's Horizon 2020 research and innovation program (H2020/2017-2020) under grant agreement n°731065.

6 Authors' contribution

B.M. and F.V. conceived the mesocosm studies. B.M., F.V. and S.M. managed the mesocosm experiments. T.S. and S.M. calibrated the automated sensors. T.S., S.M., J.C., B.M. and F.V. participated to the manual sampling of the mesocosms. J.C. and B.M. performed the dilution experiments and J.C. analyzed the dilution experiments data. T.S. and F.V. analyzed the HPLC data from the fall experiment, and performed the related data processing for both experiments. T.S. processed and analyzed the sensor data, and wrote the original draft of the manuscript, with inputs from all authors.

7 References

Voir la section Bibliographie de la thèse

Encadré – Chapitre 3

Effets du réchauffement sur la production primaire brute, la respiration communautaire et la production communautaire nette lors des expériences réalisées au printemps et en automne dans la lagune de Thau

Dans le but de pouvoir comparer l'effet d'un réchauffement de l'eau de 3°C sur les paramètres métaboliques de l'oxygène (Production Primaire Brute, Respiration et Production Communautaire Nette) des communautés planctoniques de la lagune de Thau à différentes saisons et pour plusieurs expériences testant la même perturbation, ces paramètres ont été estimés avec les données de concentration et de saturation en oxygène dissout des expériences de mésocosmes qui font l'objet du présent Chapitre, et calculés via la méthode établie dans le Chapitre 1. Les résultats présentés dans cet encadré n'étant pas présentés et discutés dans l'article scientifique qui compose le présent Chapitre, comme vu précédemment, seront discutés dans la Discussion Générale.

La PPB, la R et la PCN ont été calculées avec la méthode établie dans le Chapitre 1. La valeur du coefficient d'échange avec l'atmosphère a été corrigée pour la température et la salinité comme présenté dans l'Encadré du Chapitre 1. De plus, la PPB et la R cumulées ont été calculés en faisant la somme des valeurs de PPB et de R jusqu'au dernier jour de l'expérience via l'équation suivante (Éq. 1), dans laquelle x_i est la valeur de la PPB ou de la R au jour i, et n est le nombre de jours de l'expérience.

$$\sum_{i=1}^{n} x_i \quad \text{(Éq. 1)}$$

Lors de l'expérience de Printemps, la PPB et la R étaient significativement plus faibles dans le traitement chauffé que dans le traitement contrôle, d'en moyenne 50,9 et 47,9% respectivement (Fig E3.1, Tableau E3.1). Cependant, l'effet du réchauffement étant d'une ampleur similaire pour la PPB et la R, la PCN n'était pas significativement différente entre traitements, et était représentative d'un système globalement autotrophe au début de l'expérience, puis hétérotrophe durant la seconde partie de l'expérience. A la fin de l'expérience, la PPB et la R cumulées étaient significativement plus faibles dans le traitement chauffé que dans les contrôles.

Lors de l'expérience d'Automne, la PPB était significativement plus forte dans le traitement chauffé comparé au traitement contrôle, d'en moyenne 32,3% au début de l'expérience (jour 4 à jour 7) et 44,1% durant la seconde moitié de l'expérience (jour 12 à jour 17, Fig. E3.1, Tableau E3.1). Au contraire, la R n'était pas significativement différente entre traitements. En conséquence, la PCN était significativement plus élevée dans le traitement chauffé que dans le traitement contrôle, d'en moyenne 250,5%, et représentative d'un système globalement autotrophe à partir du jour 3. La PPB cumulée à la fin de l'expérience était significativement plus élevée dans le traitement chauffé que dans les contrôles, tandis que la R cumulée n'était pas significativement différente en fonction du traitement.

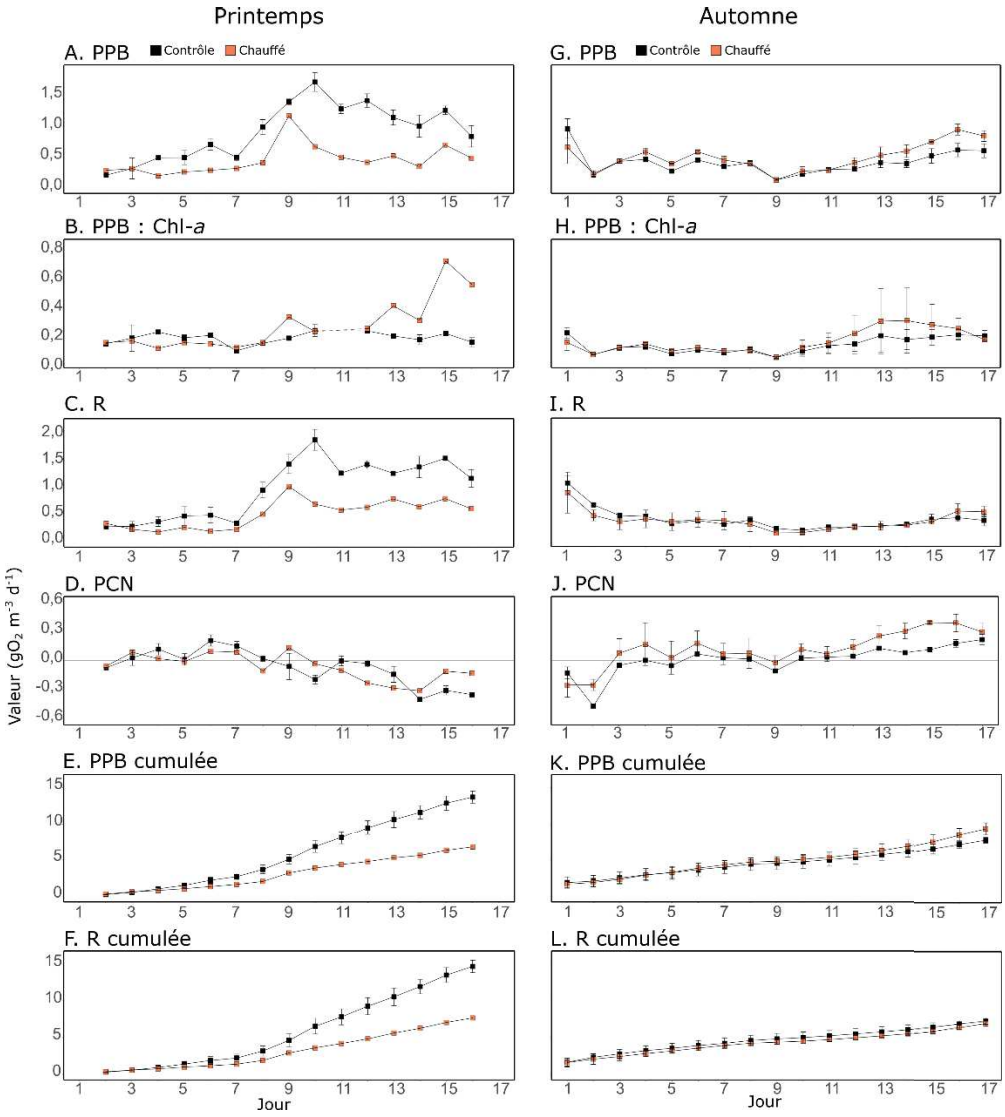

Figure E3.1. Production Primaire Brute (PPB), PPB normalisée par la chlorophylle-*a*, Respiration (R), Production Communautaire Nette (PCN), PPB cumulée et R cumulée pour l'expérience de Printemps (A, B, C, D, E, F) et d'Automne (G, H, I, J, K, L) dans les mésocosmes contrôles (en noir) et chauffés (en orange). Pour l'expérience de Printemps, les données du traitement contrôle sont la moyenne journalière ± l'étendue d'un duplicat de mésocosmes, les données du traitement chauffé sont issues d'un seul mésocosme. Pour l'expérience d'Automne, les données du traitement contrôle et du traitement chauffé sont la moyenne journalière ± l'écart-type d'un triplicat de mésocosmes.

Tableau E3.1. Résultats de la comparaison statistique (RM-ANOVA ou Kruskal-Wallis) entre les paramètres métaboliques obtenus dans le traitement chauffé et dans le traitement contrôle pour les expériences de Printemps et d'Automne dans la lagune de Thau. Les valeurs *P* inférieures ou égales à 0,05 sont considérées significatives et représentées en gras. Les parenthèses indiquent les valeurs F.

Paramètre	Printemps	Automne
PPB	**$<1,0 \times 10^{-4}$** ($F_{1,14}$=35,1)	**0,02** ($F_{1,16}$=6,1)
R	**$<1,0 \times 10^{-4}$** ($F_{1,14}$=55,5)	0,26 ($F_{1,16}$=1,3)
PCN	0,89 ($F_{1,14}$=0,1)	**$1,0 \times 10^{-4}$** ($F_{1,16}$=24,5)
PPB cumulée	**$8,0 \times 10^{-4}$** ($F_{1,14}$=18,2)	**$5,4 \times 10^{-3}$** ($F_{1,16}$=10,3)
R cumulée	**$1,0 \times 10^{-3}$** ($F_{1,14}$=17,2)	0,46 (Kruskal-Wallis)

L'ensemble des résultats présentés dans cet encadré sont discutés dans la Discussion Générale de la thèse (p 176).

Chapitre 4

Stabilité fonctionnelle d'une communauté planctonique côtière méditerranéenne face à une vague de chaleur : une expérience de mésocosmes *in situ* combinée aux mesures à haute-fréquence

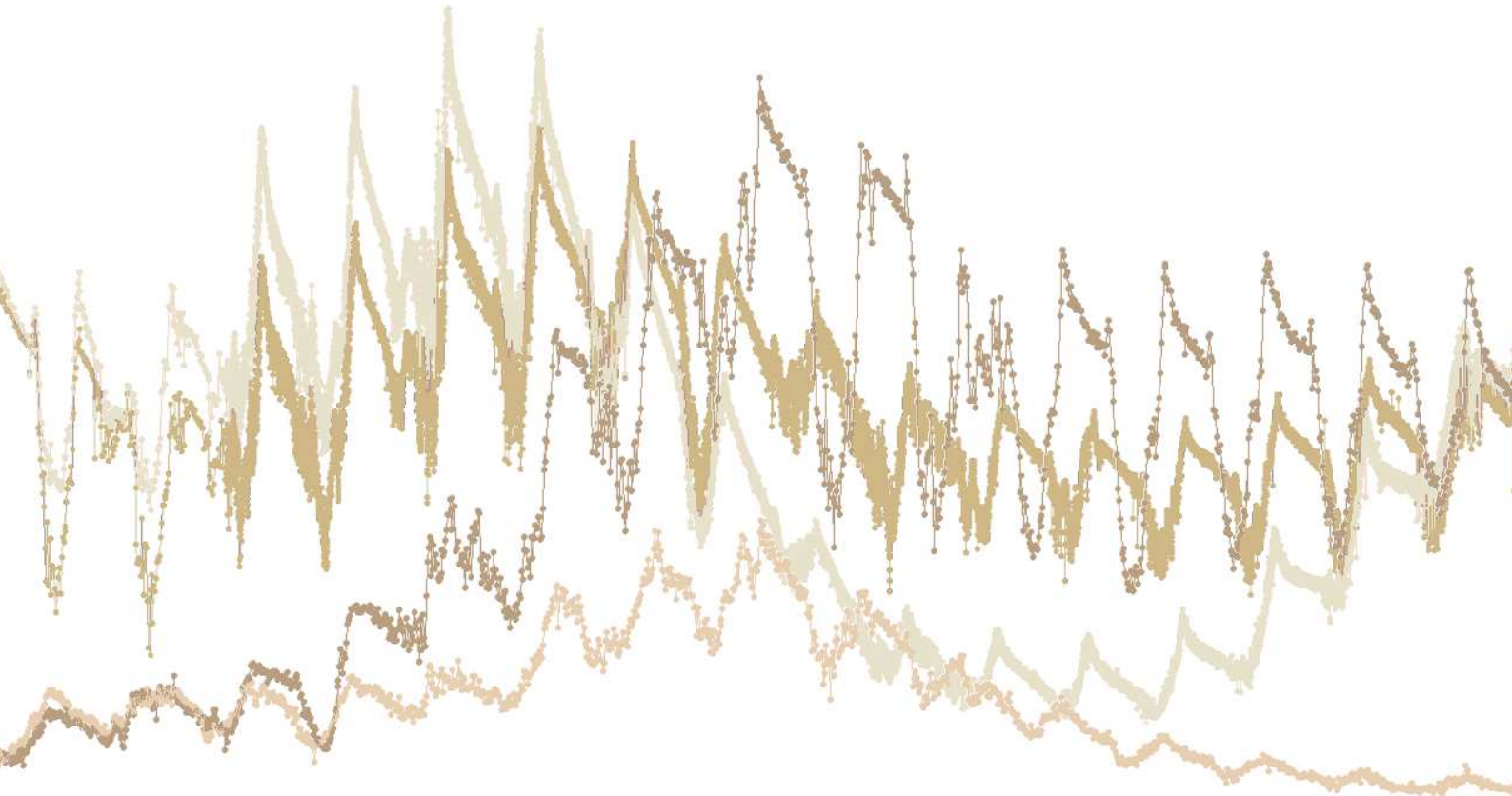

Avant-Propos

Dans la région méditerranéenne, une augmentation de la fréquence des vagues de chaleur et leur intensification sont prévues comme conséquences du changement climatique global. Néanmoins, les effets de ces épisodes extrêmes sur le fonctionnement des communautés planctoniques côtières de Méditerranée sont encore très peu étudiés et largement méconnus.

Dans ce cadre, l'objectif du présent chapitre est d'étudier la réponse d'une communauté planctonique naturelle en zone côtière méditerranéenne face à une vague de chaleur expérimentale et d'évaluer la résistance, la résilience et la trajectoire de récupération de certains processus planctoniques et de la composition de la communauté phytoplanctonique face à cette perturbation. Dans ce but, une expérience de mésocosmes *in situ* a eu lieu durant 20 jours entre Mai et Juin 2019 dans la lagune de Thau, dans le cadre du projet européen AQUACOSM (Network of Leading European AQUAtic MesoCOSM Facilities Connecting Mountains to Oceans from the Arctic to the Mediterranean). Durant cette expérience, une vague de chaleur a été simulée en augmentant la température d'un triplicat de mésocosmes à +3°C par rapport à un triplicat de mésocosmes contrôles pendant les 10 premiers jours de l'expérience. Puis, le réchauffement a été arrêté afin que la température du triplicat de mésocosmes chauffé revienne au niveau de celle des mésocosmes contrôles pendant les 10 jours suivants. Immergé à 1m de profondeur dans chaque mésocosme, un jeu de capteurs, comprenant un capteur de concentration et de saturation d'oxygène dissout, de fluorescence de la chlorophylle-*a*, de salinité, de quantité de radiations photosynthétiques actives, et trois sondes de température, a permis de suivre l'évolution des paramètres biotiques et abiotiques et de calculer les paramètres métaboliques de l'oxygène et les taux de croissance et de perte du phytoplancton. De plus, l'échantillonnage journalier manuel des mésocosmes a permis de suivre la concentration en nutriments inorganiques dissouts et d'évaluer la composition des types fonctionnels du phytoplancton via sa composition pigmentaire. Les paramètres de stabilité (i.e., résistance, résilience, récupération et stabilité temporelle) ont été calculés en termes de processus planctoniques et de types fonctionnels du phytoplancton.

Durant cette expérience, j'ai participé à la mise en place et à l'échantillonnage journalier des mésocosmes, j'ai traité et analysé l'ensemble des données des capteurs, j'ai réalisé des incubations pour mesurer les paramètres métaboliques de l'oxygène (données faisant en partie l'objet du chapitre 1) et j'ai analysé la composition pigmentaire du phytoplancton via chromatographie liquide à haute performance (HPLC). Les résultats sont présentés sous la forme d'un article rédigé en anglais intitulé « **Low functional stability of a coastal Mediterranean plankton community to an experimental marine heatwave unraveled by high-frequency measurements** », dont les auteurs sont Tanguy Soulié, Francesca Vidussi, Sébastien Mas, et Behzad Mostajir, et qui sera soumis dans une revue spécialisée très prochainement.

Participants à l'expérience simulant une vague de chaleur dans la lagune de Thau. Photo © B. Mostajir

Low functional stability of a coastal Mediterranean plankton community to an experimental marine heatwave unraveled by high-frequency measurements

Tanguy Soulié[1*], Francesca Vidussi[1], Sébastien Mas[2], Behzad Mostajir[1*]

[1]MARBEC (MARine Biodiversity, Exploitation and Conservation), Univ Montpellier, CNRS, Ifremer, IRD, Montpellier, France

[2]MEDIMEER (MEDIterranean platform for Marine Ecosystems Experimental Research), OSU OREME, CNRS, Univ Montpellier, IRD, IRSTEA, Sète, France

* corresponding authors: Tanguy Soulié, tanguy.soulie@gmail.com, Behzad Mostajir, behzad.mostajir@umontpellier.fr

Running head: Heatwave effects on plankton communities

Keywords: marine heatwave, plankton metabolism, resistance, resilience, recovery, in situ mesocosm, high-frequency measurements, Thau lagoon

Abstract

As heatwaves are expected to increase in frequency and intensity in the Mediterranean Sea due to global warming, an in situ mesocosm experiment was performed for 19 days during late-spring early-summer 2019 in a coastal Mediterranean lagoon to investigate their effects on coastal plankton community composition and functioning. A heatwave was simulated by elevating the water temperature of three mesocosms at +3°C compared to three control mesocosms with natural lagoon water temperature during 10 days. Then, the heating procedure was stopped during the next 10 days to study the resilience and the recovery of the system. Automated high-frequency monitoring of dissolved oxygen concentration and saturation, chlorophyll-*a* fluorescence, photosynthetic active radiation, salinity and water temperature was completed with manual sampling for nutrient and phytoplankton pigments analyses. The high-frequency data were used to estimate different functional processes: gross primary production (GPP), community respiration (R), and phytoplankton growth (μ) and loss (*l*) rates. Ecosystem stability was assessed by calculating resistance, resilience, recovery and temporal stability both in terms of key functions (GPP, R, μ and *l*), and phytoplankton functional types (PFT) composition assessed through chemotaxonomic pigment composition. During the heatwave, GPP, R, μ and *l* were enhanced by 31%, 49%, 16% and 21% compared to the control treatment, respectively. These positive effects persisted several days after the offset of the heatwave, resulting in a low resilience for these key functions. However, GPP and R recovered almost completely at the end of the experiment, suggesting that the effect of the heatwave on these two rates was reversible. The heatwave also impacted the PFT composition, as diatoms, prymnesiophytes and cyanobacteria were favored while dinoflagellates were depressed.

1 Introduction

The frequency and the intensity of marine heatwaves are expected to increase during this century in most regions of the world due to global climate change and plausible scenarios of greenhouse gases emissions (IPCC 2019). These marine heatwaves are defined as extreme warming events of the ocean lasting several days to multiple months (Hodbay et al. 2018). It is projected that the Mediterranean Sea will become one of the most sensitive regions to such events (Diffenbaugh et al. 2007; Darmaraki et al. 2019). In addition, coastal waters are naturally more sensitive than open water to temperature variations due to their shallowness and low thermal inertia (Nixon et al. 2004; Trombetta et al. 2019). Hence, this rise in marine heatwaves is expected to have important consequences for Mediterranean coastal planktonic communities, both in terms of functioning and composition (Stefanidou et al. 2018; Xoplaki et al. 2021).

Planktonic communities play a major role in marine ecosystems as they are major components of the food web and take an important part in several biogeochemical cycles, notably those of oxygen and carbon (Behrenfeld 2011; Falkowski 2012; Brierley 2017). Indeed, autotrophic plankton produces dissolved oxygen through photosynthesis (the Gross Primary Production, GPP), and both heterotrophic and autotrophic plankton consumes it through aerobic respiration (R). Hence, plankton plays a crucial role in the Net Community Production (NCP), which is the balance between GPP and R, and therefore in the capacity of marine ecosystems to be net producers or sinks of oxygen (Odum 1956; Duarte and Regaudie-de-Gioux 2009). Therefore, the phytoplankton growth (μ) and loss (l) rates drive the primary production dynamics, making these two parameters also necessary to understand and predict the fate of marine ecosystem functioning in the context of global change (Calbet and Landry 2004; Sherman et al. 2016). Finally, even if all phytoplankton groups contribute to the primary production, they differ according to their biogeochemical role and within the food web. These functional differences can be assessed by pigment biomarkers representing specific phytoplankton functional types (PFT) which are of prime interest in order to understand the effects of climate change on plankton community structure and functioning (Hirata et al. 2011).

The effects of warming on marine planktonic communities and on ecosystem functioning have been investigated for multiple systems and areas (Vidussi et al. 2011; Sommer et al. 2012; Moreau et al. 2014). However, less is known about the effects of heatwaves on coastal ecosystems. In Western Australia and in the Tasman sea, marine heatwaves induced significant changes both in the phytoplankton and in the zooplankton communities' composition (Berry et al. 2019; Evans et al. 2020). In the Gulf of Alaska, a two-year marine heatwave seemed to negatively affect the phytoplankton community while having neutral to positive effects on the zooplankton community (Batten et al. 2018; Suryan et al. 2021). In addition, global models predict a positive effect of marine heatwaves on

phytoplankton biomass in nutrient-replete conditions and the opposite on nutrient-poor conditions, with drastic phytoplankton biomass reductions in tropical areas (Hayashida et al. 2020; Sen Gupta et al. 2020).

However, most studies monitored the effects of one or multiple natural heatwaves on the plankton communities, but experimental studies, and notably mesocosm experiments, could be useful to elucidate the effects of heatwave on marine plankton assemblages and to refine model predictions. Indeed, mesocosm experiments allow to simulate a perturbation and to follow its effects on a natural community in controlled conditions and in a reproducible way (Stewart et al. 2013; Dzialowski et al. 2014). Nonetheless, only few mesocosm experiments were used to simulate a heatwave, and most of them were performed in freshwater ecosystems (Rasconi et al. 2017; Filiz et al. 2020; Iskin et al. 2020), so the effects of heatwaves on coastal planktonic assemblages are still uncertain.

In this regard, we performed an in situ mesocosm experiment in Thau lagoon, a coastal productive shallow lagoon located on the French coast of the Northwestern Mediterranean Sea. During this experiment, we simulated a moderate heatwave during late spring by increasing the water temperature of triplicate mesocosms by +3°C compared to triplicate control mesocosms during the first 10 days of the experiment, before switching off the heating for the remaining 10 days. High-frequency sensors immerged in every mesocosms were used to monitor dissolved oxygen concentration and saturation, chlorophyll-a (chl-*a*) fluorescence, water temperature, salinity, and photosynthetically active radiation to estimate plankton oxygen metabolism (GPP, R, NCP) and phytoplankton's μ and *l*. In combination to this high-frequency monitoring, the mesocosms were sampled daily for nutrients and phytoplankton pigment composition. Moreover, ecosystem stability parameters (i.e., resistance, resilience, recovery and temporal stability) were assessed in terms of plankton community functioning and composition.

2 Material and Methods

2 1 *In situ* mesocosm experiment set-up

An in situ mesocosm experiment was carried out in Thau lagoon, a coastal shallow lagoon located in the Northwestern Mediterranean on the coast of south of France. The lagoon has a mean depth of ca. 4 m (Derolez et al. 2020) and the mesocosms were installed directly in the lagoon using the facilities of the Mediterranean Platform for Marine Ecosystems Experimental Research (MEDIMEER, 43°24'53''N 3°41'16''). The experiment was performed during 19 days, from May 24th to June 12th 2019. Each mesocosm consisted of a 280 cm high and 120 cm wide transparent bag made of a 200 μm-thick vinyl acetate polyethylene film reinforced with nylon (Insinööritoimisto Haikonen Ky), equipped with a 50 cm long sediment trap. Mesocosms were covered with a polyvinyl-chloride dome, which transmitted 73% of the received photosynthetically active radiation (PAR), in order to avoid external

inputs and precipitations. A pump (Rule, Model 360) was immersed at 1 m depth to continuously and gently mix the water column of the mesocosms.

Two treatments, each in triplicate, were applied in six mesocosms. During the first 10 days of the experiment (from d1 to d10 included), the water temperature was raised to +3°C in three mesocosms (hereafter called 'the HW treatment') in comparison to the three other mesocosms with natural lagoon temperature referred to as 'control treatment'. This 10d period in which water temperature was elevated by 3°C compare to control mesocosms is referred to as the 'HW period' hereafter. Then, the water temperature of the HW mesocosms returned to the level of the control mesocosms for the next 10 days until the end of the experiment (from d11 to d20). This 10d period, in which the water temperature of the HW and control mesocosms was similar is called the 'Post-HW period'. Therefore, 'control mesocosms' followed the in situ lagoon temperature during the whole 20d of the experiment. A precise description of the heating procedure that enabled to increase the water temperature by +3°C in the HW mesocosms during the HW period, while still following natural temperature fluctuations of the lagoon, can be found in Nouguier et al. (2007) and Vidussi et al. (2011).

In each mesocosm, a set of automated high-frequency sensors was immersed at 1 m depth. Each set consisted of an oxygen optode (Aanderaa 3835) for dissolved oxygen (DO) concentration and saturation, a chlorophyll fluorometer (WetLabs ECO-FLNTU) for chl-*a* fluorescence, an electromagnetic induction conductivity sensor (Aanderaa 4319) for salinity, a spherical underwater quantum sensor (Li-Cor Li-193) for incident PAR. Moreover, three water temperature probes (Campbell Scientific Thermistore Probe 107) were installed at three different depths (0.5, 1 and 1.5 m) to measure water temperature. Each sensor took a measurement every minute during the entire experiment.

2 2 High-frequency sensor data acquisition, calibration and correction

The oxygen optodes, chlorophyll fluorometers, conductivity sensors and water temperature probes were calibrated before and after the experiment. The oxygen optodes were calibrated using three saturation points (0, 50 and 100%) and at three different temperatures (17, 20 and 22°C). The calibrated DO data were then corrected using temperature and salinity data obtained with the water temperature probes and the conductivity sensor following Bittig et al. (2018). To ensure high quality oxygen data, daily oxygen concentrations were also measure using the Winkler method to correct sensor data (Soulié et al. 2021). The whole calibration and correction procedures are described in Soulié et al. (2021). The chlorophyll fluorometers were calibrated using 4 algae monocultures during exponential growth phase (*Tetraselmis chui*, *Isochrisis galbana*, *Nanochloropsis occulata*, *Dunaliela salina*) and a mix of these 4 cultures and with 5 chl-*a* concentration points, which were measured using high performance liquid chromatography (HPLC, Waters) and ranged from 0 to 18.64 µg L^{-1}. In addition, the chl-*a* fluorescence sensor data were

corrected with daily measured chl-*a* concentrations analyzed by HPLC and for non-photochemical quenching (NPQ) by linearly interpolating the data from sunrise to sunset (Li et al. 2008). Moreover, the conductivity sensors were calibrated at 3 salinity points (0, 20 and 35) using sodium chloride in distilled water and at two temperatures (18 and 22°C). Finally, the water temperature probes were calibrated in a distilled water bath at 5 temperature levels ranging from 10 to 30 °C. All data presented thereafter were corrected according to the calibration coefficients obtained with the preceding procedure.

2 3 Nutrient and pigment analyses from daily manual mesocosm sampling

For dissolved nutrients and phytoplankton pigment concentrations all the mesocosms were sampled daily by a 5 L Niskin water sampler at 1 m depth between 09:00 and 10:00. For dissolved nutrient analyses (nitrate NO_3^-, nitrite NO_2^-, ammonium NH_4^+, orthophosphate PO_4^{3-}, and silicate SiO_2), 50 mL of the samples were put in an acid-washed polycarbonate bottle, before being filtered on 0.45 µm filters (Gelman) and stored in a polyethylene tube at -20°C until analyses that were performed using an automated colorimeter (Skalar Analytical). For phytoplankton pigment analyses, between 800 and 1200 mL of the samples were put on covered 2 L bottles before being directly filtered at low-light on a glass-fiber filter (Whatman GF/F 0.7 µm pore size) and at low-vacuum. Filters were frozen in liquid nitrogen before being stored at -80°C until analyses. Pigment concentrations were analyzed with HPLC (Waters), following the method of Zapata et al. (2000) and the protocol described in Vidussi et al. (2011). Phytoplankton pigments were attributed to different phytoplankton functional types (PFTs) following Vidussi et al. (2000) and Hirata et al. (2011). More precisely, fucoxanthin was attributed to diatoms, peridinin to dinoflagellates, 19'-hexanoyloxyfucoxanthin (19'-HF) to prymnesiophytes, chlorophyll-*b* (chl-*b*) to green algae, and zeaxanthin to cyanobacteria.

2 4 Daily Light Integral (DLI) using the high-frequency PAR sensor data

The high-frequency Photosynthetically Active Radiation (PAR) measurements were used to calculate the Daily Light Integral (DLI), which corresponds to the daily average amount of light received by a 1 square meter surface and over a 24-hr period (Faust and Logan 2018). DLI was calculated using Equation 1:

$$DLI = \frac{mean\ PAR * day\ length * 3600}{1 * 10^6} \qquad \text{(Equation 1)}$$

With the DLI expressed in mol m^{-2} d^{-1}, the mean PAR between sunrise and sunset in µmol m^{-2} s^{-1}, and the daylength in hr.

2 5 Estimation of phytoplankton µ and *l* using the high-frequency chl-*a* fluorescence sensor data

To estimate phytoplankton µ and *l* rates in each mesocosms, each high-frequency chl-*a* fluorescence cycle was separated into two periods: the 'increasing period' during which the chl-*a* fluorescence increases, from sunrise to when its maximum value is attained, generally a few minutes to a few hours after sunset, and the 'decreasing period' during which chl-*a* fluorescence decreases, from when its maximum value is attained until the next sunrise. For each increasing and each decreasing period, an exponential fit was applied to the chl-*a* fluorescence data using Equation 2:

$$F_{chla} = a * e^{bt} \qquad \text{(Equation 2)}$$

In this equation, F_{chla} is the chl-*a* fluorescence in µg L^{-1}, *a* a constant in µg L^{-1}, *b* a constant in min^{-1} and *t* the time (min). Then, considering the assumptions that F_{chla} changes during the night are only due to phytoplankton losses and that F_{chla} changes during the day are due to both losses and growth (Neveux et al. 2003), *l* and µ were estimated following the Equations 3 and 4:

$$l = b_{dec} \qquad \text{(Equation 3)}$$

$$\mu = b_{inc} + l \qquad \text{(Equation 4)}$$

With *l* and µ the phytoplankton loss and growth rates (min^{-1}), and b_{dec} and b_{inc} the exponential fit coefficients obtained for the decreasing and the increasing periods, respectively. Then, *l* and µ were converted in d^{-1} by multiplying rates in min^{-1} by 60 and by 24 for *l* as it is considered constant over a 24-hr period (Neveux et al. 2003)), and by 60 and by the duration of the increasing period (in hr) for µ (as it only occurs during the increasing period).

Due to the lack of a complete chl-*a* fluorescence cycle on the last day of the experiment (d20), µ and *l* were only estimated from d1 to d19.

2 6 Estimation of GPP, R and NCP using the high-frequency DO sensor data

GPP, R and NCP were estimated using the high-frequency DO sensor data with a method, based on the classical free-water diel oxygen technique (Odum and Odum 1955), that was specially developed for mesocosm experiments and that considers variability in the daytime and nighttime respirations and in the coupling between day-night and DO cycles (Soulié et al. 2021). All the equations used in the calculations are presented in Table 1. Briefly, each DO cycle was separated in 'Positive NCP periods' during which DO concentration increased, and in 'Negative NCP periods' when DO concentration decreased. For each Positive and Negative NCP periods, the DO concentrations were smoothed using a 5-point sigmoidal model. The DO data and these periods were then used to estimate the oxygen metabolic parameters which were calculated using the fundamental equation of Odum and Odum (1955)

presented in Eq. 5. In this equation, $\frac{\Delta O_2}{\Delta t}$ represents the instantaneous change in DO concentration, F the physical oxygen exchange between the water and the atmosphere, and A encompasses all other physical and chemical phenomena that could affect the DO concentration in the considered system which were considered null in the present study as well as in most other investigations (Staehr et al. 2010; Soulié et al. 2021). Then, the calculation needs to be performed following 2 important steps.

The first step concerns the calculation of the oxygen exchange term F. It can be expressed as in Eq.6., where k is the air-water constant, called piston velocity coefficient, O_2 and O_{2sat} the DO concentration and saturation, respectively, and Z_{mix} the water column mixing depth. In the case of gently mixed mesocosms as in the present study, Z_{mix} can be considered equal to the water column length of the mesocosms. The piston velocity k is generally derived from literature values (Soulié et al. 2021). However, this parameter is determined by water viscosity and O_2 solubility, which are affected by water temperature and salinity. Therefore, we modeled every minute the k as a function of the reference k (k_{ref} = 0.000156 m min^{-1}, Alcaraz et al. 2001; Soulié et al. 2021) and the high-frequency water temperature and salinity data with the following steps. First, the Schmidt number (Sc) for O_2 in freshwater and in function of temperature is given with the Eq. 7. (Wanninkhof 1992). In this equation, T is the water temperature. Then, to account for salinity, the coefficient m needs to be calculated as in Eq. 8 (Holtgrieve et al. 2010). Finally, the Schmidt number is adjusted for salinity according to Eq. 9 (Holtgrieve et al. 2010), where S is the salinity and m the coefficient previously calculated. Finally, the piston velocity k was calculated for every 1 min timestep using Eq. 10, wiith $Sc_{O2}(ref)$ referring to the Schmidt number for the conditions in which k_{ref} was experimentally measured (16°C, 37.5), which is equal to 675.58.

The second step is to estimate instantaneous and, *in fine*, daily metabolic parameters. For each 1 min timestep, the instantaneous NCP was calculated according to Eq. 11, in which $O_2(t)$ and $O_2(t-1)$ are the DO concentrations at time t and t-1, respectively, and $F(t)$ the oxygen exchange term at time t. Daily metabolic parameters could be estimated using the instantaneous NCP for each couple of Positive and Negative NCP periods. First, the respiration occurring the day, Rdaytime, was calculated according to Eq. 12. In this equation, Rdaytime was expressed in gO_2 m^{-3} d^{-1}, the mean instantaneous NCP during a 1-hr period centered around the maximum instantaneous NCP attained during the Negative NCP period was expressed in gO_2 m^{-3} min^{-1}, and the duration of the Positive NCP period in hr. Similarly, the respiration occurring during the night, Rnight, could be estimated following Eq. 13. Rnight was expressed in gO_2 m^{-3} d^{-1}, the mean instantaneous NCP during the Negative NCP period expressed in gO_2 m^{-3} min^{-1}, and the duration of the Negative NCP period in hr. Then, daily R (gO_2 m^{-3} d^{-1}) was calculated according to Eq. 14. Daily GPP was estimated using the following Eq. 15. GPP and Rdaytime were expressed in gO_2 m^{-3} d^{-1}, the mean instantaneous NCP during the Positive NCP period in gO_2 m^{-3} min^{-1}, and the duration of the Positive NCP period in hr. Finally, daily NCP was calculated

as the difference between daily GPP and daily R (Eq.16). Due to the lack of a complete DO cycle on the last day of the experiment (d20), NCP, GPP and R were only estimated from d1 to d19.

Table 1. **Equations used to calculate daily GPP, R and NCP**.

Parameter	Equation	Eq.
Governing equation (Odum and Odum 1955)	$\frac{\Delta O_2}{\Delta t} = GPP - R - F - A$	5
Oxygen physical exchange term	$F = (k \times (O_2 - O_{2sat}))/Z_{mix}$	6
Schmidt number (Sc) for O_2 in freshwater and in function of temperature (Wanninkhof 1992)	$Sc_{O_2FW}(T) = -120.1 \times T + 3.7818 \times T^2 - 0.047608 \times T^3 + 1800.6$	7
Schmidt number adjusted for salinity (Holtgrieve et al. 2010)	$m = 3.286 \times 10^{-5} \times T + 2.474 \times 10^{-3}$ $Sc_{O_2}(T,S) = Sc_{O_2FW} \times (1 + S \times m)$	8 9
Piston velocity coefficient accounting for temperature and salinity	$k(T,S) = k_{ref} \times (\frac{Sc_{O_2}(T,S)}{Sc_{O_2}(ref)})^{-0.5}$	10
Instantaneous NCP	$NCP(t) = O_2(t) - O_2(t-1) - F(t)$	11
Daytime R	$R_{daytime}$ = *(mean of NCP during a 1hr period centered around the max. NCP of the Negative NCP period) × duration of Positive NCP period ×60*	12
Nightime R	R_{night} = *(mean of NCP during the Negative NCP period) × duration of Negative NCP period ×60*	13
R	$R = R_{daytime} + R_{night}$	14
GPP	$GPP = R_{daytime}$ + *(mean of NCP during the Positive NCP period) × duration of Positive NCP period ×60*	15
NCP	$NCP = GPP - R$	16

2 7 Cumulative data

Cumulative data over the whole experimental period was calculated for GPP, R, NCP, µ, *l* and PFTs to evaluate the overall consequences of the heatwave, using Equation 17:

$$\sum_{i=1}^{n} x_i \quad \text{(Equation 17)}$$

With x_i the value of the investigated parameter on day *i* and *n* the last experimental day (*n*=19 for GPP, R, NCP, µ and *l*, *n*=20 for pigment concentrations).

2 8 Resistance, resilience, recovery and temporal stability estimates

Resistance, resilience, recovery and temporal stability were calculated for key functions (μ, *l*, GPP and R) and for PFTs following Hillebrand et al. (2018) (Table 2). For each day of the HW period, resistance was calculated as the logarithm response ratio (LRR). In addition, the change of resistance during the HW period was calculated as the regression slope of the resistance over time (resistance = slope × time + intercept) following Filiz et al. (2020). A positive change means that resistance decreases over time for parameters with an average positive resistance, while it means resistance increases over time for parameters with an average negative resistance. Resilience was calculated as the regression slope of the relative LRR function over time during the 10d of the Post-HW period. Recovery was estimated as the LRR on the last day of the experiment. Finally, temporal stability was calculated as the inverse standard deviation of residuals around resilience. An unpaired *t*-test was performed to check if there was a significant difference between resistance over time and benchmark resistance (0) using the R software.

Table 2. **Stability parameters estimated in the present study** and the experimental period they are calculated for, their mathematical definition, and interpretation. Stability parameters definition and interpretation is according to Hillebrand et al. (2018). [1] X_{HW} and X_C represent the investigated function (GPP, R, μ, *l*) or the investigated phytoplankton functional type in the HW and control treatments, respectively.

Parameter	Period	Estimation	Interpretation
Resistance (*a*)	d1-d10	$a = \ln\left(\frac{X_{HW}}{X_C}\right)$ [1]	*a* = 0 → maximum resistance *a* > 0 → overperformance *a* < 0 → underperformance
Resilience (*b*)	d11-d20	$\ln\left(\frac{X_{HW}}{X_C}\right) = b * t + i$	*b* = 0 → no recovery *b* > 0 → faster recovery (if *i* < 0) *b* < 0 → further deviation from the control (if *i* < 0)
Recovery (*c*)	d20	$c = \ln\left(\frac{X_{HW}}{X_C}\right)$	*c* = 0 → maximum recovery *c* > 0 → overcompensation *c* < 0 → incomplete recovery
Temporal stability (*d*)	d11-d20	$d = \frac{1}{(sd(res_b)}$	The larger *d* the lower fluctuations

2 9 Statistical analyses

The difference between treatments was assessed during the 10d of HW period (d1-d10), 10d of the Post-HW period (d11-d19), and during the entire experiment (d1-d19) using Repeated-Measures Analysis of Variances (RM-ANOVA) with the treatment assigned as fixed factor and time as random factor. *P*-values less or equal to 0.05 were considered significative. When the assumptions for a parametric test were not met, even if the data were transformed (logarithmic, square-root or exponential transformations), a non-parametric Kruskal-Wallis rank sum test was performed instead. Principal Component Analyses (PCA) and ordinary least-square linear relationships were assessed between LRR of GPP, R, μ, *l*, PFTs, DLI, temperature and salinity to assess potential drivers of the system responses (expressed as LRR) to the treatment. The data management and the statistical analyses were done using the R software (version 4.0.1).

3 Results

3 1 Physical and chemical conditions

In the control treatment, the water temperature ranged from 17.85 ± 0.02 °C (d7) to 20.29 ± 0.01 °C (d18). It generally decreased until d7, before increasing and peaking on d13 and d18. In the HW treatment, the water temperature was successfully enhanced by an average of 2.75 ± 0.23 °C compared to the control treatment during the HW period (d1-d10), before returning to the control level during the Post-HW period (d11-d19) (Fig 1A). The Daily Light Integral (DLI) in the control treatment varied from 7.33 ± 0.85 mol m^{-2} d^{-1} (d1) to 26.32 ± 2.54 mol m^{-2} d^{-1} (d6). It increased from d1 to d4, before being relatively stable and at high values from d6 to d14. Then, DLI values decreased until the end of the experiment, but with a peak on d16 (Fig 1B). They were significantly lower in the HW treatment compared to the control both during the HW and the Post-HW periods, by an average of 12% and 11%, respectively (Table 2). The salinity increased during the HW period and stayed relatively constant during the Post-HW period. In the control, salinity ranged from 38.27 ± 0.17 to 38.73 ± 0.18 (Fig 1C) and was significantly lower in the HW treatment compared to the control during the HW period by an average of 0.07%, while it was significantly higher during the Post-HW period by an average of 0.05% (Table 3).

The dissolved nutrient concentrations showed different trends. In the control, the ammonium (NH_4^+) concentration ranged from 0.09 ± 0.04 μM (d9) to 0.37 ± 0.04 μM (d1). It generally decreased during the HW period, before staying relatively constant during the Post-HW period (Fig 1D). There was no significant difference between the control and the HW treatment in both periods (Table 3). The nitrate and nitrite concentrations (NO_3^-+NO_2^-) varied from 0.20 ± 0.04 μM (d5) to 0.54 ± 0.03 μM (d15) in the control. It decreased from d2 to d5, then it generally increased until d14 or d15 depending on the treatment, before decreasing again until the end of the experiment (Fig 1E). Similarly to the ammonium

concentrations, there was no significant difference in the nitrate and nitrite concentrations between the control and the HW treatments during both periods (Table 3). In the control, the orthophosphate (PO_4^{3-}) concentration ranged from 0.04 ± 0.01 µM to 0.44 ± 0.02 µM and peaked three times during the experiment (d7, d11, d17). As for N-nutrients, there was no significant difference between treatments in both the HW and the Post-HW periods (Table 3). Finally, in the control treatment, the silicate (SiO_2) concentration ranged from 0.98 ± 0.27 µM (d1) to 8.84 ± 1.22 µM (d11), and increased from d4 to d11, before decreasing until the end of the experiment, except from a peak on d17 (Fig 1G). Conversely to the other nutrient concentrations, silicate concentrations were significantly higher in the HW treatment during the HW period by an average of 42%, while no significant differences between treatments were found in the Post-HW period (Table 3).

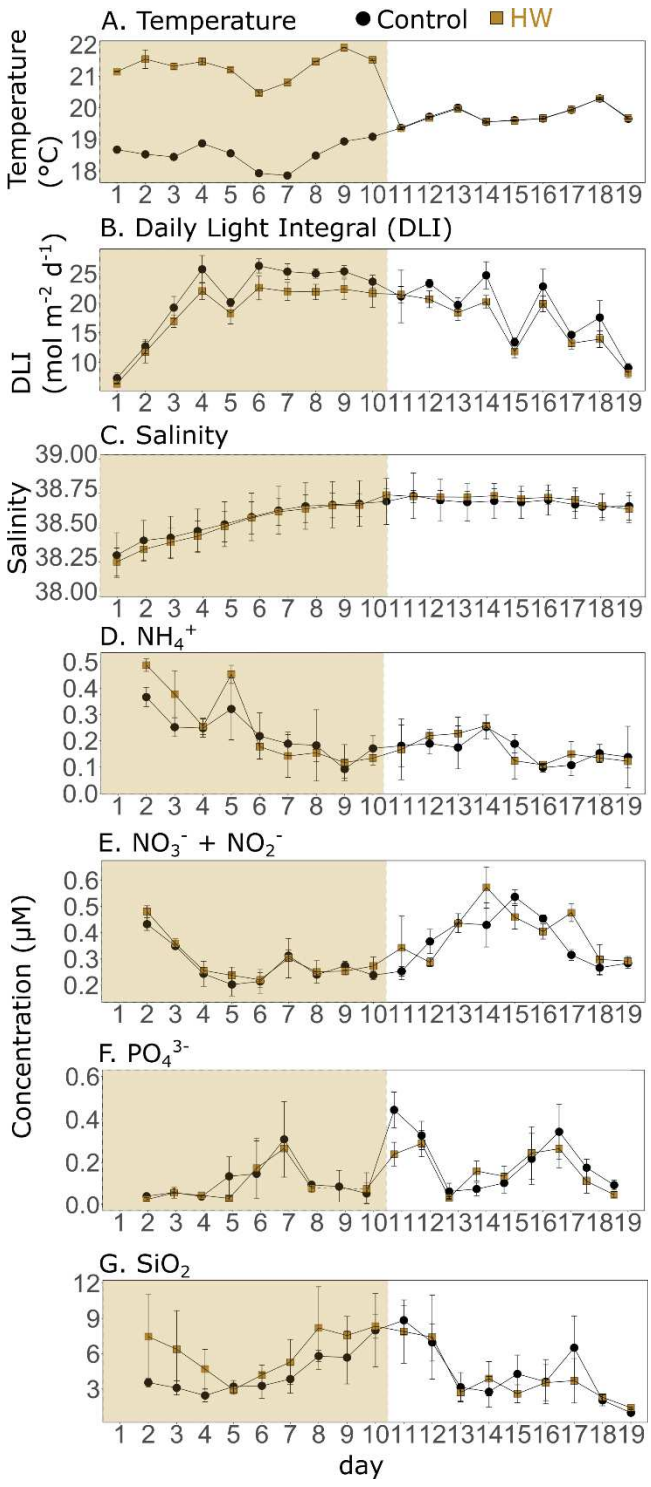

Figure 1. **Daily means of water temperature (A), Daily Light Integral (DLI, B), salinity (C), and concentrations of ammonium (NH_4^+, D), nitrate + nitrite (NO_3^-+NO_2^-, E), orthophosphate (PO_4^{3-}, F) and silicate (SiO_2, G)** in the control (black) and HW (gold) treatments. The gold shaded area represents the HW period during which the +3°C was applied in the HW mesocosms. Error bars represent the standard deviation. Note that the scales of the y-axis are different.

Table 3. **Summary table of statistical test results and relative changes between the HW and control treatments on physical and chemical parameters** during the HW period, the Post-HW period and during the entire experiment. The significance level of the statistical test was set as 0.05, and significant *p*-values were highlighted in bold in the table. When a value of relative change was smaller than 0.5%, it was set as 0 and marked by the symbol *.

Parameter	Period	*P*-value	Relative change (%)
Temperature	1-10 (HW)	**4.2×10^{-11}** (KW)	**15**
	11-19 (Post-HW)	0.91 (KW)	0*
	1-19 (All)	**1.9×10^{-12}** (KW)	**8**
Daily Light Integral (DLI)	1-10	**0.02** (KW)	**-12**
	11-19	**1.0×10^{-4}** ($F_{1,44}$=17.89)	**-11**
	1-19	**0.01** (KW)	**-12**
Salinity	1-10	**2.4×10^{-3}** ($F_{1,44}$=17.5)	**0***
	11-19	**0.01** ($F_{1,41}$=9.01)	**0***
	1-19	**7.9×10^{-3}** (KW)	**0***
NH_4^+ concentration	1-10	0.57 ($F_{1,44}$=0.31)	13
	11-19	0.77 ($F_{1,44}$=0.08)	2
	1-19	0.55 ($F_{1,89}$=0.36)	8
NO_3^-+NO_2^- concentration	1-10	0.16 ($F_{1,44}$=2.05)	5
	11-19	0.45 (KW)	7
	1-19	0.43 (KW)	6
PO_4^{3-} concentration	1-10	0.67 (KW)	-3
	11-19	0.17 ($F_{1,44}$=1.96)	-17
	1-19	0.59 (KW)	10
SiO_2 concentration	1-10	**6.0×10^{-4}** ($F_{1,44}$=13.57)	**42**
	11-19	0.63 ($F_{1,44}$=0.23)	-10
	1-19	0.05 ($F_{1,89}$=3.86)	16

3 2 Phytoplankton community: chl-*a* fluorescence, µ, *l*, and PFTs

The chl-*a* fluorescence dynamic indicated that the experiment started during a phytoplankton bloom as concentrations increased from d1 to d2 reaching 4.04 ± 0.51 µg L^{-1} in the control treatment, before decreasing until d13, with the lowest value being 1.21 ± 0.13 µg L^{-1}, and then slightly increasing again until the end of the experiment (Fig 2A). The HW treatment has a similar dynamic, peaking on d2, then decreasing however both the HW and the Post-HW periods. Concentrations were significantly higher in the HW treatment compared to the control, by an average of 13% and 20% respectively (Table 4).

In the control, µ varied from 0.26 ± 0.03 d^{-1} (d5) to 0.97 ± 0.04 d^{-1} (d19). During the HW period, it was relatively constant and generally higher than 0.3 d^{-1}, except on d5 (0.26 ± 0.03 d^{-1}). During the Post-HW period, it displayed more fluctuations, with peaks on d13, d15, d17 and d19 (Fig 2B). In the HW treatment µ was significantly higher than in the control treatment by an average of 16% during the HW period, while no significant effect was found in the Post-HW period (Table 4).

In the control, *l* ranged from 0.28 ± 0.03 d^{-1} (d5) to 1.27 ± 0.04 d^{-1} (d19). It increased from d5 to d9, and from d12 to d19 (Fig 2C). Similarly to µ, *l* was significantly higher in the HW treatment compared

to the control during the HW period by an average of 21%, but, departing from μ, *l* stayed significantly higher in the HW treatment compared to the control during the Post-HW period by an average of 6% (Table 4). In the control treatment, as μ was generally lower than *l*, the μ : *l* ratio was negative 16 days out of 19 (Fig 2D). The ratio was significantly lower in the HW treatment than in the control during the HW period, by an average of 45%, while it was not significantly changed during the Post-HW period (Table 4).

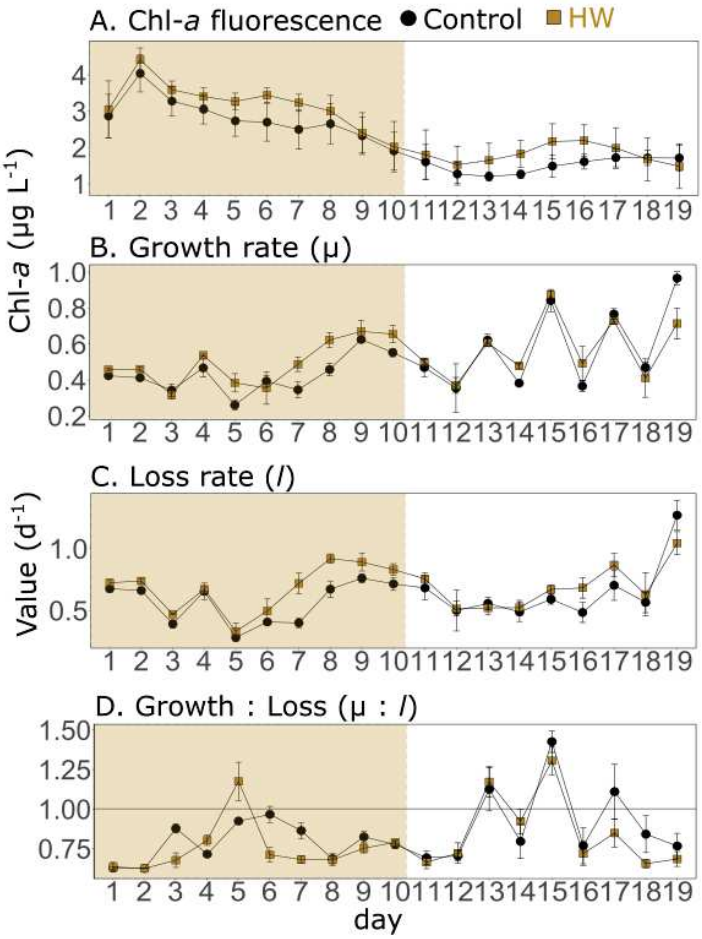

Figure 2. **Daily means of phytoplankton chlorophyll-*a* fluorescence** (corrected for NPQ, A), μ (B), *l* (C), μ : *l* (D) in the control (black) and HW (gold) treatments. The gold shaded area represents the HW period during which the +3°C was applied in the HW mesocosms. Error bars represent the standard deviation.

In the control treatment, the main phytoplankton taxonomic pigments were the fucoxanthin (associated to diatoms) and the 19'-HF (associated to prymnesiophytes), with average concentrations of 1.17 ± 0.17 and 1.27 ± 0.21 μg L^{-1}, respectively. Peridinin (associated to dinoflagellates), chl-b (associated to green algae) and zeaxanthin (associated to cyanobacteria) were present with lower concentrations. The fucoxanthin, 19'-HF, and chl-*b* concentrations followed a similar temporal trend (Fig 3A, C, D). They increased at the beginning of the experiment, then generally decreased until d12 or d13 depending on

the pigment, before increasing again at the end of the experiment. However, while fucoxanthin and chl-*b* concentrations decreased rapidly after their peak on d3, the 19'-HF concentration remained high until d10. At the beginning of the experiment, the peridinin concentration was extremely low (under the detection limits). Then, it generally increased until d14, with peaks on d9, d11 and d14, then decreased on d15 and remained relatively constant until the end of the experiment (Fig 3B). The zeaxanthin concentration stayed relatively constant during the entire experiment, peaking on d4, d7 and d15 and reaching its minimum on d9 (Fig 3E).

During the HW period, a significant increase was found in the HW treatment for the fucoxanthin and the 19'-HF concentrations, both by an average of 12% (Table 4). During the Post-HW period, the zeaxanthin concentrations were significantly higher in the HW treatment by an average of 47%, while the peridinin concentrations were significantly reduced by an average of 48% (Table 3). No other significant differences between the two treatments were found.

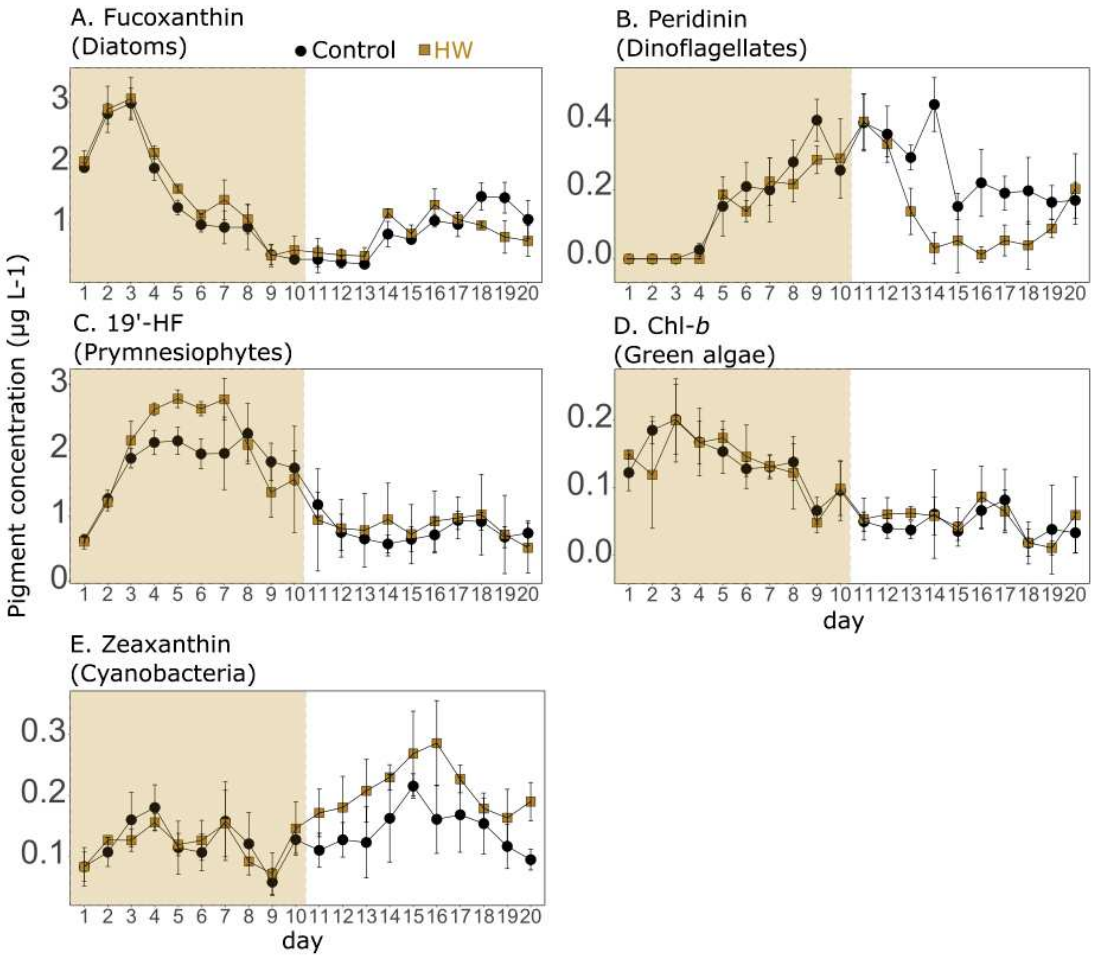

Figure 3. **Phytoplankton Functional Types (PFTs) assessed as daily mean concentrations of fucoxanthin (A), peridinin (B), 19'-hexanoyloxyfucoxanthin (19'-HF, C), chlorophyll-*b* (Chl-*b*, D), and zeaxanthin (F)** in the control (black) and HW (gold) treatments. The gold shaded area represents the HW period during which the +3°C was applied in the HW mesocosms. Error bars represent the standard deviation. Note that the scales of the y-axis are different.

Table 4. **Summary table of statistical test results and relative changes between the HW and control treatments on chl-*a* fluorescence, µ, *l*, and pigment concentrations** during the HW period, the Post-HW period and during the entire experiment. The significance level of the statistical test was set as 0.05, and significant *p*-values were highlighted in bold in the table.

Parameter	Period	*P*-value	Relative change (%)
Chl-*a* fluorescence	1-10 (HW)	**6.4×10^{-4}** ($F_{1,48}$=26.57)	**13**
	11-19 (Post-HW)	**0.02** ($F_{1,44}$=9.12)	**20**
	1-19 (All)	**1.0×10^{-4}** ($F_{1,93}$=24.14)	16
µ	1-10	**$<1.0 \times 10^{-4}$** ($F_{1,48}$=25.79)	**16**
	11-19	0.67 ($F_{1,44}$=0.19)	-1
	1-19	**2.7×10^{-3}** ($F_{1,93}$=9.52)	**6**
l	1-10	**$<1.0 \times 10^{-4}$** ($F_{1,48}$=44.40)	**21**
	11-19	**0.04** ($F_{1,44}$=3.91)	**6**
	1-19	**$<1.0 \times 10^{-4}$** ($F_{1,93}$=28.76)	**13**
µ : *l*	1-10	**0.04** (KW)	**-45**
	11-19	0.23 (KW)	18
	1-19	**0.02** (KW)	**-32**
Fucoxanthin (Diatoms)	1-10	**3.2×10^{-3}** ($F_{1,49}$=9.59)	**12**
	11-19	0.60 ($F_{1,49}$=0.28)	-4
	1-19	0.09 ($F_{1,99}$=2.97)	6
19'-HF (Prymnesiophytes)	1-10	**0.03** ($F_{1,49}$=4.73)	**12**
	11-19	0.73 ($F_{1,49}$=0.12)	7
	1-19	0.66 (KW)	10
Chl-*b* (Green algae)	1-10	0.73 ($F_{1,49}$=0.12)	-2
	11-19	0.34 (KW)	12
	1-19	0.82 (KW)	1
Zeaxanthin (Cyanobacteria)	1-10	0.87 ($F_{1,49}$=0.03)	-1
	11-19	**$<1.0 \times 10^{-4}$** ($F_{1,49}$=34.49)	**47**
	1-19	**2.0×10^{-4}** ($F_{1,99}$=15.06)	**25**
Peridinin (Dinoflagellates)	1-10	0.43 (KW)	-12
	11-19	**3.6×10^{-4}** (KW)	**-48**
	1-19	**4.7×10^{-3}** (KW)	**-35**

3 3 Plankton community metabolism: Gross Primary Production, Respiration and Net Community Production

In the control treatment, the GPP ranged from 0.27 ± 0.01 (d3) to 0.95 ± 0.08 gO_2 m^{-3} d^{-1} (d16). It peaked on d8 and d16 (Fig 4A). During both the HW and the Post-HW periods, it was significantly enhanced in the HW treatment compared to the control by an average of 32% and 31%, respectively (Table 5). The highest difference was found on d15, with the GPP being 94% higher in the HW treatment. Finally, on the two last days of the Post-HW period (d18 and d19), GPP values decreased to reach the level of the control treatment.

The R varied from 0.29 ± 0.01 gO_2 m^{-3} d^{-1} (d3) to 0.81 ± 0.09 gO_2 m^{-3} d^{-1} (d18). It remained relatively constant during the entire experiment, except between d11 and d13 and between d15 and d18 when it increased (Fig 4B). Similarly to the GPP, it was significantly increased in the HW treatment compared to the control during the HW period by an average of 49% (Table 5). In addition, R were significantly higher in the HW treatment during the Post-HW period by an average of 20%, but returned to the control level on d19. The biggest difference between treatments was found on d15 (95%).

As a consequence, in the control treatment, the NCP was positive 10 days out of 19 and ranged from -0.19 ± 0.06 (d18) to 0.20 ± 0.03 gO_2 m^{-3} d^{-1} (d8). The mean NCP (3.2×10^{-3} ± 0.03 gO_2 m^{-3} d^{-1}) indicates a globally autotrophic system (Fig 4C). In the HW treatment, the NCP was positive 7 days out of 19, with a mean value of 6.1×10^{-3} ± 0.10 gO_2 m^{-3} d^{-1}. During the HW period, the NCP was significantly reduced in the HW treatment compared to the control by an average of 157% (Table 5). In the Post-HW period however, no statistically significant differences were found between the two treatments.

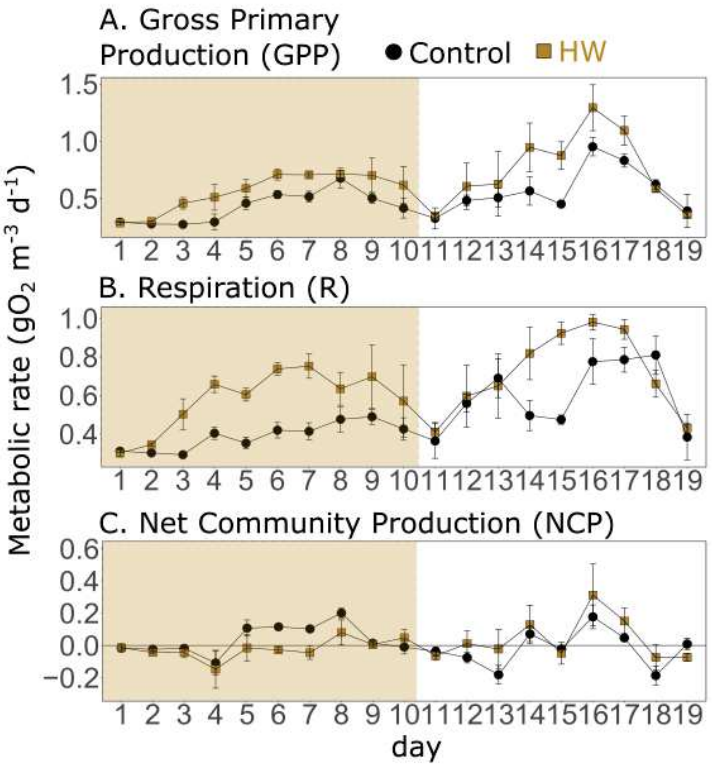

Figure 4. **Daily means of Gross Primary Production (GPP, A), Respiration (R, B), Net Community Production (NCP, C)** in the control (black) and HW (gold) treatments. The gold shaded area represents the HW period during which the +3°C was applied in the HW mesocosms. Error bars represent the standard deviation.

Table 5. **Summary table of statistical test results and relative changes between treatments on oxygen metabolism parameters** during the HW period, the Post-HW period and during the entire experiment. The significance level of the statistical test was set as 0.05, and significant *p*-values were highlighted in bold in the table.

Parameter	Period	*P*-value	Relative change (%)
GPP	1-10 (HW)	**1.7×10^{-3}** (KW)	**32**
	11-19 (Post-HW)	**4.0×10^{-4}** ($F_{1,44}$=14.92)	**31**
	1-19 (All)	**$<1.0 \times 10^{-4}$** ($F_{1,94}$=52)	**31**
R	1-10	**1.8×10^{-5}** (KW)	**49**
	11-19	**1.4×10^{-3}** ($F_{1,44}$=11.64)	**20**
	1-19	**4.5×10^{-5}** (KW)	**33**
NCP	1-10	**0.02** (KW)	**-34**
	11-19	0.37 (KW)	10
	1-19	0.37 (KW)	-11

3 4 Relationships between plankton metabolism, pigment, and environmental variables

Principal Component Analyses (PCA) were assessed to highlight potential correlations between plankton metabolic rates, PFTs, and environmental variables logarithm response ratio (LRR) during both the HW and the Post-HW periods (Fig 5). The PCAs enabled to project variables in a multidimensional space and showed general relationships between metabolic and environmental variables LRR (Fig 5A, B) and between metabolic and PFTs LRR (Fig 5C, D). Moreover, ordinary least squares linear relationships between LRR of metabolic, PFTs and environmental variables were assessed to refine the relationship between specific variables. Only relationships that were found to be significant (*p*-value < 0.05) during at least one of the tested periods are indicated in Table 6.

For both periods, GPP, R and chl-*a* fluorescence were grouped near to the first PCA axis (Fig. 5A, B). Salinity was part of this group during the HW period, and µ, *l* and orthophosphate concentration were part of it during the Post-HW period (Fig 5B). During the HW period, this group was opposed to DLI and nitrate, nitrite and ammonium concentrations, suggesting a negative relationship between them. In line with these results, a significant positive linear relationship was found between GPP and R, and between l and temperature during the HW period (Table 6). During the Post-HW period, significant relationships were found between µ and *l*, GPP, chl-*a* fluorescence, and orthophosphate concentration, between GPP and R, chl-*a* fluorescence and orthophosphate concentration, and between R and chl-*a* fluorescence.

During the HW period, µ appeared to be close to dinoflagellates, and *l* to both dinoflagellates and diatoms (Fig 5C). R was close to prymnesiophytes and green algae. During the Post-HW period, GPP , R and l were part of a group alongside prymnesiophytes and opposed to dinoflagellates (Fig 5D). A significant linear relationship was found between µ and diatoms during both periods and between µ and

dinoflagellates during the HW period (Table 6). Diatoms were also positively correlated with *I* during the HW period. In addition, GPP and diatoms and prymnesiophytes were found positively related when considering the entire experiment and during the Post-HW period, respectively. Finally, R and prymnesiophytes were also linearly related, but only during the HW period (Table 6).

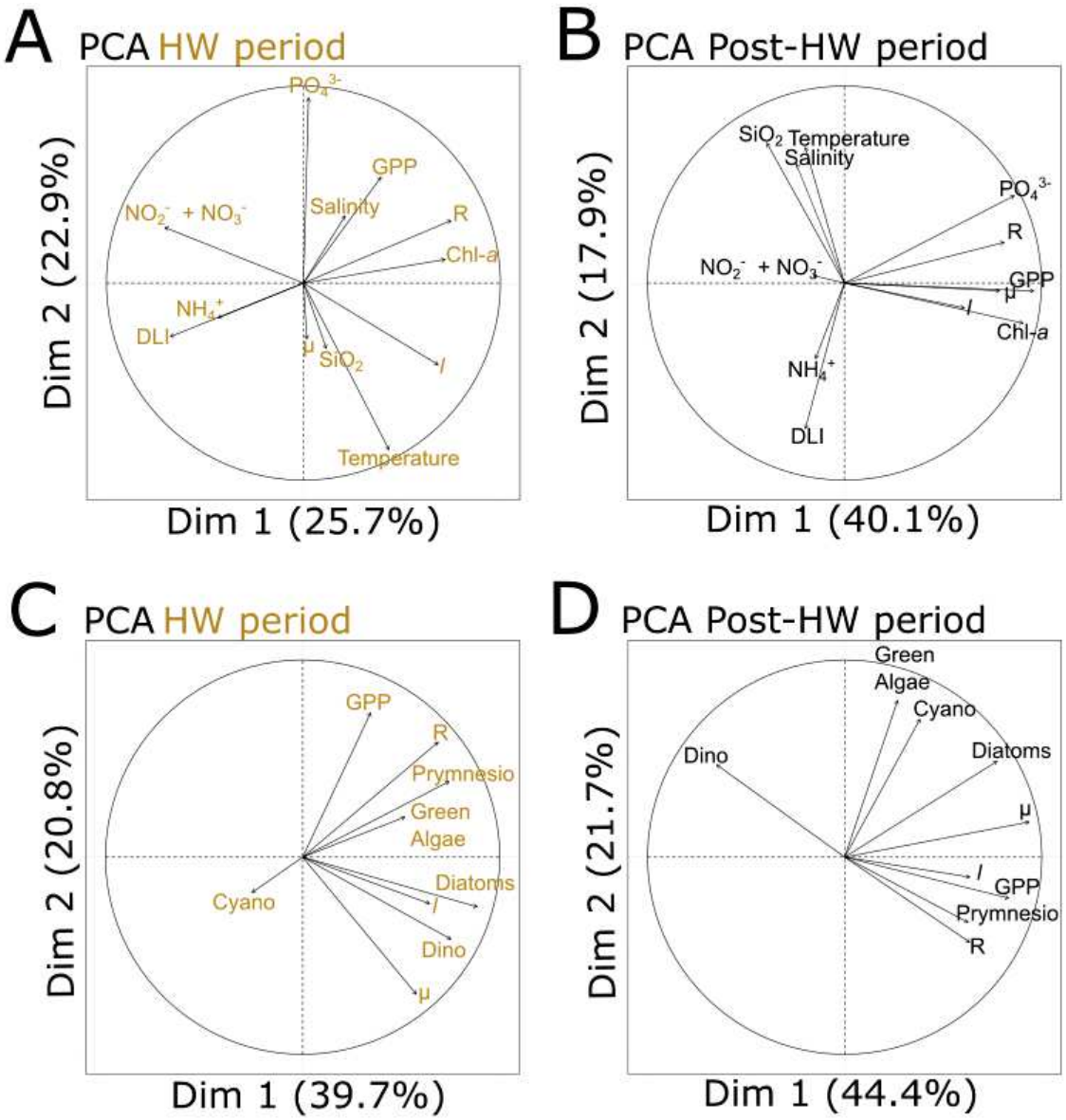

Figure 5. Principal Component Analyses (PCA) of the log response ratio (LRR) of metabolic and environmental variables during the HW period (A) and the Post-HW period (B), and PCA of the LRR of metabolic parameters and PFTs during the HW period (C) and the Post-HW period (D). When variables are close to each other, they are positively correlated. When they are opposed, they are negatively correlated. When they are orthogonally located, they are not correlated. When variables are close to the center, they are not well-represented by the analysis.

Table 6. **Ordinary least squares linear relationships between plankton community metabolism, PFTs, and environmental variables**. The significance level is indicated with * (* $p < 0.01$, ** $p < 0.001$, *** $p < 0.0001$). Only significant relationships in at least one tested period are mentioned in the table.

	HW (d1-d10)	Post-HW (d11-d19)	All (d1-d19)
μ ~ *l*	y = 0.47 x + 0.02	**y = 0.80 x - 0.02 ***	**y = 0.68 x - 0.01 ****
μ ~ GPP	y = -0.20 x + 0.08	**y = 0.46 x - 0.04 ***	y = 0.22 x + 0.01
μ ~ Chl-*a*	y = 0.08 x + 0.06	**y = 0. 69 x - 0.05 ***	y = 0.39 x + 0.01
GPP ~ R	**y = 0.65 x + 0.01 ***	**y = 0. 80 x + 0.04 ****	**y = 0. 65 x + 0.03 *****
GPP ~ Chl-*a*	y = -0.01 x + 0.13	**y = 1.31 x - 0.00 *****	**y = 0. 75 x + 0.07 ***
R ~ Chl-*a*	y = 0.67 x + 0.14	**y = 1.04 x - 0.01 ***	**y = 0. 78 x + 0.08 ***
l ~ Temperature	**y = 7.87 x + 0.39 ***	y = 8.10 x + 0.03	y = 0.93 x + 0.03
μ ~ PO_4^{3-}	y = -0.17 x + 0.05	**y = 0. 26 x + 0.03 ***	y = 0.20 x + 0.04
GPP ~ PO_4^{3-}	y = 0.47 x + 0.14	**y = 0. 44 x + 0.13 ****	**y = 0. 45 x + 0.14 ****
μ ~ Diatoms	**y = 0.71 x + 0.01 ***	**y = 0. 42 x - 0.01 ****	**y = 0. 50 x + 0.01 ****
μ ~ Dinoflagellates	**y = 0.52 x + 0.11 ***	y = -0.09 x - 0.04	y = 0.01 x + 0.04
l ~ Diatoms	**y = 0.72 x + 0.04 ***	y = 0.18 x + 0.03	**y = 0. 30 x + 0.05 ***
GPP ~ Diatoms	y = 0.23 x + 0.10	**y** = 0. 47 x + 0.09	**y = 0. 44 x + 0.09 ***
GPP ~ Prymnesiophytes	y = 0.27 x + 0.11	**y = 0.67 x + 0.04 ***	y = 0.40 x + 0.09
R ~ Prymnesiophytes	**y = 0.67 x + 0.14 ***	**y** = 0. 48 x + 0.05	**y** = 0. 51 x + 0.10

3 5 Stability parameters and cumulative data

The resistance over the 10d of the HW period was significantly different from the benchmark resistance for all studied functions (μ, *l*, GPP and R) and for diatoms, while it was not for all other PFTs (Fig 7). The change in resistance during the HW period was negative for all investigated parameters, except for prymnesiophytes, meaning that their resistance increased over time for parameters with a positive average resistance (μ, *l*, GPP, R, diatoms, cyanobacteria) while it means that their resistance decreased over time for parameters with a negative average resistance (green algae, dinoflagellates) (Fig 7).

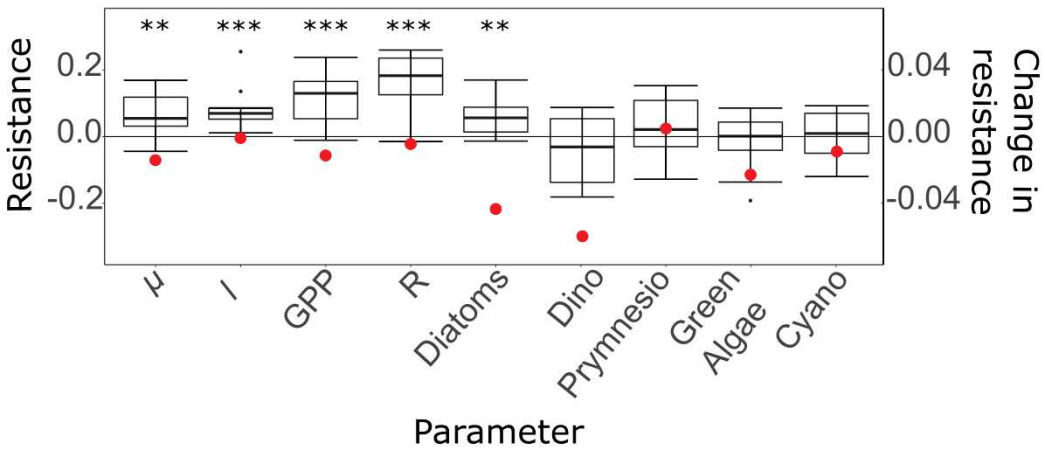

Figure 6. **Boxplot of resistance over time and change in resistance over time** (red dots) for planktonic processes (μ, *l*, GPP, R) and phytoplankton functional types (Dino: dinoflagellates,

Prymnesio: prymnesiophytes, Cyano: cyanobacteria). The results of an unpaired *t*-test testing the difference between resistance and benchmark value (0) for each parameter are presented over the boxplots when a significant *p*-value was found (**, $p < 0.01$, ***, $p < 0.001$).

The average resistance over the HW period was closer to the benchmark resistance for μ and *l* compared to GPP and R (Table 7), which indicates a better resistance for μ and *l* than for GPP and R. Among all tested functions, the system was shown to be the most resistant in terms of μ and the less resistant in terms of R. In addition, all resilience values were close to 0, the benchmark resilience, and negative, indicating that all functions continued to deviate from the control during the Post-HW period. The functions that have the worst and the best recoveries are μ and GPP. Finally, the largest temporal stability was found for μ and *l*, while GPP and R exhibited a lower temporal stability (Table 7).

Among PFTs, the highest resistance was found for cyanobacteria; and then for prymnesiophytes and green algae, while diatoms displayed the lowest (Table 7). As for the functions, all resilience values, except for prymnesiophytes, were negative and close to the benchmark, indicating a low resilience and a further deviation from the control after the Heatwave. Green algae and prymnesiophytes displayed the worst and the best recoveries, respectively. Diatoms and prymnesiophytes had the highest temporal stabilities, while dinoflagellates had the lowest (Table 7).

Table 7. **Average resistance, resilience, recovery and temporal stability** in terms of μ, *l*, GPP, R and PFTs.

	Average resistance	Resilience	Recovery	Temporal stability
Functions				
μ	0.06	-0.01	-0.13	14.96
l	0.08	-9.4×10^{-4}	-0.09	14.96
GPP	0.12	-0.01	-0.04	10.45
R	0.16	-0.0045	0.05	9.92
PFTs				
Diatoms	0.06	-0.04	-0.26	11.74
Prymnesiophytes	0.03	4.8×10^{-3}	0.02	12.05
Green algae	-0.03	-0.06	-0.05	5.92
Cyanobacteria	2.1×10^{-3}	-9×10^{-3}	0.15	6.49
Dinoflagellates	-0.04	-0.06	-0.27	2.96

When cumulated until d19, all investigated processes (GPP, R, μ, *l*) were higher in the HW treatment compared to the control (Table 8), with the lowest and the biggest differences found for μ and R, respectively. Similarly, all PFTs were higher in the HW treatment when cumulated until d20, except for dinoflagellates which were lower by an average of 35% (Table 8).

Table 8. **Cumulative GPP, R, chl-*a* fluorescence, µ, and *l* on d19, cumulative PFTs on d20 and relative difference between treatments**. When the value of relative change was smaller than 0.5%, it was set as 0 and marked by the symbol *.

Parameter	Control treatment	HW treatment	Relative change (%)
Functions			
GPP	9.38 ± 0.6 gO_2 m^{-3} d^{-1}	12.3 ± 1.32 gO_2 m^{-3} d^{-1}	31
R	9.22 ± 0.56 gO_2 m^{-3} d^{-1}	12.2 ± 0.77 gO_2 m^{-3} d^{-1}	32
Chl-*a* fluorescence	41.67 ± 7.07 µg L^{-1}	48.62 ± 7.3 µg L^{-1}	17
µ	9.53 ± 0.16 d^{-1}	10.13 ± 0.26 d^{-1}	6
l	11.47 ± 0.34 d^{-1}	13.02 ± 0.44 d^{-1}	13
PFTs			
Diatoms	23.32 ± 2.16 µg L^{-1}	24.69 ± 1.15 µg L^{-1}	6
Prymnesiophytes	25.48 ± 0.99 µg L^{-1}	28.11 ± 6.5 µg L^{-1}	10
Green algae	1.85 ± 0.11 µg L^{-1}	1.87 ± 0.15 µg L^{-1}	1
Cyanobacteria	2.71 ± 0.22 µg L^{-1}	3.18 ± 0.29 µg L^{-1}	17
Dinoflagellates	4.12 ± 0.15 µg L^{-1}	2.69 ± 0.25 µg L^{-1}	-35

4 Discussion

4 1 The heatwave enhanced functional processes and changed phytoplankton community structure.

The goal of the present study was to assess the effects of a simulated heatwave on the natural late-spring early-summer coastal Mediterranean lagoon plankton community, with a focus on phytoplankton growth and loss rates, functional types and on the whole plankton community metabolism. During the HW period, phytoplankton µ, *l*, GPP and R were increased by an average of 16%, 21%, 32% and 49% respectively in the HW treatment compared to the control.

These positive effects of the heatwave on µ and GPP are congruent with the theoretical predictions of the Metabolic Theory of Ecology (MTE, Brown et al. 2004), with observations *in situ* (López-Urrutia et al. 2006; Regaudie-de-Gioux and Duarte 2012) and with results from experimentations (Eppley 1972; Vásquez-Dominguez et al. 2007; Panigrahi et al. 2013). In the present study, µ and diatoms responses to the treatment were significantly related, meaning that the observed rise in µ is certainly due to a positive effect on diatoms. This positive effect on diatoms is in line with studies reporting higher diatom abundances under warmer conditions (Zhu et al. 2017; Sett et al. 2018; Hyun et al. 2020) and is likely due to the high silicate concentrations found in both treatments at the beginning of the experiment. Indeed, the Si : N and Si : P ratios appeared to be unusually high for the system at this time of the year (Liess et al. 2015, Trombetta et al. 2019), which likely advantaged diatoms over other phytoplankton groups. Thus, the higher silicate concentrations found in the HW treatment might have resulted in the higher diatoms associated pigment concentration in the HW treatment. This is congruent with the fact

that nutrient availabilities often override temperature in phytoplankton responses to heatwaves (Marañon et al. 2014; Hayashida et al. 2020; San Gupta et al. 2020; Domingues et al. 2021). Finally, in the present investigation, GPP was enhanced more than μ, suggesting that a substantial part of the excess carbon fixed by photosynthesis was not converted to growth, but might rather have ended as phytoplankton exudates, which joins the higher extracellular releases from phytoplankton under warming reported in the literature (Zlotnik and Dubinsky 1989, Morán et al. 2006, Engel et al. 2011).

In addition, heating enhanced *l* during the HW period, suggesting an enhancement of grazing and viral lysis. These two processes were reported to be enhanced by warming (Rose and Caron 2007; Rose et al. 2009; Aberle et al. 2012; Lara et al. 2013). Further supporting this, the positive effect of the treatment on *l* was positively related to the temperature difference between treatments. Moreover, as *l* was enhanced more than μ, the μ : *l* ratio was negatively affected by the heatwave. This is in line with a meta-analysis of μ to grazing ratio dataset estimated *in situ* in temperate coastal areas that reported a negative effect of temperature on this ratio (Cabrerizo and Marañon 2021). The μ : *l* ratio is a major factor controlling the fate of newly produced organic matter in the ocean and has important implications for element cycling. Our study implies that future heatwaves could alter the coupling between phytoplankton and their grazers, with major impacts on the structure of the microbial food web (Calbet and Landry 2004).

Similarly, community R was enhanced more than GPP during the HW period, supporting general observations in line with theoretical predictions from the MTE that reported a greater positive effect of warmer conditions on R than on GPP due to a higher activation energy for R (López-Urrutia et al. 2006; Yvon-Durocher et al. 2010; Regaudie-de-Gioux and Duarte 2012). Additionally, a strong positive relationship was found between the heatwave effects on GPP and on R, suggesting that bacterial R, which is generally the major contributor to community R in coastal waters (Robinson 2008), could be mostly dependent on autotrophic production as a carbon source, as already suggested by studies demonstrating the importance of phytoplankton exudates for bacterial metabolism (del Giorgio and Cole 1998). As a consequence of the greater increase in R than in GPP during the HW period, the NCP was reduced toward global heterotrophy. Thus, the present study indicates that moderate heatwaves could shift coastal Mediterranean lagoons from oxygen producers to oxygen sinks. Joint to the physical de-oxygenation due to global warming and higher water temperatures, heatwaves could lead to hypoxia or anoxia events, which are known to have dramatic consequences for coastal Mediterranean lagoon ecosystems (Viaroli et al. 2010).

All investigated processes showed a low resistance during the HW period, due to their higher values in the HW treatment compared to the control. However, their resistance increased as the heatwave went by. This suggests an acclimation process of the plankton community to the disturbance. Given the fact that heatwaves tend to be longer in the past decade in the Mediterranean area (Kuglitsch et al. 2010),

the effect of heatwaves on planktonic processes might be mitigated by this acclimation process. All PFTs, except diatoms, were found to be resistant to the heatwave, suggesting that heatwave-induced changes in phytoplankton community composition take more time to occur than changes in plankton processes.

4 2 Most plankton processes showed a low resilience that was associated with important changes in the phytoplankton community structure

The recovery trend of the plankton community processes accessed during the Post-HW period revealed the low resilience of GPP, R and *l* as they were significantly higher in the HW treatment relative to the control, by 6%, 31% and 20% respectively. In contrast μ quickly recovered from the heatwave as it was not significantly higher in the HW treatment compared to the control, in contrast to what was observed during the HW period.

Phytoplankton *l* was still higher in the HF treatment than in the control during the Post-HW period, but by a lower extent compared to during the HW period, suggesting that *l* partly underwent a recovery process. However, because the difference still persisted, it indicates that the heatwave probably accelerated zooplankton development and metabolism during the HW period (Hart and McLaren 1978; Vidussi et al. 2011; Wheydmann et al. 2017) which resulted in enhanced zooplankton grazing pressure that persisted during the Post-HW period, explaining the higher *l* found in the HF treatment during the Post-HW period. Nonetheless, the μ : *l* ratio was not significantly different between treatments during the Post-HW period, indicating that the unbalance toward *l* found during the HW period did not persisted during the Post-HW period, suggesting that the decoupling between phytoplankton and their predators induced by heatwaves do not extend in the long term.

Conversely to *l*, GPP and R further deviated from the control during the Post-HW period as they were higher in the HW treatment compared to the control. This phenomenon is indicated by their poor resilience values. This result is congruent with what is known for shallow lake plankton communities, as the positive effect of a simulated heatwave on GPP and R persisted several days after the end of the heatwave, regardless of nutrient status nor initial temperature (Jeppesen et al. 2021). In addition, both GPP and μ responses to the treatment were related to orthophosphate concentrations during the Post-HW period, indicating that orthophosphate availability might have regulated phytoplankton processes. This is not surprising as it is known that Thau lagoon phytoplankton can be controlled by phosphorus (Gowen et al. 2015; Derolez et al. 2020). Moreover, GPP and R were positively related to chl-*a* fluorescence and μ during the Post-HW period, in contrast to what was reported during the HW period. This could indicate that, firstly, phytoplankton had a better growth efficiency during the Post-HW period than during the HW period by converting most of the carbon fixed through photosynthesis to growth; secondly, that bacterial R still relied mainly on phytoplankton production, and finally that phytoplanktonic R might have accounted for a non-negligible part in total community R during the Post-HW period, as expected during late spring and summer (Regaudie-de-Gioux and Duarte 2012).

During the Post-HW period, NCP shifted toward autotrophy in the HW treatment, as GPP was enhanced more than R, conversely to what was observed during the HW period. This is in contradiction with the theoretical predictions of the MTE, but might be explained by indirect effects reducing the magnitude of R. Indeed, this could be explained by a trophic cascade through a positive effect of warming on the predators of bacteria (e.g. heterotrophic flagellates) during the HW period resulting in an enhanced grazing on bacteria persisting during the Post-HW period thus reducing bacteria and R, as it was shown in a previous study in the same lagoon and at the same season (Vidussi et al. 2011). Finally, it should be noted that GPP and R displayed a good recovery at the end of the Post-HW period, as they came back to the control treatment level. This recovery might be due to nutrient limitation, as nutrient concentrations tended to decreased in both treatments at the end of the experiment. Nevertheless, this indicates that HW could induce significant but reversible changes on plankton metabolism in Mediterranean coastal waters. Moreover, the cumulative data at the end of the experiment highlighted an overall positive effect of the heatwave of a similar extent on GPP and R, suggesting that heatwaves might not affect the overall balance between the capacity of coastal Mediterranean waters to produce and to consume oxygen.

In addition to important changes reported on plankton processes, the phytoplankton community structure was also significantly affected during the Post-HW period, as cyanobacteria seemed to have been favored in the HW treatment at the expense of dinoflagellates. It is well-known from the literature that cyanobacteria are often advantaged by high temperature conditions in the Mediterranean (Agawin et al. 1998; Maugendre et al. 2015; Courboulès et al. 2021). However, in the present study they increased only during the Post-HW period suggesting a potential competition with other phytoplankton groups for nutrients supply explaining this delay. As explained earlier, diatoms might have been favored by the unusually high Si : N and Si: P ratios, which could have resulted in intense competitive pressure between cyanobacteria and diatoms, as silicate concentration was shown to be a key regulator of competition between the two groups (Horn and Uhlmann 1995). Consequently, when diatoms competitive pressure decreased during the Post-HW period, cyanobacteria were potentially released from intense nutrient competition and develop. This increase was also concomitant with a strong decrease of dinoflagellates, suggesting that dinoflagellates were outcompeted by cyanobacteria during the Post-HW period in the HW treatment, maybe due to a cyanobacterial allelopathic mechanism inhibiting dinoflagellate photosynthetic activity as observed in cyanobacteria blooms (Sukenik et al. 2002). As dinoflagellates and cyanobacteria have different chemical requirements for their specific processes and play a different role within the food web, this change suggests that heatwaves could deeply alter both biogeochemical cycles and interactions among organisms. Finally, this might also explain the poor stability found for planktonic processes during the Post-HW period, as it is known that lack of compositional recovery often results in low functional resilience and recovery (Hillebrand and Kunze 2020).

4 3 Conclusions and outlooks

The unique design of the present study allowed to highlight significant changes on the metabolism of a late-spring early-summer Mediterranean coastal lagoon plankton community exposed to a simulated moderate heatwave and to assess its resistance and recovery trajectory. During the heatwave, phytoplankton growth, losses, and oxygen metabolic parameters were all enhanced by the simulated heatwave. This positive effect persisted several days after the offset of the heatwave, indicating a poor resilience of all tested functions. Nevertheless, GPP and R recovered well at the end of the experiment, indicating that heatwave effects on plankton metabolism could be reversible. In addition, the simulated heatwave induced important changes on the phytoplankton functional types structure suggesting that diatoms, prymnesiophytes and cyanobacteria could be potential winners under more frequent heatwaves occurring in late-spring early-summer in the lagoon while dinoflagellates could be the main losers.

The use of in situ mesocosm experiments and high-frequency sensors enabled to elucidate the effects of heatwaves on coastal plankton community functioning, which is necessary to refine model predictions on the future of the aquatic ecosystems. The results reported in the present study were obtained during one mesocosm experiment at one location and one season, thus their generalization to other areas or seasons must be done with care. Nevertheless, the present work contributes to broader the understanding on marine heatwaves and their potential impacts on coastal Mediterranean plankton assemblages.

5 Acknowledgements

We would like to thank Rémi Valdès, Solenn Soriano, Kevin Mestre, Camille Suarez-Bazille and David Parin, from MEDIMEER, for their precious help with the mesocosm set-up, the daily sampling, the dissolved nutrient analyses and the sensors set-up during the experiment. Moreover, we would like to thank Emilie Eveque and Jean-François Thevenot, and numerous partners from the AQUACOSM Transnational Access for their assistance with the daily sampling. The present work, plus a part of the PhD grant of TS, was funded under the AQUACOSM project, which have received funding from the European Union's Horizon 2020 research and innovation program (H2020/2017-2020) under grant agreement n°731065.

6 Authors' contributions

B.M. and F.V. conceived and designed the study and the mesocosm experiment. B.M., F.V. and S.M. managed the experiment. T.S. and S.M. calibrated all the sensors used in the study. T.S., F.V., S.M. and B.M. participated in the daily sampling of the mesocosms. T.S. and F.V. performed the phytoplankton

pigment analyses through HPLC. T.S. performed the sensor data processing, made the related analyses, and wrote the original draft of the manuscript, with inputs from all authors.

7 References

Voir la section Bibliographie de la thèse

Discussion Générale

Cette thèse a pour objectif l'étude de la réponse métabolique des communautés planctoniques côtières face à certaines perturbations liées au changement global par une approche novatrice qui repose sur l'utilisation de données acquises HF par des capteurs automatisés immergés dans des mésocosmes *in situ*. Ainsi, les travaux de cette thèse constituent des apports sur deux aspects majeurs : 1) des apports méthodologiques concernant l'utilisation de données HF issues de capteurs dans le cadre d'expériences en mésocosmes pour estimer certains processus métaboliques clés du système planctonique, et 2) des apports sur la compréhension du fonctionnement et de la réponse des communautés planctoniques côtières naturelles face à deux perturbations liées au changement global et testées de façon expérimentale.

1. Une approche novatrice : l'utilisation de données à haute-fréquence afin d'estimer les processus planctoniques en réponse à une perturbation lors d'expériences en mésocosmes

La méthode établie dans le Chapitre 1 pour estimer la production et la respiration planctoniques à partir des données HF de concentration et de saturation en O_2 dissout a été développée avec des données issues de deux expériences ayant eu lieu au même site d'étude (la lagune de Thau) mais à différentes saisons. Les différences saisonnières dans le cycle journalier d'O_2 ont ainsi été mises en évidence, ce dernier étant fortement découplé d'avec le cycle jour-nuit pour l'expérience de Mai et Juin 2019 alors que ce n'était pas le cas pour l'expérience d'Octobre 2018. La présence d'un cycle nycthéméral de l'O_2 fortement marqué, facilitant l'emploi et l'évaluation de la méthode, représentait un avantage des données issues de la lagune de Thau. L'application de la méthode sur les données acquises lors de l'expérience d'Hopavågen (Chapitre 2) a permis de confirmer qu'il était possible d'appliquer la méthode sur des données présentant un cycle nycthéméral moins prononcé qu'à Thau. Cependant, l'application de cette méthode sur les données d'Hopavågen a également mis en lumière l'impossibilité d'employer cette méthode lorsque le cycle n'est pas assez marqué, ce qui était le cas pour les jours 1, 13 et 14 de l'expérience (Chapitre 2 p 86).

Un questionnement méthodologique présenté dans l'Introduction Générale et qui n'est pas complétement résolu dans le Chapitre 1 concerne l'estimation de l'échange physique d'O_2 avec

l'atmosphère. Ce point constitue la limite principale de la méthode lorsqu'elle est appliquée dans le cadre de mésocosmes, comme expliqué dans l'Introduction Générale (p 40). Brièvement, cet échange ne peut pas être estimé via la mesure de la vitesse du vent à 10 m au-dessus de la surface comme fait généralement, car la turbulence, à l'origine de l'échange, n'est pas forcément égale dans les mésocosmes et les eaux naturelles environnantes. Dans les travaux de cette thèse, une comparaison entre les paramètres métaboliques de l'O_2 obtenus avec des valeurs du coefficient d'échange *k* faible et forte et provenant de la littérature a été réalisée dans le cadre des données complémentaires de l'article qui fait l'objet du Chapitre 1. Ces données sont présentées en Annexe III. Cette analyse avait pour but d'estimer les incertitudes générées par la valeur de *k* utilisée dans les calculs de PPB, R et PCN. Les deux valeurs de *k* choisies provenant de la littérature, 0,00936 m h^{-1} et 0,02322 m h^{-1}, correspondent à des valeurs obtenues en laboratoire dans des conditions de température et de salinité proches de celles des expériences de mésocosmes sur la lagune de Thau faisant l'objet du Chapitre 1 et via la génération de faibles et de fortes turbulences artificielles, respectivement (Alcaraz et al. 2001). Les résultats ont montré que les estimations de PPB ne sont pas significativement différentes en fonction de la valeur de *k* utilisée pour les calculs. Au contraire, les estimations de R obtenues avec la valeur de *k* faible sont significativement plus élevées que celles obtenues avec la valeur de *k* forte. Conséquemment, les estimations de PCN obtenues avec la valeur de *k* faible sont significativement moins élevées. Ainsi, une sous- ou une surestimation de la valeur de *k* entraîne potentiellement des biais dans les estimations de R et par conséquent de PCN. La difficulté d'estimer *k* dans le cadre d'expériences en mésocosmes apparaît donc toujours comme une limite. Cependant, l'intérêt des expériences de mésocosmes est de pouvoir comparer un (ou plusieurs) traitement(s) à des mésocosmes contrôles, qui ne sont pas perturbés par un traitement. Dans le cas où le(s) traitement(s) appliqué(s) n'a théoriquement aucun effet sur l'échange d'O_2 avec l'atmosphère, l'utilisation de la même valeur de *k* pour les traitements et le contrôle engendre le même potentiel biais sur les estimations de R et de PCN dans le contrôle et le(s) traitement(s), et n'a donc pas de conséquences sur la comparaison entre traitement(s) et contrôle.

Evidemment, les conditions pour lesquelles le traitement appliqué n'influe pas sur l'échange d'O_2 avec l'atmosphère ne sont pas toujours vérifiées. Par exemple, ceci n'est pas le cas pour les expériences qui testent l'effet du réchauffement, étant donné que la température joue un rôle important dans la solubilité de l'O_2 et donc dans son échange avec l'atmosphère. Dans cette situation, il est nécessaire de prendre en compte les importantes variations dans la valeur de *k* induites par la température. Dans ce but, une comparaison entre les estimations de PPB, de R et de PCN obtenues avec un *k* constant et avec un *k* qui varie en fonction de la température et de la salinité a été réalisée (Encadré Chapitre 1, p 72) à l'aide des données de l'expérience ayant eu lieu en Octobre 2018. Pour rappel, l'expérience d'Octobre 2018 comprenait un triplicat de mésocosmes contrôles, dont la température a suivi les variations naturelles *in situ*, et un triplicat de mésocosmes chauffés à +3°C par rapport aux contrôles. Dans les mésocosmes chauffés, cette comparaison a mis en évidence des estimations de R obtenues avec un *k* variable en

moyenne 7,1% plus faibles par rapport à celles obtenues avec un *k* constant, et, conséquemment, des estimations de PCN en moyenne 18,1% plus fortes. Ainsi, il apparaît nécessaire de prendre en compte les variations du *k* liées à la température et à la salinité lors d'expériences en mésocosmes dont le traitement altère ces paramètres. Pour conclure, même si l'estimation de l'échange d'O_2 avec l'atmosphère introduit toujours potentiellement des biais dans les estimations de R et de PCN, les travaux de la présente thèse permettent de comprendre et de réduire les incertitudes liées à cette estimation dans le cadre de l'application de la méthode aux expériences en mésocosmes.

Dans le cadre de la thèse, d'autres processus planctoniques ont été estimés avec les mesures des capteurs. Les données de fluorescence de la chl-*a* HF acquises lors des expériences en mésocosmes ayant eu lieu dans la lagune de Thau en Avril 2018, en Octobre 2018 et en Mai et Juin 2019 ont permis d'estimer les taux de croissance et de perte du phytoplancton (Chapitre 3, Chapitre 4). L'utilisation de ces données pour estimer ces taux permet une résolution temporelle jusqu'alors impossible avec la méthode traditionnelle des dilutions qui demande des efforts considérables d'échantillonnage, d'incubation, et des analyses très chronophages. Cependant, alors que la méthode des dilutions a été utilisée extensivement et que sa robustesse et sa fiabilité sont reconnues (Calbet 2001, Menden-Deuer et al. 2021), très peu d'études ont utilisé les données de capteurs de fluorescence de la chl-*a* pour estimer les taux de croissance et de perte du phytoplancton, et aucune dans le cadre d'expérience en mésocosmes à ma connaissance. C'est pourquoi il était nécessaire de comparer les taux estimés avec les données des capteurs de fluorescence de la chl-*a* avec ceux estimés via la méthode classique des dilutions. Cette comparaison, réalisée dans le Chapitre 3 (p 130), a mis en lumière une assez bonne concordance entre les deux méthodes malgré les différences inhérentes aux deux méthodes. Ainsi, cela tend à indiquer que les capteurs de fluorescence de la chl-*a* peuvent fournir des estimations robustes et fiables des taux de croissance et de perte du phytoplancton, au moins lorsque le problème d'advection de la masse d'eau n'existe pas, comme c'est le cas dans les mésocosmes. De plus, l'utilisation combinée des capteurs HF et de la technique des dilutions présente certains avantages : en effet, la technique des dilutions permet d'estimer la mortalité du phytoplancton liée au broutage par le microzooplancton (< 200 µm), tandis que les données des capteurs permettent d'estimer les pertes totales du phytoplancton, comprenant donc la mortalité par la prédation du micro- et mésozooplancton (> 200 µm), par la lyse virale, par la sénescence naturelle et par la sédimentation des cellules phytoplanctoniques, et donc, par comparaison, d'estimer la part liée à ces autres facteurs de perte.

La méthode présente également certaines limitations. La plus importante concerne l'estimation de la quantité de chl-*a*, et donc de la biomasse phytoplanctonique par approximation, à partir de la fluorescence de la chl-*a*. Comme expliqué dans l'Introduction Générale de la thèse (p 41), certains facteurs peuvent biaiser l'estimation de biomasse phytoplanctonique via la mesure de la fluorescence de la chl-*a*. Durant les travaux de cette thèse, cette problématique s'est particulièrement manifestée lors de l'expérience de brunissement à Hopavågen (Chapitre 2). En effet, il est apparu que la matière

humique ajoutée pour simuler le brunissement, HuminFeed®, fluoresce en partie dans les mêmes longueurs d'onde que la chl-*a*, ce qui a interféré avec le signal de fluorescence et introduit un biais systématique dans les mesures de fluorescence de la chl-*a* au sein des mésocosmes brunifiés, et c'est pourquoi les données de fluorescence ne font pas partie du Chapitre 2. Cependant, ce biais est théoriquement corrigeable en calibrant les données de fluorescence chaque jour avec une mesure de la chl-*a* non-basée sur la fluorescence, par exemple via l'analyse par chromatographie liquide à haute-performance (HPLC). La fluorométrie est l'une des approches les plus couramment utilisées pour estimer la concentration en chl-*a*, malgré les sources documentées de variabilité naturelle dans la relation entre la fluorescence et la concentration en chlorophylle. La source de variabilité la plus importante est ainsi le « quenching » non-photochimique de la fluorescence (NPQ) de la chl-*a* comme présenté dans l'Introduction générale (p 41), et sa prise en compte représente ainsi une des incertitudes majeures dans l'application de la méthode pour estimer la croissance phytoplanctonique à partir de données de fluorescence de la chl-*a*. Dans le cadre des travaux de cette thèse, ce phénomène a été pris en compte via l'interpolation linéaire des données de fluorescence de la chl-*a* entre le lever et le coucher du soleil. Cette méthode est régulièrement utilisée dans le cadre d'observations *in situ* et nécessite une homogénéité spatiale et temporelle de la communauté phytoplanctonique (Li et al. 2008, Carberry et al. 2019). Ainsi, même si cette méthode n'a pas été employée dans le cadre d'expériences en mésocosmes à ma connaissance, elle semble parfaitement adaptée aux mésocosmes, qui représentent un système fermé dont la communauté phytoplanctonique est relativement homogène. Appuyant ce constat, l'amplitude du NPQ obtenue en utilisant cette méthode pour corriger les données de fluorescence des expériences d'Avril et d'Octobre 2018 s'est révélée être significativement et linéairement corrélée à la quantité de lumière reçue dans les mésocosmes, en cohérence avec le lien théorique entre NPQ et quantité de lumière (Annexe I, p 233). Il est apparu que la fluorescence de la chl-*a* corrigée était significativement plus élevée que celle non-corrigée lors de l'expérience d'Avril 2018, tandis qu'aucune différence significative n'a été reportée pour l'expérience d'Octobre 2018, indiquant une ampleur du NPQ plus importante en Avril 2018 qu'en Octobre 2018. Finalement, une diminution significative du taux de croissance a été reporté lorsque ce dernier est calculé avec les données de fluorescence corrigées par rapport à celui obtenu avec les données non-corrigées, pour les deux expériences. Ainsi, ce résultat met en exergue l'importance que revêt la prise en compte du NPQ afin d'obtenir des estimations de croissance phytoplanctonique non-baisées, ce qui a été considéré et réalisé dans cette thèse.

2. Apports de la thèse dans la compréhension des effets du changement climatique sur le fonctionnement des communautés planctoniques côtières

2.1. Effets du réchauffement sur le fonctionnement et la composition des communautés planctoniques côtières méditerranéennes

Le même protocole expérimental a été utilisé lors des expériences d'Avril 2018, d'Octobre 2018 et pendant les 10 premiers jours de l'expérience de Mai et Juin 2019. Afin de simuler les scénarios de réchauffement de la Méditerranée d'ici la fin du siècle, ce protocole consistait en l'augmentation de la température de l'eau de 3°C d'un triplicat de mésocosmes par rapport aux mésocosmes contrôles dont la température suivait celle de la lagune de Thau (Nouguier et al. 2007, Vidussi et al. 2011). Ainsi, il est possible de comparer la réponse obtenue face à la même perturbation lors de saisons et d'années différentes : lors d'une efflorescence printanière phytoplanctonique typique de la lagune (Avril 2018, Chapitre 3), d'une période productive automnale avec une composition de la communauté planctonique particulière (Octobre 2018, Chapitre 3), et pour un système de fin de printemps et de début d'été relativement pauvre en nutriments typique d'une période de post-efflorescence (Mai et Juin 2019, Chapitre 4). Cette comparaison est importante dans le cadre d'études expérimentales investiguant les effets du changement climatique car elle permet de savoir si les résultats obtenus à un moment précis, et avec une communauté spécifique, sont représentatifs d'un patron de réponse général de ce système ou non, et si les réponses observées se conservent ou changent au fil du temps. Cette analyse est ainsi cruciale pour la construction et la calibration de modèles prédictifs.

Les réponses de la communauté planctonique en termes de production, de respiration, de croissance et de pertes face au réchauffement peuvent être séparées en deux groupes : celles qui confirment l'effet théorique d'une augmentation de la température prédit par la Théorie Métabolique de l'Ecologie (MTE), et celles qui sont en contradiction avec cette théorie. Comme détaillé dans l'Introduction Générale (p 30), cette théorie prédit un effet positif du réchauffement sur les métabolismes autotrophes et hétérotrophes, mais plus important pour le métabolisme hétérotrophe qu'autotrophe à cause d'un effet antagoniste de la température sur une des enzymes impliquées dans la photosynthèse (Allen et al. 2005). Cette différence de sensibilité à la température est supposée entraîner en conséquence un basculement des communautés vers l'hétérotrophie sous l'effet du réchauffement. Cet effet théorique a été observé pour l'expérience de Mai et de Juin 2019, durant lesquelles le réchauffement a augmenté la production primaire brute d'en moyenne 32%, contre une augmentation d'en moyenne 49% pour la respiration communautaire, résultant en une diminution de la production communautaire nette et un basculement vers l'hétérotrophie (Fig. 1). Cependant, les autres expériences ont mis en évidence des résultats différents. L'expérience d'Octobre 2018 a mis en lumière une réponse partiellement en accord avec cette théorie étant donné que le réchauffement a augmenté la production primaire brute, d'en moyenne 32%, mais pas la respiration, résultant ainsi en une augmentation de la production communautaire nette et un basculement du système vers l'autotrophie (Fig. 1). Finalement, les résultats de l'expérience d'Avril 2018 sont en complète contradiction avec la théorie, le réchauffement ayant entraîné une diminution importante de la production primaire et de la respiration, d'en moyenne 51% et 48%,

respectivement, ce qui n'a pas altéré significativement la production communautaire nette et l'état trophique du système (Fig. 1). Concernant les taux de croissance et de perte, une réponse globale et positive sous l'effet du réchauffement a été observée durant toutes les expériences. Néanmoins, même si le patron de réponse est globalement similaire, l'effet du réchauffement sur le ratio entre croissance et perte s'est révélé être différent en fonction de l'expérience considérée : un effet négatif sur ce ratio a été observé pour les expériences d'Avril 2018 et Mai et Juin 2019, tandis qu'un effet positif sur ce ratio a été reporté pour l'expérience d'Octobre 2018 (Fig. 1).

Il apparaît intéressant de proposer des mécanismes et des hypothèses pour expliquer ces différences dans la réponse métabolique du plancton face à une augmentation de la température, et notamment pour tenter d'expliquer pourquoi la théorie n'a pas été vérifiée lors des expériences d'Avril 2018 et d'Octobre 2018. En effet, dans des conditions naturelles ou quasi-naturelles comme au sein de mésocosmes *in situ*, de nombreux facteurs autres que l'effet direct de la température sur le métabolisme peuvent affecter la production et la respiration planctoniques. Parmi eux, les plus importants sont la quantité et la qualité de la lumière disponible, la quantité de nutriments disponibles, la composition de la communauté planctonique, et les interactions biotiques au sein de la communauté planctonique et avec les organismes d'échelons trophiques supérieurs. En conséquence, les conditions initiales du système jouent beaucoup dans sa réponse face au réchauffement.

Ainsi, certains paramètres abiotiques, et notamment la quantité de lumière disponible, peuvent jouer un rôle important dans la régulation du métabolisme planctonique et par conséquent dans sa sensibilité à la température (Lomas et al. 2008, Biermann et al. 2014). Dans notre cas, il apparaît peu probable que la quantité de lumière ait été importante dans la différence de sensibilité à la température reportée entre les expériences. En effet, c'est lors de l'expérience d'Octobre 2018 que la quantité de lumière disponible était la plus faible, et le réchauffement a augmenté la production primaire et le ratio croissance sur perte lors de cette expérience, suggérant que la lumière n'était pas limitante pour le métabolisme phytoplanctonique lors des expériences. Ces résultats confirment également que dans la lagune de Thau, la lumière ne semble pas limitante pour les processus phytoplanctoniques et notamment pour l'initiation des efflorescences (Trombetta et al. 2019).

La quantité et la disponibilité des ressources nutritives, et notamment des nutriments inorganiques, sont d'autres facteurs abiotiques importants dans la régulation du métabolisme planctonique. En effet, la sensibilité du métabolisme planctonique à la température est fortement dépendante des conditions nutritives du système. De nombreuses études ont ainsi montré que les prédictions de la MTE ne peuvent être vérifiées que si la quantité et la disponibilité des nutriments inorganiques ne limitent pas le métabolisme planctonique (O'Connor et al. 2009, Marañon et al. 2014, 2018). Dans le cadre des travaux de cette thèse, les concentrations en nutriments inorganiques et l'effet indirect du réchauffement sur celles-ci ont varié grandement d'une expérience à l'autre. Concernant la réponse du taux de croissance

phytoplanctonique, il semblerait que la disponibilité en nutriments inorganiques ait joué un rôle, au moins pour les expériences d'Avril et d'Octobre 2018. Plus précisément, lors de l'expérience d'Avril 2018, la croissance était sans doute limitée par le phosphate dans le traitement chauffé pendant la première moitié de l'expérience, puis stimulée par les concentrations en nitrates et nitrites plus importantes dans le traitement chauffé à partir du milieu de l'expérience. De même, lors de l'expérience d'Octobre 2018, l'augmentation de la croissance à partir du milieu de l'expérience sous l'effet du réchauffement est concomitante d'une augmentation significative de la concentration en ammonium. Concernant la réponse de la production primaire et de la respiration, le rôle de la disponibilité des nutriments est moins évident. En effet, le réchauffement a entraîné une augmentation de la production primaire pour les expériences d'Octobre 2018 et de Mai et Juin 2019 alors même que les concentrations en azote étaient plus faibles qu'en Avril 2018, expérience durant laquelle le réchauffement a diminué le métabolisme planctonique. Il semblerait donc que la disponibilité en nutriments inorganiques puisse expliquer partiellement l'effet du réchauffement sur le taux de croissance, alors qu'elle ne suffit pas pour expliquer les différences reportées dans la réponse de la production primaire et de la respiration face au réchauffement lors des expériences. D'autres mécanismes peuvent néanmoins potentiellement expliquer ces différences. Notamment, concernant l'expérience d'Octobre 2018, il est possible que ce soit la composition particulière de la communauté planctonique, majoritairement composée de cyanobactéries et de petites algues vertes, qui soit à l'origine de l'absence de réponse de la respiration face au réchauffement, en contradiction avec la théorie (Fig. 1). Comme proposé par Courboulès et al. (2021), lors de l'expérience d'Octobre 2018, la forte abondance de cyanobactéries a potentiellement résulté en un accroissement de la compétition avec les autres groupes phytoplanctoniques et les bactéries hétérotrophes pour les nutriments inorganiques sous l'effet du réchauffement, à l'avantage des cyanobactéries qui sont connues pour être de fortes compétitrices dans les eaux côtières et chaudes de la Méditerranée (Bec et al. 2011, Maugendre et al. 2015, Chen et Laws 2017), et au détriment des bactéries hétérotrophes. Or, ces dernières contribuent généralement à une part très importante de la respiration communautaire totale (Robinson 2008). Ainsi, la compétition accrue pour les ressources aurait résulté en un effet moins important du réchauffement sur le métabolisme bactérien, et donc sur la respiration communautaire, que ce qui est prédit par la MTE. D'autres interactions, et notamment avec le micro- et le mésozooplancton, peuvent potentiellement expliquer le fait que le réchauffement n'ait pas augmenté la respiration lors de l'expérience d'Octobre 2018. Ce résultat, en contradiction avec la plupart des études sur le réchauffement, a déjà été obtenu dans les mêmes conditions expérimentales dans la lagune de Thau par le passé (Vidussi et al. 2011). Les auteurs, en s'appuyant sur des données d'abondance des hétérotrophes, ont proposé un mécanisme de cascade trophique, avec un effet positif du réchauffement sur les copépodes et donc une diminution de l'abondance de leurs proies, les ciliés, libérant les flagellés hétérotrophes de la pression de prédation des ciliés, et leur permettant ainsi une prédation plus importante sur les bactéries hétérotrophes, leurs principales proies, diminuant *in fine* l'abondance, et par conséquent le métabolisme, de ces dernières. Néanmoins, aucun effet du

réchauffement sur l'abondance des bactéries n'a été reporté lors de notre étude par Courboulès et al. (2021). Dès lors, ce mécanisme ne peut pas s'appliquer à l'expérience d'Octobre 2018 et expliquer l'absence d'effet du réchauffement sur la respiration bactérienne. Par contre, c'est potentiellement la diminution de biomasse phytoplanctonique sous l'effet du réchauffement, et notamment celle des algues vertes qui étaient anormalement abondantes, qui est à l'origine de l'absence d'effet du réchauffement sur la respiration communautaire. Cela suggère une forte contribution du petit phytoplancton à la respiration communautaire, en accord avec les études qui ont montré l'importance des petits organismes planctoniques dans la lagune de Thau (Trombetta et al. 2020). Quoi qu'il en soit, il semblerait que l'absence d'effet du réchauffement sur la respiration, en contradiction avec la théorie, reportée au printemps par Vidussi et al. (2011) et dans la thèse (Encadré Chapitre 3) peut être la conséquence de différents mécanismes écologiques.

Pour l'expérience d'Avril 2018, l'effet du réchauffement sur le zooplancton peut expliquer potentiellement pourquoi le réchauffement a eu un effet négatif sur la production primaire et la respiration (Fig. 1). En effet, lors de cette expérience, le taux de perte du phytoplancton a augmenté d'en moyenne 37% sous l'effet du réchauffement, résultant en la diminution de la biomasse phytoplanctonique, évaluée par la fluorescence de la chl-*a*, d'en moyenne 64%. Cette diminution importante de la biomasse phytoplanctonique est à l'origine de la diminution de la production primaire, comme indiqué par les données de production primaire normalisée par la chl-*a* (Encadré Chapitre 3), et a probablement entraîné la diminution de la respiration communautaire, la respiration bactérienne étant fortement dépendante de la production primaire en zone côtière (Pringault et al. 2009). Il faut noter que le taux de perte est principalement dû à plusieurs paramètres : la prédation par le zooplancton, la lyse cellulaire par infection virale, la sédimentation des grosses cellules, et la senescence naturelle des cellules, cette dernière ne contribuant généralement que faiblement à la mortalité totale (Kimmance et al. 2007). Les différents prédateurs et virus n'ont pas tous la même sensibilité face au réchauffement, la composition des communautés de prédateurs et de virus modulant ainsi l'effet du réchauffement sur le taux de perte phytoplanctonique (Baudoux et al. 2008, Anderson et Harvey 2019). On peut donc émettre certaines hypothèses pour expliquer l'augmentation du taux de perte à l'origine de la diminution de la biomasse phytoplanctonique, de la production et de la respiration. Comme déjà reporté dans la littérature, le réchauffement a peut-être accéléré le métabolisme du zooplancton et/ou augmenté l'abondance des virus, résultant en des pertes plus importantes pour le phytoplancton (Aberle et al. 2007, Rose et Caron 2007, O'Connor et al. 2009, Lara et al. 2013, Courboulès et al. 2021).

En conclusion, les effets du réchauffement en contradiction avec la théorie pour les expériences d'Avril 2018 et d'Octobre 2018 pourraient être expliqués par certaines interactions de compétition ou de prédation intimement liées à la composition de la communauté planctonique étudiée. Même si la MTE a été vérifiée à l'aide d'importants jeux de données qui couvrent une grande partie de l'océan global (López-Urrutia et al. 2006, Regaudie-de-Gioux et Duarte 2012) et lors d'expérimentations en

mésocosmes (Yvon-Durocher et al. 2010), les travaux de la présente thèse montrent que la réponse métabolique des communautés planctoniques côtières méditerranéennes face au réchauffement ne suit pas toujours les prédictions théoriques. Ils mettent en évidence la complexité de cette réponse et l'importance de prendre en compte les conditions initiales du système, la composition de la communauté planctonique et les interactions biologiques lors de la construction de modèles prédictifs.

Un autre point semble également intéressant à discuter. Il s'agit du couplage entre taux de croissance et production primaire brute. En effet, il semblerait que le réchauffement ait eu un effet positif similaire sur le taux de croissance et la production primaire (normalisée par la chl-*a*) pour toutes les expériences. Ce dernier cas indique un couplage important entre photosynthèse et croissance, ce qui suggère que la majorité de l'énergie fixée par la photosynthèse est convertie en croissance. Généralement, on considère que l'efficacité de la croissance dépend de la quantité de lumière et de nutriments inorganiques disponibles ainsi que de la composition de la communauté phytoplanctonique, certains taxons ayant une meilleure efficacité que d'autres sous différentes conditions environnementales (Cloern et al. 1995, Stomp et al. 2004). Alors qu'il a été suggéré que le réchauffement diminue l'efficacité de croissance du phytoplancton de la Mer Baltique (Engel et al. 2010), il semblerait que ce ne soit pas le cas pour les communautés phytoplanctoniques de la lagune de Thau.

Les travaux de cette thèse ont mis en évidence que la composition de la communauté phytoplanctonique peut être d'une grande importance dans la réponse de certains processus phytoplanctoniques face au réchauffement (Chapitre 3 et Chapitre 4). Cette composition a été évaluée via les concentrations en pigments biomarqueurs et était propre à la saison investiguée. Il convient de noter que l'approche chemotaxonomique utilisée dans les travaux de la présente thèse s'est déjà révélée être une approche efficace dans l'estimation de la composition de la communauté phytoplanctonique de la lagune de Thau par le passé (Pecqueur et al. 2011, Deininger et al. 2016) malgré le fait qu'un même pigment peut être présent chez plusieurs groupes phytoplanctoniques, et que l'attribution taxonomique de certains pigments est parfois complexe (Roy et al. 2011). Même si la composition pigmentaire et l'effet du réchauffement sur cette dernière étaient différents en fonction de l'expérience, il est apparu dans pratiquement tous les travaux de cette thèse que ce sont principalement les diatomées qui contribuent à la biomasse et au métabolisme phytoplanctoniques dans la lagune de Thau. Ainsi, évaluer et comprendre l'effet du réchauffement sur les diatomées semblent indispensable pour prédire les effets du réchauffement sur les processus phytoplanctoniques des zones côtières méditerranéennes telles que la lagune de Thau. Les diatomées ont été affectées de façon différente en fonction de l'expérience considérée. L'effet négatif reporté en Avril 2018 est en accord avec certaines études ayant reporté une diminution de l'abondance des diatomées face au réchauffement en zone côtière méditerranéenne (Pulina et al. 2016, Pulina et al. 2020). Cependant, alors que ces études ont proposé un mécanisme de compétition avec le phytoplancton de plus petite taille pour expliquer cet effet, il semble plutôt que ce soit l'augmentation du taux de perte, comme exposé précédemment, qui en soit à l'origine dans le cas

de l'expérience d'Avril 2018. Cela suggère ainsi que les diatomées ont été l'un des groupes les plus affectés par l'accroissement du taux de perte, potentiellement parce que le métabolisme des prédateurs spécifiques des diatomées a été accéléré par le réchauffement (Peter et Sommer 2012), ou parce que le réchauffement a favorisé des espèces de diatomées plus grosses, et donc plus sujettes à la sédimentation (Riebesell 1989, Waite et al. 1997). Au contraire, les effets positifs du réchauffement sur les diatomées pour les expériences d'Octobre 2018 et de Mai et Juin 2019 sont plus inattendus, aucune étude investiguant la composition de la communauté phytoplanctonique d'une zone côtière méditerranéenne n'ayant mis en évidence un résultat similaire à ma connaissance, bien que cet effet ait été observé pour les zones côtières de la Mer Baltique et de la Mer de Corée (Sett et al. 2018, Hyun et al. 2020). Ces effets positifs sont vraisemblablement liés à la composition de la communauté planctonique et à la disponibilité en nutriments, et notamment à la disponibilité en silicate, dont on sait qu'elle régule souvent la réponse des diatomées face au réchauffement (Shatwell et al. 2008). Lors de l'expérience d'Octobre 2018, c'est sans doute l'effet négatif du réchauffement sur les petites algues vertes qui a permis de libérer les diatomées de la compétition pour l'acquisition des nutriments (Chapitre 3 p 128), les interactions avec d'autres groupes phytoplanctoniques jouant souvent un rôle important dans la réponse des diatomées face au réchauffement (Sommer et Lengfellner 2008, Lewandowska et Sommer 2010). Finalement, les travaux de la présente thèse mettent en lumière des effets du réchauffement conséquents sur la biomasse des diatomées au sein de la lagune de Thau, et tendent à indiquer un remodelage de la dynamique des diatomées au cours des saisons dans un scénario de réchauffement de la lagune dans le futur. Ce sont en majorité les diatomées qui alimentent la croissance des huîtres dans la lagune de Thau (Pernet et al. 2012), et les effets négatifs du réchauffement sur les diatomées lors de la période d'efflorescence phytoplanctonique printanière présentés dans la présente thèse (expérience d'Avril 2018) seraient ainsi lourds de conséquences pour les activités conchylicoles et économiques de la lagune.

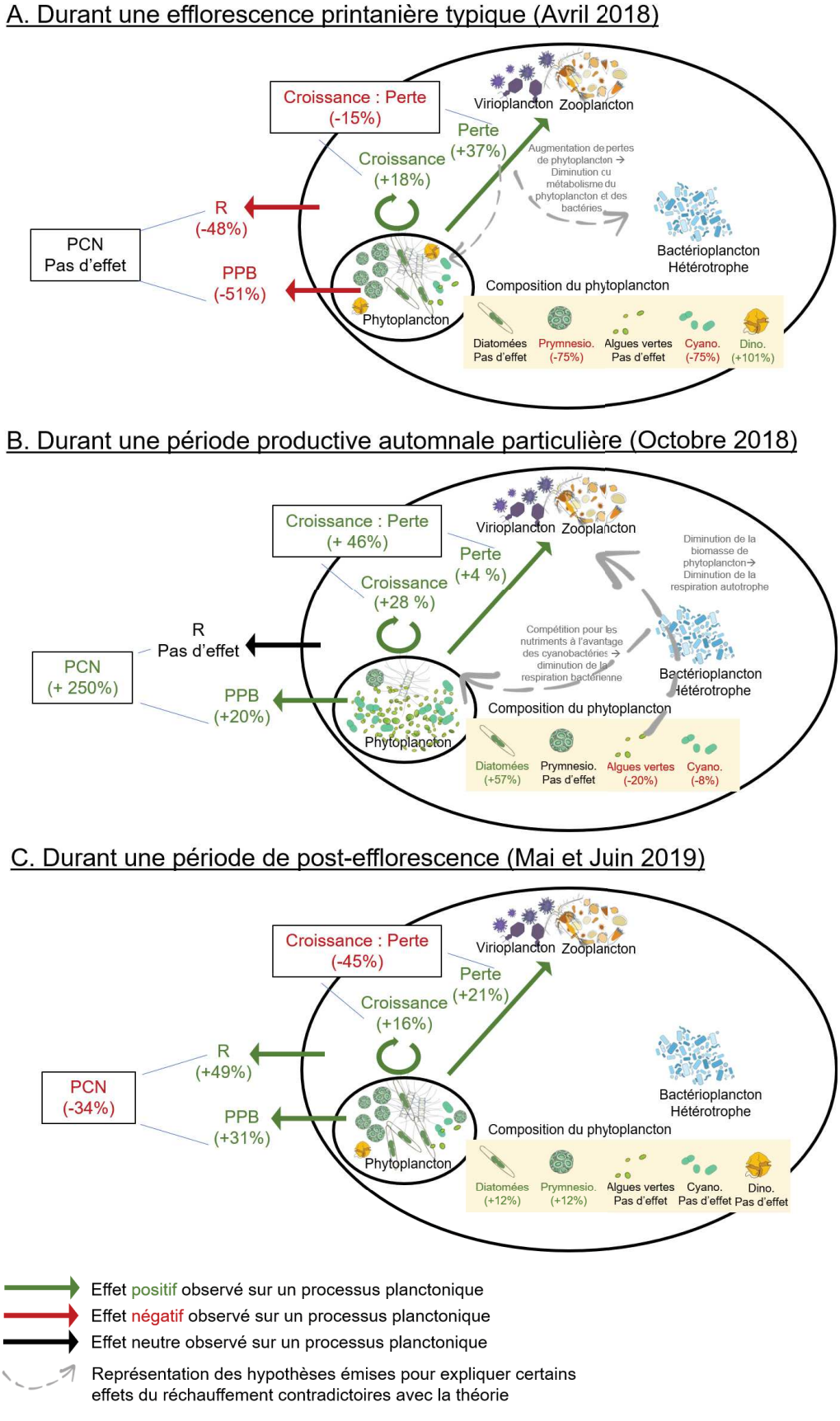

Figure 1. Représentation schématique des effets contrastés du réchauffement sur la production primaire brute (PPB), la respiration (R), la production communautaire nette (PCN), les taux de

croissance et de pertes du phytoplancton et la composition de la communauté phytoplanctonique, en comparaison des valeurs observées dans le contrôle. A. Lors d'une période d'efflorescence printanière typique de la lagune de Thau (expérience d'Avril 2018). B. Lors d'une période productive automnale particulière (expérience d'Octobre 2018). C. Lors d'une période de post-efflorescence pauvre en nutriments (expérience de Mai et Juin 2019). Les flèches vertes, rouges et noires indiquent un effet du réchauffement positif, négatif, ou non significatif respectivement. Les flèches représentées en pointillés gris correspondent aux hypothèses formulées pour expliquer certains effets du réchauffement contradictoires avec la théorie. Il faut noter que le panneau C. ne prend en compte que les 10 premiers jours de l'expérience de Mai et Juin 2019, période durant laquelle le réchauffement fut appliqué. Les dessins des organismes ont été réalisées par © J. Courboulès.

2.2. Extrapolation des conséquences d'une vague de chaleur sur une lagune déjà soumise au réchauffement constant

Les modèles simulant le réchauffement climatique prévoient que l'augmentation de la fréquence et de l'intensité des vagues de chaleur aura lieu concomitamment au réchauffement constant lié au changement climatique (IPCC 2019). L'expérience de Mai et Juin 2019, durant laquelle des mésocosmes ont été chauffés à +3°C par rapport aux mésocosmes contrôles pendant 10 jours, avant que le réchauffement ne soit stoppé pour les 10 jours suivant de l'expérience (Chapitre 4), a permis de simuler un épisode de vague de chaleur et représente la première étude expérimentale à ce sujet dans la lagune de Thau. Grâce à cette conception originale, il a été possible de caractériser les conséquences d'une vague de chaleur sur la communauté planctonique et son fonctionnement plusieurs jours après la terminaison de la vague de chaleur. Il serait donc intéressant de faire un exercice d'extrapolation afin d'évaluer si les conséquences de la vague de chaleur auront potentiellement un caractère antagoniste ou synergétique avec les effets du réchauffement constant comme ceux qui ont été observés et discutés dans la section précédente. Dans la présente section, nous allons donc évoquer les potentielles interactions entre les conséquences des vagues de chaleur comme observé lors de la deuxième partie de l'expérience de Mai et Juin 2019 (Chapitre 4) avec les effets du réchauffement constant comme ceux observés lors des expériences d'Avril et d'Octobre 2018 et lors de la première partie de l'expérience de Mai et Juin 2019 (Chapitres 3 et 4).

Les résultats de la deuxième moitié de l'expérience de Mai et Juin 2019 (Chapitre 4) montrent qu'à la suite de l'effet positif observé sur le taux de croissance du phytoplancton pendant le réchauffement, un retour au niveau du contrôle a été reporté, suggérant une capacité de résilience assez importante de ce paramètre. Cela suggère qu'une vague de chaleur, simulée dans les conditions qui caractérisent cette expérience, n'a pas d'impact à long terme (plusieurs jours ou semaines) sur la croissance de la communauté phytoplanctonique, et que c'est bien le réchauffement constant qui modifierait le plus fortement cette dernière dans le futur. Au contraire, l'effet positif observé sur le taux de perte du phytoplancton a continué après la fin de la vague de chaleur, indiquant une résilience plus faible pour

ce paramètre probablement due au temps de développement plus long des prédateurs que du phytoplancton (Aberle et al. 2012), qui ont maintenu leur capacité de prédation après l'arrêt de la vague de chaleur. Cela suggèrerait une accentuation de l'effet positif du réchauffement constant sur le taux de perte par les vagues de chaleur. Finalement, la diminution du ratio croissance sur perte observée pendant la vague de chaleur a persisté après l'arrêt de cette dernière, ce qui impliquerait un effet synergétique négatif des vagues de chaleur et du réchauffement constant sur le ratio croissance sur perte, ce qui engendrerait potentiellement une diminution importante de la biomasse phytoplanctonique et aurait des conséquences pour tout le réseau trophique.

La production primaire et la respiration ont elles-aussi continué à être plus élevées que dans le contrôle après la fin de la vague de chaleur, et cet écart a même augmenté par rapport à l'effet positif reporté pendant les 10 jours de réchauffement. Les conséquences de cette très faible résilience de la production primaire et de la respiration dépendront certainement de l'effet qu'aura le réchauffement constant sur ces paramètres. En effet, les travaux de la thèse ont mis en évidence plusieurs effets opposés du réchauffement constant sur la production primaire et la respiration dépendant notamment des conditions nutritives et des interactions au sein de la communauté planctonique (Section 2.1). Si le réchauffement constant a déjà un effet positif sur ces paramètres, comme dans les expériences d'Octobre 2018 et de Mai et Juin 2019, cela suggérerait que les vagues de chaleur vont potentiellement accroître l'effet positif du réchauffement constant. Si, au contraire, le réchauffement a un effet négatif sur la production et la respiration, comme lors de l'expérience d'Avril 2018, les conséquences des vagues de chaleur semblent être plus incertaines. Elles résulteront peut-être en une augmentation de la production primaire et de la respiration, ce qui permettrait ainsi d'atténuer les effets négatifs du réchauffement constant. Cela a été le cas lors d'une expérience de mésocosmes dans le golfe de Bothnie reportant l'atténuation des effets négatifs d'un réchauffement constant par des fluctuations de température simulant une succession de vagues de chaleur (Cabrerizo et al. 2021). Cependant, il est aussi possible que les effets combinés du réchauffement constant et de la vague de chaleur soient synergétiques et dans ce cas, la vague de chaleur amplifierait la diminution du métabolisme induite par le réchauffement constant, aggravant ainsi les conséquences de ce dernier.

Finalement, il est également possible de mettre en relation les conséquences des vagues de chaleur avec celles du réchauffement constant en termes de composition de la communauté phytoplanctonique. Nous avons montré dans le Chapitre 4 (p 159) qu'après l'arrêt du réchauffement, une augmentation importante du pigment associé aux cyanobactéries a été observée dans le traitement préalablement chauffé. Cette augmentation semble avoir eu lieu au détriment des dinoflagellés péridiniens et a potentiellement comme origine une plus grande compétitivité des cyanobactéries pour l'acquisition des nutriments inorganiques à des températures plus élevées. Etant donné qu'il a été reporté dans la littérature que le réchauffement constant favorisera probablement les cyanobactéries, et notamment en zones côtières méditerranéennes telles que la lagune de Thau (Bec et al. 2005, Courboulès et al. 2021),

les résultats du Chapitre 4 laissent supposer que les vagues de chaleur vont accélérer encore plus ce phénomène. Dans le cas spécifique de la lagune de Thau, les changements induits dans la structure de la communauté phytoplanctonique par un épisode de vague de chaleur pourraient ainsi avoir des conséquences importantes pour l'activité ostréicole, et donc pour un secteur d'activités très important de la région, car les huîtres ne peuvent se nourrir que d'organismes dont la taille est bien supérieure à celle des cyanobactéries (Dupuy et al. 2000, Pernet et al. 2012). Cependant, les cyanobactéries seraient broutées par les ciliés, dont l'abondance augmenterait. Les ciliés pourraient à leur tour servir de nourriture aux huîtres, et, *in fine*, les vagues de chaleur induiraient donc un effet positif sur les huîtres.

En conclusion, les conséquences des vagues de chaleur sur les processus planctoniques pourraient interagir avec les effets du réchauffement constant, et souvent de manière synergétique, notamment quant à l'augmentation des taux de croissance et de perte du phytoplancton. Il est cependant prudent de noter qu'une généralisation des résultats observés lors d'une seule expérience en mésocosmes est à faire avec précaution. Dans tous les cas, les travaux de la thèse accentuent la nécessité de prendre en compte les effets des vagues de chaleurs, trop souvent négligés, dans l'élaboration des modèles prédictifs.

2.3. Effets du brunissement sur le fonctionnement et la composition des communautés planctoniques côtières septentrionales

2.3.1. Avantages et inconvénients de l'utilisation de matière humique artificielle pour simuler un épisode de brunissement naturel

Le phénomène de brunissement au sein des écosystèmes aquatiques dépend fortement de plusieurs facteurs environnementaux locaux, notamment la topographie de la zone et le type de sol ainsi que la couverture végétale à proximité (Roulet et Moore 2006, Frigstad et al. 2020). Ainsi, de par sa complexité et sa multiplicité, le brunissement est difficile à simuler dans le cadre d'une expérimentation. Plusieurs méthodes sont employées dans les études expérimentales testant le brunissement sur les écosystèmes aquatiques. La première option consiste à prélever de la matière organique (soit directement depuis le sol, soit avec de l'eau d'un système aquatique très humique), à la filtrer par osmose inverse et/ou la faire maturer, et à l'ajouter directement au système étudié (Deininger et al. 2016, Mustaffa et al. 2020). Cette méthode a l'avantage de simuler assez fidèlement les processus naturels de brunissement de la zone étudiée, cependant une caractérisation de la matière organique utilisée, trop souvent absente des études, est nécessaire afin de connaître avec précision la composition de la matière organique, la quantité de nutriments organiques et inorganiques et son spectre d'absorption. De plus, une extrême précaution est nécessaire afin d'éviter les contaminations biotiques provenant de l'ajout de matière humique naturelle dans les mésocosmes, et ces contaminations ne sont pas toujours facilement détectables (Scharnweber et al. 2021). Au contraire, une autre méthode,

employée dans les travaux de la présente thèse (Chapitre 2) et couramment dans le cadre d'études en écologie aquatique, consiste à utiliser une matière humique commerciale, telles qu'HuminFeed® (HuminTech, Allemagne) ou SuperHume® (Ag Concepts, États-Unis), pour simuler le brunissement. Ces matières humiques commerciales sont presque exclusivement dérivées de léonardite (i.e., de lignine oxydée) et furent conçues pour des applications agricoles (Quilty et Cattle 2011). L'utilisation de ces sources commerciales présente les avantages de pouvoir répliquer une même expérience dans des systèmes et à des saisons différentes avec la même source de matière humique, d'éviter avec certitude une contamination biotique, et enfin de connaître avec une grande précision la composition chimique de la matière ajoutée. Cependant, un inconvénient réside dans le fait que la matière ajoutée n'est pas forcément représentative des épisodes naturels de brunissement ayant lieu dans la zone étudiée (Scharnweber et al. 2021).

Ainsi, une expérience de mésocosmes dans un lac à l'est de la Suède a mis en évidence un effet positif sur la concentration en chlorophylle-*a* plus important avec un ajout d'HuminFeed® qu'avec un ajout de matière humique naturelle filtrée par osmose inverse ou un ajout d'un mélange de matière humique naturelle filtrée par osmose inverse et d'HuminFeed® (Nydahl et al. 2019). Dans le cadre de la présente thèse, la question se pose de savoir si HuminFeed®, la matière humique commerciale utilisée pour simuler le brunissement à Hopavågen, peut engendrer les mêmes conséquences que les épisodes naturels de brunissement des eaux côtières norvégiennes. Pour le cas du fjord de Trondheim spécifiquement, le brunissement est attribué essentiellement à des apports terrestres de matière organique dissoute colorée (*colored dissolved organic matter*, cDOM) et de matière suspendue particulaire d'origine terrestre (*terrestrial suspended matter*, TSM), et a pour conséquence une diminution de la quantité de lumière disponible et un enrichissement en nutriments organiques et inorganiques (Mascarenhas et al. 2017, Mascarenhas et Zielinski 2018). La baie d'Hopavågen étant directement connectée au fjord de Trondheim et échangeant quotidiennement en moyenne 14% de son volume d'eau avec le fjord (van Marion 1996), nous pouvons considérer que les épisodes de brunissement ayant lieu dans la baie d'Hopavågen possèdent des caractéristiques similaires à ceux affectant le fjord de Trondheim. L'ajout d'HuminFeed® permet de simuler fidèlement une des conséquences du brunissement comme observé dans le fjord de Trondheim : l'atténuation de la lumière (Lebret et al. 2018). Par contre, pour ce qui est de l'apport de nutriments organiques et inorganiques, l'ajout d'HuminFeed® n'est potentiellement pas représentatif des apports naturels liés aux épisodes de brunissement, pour plusieurs raisons, et notamment une composition en éléments nutritifs différente et une biodisponibilité moins importante (Scharnweber et al. 2021).

Ainsi, dans le cadre de l'expérience de brunissement effectuée pendant cette thèse, les effets observés de l'ajout d'HuminFeed® sur la composition pigmentaire du phytoplancton et la diminution de la production primaire, attribués à l'atténuation de la lumière, sont probablement représentatifs de l'effet du brunissement naturel à Hopavågen. La diminution de la respiration communautaire, par contre, est

probablement due au fait qu'HuminFeed® ne représente pas une source de matière organique dissoute facilement disponible pour les bactéries, contrairement aux apports liés aux épisodes de brunissement naturels qui peuvent contenir de la matière labile et réfractaire en différentes proportions. Par conséquent, ces derniers ont potentiellement un effet positif sur la respiration communautaire, principalement composée de la respiration bactérienne (Robinson 2008), qui n'a pas été observé dans les résultats obtenus dans la thèse (Chapitre 2). Ce point démontre ainsi la difficulté de mettre en place une simulation du brunissement qui répond à la fois aux exigences de reproductibilité des expérimentations en mésocosmes et qui permet également de simuler fidèlement les phénomènes naturels.

2.3.2. Conséquences du brunissement sur les communautés planctoniques des eaux côtières septentrionales

Contrairement au réchauffement, qui touche tous les océans du monde, le brunissement est un phénomène qui ne concerne que certaines régions, notamment les zones côtières septentrionales. Néanmoins, les régions touchées font partie des écosystèmes les plus productifs au monde et constituent ainsi d'importantes zones de séquestration du carbone (Cloern et al. 2014, Smith et al. 2015). Elles délivrent également de nombreux services écosystémiques (Barbier et al. 2011), en étant notamment une zone privilégiée pour le développement d'espèces majeures pour les pêcheries et pour la pisciculture (Skogen et al. 2009, Checkley et al. 2017). Alors qu'au cours des dernières décennies, les apports de matière organique d'origine terrigène dans les écosystèmes d'eau douce septentrionaux n'ont cessé d'augmenter, résultant en un accroissement de l'afflux de matière organique au sein des écosystèmes côtiers ayant pour conséquence leur brunissement, les conséquences de ce phénomène sur les écosystèmes côtiers sont encore très incertaines, car peu d'études s'y sont intéressées (Monteith et al. 2007, Aksnes et al. 2009, de Wit et al. 2016, Frigstad et al. 2020a). L'étude effectuée pendant la thèse et faisant l'objet du Chapitre 2 apporte certains éléments de réponse quant aux conséquences du brunissement sur le métabolisme des communautés planctoniques côtières septentrionales.

Nous avons montré une réduction de la production primaire et de la respiration d'environ un tiers sous l'effet du brunissement, pour la première fois à ma connaissance. Même s'il semblerait que cette réduction n'ait pas de conséquences significatives sur le bilan total d'O_2 au sein des écosystèmes côtiers, étant donné que les capacités de production et de consommation d'O_2 ont été réduites d'une ampleur similaire, cette réduction des flux de production et de consommation d'O_2 est le signe d'un dysfonctionnement de la communauté planctonique engendré par le brunissement. En effet, le métabolisme planctonique, qu'il soit autotrophe ou hétérotrophe, est en relation avec la biomasse des organismes. Par exemple, nous avons mis en évidence que le brunissement a réduit la biomasse phytoplanctonique (Chapitre 2). De façon générale, les changements qu'induit le brunissement peuvent

altérer les stocks de producteurs primaires et secondaires et entraîner des effets en cascade sur les consommateurs de ces stocks. Par exemple, dans les eaux côtières norvégiennes, on sait que le brunissement a favorisé l'extrême prolifération des méduses, à l'origine de phénomènes d'hypoxie et d'anoxie localisés (Aksnes et al. 2009, Sweetman et al. 2016). Ces derniers ont souvent des conséquences majeures pour les organismes des écosystèmes côtiers (Breitburg 2002, Conley et al. 2007), et les effets du brunissement sur le métabolisme planctonique reportés dans la thèse pourraient être accompagnés par d'autres mécanismes affectant le fonctionnement des communautés planctoniques côtières septentrionales.

Nous avons également montré que le brunissement est à l'origine d'importants changements au sein de la composition des communautés phytoplanctoniques et zooplanctoniques. Le brunissement a favorisé le genre d'appendiculaire *Oikopleura*, qui se nourrit par filtration. Ce résultat corrobore certaines études ayant reporté un effet positif du brunissement sur les organismes filtreurs, au détriment d'organismes ayant un mode de prédation basé sur la vision (Aksnes et al. 2004, Frigstad et al. 2020b). Les larves de poisson, des prédateurs visuels, pourraient ainsi pâtir du brunissement. Couplée à la baisse de biomasse phytoplanctonique reportée dans notre étude, premier maillon du réseau trophique dont les stocks de poissons dépendent, le brunissement pourrait ainsi avoir de lourdes conséquences pour les pêcheries, l'une des activités socio-économiques les plus importantes des eaux côtières septentrionales (Aksnes 2007). De plus, dans le Chapitre 2, le changement dans la composition de la communauté zooplanctonique engendré par le brunissement aurait impacté la composition de la communauté phytoplanctonique, en modifiant la pression de broutage sur certains groupes taxonomiques. Or, il a été montré que la composition de la communauté phytoplanctonique régule la production primaire (Fu et al. 2016, Mayot et al. 2017). La diminution de la biomasse des diatomées, qui sont d'importantes contributrices à la production primaire des écosystèmes nordiques (Larsen et al. 2004), sous l'effet du brunissement reportée dans le Chapitre 2 montre ainsi que l'effet du brunissement sur la composition du phytoplancton pourrait impacter la productivité des communautés phytoplanctoniques à long-terme, bien que cela soit non reporté dans la littérature à ce jour à ma connaissance.

2.4. Comparaison de la stabilité des communautés planctoniques de la lagune de Thau et de la baie d'Hopavågen face aux évènements ponctuels liés au changement global

Nous évaluons dans ce sous-chapitre la stabilité, tant en termes de fonctions que de composition pigmentaire, des communautés planctoniques côtières étudiées dans cette thèse, à savoir celles de la lagune de Thau et de la baie d'Hopavågen, face aux perturbations ponctuelles liées au changement global, comme c'est le cas des vagues de chaleur et du brunissement. Bien qu'il s'agisse de deux zones

d'études différentes qui ont été soumises à deux perturbations différentes, cette comparaison a pour but de donner quelques éléments afin d'identifier la communauté planctonique susceptible d'être la plus sensible aux perturbations ponctuelles liées au changement climatique global. Il s'agit également de répondre à un questionnement écologique plus théorique que réel : observe-t-on une résistance et une trajectoire de récupération similaire quand on soumet deux communautés planctoniques différentes à deux perturbations différentes ? Ou bien la réponse est indépendante de la communauté et de la perturbation ? Pour répondre à ces questionnements, les paramètres de stabilité (résistance, résilience, récupération et stabilité temporelle) obtenues pour certaines fonctions (production primaire et respiration) et pour les concentrations des pigments communs aux deux expériences (Encadré Chapitre 2, Chapitre 4) ont été comparés dans le Tableau 1. Ce tableau indique pour chaque paramètre testé (production primaire, respiration, concentrations pigmentaires), l'expérience pour laquelle il a présenté les meilleurs résistance, résilience, récupération et stabilité temporelle.

Tableau 1. Récapitulatif de la comparaison des paramètres de stabilité pour la production primaire brute (PPB), la respiration (R) et pour les concentrations pigmentaires entre les expériences de vague de chaleur à Thau et de brunissement à Hopavågen (Hop.). Pour simplifier la comparaison, pour la résistance et la récupération, si la valeur absolue était supérieure à 0,4, « Médiocre » a été attribué, si la valeur absolue était comprise entre 0,1 et 0,4, « Moyen » a été attribué, et si la valeur absolue était inférieure à 0,1, « Bon » a été attribué. Pour la résilience, si la valeur absolue était supérieure à 0,4, « Bon » a été attribué, si la valeur absolue était comprise entre 0,1 et 0,4, « Moyen » a été attribué, et si la valeur absolue était inférieure à 0,1, « Médiocre » a été attribué. Pour la stabilité temporelle, si la valeur absolue était inférieure à 3, « Médiocre » a été attribué, si la valeur absolue était comprise entre 3 et 7, « Moyen » a été attribué, et si la valeur absolue était supérieure à 7, « Bon » a été attribué. Les signes >, < et = indiquent le résultat de la comparaison entre les deux expériences.

Paramètre	Résistance		Résilience		Récupération		Stabilité temporelle	
	Thau	Hop.	Thau	Hop.	Thau	Hop.	Thau	Hop.
PPB	Moyen	> Médiocre	Médiocre	< Moyen	Bon	> Médiocre	Bon	> Médiocre
R	Moyen	> Médiocre	Médiocre	< Médiocre	Bon	> Médiocre	Bon	> Médiocre
Fucoxanthine	Bon	< Bon	Médiocre	= Médiocre	Moyen	> Moyen	Bon	> Bon
19'-HF	Bon	> Moyen	Médiocre	< Médiocre	Bon	> Moyen	Bon	> Moyen
Chl-*b*	Bon	> Bon	Médiocre	> Médiocre	Bon	> Moyen	Moyen	< Moyen
Zéaxanthine	Bon	> Moyen	Médiocre	< Médiocre	Moyen	> Moyen	Moyen	< Moyen

Lors de l'expérience de vague de chaleur à Thau, la communauté planctonique a généralement montré de bonnes résistance, récupération et stabilité temporelle en termes de processus et de concentrations pigmentaires, tandis que les valeurs de résilience étaient faibles. Lors de l'expérience de brunissement à Hopavågen, la résistance était moins bonne qu'à Thau, sauf pour la concentration en fucoxanthine (représentative des diatomées). Similairement, la récupération était moins bonne pour tous les paramètres testés. La stabilité temporelle était également généralement plus faible qu'à Thau, sauf pour les concentrations en chl-*b* et zéaxanthine (représentatives des algues vertes et des cyanobactéries, respectivement). Finalement, la résilience s'est avérée être médiocre, même si elle était légèrement supérieure qu'à Thau.

Le fait que la production primaire et la respiration aient montré une résistance et une récupération bien supérieures lors de l'expérience de vague de chaleur à Thau que lors du brunissement à Hopavågen suggère ainsi une plus grande sensibilité des communautés planctoniques côtières septentrionales face au changement climatique global. Appuyant ce constat, alors que les valeurs de résilience obtenues pour la production primaire et la respiration lors de l'expérience sur la vague de chaleur à Thau suggèrent que ces fonctions retournent à un état comparable au contrôle, ce n'est pas le cas pour la respiration à Hopavågen (Encadré Chapitre 2). Il faut noter que stabilité fonctionnelle et compositionnelle (ici pigmentaire) sont très souvent liées, une méta-analyse ayant montré que les paramètres compositionnels récupèrent généralement plus difficilement que les fonctions écosystémiques (Baert et al. 2020, Hillebrand et Kunze 2020). Ce fut généralement le cas lors de l'expérience de vague de chaleur à Thau, tandis que ce fut globalement le contraire lors de l'expérience de brunissement à Hopavågen, avec une meilleure récupération des concentrations pigmentaires que des fonctions testées, soulignant

l'impossibilité des communautés d'Hopavågen à rétablir ces dernières malgré d'important changements dans la composition pigmentaire du phytoplancton. Ceci est peut-être dû au fait que les changements dans la quantité et la qualité de la lumière induits par le brunissement ont entraîné des changements dans la concentration intra-cellulaire de certains pigments en tant que mécanisme d'acclimatation du phytoplancton (Chapitre 2). Ces changements ont certainement engendré les faibles valeurs de stabilité trouvées pour les concentrations pigmentaires lors de l'expérience d'Hopavågen.

Finalement, la résilience est le seul paramètre qui semble très faible quelles que soient l'expérience et la perturbation investiguées. Cette faible résilience pour pratiquement tous les paramètres étudiés implique une vitesse de récupération assez lente des communautés. C'est sans doute cette faible résilience qui est à l'origine de la récupération incomplète pour les paramètres de l'expérience d'Hopavågen, car résilience et récupération sont souvent corrélées (Hillebrand et al. 2018). Dans le cas de l'expérience à Thau, la faible résilience n'empêche pas une bonne récupération à la fin de l'expérience, cette absence de relation entre résilience et récupération s'expliquant parce qu'un brusque retour au niveau du contrôle a été observé quelques jours avant la fin de l'expérience pour de nombreux paramètres (Chapitre 4, pp 158-161). Quoi qu'il en soit, il semblerait que les communautés planctoniques côtières ne soient que très peu résilientes face aux perturbations ponctuelles liées au changement climatique global. Les données d'expériences supplémentaires pourraient permettre de vérifier ou d'infirmer cette tendance.

3. Conclusion et perspectives

L'objectif principal de la thèse était d'évaluer la réponse métabolique des communautés planctoniques côtières face à des perturbations en utilisant des données HF acquises via des capteurs immergés dans des mésocosmes *in situ*. Ainsi, de nouvelles méthodes pour estimer les processus planctoniques à partir de données d'O_2 dissout et de fluorescence de la chl-*a* ont été développées et employées pour caractériser la réponse de communautés planctoniques face à plusieurs perturbations liées au changement climatique. Notamment, l'application de la nouvelle méthode pour estimer la PPB, la R et la PCN à partir des cycles journaliers d'O_2 a permis de mettre en évidence une diminution d'environ un tiers du métabolisme planctonique de l'O_2 sous l'effet du brunissement en zone côtière norvégienne, des effets contrastés en réponse à un réchauffement continu de 3°C pour les communautés de la lagune de Thau, et, enfin, une augmentation d'environ un tiers du métabolisme planctonique lorsque ces dernières furent soumises à un épisode de vague de chaleur. Similairement, la méthode développée pour estimer les taux de croissance et de perte du phytoplancton a révélé une réponse globalement similaire et positive des communautés de la lagune de Thau face au réchauffement pour ces paramètres, malgré d'importantes différences dans la composition de la communauté phytoplanctonique.

Il faut noter que les travaux de cette thèse sont basés sur une approche expérimentale de mésocosmes ne prenant pas en considération la potentielle capacité d'adaptation à long terme des communautés planctoniques, par exemple face à un phénomène agissant sur plusieurs années tel que le réchauffement climatique. Néanmoins, ces travaux ont apporté des connaissances supplémentaires quant aux effets de certaines perturbations liées au changement climatique sur les processus métaboliques du plancton et permettront d'affiner les modèles prédictifs pour le futur des océans et de leur fonctionnement.

De nombreuses perspectives s'ouvrent quant à la suite de ces travaux. Plusieurs méthodes dérivées de la méthode initiale des changements journaliers dans le cycle d'O_2 existent dans la littérature et ont produit une quantité importante de données de production et de respiration. Il pourrait être intéressant de comparer ces méthodes et estimations dans un but d'harmonisation et de compréhension des différences inhérentes aux méthodes. Notamment, il serait judicieux pour de futurs travaux de comparer les estimations obtenues avec la méthode développée dans la thèse (Soulié et al. 2021) avec des estimations obtenues via modélisation inversée (Grace et al. 2015, Winslow et al. 2016, Appling et al. 2018), cette comparaison entre modélisation directe et inversée n'ayant jamais été réalisée à ma connaissance. Par rapport à la méthode développée dans cette thèse (Soulié et al. 2021) et aux autres méthodes de modélisation directe (Cole et al. 2000, Staehr et al. 2010, Mostajir et al. 2013), la modélisation inversée (Grace et al. 2015, Winslow et al. 2016, Appling et al. 2018) présente certains avantages et inconvénients. En effet, elle permet d'estimer l'échange d'O_2 avec l'atmosphère concomitamment aux estimations de PPB, de R et de PCN, et permettrait potentiellement de s'affranchir des incertitudes liées à l'estimation de l'échange avec l'atmosphère. Cependant, elle est basée sur des relations empiriques entre métabolisme du plancton et paramètres environnementaux (lumière, température etc.), ces relations n'étant pas forcément adaptées à tous les systèmes planctoniques.

Il serait également intéressant de combiner les estimations des taux de perte du phytoplancton à partir des mesures HF de fluorescence avec les estimations de broutage par le microzooplancton obtenues avec la technique des dilutions, afin de discriminer la part de la prédation par le microzooplancton dans les pertes totales du phytoplancton, et, dans le cadre d'expériences en mésocosmes, d'affiner la compréhension de la réponse du réseau trophique face à une perturbation. De plus, il existe des capteurs mesurant la fluorescence à d'autres longueur d'ondes que celle de la chl-*a*, notamment pour estimer la quantité de phycocyanine, pigment des cyanobactéries (Hodges et al. 2018, Bosse et al. 2019). Couplés aux capteurs de fluorescence de la chl-*a*, ces capteurs permettraient d'estimer la part des cyanobactéries dans les estimations de croissance et de pertes totales du phytoplancton, cette information revêtant une grande importance par exemple pour les systèmes d'eau douce régulièrement sujets aux efflorescences de cyanobactéries toxiques, et permettraient de s'affranchir en partie des interférences liées aux matières humiques fluoresçant dans les mêmes longueurs d'onde que la chl-*a*.

Mais les travaux de la thèse ouvrent aussi de nombreuses perspectives sur le plan écologique. Les différences dans les effets du réchauffement reportés dans les Chapitres 3 et 4 mettent en lumière la variabilité dans la réponse des communautés de la lagune de Thau face au réchauffement climatique. La réponse de certains processus planctoniques face à la même perturbation de réchauffement s'est avérée être différente pour les communautés printanières et automnales. Qu'en est-il de l'été et de l'hiver ? L'été est généralement une saison importante pour la production primaire de la lagune et pour la croissance des bivalves (Souchu et al. 2001), et donc pour l'ostréiculture. Il serait donc intéressant de tester les effets du réchauffement sur cette période écologiquement et économiquement importante. De plus, lors de certains étés, des phénomènes d'anoxie localisés, appelés « malaigues », sont à l'origine d'épisodes de mortalité de masse des huîtres (Derolez et al. 2020b). Comprendre comment le réchauffement affecte les communautés dysfonctionnelles à l'origine des malaigues revêt une importance majeure afin de comprendre et de prévoir ces phénomènes, cependant très peu d'études expérimentales ont été réalisées dans ce cadre dans la lagune. Les hivers sont également de plus en plus chauds. Il a été montré que les efflorescences printanières qui suivent un hiver plus chaud dans la lagune de Thau sont d'une ampleur moindre que pour une efflorescence suivant un hiver avec des températures de saison (Trombetta et al. 2019). Néanmoins, les mécanismes derrière cette diminution de biomasse sont encore méconnus, et c'est pourquoi il serait intéressant de tester le réchauffement en hiver.

En plus d'être sujette au réchauffement, la lagune de Thau est caractérisée au printemps et en automne par des crues typiques de la Méditerranée via les rivières qui alimentent la lagune et qui conduisent parfois au brunissement d'une partie de la lagune (Pecqueur et al. 2011, Fouilland et al. 2012). Cependant, très peu d'études ont investigué ce phénomène, et, pour la lagune de Thau, aucune ne l'a combinée au réchauffement à ma connaissance. Or, il est prévu que ces deux perturbations gagnent en intensité durant le siècle à venir (Adloff et al. 2015, Hoegh-Guldberg et al. 2018), et il pourrait être intéressant de combiner brunissement et réchauffement : on pourrait s'attendre à ce que les effets positifs théoriques du réchauffement sur la production primaire brute soient contrebalancés par les effets négatifs de la diminution de la quantité de lumière induite par le brunissement. Néanmoins, la quantité de lumière est très rarement limitante pour les processus phytoplanctoniques dans la lagune de Thau (Trombetta et al. 2019). Dès lors, l'apport de nutriments inorganiques que représente le brunissement suffirait-il pour soutenir la production primaire malgré la diminution de lumière ?

Le manque d'études expérimentales testant les impacts du brunissement sur le métabolisme et le fonctionnement des communautés planctoniques côtières septentrionales est aujourd'hui reconnu (Frigstad et al. 2020a, 2020b). L'étude réalisée dans le Chapitre 2 constitue ainsi une première étape pour la compréhension de ce phénomène et de ces conséquences. Elle met néanmoins en lumière la nécessité de réaliser d'autres études afin d'obtenir une vision plus générale des conséquences du changement climatique sur ces systèmes. Notamment, il faudrait combiner le brunissement avec d'autres perturbations affectant les systèmes côtiers septentrionaux, par exemple le réchauffement. À

ma connaissance, toutes les études qui ont investigué les effets du brunissement combiné au réchauffement pour les systèmes nordiques l'ont fait pour des lacs, et dans la majorité des cas, c'est le réchauffement qui a eu le plus de conséquences sur le métabolisme du plancton (Nicolle et al. 2012, Rasconi et al. 2015, Wilken et al. 2018, Feuchtmayr et al. 2019). Est-ce également le cas pour les zones côtières ? Il serait également extrêmement intéressant de tester le brunissement lors d'une autre saison, au printemps notamment. En effet, on s'attend à ce que l'atténuation de la lumière induite par le brunissement altère le déclenchement et la physiologie des efflorescences printanières (Frigstad et al. 2020a), qui sont d'une importance capitale dans les cycles biogéochimiques des écosystèmes nordiques (Degerlund et Eilertsen 2010). On sait également qu'il existe une grande hétérogénéité régionale et latitudinale dans les apports terrigènes à l'origine du brunissement (Frigstad et al. 2020a). Il serait donc avisé de comparer la réponse des communautés planctoniques côtières face au brunissement pour plusieurs systèmes côtiers septentrionaux le long d'un gradient latitudinal.

En conclusion, les travaux de cette thèse ont mis en lumière des effets parfois contrastés du changement climatique sur les processus et la composition des communautés planctoniques côtières, et mettent en avant la nécessité des expérimentations prenant en compte cette complexité afin d'affiner toujours plus notre compréhension des processus planctoniques face à un environnement en perpétuel changement. Les efforts de normalisation des protocoles et des analyses doivent être poursuivis afin d'établir une base de données toujours plus fournie et d'augmenter la résolution spatio-temporelle de notre compréhension du fonctionnement des communautés planctoniques. Ainsi, la présente thèse contribue à la poursuite de ces objectifs et constitue une humble étape dans l'enrichissement de la connaissance des processus qui façonnent le monde qui nous entoure.

Bibliographie

-A-

Aberle, N., K. Lengfellner, and U. Sommer. 2007. Spring bloom succession, grazing impact and herbivore selectivity of ciliate communities in response to winter warming. *Oecologia* **150**: 668–681. doi:10.1007/s00442-006-0540-y

Aberle, N., B. Bauer, A. Lewandowska, U. Gaedke, and U. Sommer. 2012. Warming induces shifts in microzooplankton phenology and reduces time-lags between phytoplankton and protozoan production. *Mar. Biol*. **159**: 2441–2453. doi:10.1007/s00227-012-1947-0

Adloff, F., S. Somot, F. Sevault, and others. 2015. Mediterranean Sea response to climate change in an ensemble of twenty first century scenarios. *Clim. Dyn*. **45**: 2775–2802. doi:10.1007/s00382-015-2507-3

Agawin, N. S. R., C. M. Duarte, and S. Agusti. 1998. Growth and abundance of *Synechococcus* sp. in a Mediterranean Bay: seasonality and relationship with temperature. *Mar. Ecol. Prog. Ser*. 170: 45–53. doi:10.3354/meps170045

Agusti, S., J. Martinez-Ayala, A. Regaudie-de-Gioux, and C. M. Duarte. 2017. Oligotrophication and Metabolic Slowing-Down of a NW Mediterranean Coastal Ecosystem. *Front. Mar. Sci.* **4**. doi:10.3389/fmars.2017.00432

Aksnes, D., J. Nejstgaard, E. Sædberg, and T. Sørnes. 2004. Optical control of fish and zooplankton populations. *Limnol. Oceanogr*. **49**(1): 233-238. doi: 10.4319/lo.2004.49.1.0233

Aksnes, D. 2007. Evidence for visual constraints in large marine fish stocks. *Limnol. Oceanogr*. **52**(1): 198-203. doi: 10.4319/lo.2007.52.1.0198

Aksnes, D., N. Dupont, A. Staby, O. Fiksen, S. Kaartvedt, and J. Aure. 2009. Coastal water darkening and implications for mesopelagic regime shifts in Norwegian fjords. *Mar. Ecol. Prog. Ser.* **387**: 39–49. doi:10.3354/meps08120

Albretsen, J., J. Aure, R. Sætre, and D. S. Danielssen. 2012. Climatic variability in the Skagerrak and coastal waters of Norway. *ICES J. of Mar. Sci* **69**(5): 758-736. doi:10.1093/icesjms/fsr187

Alcaraz, M., C. Marrasé, F. Peters, L. Arin, and A. Malits. 2001. Seawater–atmosphere O_2 exchange rates in open top laboratory microcosms: application for continuous estimates of planktonic primary production and respiration. *J. Exp. Mar. Biol. Ecol.* **257**: 1–12. doi:10.1016/ S0022-0981(00)00328-2

Alfonso, M. B., A. S. Brendel, A. J. Vitale, C. Seitz, M. C. Piccolo, and G. M. E. Perillo. 2018. Drivers of ecosystem metabolism in two managed shallow lakes with different salinity and trophic conditions: The Sauce Grande and La Salada Lakes (Argentina). *Water* **10**: 1136. doi:10.3390/ w10091136

Alkire, M. B., and others. 2012. Estimates of net community production and export using high-resolution, Lagrangian measurements of O_2, NO_3^-, and POC through the evolution of a spring diatom bloom in the North Atlantic. *Deep Sea Res. I Oceanogr. Res. Pap*. **64**: 157–174. doi:10.1016/ j.dsr.2012.01.012

Allen, A.P., J. F. Gillooly, and J. H. Brown. 2005. Linking the global carbon cycle to individual metabolism. *Functional Ecol.* **19**(2): 202-213. doi:10.1111/j.1365-2435.2005.00952.x

Anderson, S. R., and E. L. Harvey. 2019. Seasonal variability and drivers of microzooplankton grazing and phytoplankton growth in a subtropical estuary. *Front. Mar. Sci*. **6**:174. doi: 10.3389/fmars.2019.00174

Antoine, D., J.-M. André, and A. Morel. 1996. Oceanic primary production: 2. Estimation at global scale from satellite (Coastal Zone Color Scanner) chlorophyll. *Glob. Biogeochem. Cycles* **10**: 57– 732. doi:10.1029/95GB02832

Appling, A. P., R. O. Hall Jr, C. B. Yackulic, and M. Arroita. 2018. Overcoming Equifinality: Leveraging Long Time Series for Stream Metabolism Estimation. *JGR Biogeosciences* **123**: 624–645. doi:10.1002/2017JG004140

Arhonditsis, G., G. Tsirtsis, and M. Karydis. 2002. The effects of episodic rainfall events to the dynamics of coastal marine ecosystems: applications to a semi-enclosed gulf in the Meditteranean Sea. *J. Mar. Sys.* **35**: 183–205. doi:10.1016/S0924-7963(02)00081-7

Arroita, M., A. Elosegi, and R. O. Hall Jr. 2019. Twenty years of daily metabolism show riverine recovery following sewage abatement. *Limnol. Oceanogr*. **64**: S77–S92. doi:10.1002/lno.11053

-B-

Baert, J. M., F. De Laender, K. Sabbe, C. R. Janssen. 2020. Biodiversity increases functional and compositional resistance, but decreases resilience in phytoplankton communities. *Ecology* **97**:3433-3440. doi: 10.1002/ecy.1601

Bährs, H., and C. E. W. Steinberg. 2012. Impact of two different humic substances on selected coccal green algae and cyanobacteria—changes in growth and photosynthetic performance. *Env. Sci. Pollut. Res*. **19**: 335–346. doi:10.1007/s11356-011-0564-7

Baird, M. E., S. M. Emsley, and J. M. Mcglade. 2001. Modelling the interacting effects of nutrient uptake, light capture and temperature on phytoplankton growth. *J Plankt. Res*. **23**: 829–840. doi:10.1093/plankt/23.8.829

Barbier, E. B., S. D. Hacker, C. Kennedy, E. W. Koch, A. C. Stier, and B. R. Silliman. 2011. The value of estuarine and coastal ecosystem services. *Ecol. Monogr*. **81**(2): 169-193. doi:10.1890/10-1510.1

Barton, S., and G. Yvon-Durocher. 2019. Quantifying the temperature dependence of growth rate in marine phytoplankton within and across species. *Limnol. Oceanogr*. **64**: 2081–2091. doi:10.1002/lno.11170

Batten, S. D., D. E. Raitsos, S. Danielson, R. Hopcroft, K. Coyle, and A. McQuatters-Gollop. 2018. Interannual variability in lower trophic levels on the Alaskan Shelf. *Deep Sea Res. II Top. Studies Oceanogr* **147**: 58–68. doi:10.1016/j.dsr2.2017.04.023

Baudoux, A.-C., M. J. W. Veldhuis, A. A. M. Noordeloos, G. van Noort, and C. P. D. Brussaard. 2008. Estimates of virus- vs. grazing induced mortality of picophytoplankton in the North Sea during summer. *Aq. Microb. Ecol*. **52**: 69–82. doi:10.3354/ame01207

Beardall, J., T. Burger-Wiersma, M. Rijkeboer, A. Sukenik, J. Lemoalle, Z. Dubinsky, and D. Fontvielle. 1994. Studies on enhanced post-illumination respiration in microalgae. *J. Plankt. Res*. **16**: 1401–1410. doi:10.1093/plankt/16.10. 1401

Beaulieu, J. J., C. P. Arango, D. A. Balz, and W. D. Shuster. 2013. Continuous monitoring reveals multiple controls on ecosystem metabolism in a suburban stream. *Fresh. Biol*. **58**: 918–937. doi:10.1111/fwb.12097

Bec, B., J. Husseini-Ratrema, Y. Collos, P. Souchu, and A. Vaquer. 2005. Phytoplankton seasonal dynamics in a Mediterranean coastal lagoon: emphasis on the picoeukaryote community. *J. Plankt. Res*. **27**: 881–894. doi:10.1093/plankt/fbi061

Bec, B., Y. Collos, P. Souchu, A. Vaquer, J. Lautier, A. Fiandrino, L. Benau, V. Orsoni, and T. Laugier. 2011. Distribution of picophytoplankton and nanophytoplankton along an anthropogenic eutrophication gradient in French Mediterranean coastal lagoons. *Aq. Microb. Ecol*. **63**:29–45. doi:10.3354/ame01480

Behrenfeld, M. J. 2011. Uncertain future for ocean algae. *Nat. Clim. Change* **1**: 33–34. doi:10.1038/nclimate1069

Bénard, R., M. Levasseur, M. Scarratt, and others. 2018. Experimental assessment of the sensitivity of an estuarine phytoplankton fall bloom to acidification and warming. *Biogeosciences* **15**: 4883–4904. doi:10.5194/bg-15-4883-2018

Bender, M., and others. 1987. A comparison of four methods for determining planktonic community production. *Limnol. Oceanogr*. **32**: 1085–1098. doi:10.4319/lo.1987.32. 5.1085

Benoiston, A.-S., F. M. Ibarlalz, L. Bittner, L. Guidi, O. Jahn, S. Dutkiewicz, and C. Bowler. 2017. The evolution of diatoms and their biogeochemical functions. *Phil. Trans. Royal Society B: Biol. Sci*. **372**: 20160397. doi:10.1098/rstb.2016.0397

Berggreen, U., B. Hansen, and T. Kiørboe. 1988. Food size spectra, ingestion and growth of the copepod *Acartia tonsa* during development: Implications for determination of copepod production. *Mar Biol* **99**:341-352

Berry, T. E., B. J. Saunders, M. L. Coghlan, and others. 2019. Marine environmental DNA biomonitoring reveals seasonal patterns in biodiversity and identifies ecosystem responses to anomalous climatic events. *PLOS Genetics*. doi:10.1371/journal.pgen.1007943

Biermann, A., A. Engel, and U. Riebesell. 2014. Changes in organic matter cycling in a plankton community exposed to warming under different light intensities. *J. Plankt. Res*. **36**(3): 658-671. doi:10.1093/plankt/fbu005

Birk, S., D. Chapman, L. Carvalho, and others. 2020. Impacts of multiple stressors on freshwater biota across spatial scales and ecosystems. *Nat. Ecol. Evol*. **4**: 1060-1068. doi:10.1038/s41559-020-1216-4

Bittig, H. C., and others. 2018. Oxygen optode sensors: Principle, characterization, calibration, and application in the ocean. *Front. Mar. Sci*. **4**: 429. doi:10.3389/fmars.2017. 00429

Bosse, K. R., M. J. Sayers, R. A. Shuchman, G. L. Fahnenstiel, S. A. Ruberg, D. A. Fanslow, D. G. Stuart, T. H. Johengen, and A. M. Burtner. 2019. Spatial-temporal variability of in situ cyanobacteria vertical structure in Western Lake Erie: Implications for remote sensing observations. *J. Great Lakes Res*. **45**(3): 480-489. doi:10.1016/j.jglr.2019.02.003

Boyd, C. E., E. E. Prather, and R. W. Parks. 1975. Sudden Mortality of a Massive Phytoplankton Bloom. *Weed Sci*. **23**: 61–67. doi:10.1017/S0043174500062536

Boyd, P. W., T. A. Rynearson, E. A. Armstrong, and others. 2013. Marine phytoplankton temperature versus growth responses from polar to tropical waters – outcome of a scientific community-wide study. *Plos ONE* **8**(5): e63091. doi:10.1371/journal.pone.0063091

Bratbak, G., J. K. Egge, and M. Heldal. 1993. Viral mortality of the marine alga *Emiliania huxleyi* (Haptophyceae) and termination of algal blooms. *Mar. Ecol. Prog. Ser*. **93**: 39–48

Breitburg, D. 2002. Effects of hypoxia, and the balance between hypoxia and enrichment, on coastal fishes and fisheries. *Estuaries* **25**: 767-781. doi: 10.1007/BF02804904

Briand, E., O. Pringault, S. Jacquet, and J. P. Torreton. 2004. The use of oxygen microprobes to measure bacterial respiration for determining bacterioplankton growth efficiency. *Limnol. Oceanogr*. **2**: 406–416. doi:10.4319/lom.2004.2. 4066

Brierley, A. S. 2017. Plankton. *Curr. Biol.* **27**: R478–R483. doi:10.1016/j.cub.2017.02.045

Briggs, N., K. Guðmundsson, I. Cetinic, E. D'Asaro, E. Rehm, C. Lee, and M. J. Perry. 2018. A multi-method autonomous assessment of primary productivity and export efficiency in the springtime North Atlantic. *Biogeosciences* **15**: 4515– 4532. doi:10.5194/bg-15-4515-2018

Brinkman, A. G., C. J. M. Philippart, and A. F. Zuur. 1995. Model methods for the analysis of mesocosm experimental studies. *Helgoländer Meeresuntersuchungen* **49**: 771–784. doi:10.1007/BF02368400

Brown, J. H., J. F. Gillooly, A. P. Allen, V. M. Savage, and G. B. West. 2004. Toward a Metabolic Theory of Ecology. *Ecology* **85**: 1771–1789. doi:10.1890/03-9000@10.1002/(ISSN)1939-9170.MacArthurAward

Brussaard, C. P. D. 2004. Viral Control of Phytoplankton Populations—a Review. *J. Euk. Microbiol*. **51**: 125–138. doi:10.1111/j.1550-7408.2004.tb00537.x

Butler, E. I., S. Knox, and M. I. Liddicoat. 1979. The relationship between inorganic and organic nutrients in sea water. *J. Mar. Biol. Asso. Uni. Kingdom* **59**: 239–250. doi:10.1017/S0025315400046312

-C-

Cabrerizo, M. J., J. M. Medina-Sanchez, M. Villar-Argaiz, and P. Carrillo. 2019. Interplay between resistance and resilience governs the stability of a freshwater microbial food web under multiple stressors. *Sci. Tot. Env*. **691**: 908-918. doi: 10.1016/j.scitotenv.2019.07.173

Cabrerizo, M. J., and E. Marañón. 2021. Geographical and Seasonal Thermal Sensitivity of Grazing Pressure by Microzooplankton in Contrasting Marine Ecosystems. *Front. Microbiol.* doi:10.3389/fmicb.2021.679863

Cabrerizo, M., E. Marañon, C. Fernandez-Gonzalez, A. Alonso-Nunez, H. Larsson, and M. Arrenguren-Gassis. 2021. Temperature fluctuation attenuates the effects of warming in estuarine microbial communities. *Front. Mar. Sci*. **8**:351. doi: 10.3389/fmars.2021.656282

Calbet, A. 2001. Mesozooplankton grazing effect on primary production: A global comparative analysis in marine ecosystems. *Limnol. Oceanogr*. **46**(7): 1824-1830. doi:10.4319/lo.2001.46.7.1824

Calbet, A., and M. R. Landry. 2004. Phytoplankton growth, microzooplankton grazing, and carbon cycling in marine systems. *Limnol. Oceanogr.* **49**: 51–57. doi:10.4319/lo.2004.49.1.0051

Carberry, L., C. Roesler, and S. Drapeau. 2019. Correcting in situ chlorophyll fluorescence time-series observations for nonphotochemical quenching and tidal variability reveals nonconservative phytoplankton variability in coastal waters. *Limnol. Oceanogr.: Methods* **17**: 462–473. doi:10.1002/lom3.10325

Carignan, R., D. Planas, and C. Vis. 2000. Planktonic production and respiration in oligotrophic Shield lakes. *Limnol. Oceanogr*. **45**: 189–199. doi:10.4319/lo.2000.45.1.0189

Carpenter, J. H. 1965. The accuracy of the Winkler method for dissolved oxygen analysis. *Limnol. Oceanogr*. **10**: 135–140. doi:10.4319/lo.1965.10.1.0135

Carrit, D. E. 1966. Comparison and evaluation of currently employed modifications of the Winkler method for determining oxygen in seawater. A NASCO report. *J. Mar. Res*. **24**: 286–318.

Carvalho, M. C., and B. D. Eyre. 2012. Measurement of planktonic CO_2 respiration in the light. *Limnol. Oceanogr.: Methods* **10**: 167–178. doi:10.4319/lom.2012.10.167

Checkley, D. M. Jr., R. G. Asch, and R. R. Rykaczewski. 2017. Climate, anchovy and sardine. *Ann. Rev. Mar. Sci*. **9**: 469-493. doi: 10.1146/annurev-marine-122414-033819

Chekalyuk, A., and M. Hafez. 2011. Photo-physiological variability in phytoplankton chlorophyll fluorescence and assessment of chlorophyll concentration. *Optics Express* **19**: 22643–22658. doi:10.1364/OE.19.022643

Chen, B. 2015. Assessing the accuracy of the “two-point” dilution technique. *Limnol. Oceanogr: Methods* **13**: 521–526. doi:10.1002/lom3.10044

Chen, B., M. R. Landry, B. Huang, and H. Liu. 2012. Does warming enhance the effect of microzooplankton grazing on marine phytoplankton in the ocean? *Limnol. Oceanogr*. **57**: 519–526. doi:10.4319/lo.2012.57.2.0519

Chen, B., H. Liu, B. Huang, and J. Wang. 2014. Temperature effects on the growth rate of marine picoplankton. *Mar. Ecol. Prog. Ser*. **505**:37-47. doi: 10.3354/meps10773

Chen, B., and E. A. Laws. 2017. Is there a difference of temperature sensitivity between marine phytoplankton and heterotrophs? *Limnol Oceanogr* **62**:806–817. doi:10.1002/lno.10462

Chiu, C.-Y., and others. 2020. Terrestrial loads of dissolved organic matter drive inter-annual carbon flux in subtropical lakes during times of drought. *Sci. Total Environ*. **717**. doi: 10.1016/j.scitotenv.2020.137052

Chowanski, K., L. Kunza, G. Hoffman, L. Genzoli, and E. Stickney. 2020. River management alters ecosystem metabolism in a large oligotrophic river. *Fresh. Sci*. **39**: 534–548. doi:10.1086/710082

Cloern, J. E., C. Grenz, and L. Vidergas-Lucas. 1995. An empirical model of the phytoplankton chlorophyll-carbon ratio – the conversion factor between productivity and growth rate. *Limnol. Oceanogr.* **40**(7): 1313-1321. doi:10.4319/lo.1995.40.7.1313

Cloern, J. E., S. Q. Foster, and A. E. Kleckner. 2014. Phytoplankton primary production in the world's estuarine-coastal ecosystems. *Biogeosciences* **11**: 2477-2501. doi: 10.5194/bg-11-2477-2014

Clutterbuck, B., and A. Yallop. 2010. Land management as a factor controlling dissolved organic carbon release from upland peat soils 2: Changes in DOC productivity over four decades. *Sci. Tot. Env.* **408**: 6179–6191. doi:doi.org/10.1016/j.scitotenv.2010.08.038

Cohen, J. 1977. Statistical Power Analysis for the Behavioral Sciences, Revised Edition, Academic Press.

Cole, J. J., M. L. Pace, S. R. Carpenter, and J. F. Kitchell. 2000. Persistence of net heterotrophy in lakes during nutrient addition and food web manipulations. *Limnol. Oceanogr*. **45**: 1718–1730. doi:10.4319/lo.2000.45.8.1718

Collos, Y., A. Vaquer, B. Bibent, G. Slawyk, N. Garcia, and P. Souchu. 1997. Variability in nitrate uptake kinetics of phytoplankton communities in a Mediterranean coastal lagoon. *Estuar. Coast. Shelf Sci* **44**: 369-375. doi: 10.1006/ecss.1996.0121

Collos, Y., B. Bec, C. Jauzein, and others. 2009. Oligotrophication and emergence of picocyanobacteria and a toxic dinoflagellate in Thau lagoon, southern France. *J. Sea Res.* **61**: 68–75. doi:10.1016/j.seares.2008.05.008

Conley, D. J., J. Cartensen, G. Ærtebjerg, P. B. Christensen, T. Dalsgaard, J. L. S. Hansen, and A. B. Josefson. 2007. Long-term changes and impacts of hypoxia in Danish coastal waters. *Ecol. Appl*. **17**: S165-S184. doi: 10.1890/05-0766.1

Coppola, L., L. Legendre, D. Lefevre, L. Prieur, V. Taillandier, and E. Diamond Riquier. 2018. Seasonal and inter-annual variations of dissolved oxygen in the northwestern Mediterranean Sea (DYFAMED site). *Prog. Oceanogr*. **162**: 187-201. doi: 10.1016/j.pocean.2018.03.001

Correll, D. L., T. E. Jordan, and D. E. Weller. 2001. Effects of Precipitation, Air Temperature, and Land Use on Organic Carbon Discharges from Rhode River Watersheds. *Water, Air and Soil Pollut.* **128**: 139–159. doi:10.1023/A:1010337623092

Cottrell, M. T., R. R. Malmstrom, V. Hill, A. E. Parker, and D. L. Kirchman. 2006. The metabolic balance between autotrophy and heterotrophy in the western Arctic Ocean. *Deep Sea Res. I: Oceanogr. Res. Pap*. **53**: 1831–1844. doi:10.1016/j.dsr.2006.08.010

Courboulès, J. 2020. Effets du réchauffement sur la croissance et la mortalité par prédation des communautés phytoplanctoniques et bactériennes en zone côtière Méditerranéenne : Approche expérimentale en mésocosmes *in situ* et étude combinée avec l'acidification. PhD Thesis. Université de Montpellier. https://tel.archives-ouvertes.fr/tel-03340319

Courboulès, J., F. Vidussi, **T. Soulié**, S. Mas, D. Pecqueur, and B. Mostajir. 2021. Effects of experimental warming on small phytoplankton, bacteria and viruses in autumn in the Mediterranean coastal Thau Lagoon. *Aq. Ecol.* **55**: 647–666. doi:10.1007/s10452-021-09852-7

Cox, B. A. 2003. A review of dissolved oxygen modelling techniques for lowland rivers. *Sci. Tot. Env*. **314–316**: 303–334. doi:10.1016/S0048-9697(03)00062-7

Cramer, W., J. Guiot, and K. Marini. 2020. Climate and Environmental Change in the Mediterranean Basin – Current Situation and Risks for the Future. First Mediterranean Assessment Report. Union for the Mediterranean, Plan Bleu, UNEP/MAP.

Creed, I. F., A.-K. Bergström, C. G. Trick, and others. 2018. Global change-driven effects on dissolved organic matter composition: Implications for food webs of northern lakes. *Glob. Change Biol*. **24**: 3692–3714. doi:10.1111/gcb.14129

Crossland, N. O., and T. W. L. Point. 1992. The design of mesocosm experiments. *Environ. Toxicol. Chem*. **11**: 1–4. doi:10.1002/etc.5620110101

-D-

Darmaraki, S., S. Somot, F. Sevault, and others. 2019. Future evolution of Marine Heatwaves in the Mediterranean Sea. *Clim. Dyn*. **53**: 1371–1392. doi:10.1007/s00382-019-04661-z

Das, K., and S. Ray. 2008. Effect of delay on nutrient cycling in phytoplankton-zooplankton interactions in estuarine system. *Ecol. Modell*. **215**(1-3): 69-76. doi: 10.1016/j.ecolmodel.2008.02.019

Degerlund, M., and H. C. Eilertsen. 2010. Main species characteristics of phytoplankton spring blooms in NE Atlantic and Arctic waters (68-80°N). *Est. Coasts* **33**: 242-269. doi: 10.1007/s12237-009-9167-7

Deininger, A., C. L. Faithfull, K. Lange, T. Bayer, F. Vidussi, and A. Liess. 2016. Simulated terrestrial runoff triggered a phytoplankton succession and changed seston stoichiometry in coastal lagoon mesocosms. *Mar. Env. Res.* **119**: 40–50. doi:10.1016/j.marenvres.2016.05.001

Demars, B. O. L., J. Thompson, and J. R. Manson. 2018. Stream metabolism and the open diel oxygen method: Principles, practice, and perspectives. *Limnol. Oceanogr.: Methods* **13**: 356–374. doi:10.1002/lom3.10030

Demers, S., S. Roy, R. Gagnon, and C. Vignault. 1991. Rapid light-induced changes in cell fluorescence and in xanthophyll-cycle pigments of Alexandrium excavatum (Dinophyceae) and Thalassiosira pseudonana (Bacillariophyceae): a photo-protection mechanism. *Mar. Ecol. Prog. Ser.* **76**: 185–193.

Derolez, V., D. Soudant, N. Malet, C. Chiantella, M. Richard, E. Abadie, C. Aliaume, and B. Bec. 2020a. Two decades of oligotrophication: Evidence for a phytoplankton community shift in the coastal lagoon of Thau (Mediterranean Sea, France). *Estuar. Coast. Shelf Sci* **241**: 106810. doi:10.1016/j.ecss.2020.106810

Derolez, V., N. Malet, A. Fiandrino, F. Lagarde, M. Richard, V. Ouisse, B. Bec, and C. Aliaume. 2020b. Fifty years of ecological changes : regime shifts and drivers in a coastal Mediterranean lagoon during oligotrophication. *Sci. Tot. Env*. **732**: 139292. doi: 10.1016/j.scitotenv.2020.139292

Diffenbaugh, N. S., J. S. Pal, F. Giorgi, and X. Gao. 2007. Heat stress intensification in the Mediterranean climate change hot spot. *Geophys. Res. Lett*. **34**. doi:10.1029/2007GL030000

Domingues, R.B., M. Barreto, V. Brotas, H.M. Galvao, and A.B. Barbosa. 2021. Short-term effects of winter warming and acidification on phytoplankton growth and mortality: more losers than winners in a temperate coastal lagoon. *Hydrobiologia*. doi: 10.1007/s10750-021-04672-0

Doney, S. C. 2006. Plankton in a warmer world. *Nature* **444**: 695-696. doi:10.1038/444695a

Duarte, C. M., S. Agustí, and D. Vaqué. 2004. Controls on planktonic metabolism in the Bay of Blanes, northwestern Mediterranean littoral. *Limnol. Oceanogr.* **49**: 2162–2170. doi:10.4319/lo.2004.49.6.2162

Duarte, C. M., and A. Regaudie-de-Gioux. 2009. Thresholds of gross primary production for the metabolic balance of marine planktonic communities. *Limnol. Oceanogr*. **54**: 1015–1022. doi:10.4319/lo.2009.54.3.1015

Dugan, H. A., R. I. Woolway, A. B. Santoso, and others. 2016. Consequences of gas flux model choice on the interpretation of metabolic balance across 15 lakes. *Inland Waters* **6**: 581–592. doi:10.1080/IW-6.4.836

Dupuy, C., A. Vaquer, T. Lam-Hoai, C. Rougier, N. Mazouni, J. Lautier, Y. Collos, and S. Le Gall. 2000. Feeding rate of the oyster Crassostrea gigas in a natural planktonic community of the Mediterranean Thau Lagoon. *Mar. Ecol. Prog. Ser.* **205**:171–184. doi:10.3354/meps205171

Dzialowski, A. R., M. Rzepecki, I. Kostrzewska-Szlakowska, K. Kalinowska, A. Palash, and J. T. Lennon. 2014. Are the abiotic and biotic characteristics of aquatic mesocosms representative of *in situ* conditions? J. *Limnol*. **73**: 603–612. doi: 10.4081/jlimnol.2014.721

-E-

Ejankowski, W., and T. Lenard. 2015. Climate driven changes in the submerged macrophyte and phytoplankton community in a hard water lake. *Limnologica* **52**:59-66. doi:10.1016/j.limno.2015.03.003

Engel, A., N. Händel, J. Wohlers, M. Lunau, H-P. Grossart, U. Sommer and U. Riebesell. 2011. Effects of sea surface warming on the production and composition of dissolved organic matter during phytoplankton blooms: results from a mesocosm study. *J. Plankt. Res*. **33**(3) :357-372. doi:10.1093/plankt/fbq122

Eppley, R. 1972. Temperature and phytoplankton growth in the sea. *Fish. Bul.*

Evans, R., M.-A. Lea, M. A. Hindell, and K. M. Swadling. 2020. Significant shifts in coastal zooplankton populations through the 2015/16 Tasman Sea marine heatwave. *Estuar. Coast. Shelf Sci* **235**: 106538. doi:10.1016/j.ecss.2019.106538

de Eyto, E., and others. 2019. High frequency monitoring reveals fine scale spatial and temporal dynamics of the deep chlorophyll maximum of a stratified coastal lagoon. *Estuar. Coast. Shelf Sci*. **218**: 278–291. doi:10.1016/j.ecss.2018. 12.010

-F-

Fahnenstiel, G. L., M. J. McCormick, G. A. Lang, D. G. Redalge, S. E. Lohrenz, M. Markowitz, B. Wagoner, and H. J. Carrick. 1995. Taxon-specific growth and loss rates for dominant phytoplankton populations from the northern Gulf of Mexico. *Mar. Ecol. Prog. Ser*. **117**:229-239.

Falkowski, P., and D. A. Kiefer. 1985. Chlorophyll *a* fluorescence in phytoplankton: relationship to photosynthesis and biomass. *J. Plankt. Res.* **7**: 715–731. doi:10.1093/plankt/7.5.715

Falkowski, P. G., Z. Dubinsky, and G. Santostefano. 1985. Light-enhanced dark respiration in phytoplankton. *SIL Proc. 1922-2010* **22**: 2830–2833. doi:10.1080/03680770. 1983.11897784

Falkowski, P. 2012. Ocean Science: The power of plankton. *Nature* **483**: S17–S20. doi:10.1038/483S17a

Faust J.E., and J. Logan. 2018. Daily Light Integral: a research review and high-resolution maps of the United States. *Hort. Sci*. **53**(9): 1250-127. doi:10.21273/HORTSCI13144-18

Feuchtmayr, H., T. Pottinger, A. Moore, M. De Ville, L. Caillouet, H. Carter, G. Pereira, and S. Maberly. 2019. Effects of brownification and warming on algal blooms, metabolism and higher trophic levels in productive shallow lake mesocosms. *Sci. Tot. Env*. **678**: 227–238. doi:10.1016/j.scitotenv.2019.04.105

Fiandrino, A., V. Ouisse, F. Dumas, F. Lagarde, R. Pete, N. Malet, S. Le Noc, and R. de Wit. 2017. Spatial patterns in coastal lagoons related to the hydrodynamics of seawater intrusion. *Mar. Pollut. Bul.* **119**: 132–144. doi:10.1016/j.marpolbul.2017.03.006

Field, C. B., M. J. Behrenfeld, J. T. Randerson, and P. Falkowski. 1998. Primary Production of the Biosphere: Integrating Terrestrial and Oceanic Components. *Science* **281**: 237–240. doi:10.1126/science.281.5374.237

Filiz, N., U. Iskin, M. Beklioğlu, and others. 2020. Phytoplankton Community Response to Nutrients, Temperatures, and a Heat Wave in Shallow Lakes: An Experimental Approach. *Water* **12**: 3394. doi:10.3390/w12123394

Findlay, S., and R. Sinsabaugh. 2002. Aquatic ecosystems: interactivity of dissolved organic matter, Academic Press

Førland, E. J., and I. Hanssen-Bauer. 2000. Increased precipitation in the Norwegian Arctic: true or false? *Clim. Change* **46**: 485–509. doi:10.1023/A:1005613304674

Fouilland, E., A. Trottet, C. Bancon-Montigny, and others. 2012. Impact of a river flash flood on microbial carbon and nitrogen production in a Mediterranean lagoon (Thau lagoon, France). *Est. Coast. Shelf Sci.* **113**: 192-204. doi: 10.1016/j.ecss.2012.08.004

Frigstad, H. O. Kaste, A. Deininger, K. Kvalsund, G. Christensen, R. G. J. Bellerby, K. Sorensen, M. Norli, and A. L. King. 2020a. Influence of riverine input on Norwegian coastal systems. *Front. Mar. Sci*. **7**:332. doi:10.3389/fmars.2020.00332

Frigstad, H., E. T. Harvey, A. Deininger, and A. Poste. 2020b. Increased light attenuation in Norwegian coastal waters – A literature review. Norwegian Institute for Water Research. Report SNO. 7551-2020

Fu, W., J. T. Randerson, and J. K. Moore. 2016. Climate change impacts on net primary production (NPP) and export production (EP) regulated by increasing stratification and phytoplankton community structure in the CMIP5 models. *Biogeosciences* **13**: 5151-5170. doi: 10.5194/bg-13-5151-2016

Fuhrman, J. A. 1999. Marine viruses and their biogeochemical and ecological effects. *Nature* **399**: 541–548. doi:10.1038/21119

-G-

Garcia-Corral, L.S., C.M. Duarte, and S. Agusti. 2021. Plankton community metabolism in Western Australia: Estuarine, Coastal and Oceanic surface waters. *Front. Mar. Sci*. **7**: 1142. doi: 10.3389/fmars.2020.582136

Gillooly, J. F., J. H. Brown, G. B. West, V. M. Savage, and E. L. Charnov. 2001. Effects of Size and Temperature on Metabolic Rate. *Science* **293**: 2248–2251. doi:10.1126/science.1061967

del Giorgio, P., and J. J. Cole. 1998. Bacterial growth efficiency in natural aquatic systems. *Ann. Rev. Ecol. Sys*. **29**: 503–541. doi:10.1146/annurev.ecolsys.29.1.503

del Giorgio, P., and C. M. Duarte. 2002. Respiration in the open ocean. *Nature* **420**: 379–384. doi:10.1038/nature01165

del Giorgio, P., and P. Williams. 2005. Respiration in aquatic ecosystems, OUP Oxford.

Goericke, R., and J. P. Montoya. 1998. Estimating the contribution of microalgal taxa to chlorophyll *a* in the field--variations of pigment ratios under nutrient- and light-limited growth. *Mar. Ecol. Prog. Ser.* **169**: 97–112. doi:10.3354/meps169097

Goss, R., and T. Jakob. 2010. Regulation and function of xanthophyll cycle-dependent photoprotection in algae. *Photosynthetic Res.* **106**: 103–122. doi:10.1007/s11120-010-9536-x

Gowen, R. J., Y. Collos, P. Tett, C. Scherer, B. Bec, E. Abadie, M. Allen, and T. O'Brien. 2015. Response of diatom and dinoflagellate lifeforms to reduced phosphorus loading: A case study in the Thau lagoon, France. *Estuar. Coast. Shelf Sci* **162**: 45–52. doi:10.1016/j.ecss.2015.03.033

Grace, M. R., D. P. Giling, S. Hladyz, V. Caron, R. M. Thompson, and R. Mac Nally. 2015. Fast processing of diel oxygen curves: Estimating stream metabolism with BASE (BAyesian Single-station Estimation). *Limnol. Oceanogr.: Methods* **13**: 103–114. doi:10.1002/lom3.10011

Granum, E., J. A. Raven, and R. C. Leegood. 2005. How do marine diatoms fix 10 billion tons of inorganic carbon per year? *Can. J. Bot*. **83**(7). doi:10.1139/b05-077

Grasshoff, K., K. Kremling, M. Ehrhardt, L.G. Anderson. 1999. Determination of nutrients. In: Grasshoff K., Kremling K., Ehrhardt M. (eds), *Methods of seawater analysis*. Wiley-VCH, Weinheim, p159-226

Grytaas, A. 2020. Does Brownification and Iron Affect Microbial Communities and Mixotrophic Activities? Experiences From a Mesocosm Experiment. Master thesis. University of Bergen.

-H-

Haaland, S., D. Hongve, H. Laudon, G. Riise, and R. D. Vogt. 2010. Quantifying the Drivers of the Increasing Colored Organic Matter in Boreal Surface Waters. *Env. Sci. Tech*. **44**: 2975–2980. doi:10.1021/es903179j

Hall, R. O., Jr, and A. J. Ulseth. 2021. Gas exchange in streams and rivers. *WIREs Water* **7**: e1391. doi:10.1002/wat2.1391

Hanson, P. C., D. L. Bade, S. R. Carpenter, and T. K. Kratz. 2003. Lake metabolism: Relationships with dissolved organic carbon and phosphorus. *Limnol. Oceanogr*. **48**: 1112–1119. doi:10.4319/lo.2003.48.3.1112

Hanson, P. C., S. R. Carpenter, N. Kimura, C. Wu, S. P. Cornelius, and T. K. Kratz. 2008. Evaluation of metabolism models for free-water dissolved oxygen methods in lakes. *Limnol. Oceanogr.: Methods* **6**: 454–465. doi:10.4319/lom. 2008.6.454

Hart, R. C., and McLaren I.A. 1978. Temperature acclimation and other influences on embryonic duration in the copepod *Pseudocalanus* sp. *Mar. Biol*. **45**: 23–30. doi:10.1007/BF00388974

Hayashida, H., R. J. Matear, and P. G. Strutton. 2020. Background nutrient concentration determines phytoplankton bloom response to marine heatwaves. *Glob. Change Biol*. doi:10.1111/gcb.15255

Henriksen, P., B. Riemann, H. Kaas, H. Munk Sørensen, and H. Lang Sørensen. 2002. Effects of nutrient-limitation and irradiance on marine phytoplankton pigments. *J. Plank. Res.* **24**: 835–858. doi:10.1093/plankt/24.9.835

Hensley, R. T., and M. J. Cohen. 2020. Nitrate depletion dynamics and primary production in riverine benthic chambers. *Freshw. Sci*. **39**: 169–182. doi:10.1086/707650

Hernández-León, S., and T. Ikeda. 2005. A global assessment of mesozooplankton respiration in the ocean, *J. Plankt. Res*. **27**(2) 153 :158. doi: 10.1093/plankt/fbh166

Herrera, E. C., and K. Nadaoka. 2021. Temporal dynamics and drivers of lake ecosystem metabolism using high resolution observations in a shallow, tropical, eutrophic lake (Laguna Lake, Philippines). *J Great Lakes Res.* **47**: 997–1020. doi:10.1016/j.jglr.2021.03.017

Hillebrand, H., S. Langenheder, K. Lebret, E. Lindström, Ö. Östman, and M. Striebel. 2018. Decomposing multiple dimensions of stability in global change experiments. *Ecol. Lett*. **21**: 21–30. doi:10.1111/ele.12867

Hillebrand, H., and C. Kunze. 2020. Meta-analysis on pulse disturbances reveals differences in functional and compositional recovery across ecosystems. *Ecol. Lett*. **23**: 575-585. doi: 10.1111/ele.13457

Hirata, T., N. J. Hardman-Mountford, R. J. W. Brewin, and others. 2011. Synoptic relationships between surface chlorophyll-a and diagnostic pigments specific to phytoplankton functional types. *Biogeosciences* **8**: 311-327. doi: 10.5194/bg-8-311-2011

Hintz, N. H., M. Zeising, and M. Striebel. 2021. Changes in spectral quality of underwater light alter phytoplankton community composition. *Limnol. Oceanogr*. doi:10.1002/lno.11882

Hobday, A. J., E. C. J. Oliver, A. Sen Gupta, and others. 2018. Categorizing and Naming Marine Heatwaves. *Oceanography* **31**: 162–173. doi:10.5670/oceanog.2018.205

Hodges, C. M., S. A. Wood, J. Puddick, and others. 2018. Sensor manufacturer, temperature, and cyanobacteria morphology affect phycocyanin fluorescence measurements. *Environ. Sci. Pollut. Res.* **25**: 1079-1088. doi:10.1007/s11356-017-0473-5

Hoegh-Guldberg, O., D. Jacob, M. Bindi, and others. 2018. Impacts of 1.5°C Global Warming on Natural and Human Systems . in V Masson-Delmotte , P Zhai , H O Pörtner , D Roberts , J Skea , P R Shukla , A Pirani , W Moufouma-Okia , C Péan , R Pidcock , S Connors , J B R Matthews , Y Chen , X Zhou , M I Gomis , E Lonnoy , T Maycock , M Tignor & T Waterfield (eds) , Global warming of 1.5°C. : An IPCC Special Report . IPCC Secretariat , pp. 175-311

Holtgrieve, G. W., D. E. Schindler, T. A. Branch, and Z. T. A'mar. 2010. Simultaneous quantification of aquatic ecosystem metabolism and reaeration using a Bayesian statistical model of oxygen dynamics. *Limnol. Oceanogr*. **55**: 1047–1063. doi:10.4319/lo.2010.55.3.1047

Hongve, D., G. Riise, and J. F. Kristiansen. 2004. Increased colour and organic acid concentrations in Norwegian forest lakes and drinking water - a result of increased precipitation? *Aq. Sci.* **66**: 231–238. doi:10.1007/s00027-004-0708-7

Hoppe, H.-G., P. Breithaupt, K. Walther, R. Koppe, S. Bleck, U. Sommer, and K. Jürgens. 2008. Climate warming in winter affects the coupling between phytoplankton and bacteria during the spring bloom: a mesocosm study. *Aq. Microb. Ecol*. **51**: 105–115. doi:10.3354/ame01198

Horn, H., and D. Uhlmann. 1995. Competitive growth of blue-greens and diatoms (*Fragilaria*) in the Saidenbach reservoir, Saxony. *Water Sci. Technol*. **32**: 77–88. doi:10.2166/wst.1995.0168

Hotchkiss, E. R., and R. O. Hall Jr. 2014. High rates of daytime respiration in three streams: Use of $\delta^{18}O_{O2}$ and O_2 to model diel ecosystem metabolism. *Limnol. Oceanogr*. **59**: 798– 810. doi:10.4319/lo.2014.59.3.0798

Hyun, B., J.-M. Kim, P.-G. Jang, and others. 2020. The Effects of Ocean Acidification and Warming on Growth of a Natural Community of Coastal Phytoplankton. *J. Mar. Sci. Engineer*. **8**: 820. doi:10.3390/jmse8100821

Hyvärinen, V. 2003. Trends and characteristics of hydrological time series in Finland. *Nord. Hydro.* **34**: 71–90.

-I-

Idrizag, A., A. Laas, U. Anijalg, and P. Noges. 2016. Horizontal differences in ecosystem metabolism of a large shallow lake. *J. Hydrol*. **535**: 93–100. doi:10.1016/j.jhydrol.2016. 01.037

IPCC, 2018: Summary for Policymakers. In: Global Warming of 1.5°C. An IPCC Special Report on the impacts of global warming of 1.5°C above pre-industrial levels and related global greenhouse gas emission pathways, in the context of strengthening the global response to the threat of climate change, sustainable development, and efforts to eradicate poverty [Masson-Delmotte, V., P. Zhai, H.-O. Pörtner, D. Roberts, J. Skea, P.R. Shukla, A. Pirani, W. Moufouma-Okia, C. Péan, R. Pidcock, S. Connors, J.B.R. Matthews, Y. Chen, X. Zhou, M.I. Gomis, E. Lonnoy, T. Maycock, M. Tignor, and T. Waterfield (eds.)]. In Press.

IPCC, 2019: Summary for Policymakers. In: IPCC Special Report on the Ocean and Cryosphere in a Changing Climate [H.-O. Pörtner, D.C. Roberts, V. Masson-Delmotte, P. Zhai, M. Tignor, E. Poloczanska, K. Mintenbeck, A. Alegría, M. Nicolai, A. Okem, J. Petzold, B. Rama, N.M. Weyer (eds.)]. In press.

Iskin, U., N. Filiz, Y. Cao, and others. 2020. Impact of Nutrients, Temperatures, and a Heat Wave on Zooplankton Community Structure: An Experimental Approach. *Water* **12**: 3416. doi:10.3390/w12123416

-J-

Jankowski, K. J., F. H. Mejia, J. R. Blaszczak, and G. W. Holtgrieve. 2021. Aquatic ecosystem metabolism as a tool in environmental management. *WIREs Water*. doi:10.1002/wat2.1521

Jeppesen, E., J. Audet, T. A. Davidson, and others. 2021. Nutrient Loading, Temperature and Heat Wave Effects on Nutrients, Oxygen and Metabolism in Shallow Lake Mesocosms Pre-Adapted for 11 Years. *Water* **13**: 127. doi:10.3390/w13020127

Joint, I., A. Pomroy, G. Savidge, and P. Boyd. 1993. Size-fractionated primary productivity in the northeast Atlantic in May–July 1989. *Deep Sea Res. II: Top. Stud. Oceanogr* **40**: 423–440. doi:10.1016/0967-0645(93)90025-I

Joint, I., P. Henriksen, G. A. Fonnes, D. Bourne, T. F. Thingstad, and B. Riemann. 2002. Competition for inorganic nutrients between phytoplankton and bacterioplankton in nutrient manipulated mesocosms. *Aq. Microb. Ecol*. **29**: 145–159. doi:10.3354/ame029145

Jones, R. I. 1977. The importance of temperature conditioning to the respiration of natural phytoplankton communities. *Br. Phycol. J*. **12**: 277–285. doi:10.1080/ 00071617700650291

-K-

Kammerlander, B., K. A. Koinig, E. Rott, R. Sommaruga, B. Tartarotti, F. Trattner, and B. Sonntag. 2016. Ciliate community structure and interactions within the planktonic food web in two alpine lakes of contrasting transparency. *Freshw. Biol*. **61**: 1950–1965. doi:10.1111/fwb.12828

Karl, D. M., E. A. Laws, P. Morris, P. J. le B. Williams, and S. Emerson. 2003. Karl, D. M., Laws, E. A., & Morris, P. PJ leB. Williams, and S. Emerson. 2003. Metabolic balance of the open sea. *Nature* **426**(5). doi:10.1038/426032a

Karlsson, J., P. Byström, J. Ask, P. Ask, L. Persson, and M. Jansson. 2009. Light limitation of nutrient-poor lake ecosystems. *Nature* **460**: 506–509. doi:10.1038/nature08179

Kasprzak P., J. Padisak, R. Koschel, L. Krienitz, and F. Gervais. 2008. Chlorophyll *a* concentration across a trophic gradient of lakes: An estimator of phytoplankton biomass? *Limnologica* **38**(3-4): 327-338.doi: 10.1016/j.limno.2008.07.002

Katechakis, A., and H. Stibor. 2004. Feeding selectivities of the marine cladocerans *Penilia avirostris*, *Podon intermedius*, and *Evadne nordmanni*. *Mar. Biol.* **145**:529-539. doi: 10.1007/s00227-004-1347-1

Kimmance, S. A., W; H. Wilson, and S. D. Archer. 2007. Modified dilution technique to estimate viral lysis versus grazing mortality of phytoplankton: limitations associated with method sensitivity in natural waters. *Aq. Microb. Ecol*. **49**: 207-222. doi: 10.3354/ame01136

Kirk, J. T. O. 1983. Light and photosynthesis in aquatic ecosystems, Cambridge University Press.

Kritzberg, E. S., W. Granéli, J. Björk, C. Brönmark, P. Hallgren, A. Nicolle, A. Persson, and L.-A. Hansson. 2014. Warming and browning of lakes: consequences for pelagic carbon metabolism and sediment delivery. *Freshw Biol*. **59**: 325– 336. doi:10.1111/fwb.12267

Kritzberg, E. S. 2017. Centennial-long trends of lake browning show major effect of afforestation. *Limnol. Oceanogr.: Lett.* **2**: 105–112. doi:10.1002/lol2.10041

Kritzberg, E. S., E. M. Hasselquist, M. Skerlep, and others. 2020. Browning of freshwaters: Consequences to ecosystem services, underlying drivers, and potential mitigation measures. *Ambio* **49**: 375–390. doi:10.1007/s13280-019-01227-5

Kruskopf, M., and K.J. Flynn. 2005. Chlorophyll content and fluorescence responses cannot be used to gauge reliably phytoplankton biomass, nutrient status or growth rate. *New Phytol.* **169**(3): 525-536.doi: 10.1111/j.1469-8137.2005.01601.x

Kuczynska, P., M. Jemiola-Rzeminska, Nowicka Beatrycze, A. Jakubowska, W. Strzalka, K. Burda, and K. Strzalka. 2020. The xanthophyll cycle in diatom *Phaeodactylum tricornutum* in response to light stress. *Plant Physio. Biochem.* **152**: 125–137. doi:10.1016/j.plaphy.2020.04.043

Kuglitsch, F. G., A. Toreti, E. Xoplaki, P. M. Della-Marta, C. S. Zerefos, M. Türkeş, and J. Luterbacher. 2010. Heat waves changes in the eastern Mediterranean since 1960. *Geophys. Res. Lett*. **37**(4). doi:10.1029/2009GL041841

-L-

Laas, A., Noges, P., Koiv, T., and Noges, T. 2012. High-frequency metabolism study in a large and shallow temperate lake reveals seasonal switching between net autotrophy and net heterotrophy. *Hydrobiologia* **694**: 57–74. doi:10. 1007/s10750-012-1131-z

Laidler, K. J. 1984. The development of the Arrhenius equation. *J. Chem. Educ*. 61: 494

La Jeunesse, I., J. M. Deslous-Paoli, M. C. Ximénès, J. C. Cheylan, C. Mende, C. Borrero, and L. Scheyer. 2002. Changes in point and non-point sources phosphorus loads in the Thau catchment over 25 years (Mediterranean Sea – France). *Hydrobiologia* **475**: 403–411. doi:10.1023/A:1020351711877

La Jeunesse, I., C. Cirelli, H. Sellami, D. Aubin, R. Deidda, and N. Baghdadi. 2015. Is the governance of the Thau coastal lagoon ready to face climate change impacts? *Ocean Coast. Manag*. **118**: 234–246. doi:10.1016/j.ocecoaman.2015.05.014

Lal, R. 2008. Carbon sequestration. *Phil. Tran. R. Soc. B* **363**: 815-830. doi:10.1098/rstb.2007.2185

Landry, M. R., and R. P. Hassett. 1982. Estimating the grazing impact of marine micro-zooplankton. *Mar. Biol.* **67**: 283–288. doi:10.1007/BF00397668

Landry, M. R., K. E. Selph, A. G. Taylor, M. Decima, W. M. Balch, and R. R. Bidigare. 2011. Phytoplankton growth, grazing and production balances in the HNLC equatorial Pacific. *Deep Sea Res. II Top. Studies Oceanogr* **58**(3-4): 524-535. doi:10.1016/j.dsr2.2010.08.011

Lara, E., J. M. Arrieta, I. Garcia-Zarandona, J. A. Boras, C. M. Duarte, S. Agusti, P. Wassmann, and D. Vacqué. 2013. Experimental evaluation of the warming effect on viral, bacterial and protistan communities in two contrasting Arctic systems. *Aq. Microb. Ecol*. **70**: 17–32. doi:10.3354/ame01636

Larsen, A., G. A. Fonnes Flaten, R-A. Sandaa, T. Castberg, R. Thyrhaug, S. R. Erga, S. Jacquet, and G. Bratbak. 2004. Spring phytoplankton bloom dynamics in Norwegian coastal waters: Microbial community succession and diversity. *Limnol. Oceanogr.* **49**(1): 180-190. doi: 10.4319/lo.2004.49.1.0180

Larsen, S., T. Andersen, and D. O. Hessen. 2011. Climate change predicted to cause severe increase of organic carbon in lakes. *Glob Change Biol.* **17**: 1186–1192. doi:10.1111/j.1365-2486.2010.02257.x

Larsson, U., and A. Hagtsröm. 1979. Phytoplankton exudate release as an energy source for the growth of pelagic bacteria. *Mar. Biol.* **52**: 199–206

Lauster, G. H., P. C. Hanson, and T. K. Kratz. 2006. Gross primary production and respiration differences among littoral and pelagic habitats in northern Wisconsin lakes. *Can. J. Fish. Aquat. Sci*. **63**: 1130–1141.

Lebret, K., S. Langenheder, N. Colinas, Ö. Östman, and E. S. Lindström. 2018. Increased water colour affects freshwater plankton communities in a mesocosm study. *Aq. Microb. Ecol*. **81**: 1–17. doi:10.3354/ame01858

Leclercq, N., J.-P. Gattuso, and J. Jaubert. 1999. Measurement of oxygen metabolism in open-top aquatic mesocosms: Application to a coral reef community. *Mar. Ecol. Prog. Ser*. **177**: 299–304. doi:10.3354/meps177299

Lee, K. H., H. J. Jeong, K. Lee, and others. 2019. Effects of warming and eutrophication on coastal phytoplankton production. *Harmful Algae* **81**: 106-118. doi: 10.1016/j.hal.2018.11.017

Lefèvre, D., C. Guigue, and I. Obernosterer. 2008. The metabolic balance at two contrasting sites in the Southern Ocean: The iron-fertilized Kerguelen area and HNLC waters. *Deep Sea Res. II: Top. Stu. Oceanogr*. **55**: 766–776. doi:10.1016/j.dsr2.2007.12.006

Lejeusne, C., P. Chevaldonné, C. Pergent-Martini, C. F. Boudouresque, and T. Perez. 2010. Climate change effects on a miniature ocean: the highly diverse, highly impacted Mediterranean Sea. *Trends Ecol. Evol*. **25**: 250–260. doi:10.1016/j.tree.2009.10.009

Lenard, T., and W. Ejankowski. 2017. Natural water brownification as a shift in the phytoplankton community in a deep hard water lake. *Hydrobiologia* **787**: 153–166. doi:10.1007/s10750-016-2954-9

Lewandowska, A., and U. Sommer. 2010. Climate change and the spring bloom: a mesocosm study on the influence of light and temperature on phytoplankton and mesozooplankton. *Mar. Ecol. Prog. Ser*. **405**:101-111. doi:10.3354/meps08520

Lewandowska, A. M., D. G. Boyce, M. Hofmann, B. Matthiessen, U. Sommer, and B. Worm. 2014. Effects of sea surface warming on marine plankton. *Ecol. Lett.* **17**: 614–623. doi:10.1111/ele.12265

Li, W. K. W., M. R. Lewis, and W. G. Harrison. 2008. Multiscalarity of the Nutrient–Chlorophyll Relationship in Coastal Phytoplankton. *Est. Coas*. **33**: 440–447. doi:10.1007/s12237-008-9119-7

Liess, A., C. Faithfull, B. Reichstein, O. Rowe, J. Guo, R. Pete, G. Thomsson, W. Uszko, and S. N. Francoeur. 2015. Terrestrial runoff may reduce microbenthic net community productivity by increasing turbidity: a Mediterranean coastal lagoon mesocosm experiment. *Hydrobiologia* **753**: 205-218. doi: 10.1007/s10750-015-2207-3

Liess, A., O. Rowe, S. N. Francoeur, and others. 2016. Terrestrial runoff boosts phytoplankton in a Mediterranean coastal lagoon, but these effects do not propagate to higher trophic levels. *Hydrobiologia* **766**: 275–291. doi:10.1007/s10750-015- 2461-4

Litchman, E. 1998. Population and community responses of phytoplankton to fluctuating light. *Oecologia* **117**: 247–257.

Lomas, M. W., P. M. Gilbert, F.-K. Shiah, and E. M. Smith. 2008. Microbial processes and temperature in Chesapeake Bay: current relationships and potential impacts of regional warming. *Glob. Change Biol*. **8**(1): 51-70. doi:10.1046/j.1365-2486.2002.00454.x

López-Sandoval, D., K. Rowe, P. Carillo-de-Albonoz, C. M. Duarte, and S. Agusti. 2019. Rates and drivers of Red Sea plankton community metabolism. *Biogeosciences* **16**: 2983–2995. doi:10.5194/bg-16-2983-2019

López-Sandoval, D., C. M. Duarte, and S. Agusti. 2021. Nutrient and temperature constraints on primary production and net phytoplankton growth in a tropical ecosystem. *Limnol. Oceanogr*. **66**(7): 2923-2935. doi:10.1002/lno.11849

López-Urrutia, Á., E. S. Martin, R. P. Harris, and X. Irigoien. 2006. Scaling the metabolic balance of the oceans. *PNAS* **103**: 8739–8744. doi:10.1073/pnas.0601137103

-M-

Maazouzi, C., G. Masson, M. S. Izquierdo, and J.-P. Pihan. 2008. Midsummer heatwave effects on lacustrine plankton: variation of assemblage structure and fatty acid composition. *Therm. Biol*. **33**(5): 287-296. doi:10.1016/j.therbio.2008.03.002

Mackey, M. D., D. J. Mackey, H. W. Higgins, and S. W. Wright. 1996. CHEMTAX- a program for estimating class abundances from chemical markers: application to HPLC measurements of phytoplankton. *Mar. Ecol. Prog. Ser*. **144**:265-283. doi:10.3354/meps144265

Mantikci, M., J. L. S. Hansen, and S. Markager. 2017. Photosynthesis enhanced dark respiration in three marine phytoplankton species. *J. Exp. Mar. Biol. Ecol*. **497**: 188–196. doi: 10.1016/j.jembe.2017.09.015

Mantikci, M., P. A. Staerh, J. L. S. Hansen, and S. Markager. 2019. Patterns of dark respiration in aquatic systems. *Mar. Freshw. Res*. **71**: 432–442. doi:10.1071/MF18221

Marañón, E., P. Cermeno, M. Huete-Ortega, D. C. Lopez-Sandoval, B. Mouriño-Carballido, and T. Rodriguez-Ramos. 2014. Resource Supply Overrides Temperature as a Controlling Factor of Marine Phytoplankton Growth. *PLOS ONE* **9**: e99312. doi:10.1371/journal.pone.0099312

van Marion, P. 1996. Ecological studies in Hopavågen, a landlocked bay at Agdenes, Sør-Trøndelag, Norway. *Gunneria* **71**: 1–38

Markager, S., and K. Sand-Jensen. 1989. Patterns of night-time respiration in a dense phytoplankton community under a natural light regime. *J. Ecol*. **77**: 49. doi:10.2307/2260915

Markager, S., A.-M. Jespersen, T. V. Madsen, E. Berdalet, and R. Weisburd. 1992. Diel changes in dark respiration in a plankton community, p. 119–130.In T. Berman, H. J. Gons, and L. R. Mur [eds.], The daily growth cycle of phytoplankton: Proceedings of the fifth International Workshop of the Group for Aquatic Primary Productivity (GAP), held at Breukelen, The Netherlands 20–28 April 1990. Springer.

Marra, J., and R. T. Barber. 2004. Phytoplankton and heterotrophic respiration in the surface layer of the ocean. *Geophys. Res. Lett*. **31**. doi:10.1029/2004GL019664

Mascarenhas, V. J., D. Voß, J. Wollschlaeger, and O. Zielinski. 2017. Fjord light regime: Bio-optical variability, absorption budget, and hyperspectral light availability in Sognefjord and Trondheimsfjord, Norway. *JGR Oceans* **122**(5): 3828-3847. doi:10.1002/2016JC012610

Mascarenhas, V. J., and O. Zielinski. 2018. Parametrization of spectral particulate and phytoplankton absorption coefficients in Sognefjord and Trondheimsfjord, two contrasting Norwegian fjord ecosystems. *Rem. Sens*. **10**(6): 977. doi:10.3390/rs10060977

Maugendre, L., J.-P. Gattuso, J. Louis, A. de Kluijver, S. Marro, K. Soetaert, and F. Gazeau. 2015. Effect of ocean warming and acidification on a plankton community in the NW Mediterranean Sea. *ICES J Mar Sci* **72**: 1744–1755. doi:10.1093/icesjms/fsu161

Mayot, N., F. d'Ortenzio, J. Uitz, B. Gentili, J. Ras, V. Vellucci, M. Golbol, D. Antoine, and H. Claustre. 2017. Influence of the phytoplankton structure on the spring and annual primary production in the Northwestern Mediterranean Sea. *JGR Oceans* **122**(2): 9918-9936. doi: 10.1002/2016JC012668

McLaren, I. A. 1978. Generation Lengths of Some Temperate Marine Copepods: Estimation, Prediction, and Implications. *J. Fish. Res. Board Can*. **35**. doi:10.1139/f78-208

Meinelt, T., A. Paul, T. M. Phan, E. Zwirnmann, A. Krüger, A. Wienke, and C. E. W. Steinberg. 2007. Reduction in vegetative growth of the water mold *Saprolegnia parasitica* (Coker) by humic substance of different qualities. *Aq. Tox*. **83**: 93–103. doi:10.1016/j.aquatox.2007.03.013

Menden-Deuer, S., W. H. Slade, and H. Dierssen. 2021. Promoting instrument development for new research avenues in ocean science: opening the black box of grazing. *Front. Mar. Sci.* **8**:695938. doi:10.3389/fmars.2021.695938

Mesa, E., and others. 2017. Continuous daylight in the high Arctic summer supports high plankton respiration rates compared to those supported in the dark. *Sci. Rep*. **7**: 1247. doi:10.1038/s41598-017-01203-7

Meunier, C. L., A. Liess, A. Andersson, S. Brugel, J. Paczkowska, H. Rahman, B. Skoglund, and O. F. Rowe. 2017. Allochthonous carbon is a major driver of the microbial food web – A mesocosm study simulating elevated terrestrial matter runoff. *Mar. Env. Res*. **129**: 236–244. doi:10.1016/j.marenvres.2017.06.008

Mignot, A., H. Claustre, J. Uitz, A. Poteau, F. D'Ortenzio, and X. Xing. 2014. Understanding the seasonal dynamics of phytoplankton biomass and the deep chlorophyll maximum in oligotrophic environments: A Bio-Argo float investigation. *Glob. Biogeochem. Cycles* **28**: 856–876. doi:10.1002/2013GB004781

Mills, G., and G. Fones. 2012. A review of *in situ* methods and sensors for monitoring the marine environment. *Sensor Review* **32**: 17–28. doi:10.1108/02602281211197116

Minguez, L., E. Sperfeld, S. A. Berger, J. C. Nejstgaard, and M. O. Gessner. 2020. Changes in food characteristics reveal indirect effects of lake browning on zooplankton performance. *Limnol. Oceanogr*. **65**: 1028–1040. doi:10.1002/lno.11367

Monteith, D. T., J. L. Stoddard, C. D. Evans, and others. 2007. Dissolved organic carbon trends resulting from changes in atmospheric deposition chemistry. *Nature* **450**: 537–540. doi:10.1038/nature06316

Moore, M.C., D.J. Suggett, A.E. Hickman, Y.-N. Kim, J.F. Tweedle, J. Sharples, R.J. Geider, and P.M. Holligan. 2006. Phytoplankton photoacclimation and photoadaptation in response to environmental gradients in a shelf sea. *Limnol. Oceanogr*. **51**(2): 936-949. doi: 10.4319/lo.2006.51.2.0936

Morán, X. A. G., M. Estrada, J. M. Gasol, and C. Pedrós-Alió. 2002. Dissolved Primary Production and the Strength of Phytoplankton– Bacterioplankton Coupling in Contrasting Marine Regions. *Microb. Ecol.* **44**: 217–233. doi:10.1007/s00248-002-1026-z

Morán, X.A.G., M. Sebastián, C. Pedris-Alli, and M. Estrada. 2006. Response of Southern Ocean phytoplankton and bacterioplankton production to short-term experimental warming. *Limnol. Oceanogr*. **51**(4): 1791-1800. doi:10.4319/lo.2006.51.4.1791

Morán, X. A. G, V. Pérez, and E. Fernández. 2007. Mismatch between community respiration and the contribution of heterotrophic bacteria in the NE Atlantic open ocean: What causes high respiration in oligotrophic waters? *J. Mar. Res*. **65**: 545-560. doi: 10.1357/002224007782689102

Moreau, S., B. Mostajir, G. O. Almandoz, and others. 2014. Effects of enhanced temperature and ultraviolet B radiation on a natural plankton community of the Beagle Channel (southern Argentina): a mesocosm study. *Aq. Microb. Ecol*. **72**: 155–173. doi:10.3354/ame01694

Morison, F., G. Franzè, E. Harvey, and S. Menden-Deuer. 2020. Light fluctuations are key in modulating plankton trophic dynamics and their impact on primary production. *Limnol. Oceanogr.: Lett*. **5**: 346–353. doi:10.1002/lol2.10156

Mostajir, B., J. Nouguier, E. Le Floc'h, S. Mas, R. Pete, D. Parin, and F. Vidussi. 2012. Use of sensors in marine mesocosm experiments to study the effect of environmental changes on planktonic food webs, p. 309–329. In Sensors for ecology, toward integrated knowledge of ecosystems. Publication CNRS.

Mostajir, B., E. Le Floc'h, S. Mas, R. Pete, D. Parin, J. Nouguier, E. Fouilland, and F. Vidussi. 2013. A new transportable floating mesocosm platform with autonomous sensors for real-time data acquisition and transmission for studying the pelagic food web functioning. *Limnol. Oceanogr.: Methods* **11**: 394–409. doi:10.4319/lom.2013.11.394

Mostajir, B., C. Amblard, E. Buffan-Dubau, R. de Wit, R. Lensi, and T. Sime-Ngando. 2015. Microbial Food Webs in Aquatic and Terrestrial Ecosystems. In: Environmental Microbiology: Fundamentals and Applications. Bertrand J-C, Caumette P, Lebaron P, Matheron R, Normand P, Sime-Ngando T (eds) Springer Netherlands, Dordrecht, p 485– 509

Münster, U., and R. J. Chróst. 1990. Origin, Composition, and Microbial Utilization of Dissolved Organic Matter, In Aquatic Microbial Ecology

Mustaffa, N., L. Kallajoki, J. Biederbick, F. Binder, A. Schlenker, and M. Striebel. 2020. Coastal ocean darkening effects via terrigenous DOM addition on plankton: an indoor mesocosm experiment. *Front. Mar. Sci*. **7**. doi:10.3389/fmars.2020.547829

-N-

Nagata, T. 2000. Production mechanisms of dissolved organic matter, p. 121–152. In Microbial Ecology of the Oceans. Wiley-Liss.

Neveux, J., C. Dupouy, J. Blanchot, A. Le Bouteiller, M. R. Landry, and S. L. Brown. 2003. Diel dynamics of chlorophylls in high-nutrient, low-chlorophyll waters of the equatorial Pacific (180°): Interactions of growth, grazing, physiological responses, and mixing. *J. Geophys. Res*. **108**. doi:10.1029/2000JC000747

Neveux, J., J. P. Lefèbvre, R. Le Gendre, C. Dupouy, F. Gallois, C. Courties, P. Gérard, J.-M. Fernandez, and S. Ouillon. 2010. Phytoplankton dynamics in the southern New Caledonian lagoon during a southeast trade wind event. *J. Mar. Sys.* **82**:230-244. doi: 10.1016/j.jmarsys.2010.05.010

Nicolle, A., P. Hallgren, J. V. Einem, E. S. Kritzberg, W. Granéli, A. Persson, C. Brönmark, and L.-A. Hansson. 2012. Predicted warming and browning affect timing and magnitude of plankton phenological events in lakes: a mesocosm study. *Freshw. Biol*. **57**: 684–695. doi:10.1111/j.1365-2427.2012.02733.x

Nixon, S. W., S. Granger, B. A. Buckley, M. Lamont, and B. Rowell. 2004. A one hundred and seventeen year coastal water temperature record from Woods Hole, Massachusetts. *Estuaries* **27**: 397–404. doi:10.1007/BF02803532

Nouguier, J., B. Mostajir, E. L. Floc'h, and F. Vidussi. 2007. An automatically operated system for simulating global change temperature and ultraviolet B radiation increases: application to the study of aquatic ecosystem responses in mesocosm experiments. *Limnol. Oceanogr: Methods* **5**: 269–279. doi:10.4319/lom.2007.5.269

Nydahl, A. C., M. B. Wallin, L. J. Tranvik, C. Hiller, K. Attermeyer, J. A. Garrison, F. Chaguaceda, K. Scharnweber, G. A. Weyhenmeyer. 2019. Colored organic matter increases CO2 in meso-eutrophic lake water through altered light climate and acidity. *Limnol. Oceanogr*. **64**(2): 744-756. doi:10.1002/lno.11072

-O-

O'Connor MI, Piehler MF, Leech DM, Anton A, Bruno JF (2009) Warming and Resource Availability Shift Food Web Structure and Metabolism. *PLOS Biology* **7**(8): e1000178. doi: 10.1371/journal.pbio.1000178

Odum, E. P. 1984. The mesocosm. *Bioscience* **34**: 558–562. doi:10.2307/1309598

Odum, H. T. 1956. Primary production in flowing waters. *Limnol. Oceanogr*. **1**: 102–117. doi:10.4319/lo.1956.1.2. 0102

Odum, H. T., and E. P. Odum. 1955. Trophic structure and productivity of a windward coral reef community on Eniwetok Atoll. *Ecol. Monogr*. **25**: 291–320. doi:10.2307/ 1943285

Olsen, Y., S. Agusti, T. Andersen, and others. 2006. A comparative study of responses in planktonic food web structure and function in contrasting European coastal waters exposed to experimental nutrient addition. *Limnol. Oceanogr*. **51**(1): 488-503. doi: 10.4319/lo.2006.51.1_part_2.0488

Oviatt, C., M. Pilson, S. Nixon, J. Frithsen, D. Rudnick, J. Kelly, J. Grassle, and J. Grassle. 1984. Recovery of a polluted estuarine system: A mesocosm experiment. *Mar. Ecol. Prog. Ser*. **16**: 203–217. doi:10.3354/meps016203

Oviatt, C., A. Keller, P. Sampou, and L. Beatty. 1986. Patterns of productivity during eutrophication: A mesocosm experiment. *Mar. Ecol. Prog. Ser*. **28**: 69–80. doi:10.3354/ meps028069

Oztürk, M., O. Vadstein, and E. Sakshaug. 2003. The effects of enhanced phytoplankton production on iron speciation and removal in mesocosm experiments in a landlocked basin of Hopavågen, Norway. *Mar. Chem*. **84**: 3–17. doi:10.1016/S0304-4203(03)00087-2

-P-

Paczkowska, J., S. Brugel, O. Rowe, R. Lefébure, A. Brutemark, and A. Andersson. 2020. Response of coastal phytoplankton to high inflows of terrestrial matter. *Front. Mar. Sci*. **7**:80. doi:10.3389/fmars.2020.00080

Panigrahi, S., A. Nydahl, P. Anton, and J. Wikner. 2013. Strong seasonal effect of moderate experimental warming on plankton respiration in a temperate estuarine plankton community. *Estuar. Coast. Shelf Sci.* **135**: 269–279. doi:10.1016/j.ecss.2013.10.029

Park, M. G., W. Yih, and D. W. Coats. 2004. Parasites and Phytoplankton, with Special Emphasis on Dinoflagellate Infections. *J. Euk. Microbiol*. **51**: 145–155. doi:10.1111/j.1550-7408.2004.tb00539.x

Pecqueur, D., F. Vidussi, E. Fouilland, E. Le Floc'h, S. Mas, C. Roques, C. Salles, M.-G. Tournoud, and B. Mostajir. 2011. Dynamics of microbial planktonic food web components during a river flash flood in a Mediterranean coastal lagoon. *Hydrobiologia* **673**: 13-27. doi:10.1007/s10750-011-0745-x

Pernet, F., N. Malet, A. Pastoureaud, A. Vaquer, C. Quéré, and L. Dubroca. 2012. Marine diatoms sustain growth of bivalves in a Mediterranean lagoon. *J. Sea Res.* **68**: 20–32. doi:10.1016/j.seares.2011.11.004

Peter, K. H., and U. Sommer. 2012. Phytoplankton cell size: intra- and interspecific effects of warming and grazing. *Plos ONE* **7**(11): e49632. doi: 10.1371/journal.pone.0049632

Pomeroy, L. R. 1974. The Ocean's Food Web, A Changing Paradigm. *BioScience* **24**: 499–504. doi:10.2307/1296885

Pörtner, H.-O., D. C. Roberts, V. Masson-Delmotte, and others. 2019. IPCC Special Report on the Ocean and Cryosphere in a Changing Climate. IPCC

Powles, S. B. 1984. Photoinhibition of photosynthesis induced by visible light. *Annu. Rev. Plant Physiol*. **35**: 15–44. doi: 10.1146/annurev.pp.35.060184.000311

Pringault, O., V. Tassas, and E. Rochelle-Newall. 2007. Consequences of respiration in the light on the determination of production in pelagic systems. *Biogeosciences* 4: 105–114.

Pringault, O., S. Tesson, and E. Rochelle-Newall. 2009. Respiration in the Light and Bacterio-Phytoplankton Coupling in a Coastal Environment. *Microb. Ecol*. **57**: 321–334. doi:10.1007/s00248-008-9422-7

Pulina, S., A. Brutemark, S. Suikkanen, and others. 2016. Effects of warming on a Mediterranean phytoplankton community. *Web Ecol.* **16**: 89-92. doi:10.5194/we-16-89-2016

Pulina, S., S. Suikkanen, B. M. Padedda, A. Brutemark, L. M. Grubisic, C. T. Satta, T. Caddeo, P. Farina, and A. Lugliè. 2020. Responses of a Mediterranean coastal lagoon plankton community to experimental warming. *Mar. Biol*. **167**:22. doi:10.1007/s00227-019-3640-z

-Q-

Quilty, J. R., and S. R. Cattle. 2011. Use and understanding of organic amendments in Australian agriculture: a review. *Soil Res*. **49**(1): 1-26. doi:10.1071/SR10059

-R-

Rasconi, S., A. Gall, K. Winter, and M. J. Kainz. 2015. Increasing Water Temperature Triggers Dominance of Small Freshwater Plankton. *PLoS One* **10**: e0140449. doi:10.1371/journal.pone.0140449

Ratcovich, J. 2014. The impact of climate change and brownification on primary and bacterial production. Master thesis. Lund University.

Raven, J. A., and P. G. Falkowski. 1999. Oceanic sinks for atmospheric CO_2. *Plant Cell Env*. **22**: 741–755. doi:10.1046/j.1365-3040.1999.00419.x

Regaudie-de-Gioux, A., and C. M. Duarte. 2012. Temperature dependence of planktonic metabolism in the ocean. *Glob. Biogeochem. Cycles* **26**. doi:10.1029/2010GB003907

Reichwaldt, E.S., I.D. Wolf, and H. Stibor. 2004. The effect of different zooplankton grazing patterns resulting from diel vertical migration on phytoplankton growth and composition: a laboratory experiment. *Oecologia* **141**:411–419. doi:10.1007/s00442-004-1645-9

Reijo, C. J., R. T. Hensley, and M. J. Cohen. 2018. Isolating stream metabolism and nitrate processing at point-scales, and controls on heterogeneity. *Freshw. Sci*. **37**: 238–250. doi:10.1086/697319

Richardson, D. C., C. C. Carey, D. A. Bruesewitz, and K. C. Weathers. 2017. Intra- and inter-annual variability in metabolism in an oligotrophic lake. *Aquat. Sci.* **79**: 319– 333. doi:10.1007/s00027-016-0499-7

Richardson, A. J., J. Savage, F. Coman, C. Davies, R. Eriksen, F. McEnnulty, A. Slotwinksi, M. Tonks, and J. Uribe-Palomino. 2020. The impact on zooplankton of the 2011 heatwave off Western Australia. *IMOS*. doi:10.26198/5e16adc449e87

Riebesell, U. 1989. Comparison of sinking and sedimentation rate measurements in a diatom winter/spring bloom. *Mar. Ecol. Prog. Ser*. **54**: 109-119

Rivkin, R., M. Anderson, and C. Lajzerowicz. 1996. Microbial processes in cold oceans. I. Relationship between temperature and bacterial growth rate. *Aq. Microb. Ecol.* **10**: 243–254. doi:10.3354/ame010243

Robinson, C., and P. J. le B. Williams. 1999. Plankton net community production and dark respiration in the Arabian Sea during September 1994. *Deep Sea Res. II Top. Studies Oceanogr*. **46**: 745–765. doi:10.1016/S0967-0645(98)00126-X

Robinson, C. 2008. Heterotrophic bacterial respiration, p. 299–334.In D. L. Kirchman [ed.], Microbial ecology of the oceans. Wiley.

Roesler, C., J. Uitz, H. Claustre, and others. 2017. Recommendations for obtaining unbiased chlorophyll estimates from in situ chlorophyll fluorometers: A global analysis of WET Labs ECO sensors. *Limnol. Oceanogr: Methods* **15**: 572–585. doi:10.1002/lom3.10185

Rose, J. M., and D. A. Caron. 2007. Does low temperature constrain the growth rates of heterotrophic protists? Evidence and implications for algal blooms in cold waters. *Limnol. Oceanogr.* **52**: 886–895. doi:10.4319/lo.2007.52.2.0886

Rose, J. M., Y. Feng, C. J. Gobler, R. Gutierrez, C. E. Hare, K. Leblanc, and D. A. Hutchins. 2009. Effects of increased pCO2 and temperature on the North Atlantic spring bloom. II. Microzooplankton abundance and grazing. *Mar. Ecol. Prog. Ser*. **388**: 27–40. doi:10.3354/meps08134

Roulet, N., and T. Moore. 2006. Browning the waters. Nature 444: 283–284. doi:10.1038/444283a

Roy, S., C. A. Llewellyn, E. S. Egeland, and G. Johnsen. 2011. Phytoplankton pigments: Characterization, chemotaxonomy and applications in oceanography, Cambridge University Press. Cambridge.

Ruivo, M., A. Amorim, and P. Cartaxana. 2011. Effects of growth phase and irradiance on phytoplankton pigment ratios: implications for chemotaxonomy in coastal waters. *J. Plankt. Res*. **33**: 1012–1022. doi:10.1093/plankt/fbr019

-S-

Sadro, S., C. E. Nelson, and J. M. Melack. 2011. Linking diel patterns in community respiration to bacterioplankton in an oligotrophic high-elevation lake. *Limnol. Oceanogr.* **56**: 540–550. doi:10.4319/lo.2011.56.2.0540

Sampou, P., and W. M. Kemp. 1994. Factors regulating plankton community respiration in Chesapeake Bay. *Mar. Ecol. Prog. Ser.* **110**: 249–258

SanClements, M. D., G. P. Oelsner, D. M. McKnight, J. L. Stoddard, and S. J. Nelson. 2012. New Insights into the Source of Decadal Increases of Dissolved Organic Matter in Acid-Sensitive Lakes of the Northeastern United States. *Env. Sci. Tech*. **46**: 3212–3219. doi:10.1021/es204321x

Scharnweber, K., S. Peura, K. Attermeyer, and others. 2021. Comprehensive analysis of chemical and biological problems associated with browning agents used in aquatic studies. *bioRxiv* 2021.02.26.433092. doi:10.1101/2021.02.26.433092

von Scheibner, M., P. Dörge, A. Biermann, U. Sommer, H-.G. Hoppe, and K. Jürgens. 2013. Impact of warming on phyto-bacterioplankton coupling and bacterial community composition in experimental mesocosms. *Env. Microbiol*. **16**(3): 718-733. doi: 10.1111/1462-2920.12195

Schlüter, L., M. Møhlenberg, H. Havskum, and S. Larsen. 2000. The use of phytoplankton pigments for identifying and quantifying phytoplankton groups in coastal areas: testing the influence of light and nutrients on pigment/chlorophyll *a* ratios. *Mar. Ecol. Prog. Ser.* **192**: 49–63.

Schwaderer, A. S., K. Yoshiyama, P. de Tezanos Pinto, N. G. Swenson, C. A. Klausmeier, and E. Litchman. 2011. Eco-evolutionary differences in light utilization traits and distributions of freshwater phytoplankton. *Limnol. Oceanogr*. **56**: 589–598. doi:10.4319/lo.2011.56.2.0589

Seekell, D. A., J.-F. Lapierre, J. Ask, A.-K. Bergström, A. Deininger, P. Rodríguez, and J. Karlsson. 2015. The influence of dissolved organic carbon on primary production in northern lakes. *Limnol. Oceanogr*. **60**: 1276–1285. doi:10.1002/lno.10096

Seneviratne, S.I., M.G. Donat, A.J. Pitman, R. Knutti, and R. L. Wilby, 2016. Allowable CO_2 emissions based on regional and impact-related climate targets. *Nature* **529**(7587): 477-483. doi:10.1038/nature16542

Sen Gupta, A., M. Thomsen, J. A. Benthuysen, and others. 2020. Drivers and impacts of the most extreme marine heatwave events. *Sci. Rep.* **10**: 19359. doi:10.1038/s41598-020-75445-3

Sepp, M., T. Koiv, P. Noges, and T. Noges. 2018. Do organic matter metrics included in lake surveillance monitoring in Europe provide a broad picture of brownification and enrichment with oxygen consuming substances? *Sci. Total Environ*., 610–611,1288-1297.

Serre-Fredj, L., F. Jacqueline, M. Navon, G. Izabel, L. Chasselin, O. Jolly, M. Repecaud, and P. Claquin. 2021. Coupling high-frequency monitoring and bioassay experiments to investigate a harmful algal bloom in the Bay of Seine (French-English Channel). *Mar. Pol. Bul*. **168**:112387. doi: 10.1016/j.marpolbul.2021.112387

Serret, P., C. Robinson, M. Aranguren-Gassis, and others. 2015. Both respiration and photosynthesis determine the scaling of plankton metabolism in the oligotrophic ocean. *Nature Comm*. **6**. doi:10.1038/ncomms7961

Sett, S., K. G. Schulz, L. T. Bach, and U. Riebesell. 2018. Shift towards larger diatoms in a natural phytoplankton assemblage under combined high-CO_2 and warming conditions. *J Plankton Res* **40**: 391–406. doi:10.1093/plankt/fby018

Shatwell, T., J. Köhler, and A. Nicklish. 2008. Warming promotes cold-adapted phytoplankton in temperate lakes and opens a loophole for Oscillatoriales in spring. *Glob. Change Biol*. **14**: 2194-2200. doi: 10.1111/j.1365-2486.2008.01630.x

Sherman, E., J. K. Moore, F. Primeau, and D. Tanouye. 2016. Temperature influence on phytoplankton community growth rates. *Glob. Biogeochem. Cycles* **30**: 550–559. doi:10.1002/2015GB005272

Siegel, D. A., T. D. Dickey, L. Washburn, M. K. Hamilton, and B. G. Mitchell. 1989. Optical determination of particulate abundance and production variations in the oligotrophic ocean. *Deep Sea Res. I Oceanogr. Res. Pap* **36**: 211–222. doi:10.1016/0198-0149(89)90134-9

Skogen, M. D., M. Eknes, L. C. Asplin, and A. D. Sandvik. 2009. Modelling the environmental effects of fish farming in a Norwegian fjord. *Aquaculture* **298**(1-2): 70-75. doi: 10.1016/j.aquaculture.2009.10.018

Skovgaard, A. 2014. Dirty Tricks in the Plankton: Diversity and Role of Marine Parasitic Protists. *Acta Protozoologica* **53**. doi:10.4467/16890027AP.14.006.1443

Smetacek, V. 1999. Diatoms and the Ocean Carbon Cycle. *Protist* **150**: 25–32. doi:10.1016/S1434-4610(99)70006-4

Smith, E., and W. Kemp. 1995. Seasonal and regional variations in plankton community production and respiration for Chesapeake Bay. *Mar. Ecol. Prog. Ser*. **116**: 217–231. doi:10.3354/meps116217

Smith, R. W., T. S. Bianchi, M. Allison, C. Savage, and V. Galy. 2015. High rates of organic carbon burial in fjord sediments globally. *Nat. Geosci*. **8**: 450-453. doi: 10.1038/ngeo2421

Solomon, C. T., and others. 2013. Ecosystem respiration: Drivers of daily variability and background respiration in lakes around the globe. *Limnol. Oceanogr*. **58**: 849–866. doi:10.4319/lo.2013.58.3.0849

Solomon, C. T., S. E. Jones, B. C. Weidel, and others. 2015. Ecosystem Consequences of Changing Inputs of Terrestrial Dissolved Organic Matter to Lakes: Current Knowledge and Future Challenges. *Ecosystems* **18**: 376–389. doi:10.1007/s10021-015-9848-y

Sommer, U., and K. Lengfellner. 2008. Climate change and the timing, magnitude, and composition of the phytoplankton spring bloom. *Global Change Biol*. **14**: 1199–1208. doi:10.1111/j.1365-2486.2008.01571.x

Sommer, U., N. Aberle, K. Lengfellner, and A. Lewandowska. 2012. The Baltic Sea spring phytoplankton bloom in a changing climate: an experimental approach. *Mar. Biol*. **159**: 2479–2490. doi:10.1007/s00227-012-1897-6

Sommer, U., E. Charalampous, S. Genitsaris, and M. Moustaka-Gouni. 2017. Benefits, costs and taxonomic distribution of marine phytoplankton body size. *J. Plankt. Res.* **39**(3): 494-508. doi: 10.1093/plankt/fbw071

Souchu, P., A. Gasc, Y. Collos, A. Vaquer, H. Tournier, B. Bibent, and J.-M. Deslous-Paoli. 1998. Biogeochemical aspects of bottom anoxia in a Mediterranean lagoon (Thau, France). *Mar. Ecol. Prog. Ser*. **164**: 135-146. doi:10.3354/meps164135

Souchu, P., A. Vaquer, Y. Collos, S. Landrein, J.-M. Deslous-Paoli, and B. Bibent. 2001. Influence of shellfish farming activities on the biogeochemical composition of the water column in Thau lagoon. *Mar. Ecol. Prog. Ser*. **218**: 141-152. doi: 10.3354/meps218141

Soulié, T., S. Mas., D. Parin, F. Vidussi and B. Mostajir. 2021. A new method to estimate planktonic oxygen metabolism using high-frequency sensor measurements in mesocosm experiments and considering daytime and nighttime respirations. *Limnol. Oceanogr.: Methods* **19**(5): 303-316. doi: 10.1002/lom3.10424

Staehr, P. A., D. Bade, M. C. V. de Bogert, G. R. Koch, C. Williamson, P. Hanson, J. J. Cole, and T. Kratz. 2010a. Lake metabolism and the diel oxygen technique: State of the science. *Limnol. Oceanogr.: Methods* **8**: 628–644. doi:10. 4319/lom.2010.8.0628

Staehr, P. A., K. Sand-Jensen, A. L. Raun, B. Nilsson, and J. Kidmose. 2010b. Drivers of metabolism and net heterotrophy in contrasting lakes. *Limnol. Oceanogr*. **55**: 817–830. doi:10.4319/lo.2010.55.2.0817

Staehr, P. A., J. M. Testa, W. M. Kemp, J. J. Cole, K. Sand-Jensen, and S. V. Smith. 2012. The metabolism of aquatic ecosystems: History, applications, and future challenges. *Aquat. Sci*. **74**: 15–29. doi:10.1007/s00027-011-0199-2

Stefanidou, N., S. Genitsaris, J. Lopez-Bautista, U. Sommer, and M. Moustaka-Gouni. 2018. Effects of heat shock and salinity changes on coastal Mediterranean phytoplankton in a mesocosm experiment. *Mar Biol* **165**: 154. doi:10.1007/s00227-018-3415-y

Stewart, R. I. A., and others. 2013. Chapter two - Mesocosm experiments as a tool for ecological climate-change research, p. 71–181.In G. Woodward and E. J. O'Gorman [eds.], Advances in ecological research. Academic Press.

Stibor, H., O. Vadstein, S. Diehl, and others. 2004. Copepods act as a switch between alternative trophic cascades in marine pelagic food webs. *Ecol. Lett*. **7**: 321–328. doi:10.1111/j.1461-0248.2004.00580.x

Stomp, M., J. Huisman, F. de Jongh, A. J Veraart, D. Gerla, M. Rijkeboer, B. W. Ibelings, U. I. A. Wollenzien, and L. J. Stal. 2004. Adaptative divergence in pigment composition promotes phytoplankton biodiversity. *Nature* **432**:104-107. doi:10.1038/nature03044

Sukenik, A., R. Eshkol, A. Livne, O. Hadas, H. Rom, D. Tchernov, A. Vardi, and A. Kaplan. 2002. Inhibition of growth and photosynthesis of the dinoflagellate *Peridinium gatunense* by *Microcystis* sp. (cyanobacteria): A novel allelopathic mechanism. *Limnol. Oceanogr*. **47**: 1656–1663. doi:10.4319/lo.2002.47.6.1656

Suryan, R. M., M. L. Arimitsu, R. Hopcroft, and others. 2021. Ecosystem response persists after a prolonged marine heatwave. *Sci. Rep*. **11**: 6235. doi:10.1038/s41598-021-83818-5

Suttle, C. A., and A. M. Chan. 1994. Dynamics and Distribution of Cyanophages and Their Effect on Marine *Synechococcus* spp. *App. Env. Microbiol*. **60**: 3167–3174. doi:10.1128/aem.60.9.3167-3174.1994

Sverdrup, H. U. 1953. On Conditions for the Vernal Blooming of Phytoplankton. *ICES J Mar. Sci*. **18**: 287–295. doi:10.1093/icesjms/18.3.287

Sweetman, A. K., A. Chelsky, K. A. Pitt, H. Andrade, D. van Oevelen, and P. E. Renaud. 2016. Jellyfish decomposition at the seafloor rapidly alters biogeochemical cycling and carbon flow through benthic food-webs. *Limnol. Oceanogr*. **61**(4): 1449-1461. doi: 10.1002/lno.10310

-T-

Talling, J. F. 1971. The underwater light climate as a controlling factor in the production ecology of freshwater phytoplankton. *SIL Comm.* **19**: 214–243. doi:10.1080/05384680.1971.11903932

Tans, P. P., I. Y. Fung, and T. Takahashi. 1990. Observational constraints on the global atmospheric CO2 budget. *Science* **247**:1431-1438. doi:10.1126/science.247.4949.1431

Thompson, P. A., P. I. Bonham, and K. M. Swadling. 2008. Phytoplankton blooms in the Huon Estuary, Tasmania: top-down or bottom-up control? *J. Plankt. Res*. **30**: 735–753. doi:10.1093/plankt/fbn044

Tiller, R. G., J. Mork, R. Richards, L. Eisenhauer, Y. Liu, J.-F. Nakken, and A. L. Borgersen. 2014. Something fishy: Assessing stakeholder resilience to increasing jellyfish (*Periphylla periphylla*) in Trondheimsfjord, Norway. *Mar. Pol.* **46**: 72-83. doi: 10.1016/j.marpol.2013.12.006

Tobias, C. R., J. K. Böhlke, and J. W. Harvey. 2007. The oxygen-18 isotope approach for measuring aquatic metabolism in high productivity waters. *Limnol. Oceanogr*. **52**: 1439–1453. doi:10.4319/lo.2007.52.4.1439

Troedsson, C., M.E. Frischer, J.C. Nejstgaard, and E.M. Thompson. 2007. Molecular quantification of differential ingestion and particle trapping rates by the appendicularian *Oikopleura dioica* as a function of prey size and shape. *Limnol. Oceanogr*. **52**(1): 416:427. doi:10.4319/lo.2007.52.1.0416

Trombetta, T., F. Vidussi, S. Mas, D. Parin, M. Simier, and B. Mostajir. 2019. Water temperature drives phytoplankton blooms in coastal waters. *PLOS One* **14**: e0214933. doi:10. 1371/journal.pone.0214933

Trombetta, T., F. Vidussi, C. Roques, M. Scotti, and B. Mostajir. 2020. Marine microbial food web networks during phytoplankton bloom and non-bloom periods: warming favors smaller organism interactions and intensifies trophic cascade. *Front. Microbiol.* **11**. doi:10.3389/fmicb.2020.502336

Trombetta, T., F. Vidussi, C. Roques, S. Mas, M. Scotti, and B. Mostajir. 2021. Co-occurrence networks reveal the central role of temperature in structuring the plankton community of the Thau lagoon. *Sci. Rep*. **11**: 17675. doi: 10.1038/s41598-021-97173-y

-U-

Uitz, J., D. Stramski, B. Gentili, F. D'Ortenzio, and H. Claustre. 2012. Estimates of phytoplankton class-specific and total primary production in the Mediterranean Sea from satellite ocean color observations. *Glob. Biogeochem. Cycles* **26**. doi:10.1029/2011GB004055

Urrutia-Cordero, P., M. K. Ekvall, and L.-A. Hansson. 2016. Local food web management increases resilience and buffers against global change effects on freshwaters. *Sci. Rep*. **6**: 29542. doi:10.1038/srep29542

Urrutia-Cordero, P., M. K. Ekvall, J. Ratcovich, M. Soares, S. Wilken, H. Zhang, and L.-A. Hansson. 2017. Phytoplankton diversity loss along a gradient of future warming and brownification in freshwater mesocosms. *Freshw. Biol*. **62**: 1869–1878. doi:10.1111/fwb.13027

Utermöhl, H. 1958. Zur Verfollkommnung der quantitativen Phytoplankton-Methodik. *Mitt Int Ver Theor Angew Limnol* **9**:1-38

-V-

Van de Bogert, M. C., S. R. Carpenter, J. J. Cole, and M. L. Pace. 2007. Assessing pelagic and benthic metabolism using free water measurements. *Limnol. Oceanogr.: Methods* **5**: 145–155. doi:10.4319/lom.2007.5.145

Vaquer-Sunyer, R., and C. M. Duarte. 2013. Experimental Evaluation of the Response of Coastal Mediterranean Planktonic and Benthic Metabolism to Warming. *Est. Coasts* **36**: 697–707. doi:10.1007/s12237-013-9595-2

Vaquer-Sunyer, R., D. J. Conley, S. Muthusamy, M. Lindh, and E. S. Kritzberg. 2015. Dissolved Organic Nitrogen Inputs from Wastewater Treatment Plant Effluents Increase Responses of Planktonic Metabolic Rates to Warming. *Env. Sci. Tech*. **49**: 11411–11420.

Vázquez-Domínguez, E., D. Vaqué, and J. M. Gasol. 2007. Ocean warming enhances respiration and carbon demand of coastal microbial plankton. *Glob. Change Biol*. **13**: 1327–1334. doi:10.1111/j.1365-2486.2007.01377.x

Vidussi, F., J.-C. Marty, and J. Chiavérini. 2000. Phytoplankton pigment variations during the transition from spring bloom to oligotrophy in the northwestern Mediterranean Sea. *Deep Sea Res. I Oceanogr. Res. Pap*. **47**: 423–445. doi:10.1016/S0967-0637(99)00097-7

Vidussi, F., H. Claustre, B. B. Manca, A. Luchetta, and J.-C. Marty. 2001. Phytoplankton pigment distribution in relation to upper thermocline circulation in the eastern Mediterranean Sea during winter. *J. Geophys. Res.: Oceans* **106**: 19939–19956. doi:10.1029/1999JC000308

Vidussi, F., B. Mostajir, E. Fouilland, and others. 2011. Effects of experimental warming and increased ultraviolet B radiation on the Mediterranean plankton food web. *Limnol. Oceanogr*. **56**: 206–218. doi:10.4319/lo.2011.56.1.0206

-W-

Waite, A., A. Fischer, P. A. Thompson, and P. J. Harrison. 1997. Sinking rate versus cell volume relationships illuminate sinking rate control mechanisms in marine diatoms. *Mar. Ecol. Prog. Ser*. **157**: 97-108. doi:10.3354/meps157097

Wanninkhof, R. 1992. Relationship between wind speed and gas exchange over the ocean. *JGR Oceans* **97**: 7373–7382. doi:10.1029/92JC00188

Ward, B. B. 2011. Nitrification in the Ocean, In Nitrification. B.B. Ward, D.J. Arp and M.G. Klotz

Wartenburger, R. et al., 2017: Changes in regional climate extremes as a function of global mean temperature: an interactive plotting framework. *Geosci. Mod. Dev*. **10**:3609-3634. doi:10.5194/gmd-2017-33

Welschmeyer, N.A., A.E. Copping, M. Vernet, and C.J. Lorenzen. 1984. Diel fluctuation in zooplankton grazing rate as determined from the downward vertical flux of pheopigments. *Mar. Biol*. **83**: 263-270.doi: 10.1007/BF00397458

Welti, N., M. Striebel, A. J. Ulseth, and others. 2017. Bridging Food Webs, Ecosystem Metabolism, and Biogeochemistry Using Ecological Stoichiometry Theory. *Front. Microbiol*. **8**: 1298. doi:10.3389/fmicb.2017.01298

Westra, S., L. V. Alexander, and F. W. Zwiers. 2013. Global Increasing Trends in Annual Maximum Daily Precipitation. *J. Climate* **26**: 3904–3918. doi:10.1175/JCLI-D-12-00502.1

Weydmann, A., W. Walczowski, J. Carstensen, and S. Kwaśniewski. 2017. Warming of Subarctic waters accelerates development of a key marine zooplankton *Calanus finmarchicus*. *Glob. Change Biol* **24**: 172–183. doi:10.1111/gcb.13864

Weyhenmeyer, G. A., Y. T. Prairie, and L. J. Tranvik. 2014. Browning of Boreal Freshwaters Coupled to Carbon-Iron Interactions along the Aquatic Continuum. *PLOS ONE* **9**: e88104. doi:10.1371/journal.pone.0088104

Wikner, J., and A. Andersson. 2012. Increased freshwater discharge shifts the trophic balance in the coastal zone of the northern Baltic Sea. *Glob. Change Biol*. **18**: 2509–2519. doi:10.1111/j.1365-2486.2012.02718.x

Wilken, S., M. Soares, P. Urrutia-Cordero, J. Ratcovich, M. K. Ekvall, E. Van Donk, and L-A. Hansson. 2017. Primary producers or consumers? Increasing phytoplankton bacterivory along a gradient of lake warming and browning. *Limnol*. *Oceanogr*. **63**(S1): S142-S155. doi: 10.1002/lno.10728

Williams, P. J. le B., P. J. Morris, and D. M. Karl. 2004. Net community production and metabolic balance at the oligotrophic ocean site, station ALOHA. *Deep Sea Res. I: Oceanogr. Res. Pap*. **51**: 1563–1578. doi:10.1016/j.dsr.2004.07.001

Williams, P. J. le B., and D. A. Purdie. 1991. *In vitro* and *in situ* derived rates of gross production, net community production and respiration of oxygen in the oligotrophic subtropical gyre of the North Pacific Ocean. *Deep Sea Res. I: Oceanogr. Res. Pap*. **38**: 891–910. doi:10.1016/0198-0149(91)90024-A

Williams, P. J. le B., P. D. Quay, T. K. Westberry, and M. J. Behrenfeld. 2013. The Oligotrophic Ocean Is Autotrophic. *Ann. Rev. Mar. Sci*. **5**: 535–549. doi:10.1146/annurev-marine-121211-172335

Williamson, C. E., E. P. Overholt, R. M. Pilla, T. H. Leach, J. A. Brentrup, L. B. Knoll, E. M. Mette, and R. E. Moeller. 2015. Ecological consequences of long-term browning in lakes. *Sci. Rep*. **5**: 18666. doi:10.1038/srep18666

Winder, M., and U. Sommer. 2012. Phytoplankton response to a changing climate. *Hydrobiologia* **698**: 5–16. doi:10.1007/s10750-012-1149-2

Winslow, L. A., J. A. Zwart, R. D. Batt, H. A. Dugan, R. I. Woolway, J. R. Corman, P. C. Hanson, and J. S. Read. 2016. LakeMetabolizer: an R package for estimating lake metabolism from free-water oxygen using diverse statistical models. *Inland Waters* **6**. doi:10.1080/IW-6.4.883

de Wit, H. A., S. Valinia, G. A. Weyhenmeyer, and others. 2016. Current Browning of Surface Waters Will Be Further Promoted by Wetter Climate. *Env. Sci. Tech. Lett*. **3**: 430–435. doi:10.1021/acs.estlett.6b00396

Whitledge, G. W., and C. F. Rabeni. 2000. Benthic community metabolism in three habitats in an Ozark stream. *Hydrobiologia* **437**: 165–170.

Wikner, J., S. Panigrahi, A. Nydahl, E. Lundberg, U. Båmstedt, and A. Tengberg. 2013. Precise continuous measurements of pelagic respiration in coastal waters with oxygen optodes. *Limnol. Oceanogr.: Methods* **11**: 1–15. doi:10.4319/lom.2013.11.1

Winkler, L. W. 1888. Die Bestimmung des in Wasser gelösten Sauerstoffen. *Berichte der Deutschen Chemischen Gesellschaft* **21**: 2843–2855

Worden, A. Z., and B. J. Binder. 2003. Application of dilution experiments for measuring growth and mortality rates among *Prochlorococcus* and *Synechococcus* populations in oligotrophic environments. *Aq. Microb. Ecol*. **30**: 159–174. doi:10.3354/ame030159

-X-

Xoplaki, E., E. Tragou, A. Gogou, V. Zervakis, D. Koutsoubas, L. Behr, S. Petalas, and M. Sini. 2021. EM-MHeatwaves: Eastern Mediterranean marine heatwaves - Ocean responses to atmospheric forcing and impacts on marine ecosystems. *EGU General Assemby 2021*. doi:10.5194/egusphere-egu21-9907

Xue, X., D. A. Gauthier, D. H. Turpin, and H. G. Weger. 1996. Interactions between photosynthesis and respiration in the green alga *Chlamydomonas reinhardtii* (characterization of light-enhanced dark respiration). *Plant Physiol*. **112**: 1005– 1014. doi:10.1104/pp.112.3.1005

-Y-

Yvon-Durocher, G., J. I. Jones, M. Trimmer, G. Woodward, and J. M. Montoya. 2010. Warming alters the metabolic balance of ecosystems. *Philosoph. Trans. Royal Society B: Biol. Sci*. **365**: 2117–2126. doi:10.1098/rstb.2010.0038

-Z-

Zapata, M., F. Rodríguez, and J. L. Garrido. 2000. Separation of chlorophylls and carotenoids from marine phytoplankton: a new HPLC method using a reversed phase C8 column and pyridine-containing mobile phases. *Mar. Ecol. Prog. Ser*. **195**: 29–45. doi:10.3354/meps195029

Zhu, Z., P. Qu, N. Tennenbaum, A. O. Tatters, and D. A. Hutchins. 2017. Understanding the blob bloom: Warming increases toxicity and abundance of the harmful bloom diatom *Pseudo-nitzschia* in California coastal waters. *Harmful Algae* **67**: 36–43. doi:10.1016/j.hal.2017.06.004

Zlotnik, I., and Z. Dubinsky. 1989. The effect of light and temperature on DOC excretion by phytoplankton. *Limnol. Oceanogr*. **34**(5): 831-839. doi:10.4319/lo.1989.34.5.0831

Annexe I

Évaluation de l'estimation du quenching non-photochimique de la fluorescence de la chlorophylle-*a* par interpolation linéaire lors des expériences réalisées au printemps et en automne dans la lagune de Thau

Le quenching non-photochimique (NPQ) de la fluorescence de la chlorophylle-*a* est un phénomène qui permet au phytoplancton de se protéger d'une intensité lumineuse trop importante en dissipant l'excès d'énergie lié à cet excès de lumière sans utiliser le mécanisme principal de la fluorescence. Ainsi, ce phénomène entraîne un biais dans l'estimation de la concentration en chlorophylle-*a* via la mesure de sa fluorescence, puisque une partie de la chlorophylle ne fluoresce pas. Pour prendre en compte ce biais dans les travaux de cette thèse, la fluorescence de la chl-a a été interpolée linéairement entre le lever et le coucher du soleil, d'après Li et al. (2008) et comme expliqué dans le présent chapitre. Cependant, cette correction étant appliquée pour la première fois dans le cadre de données issues de mésocosmes *in situ*, nous avons quantifié la différence entre données corrigées et non-corrigées et de comparer les estimations de croissance phytoplanctonique dérivées de ces données (Fig. A1 et Tableau A1). Ces comparaisons ne font pas l'objet du Chapitre 3 mais sont discutées dans la Discussion générale de la thèse (p 176).

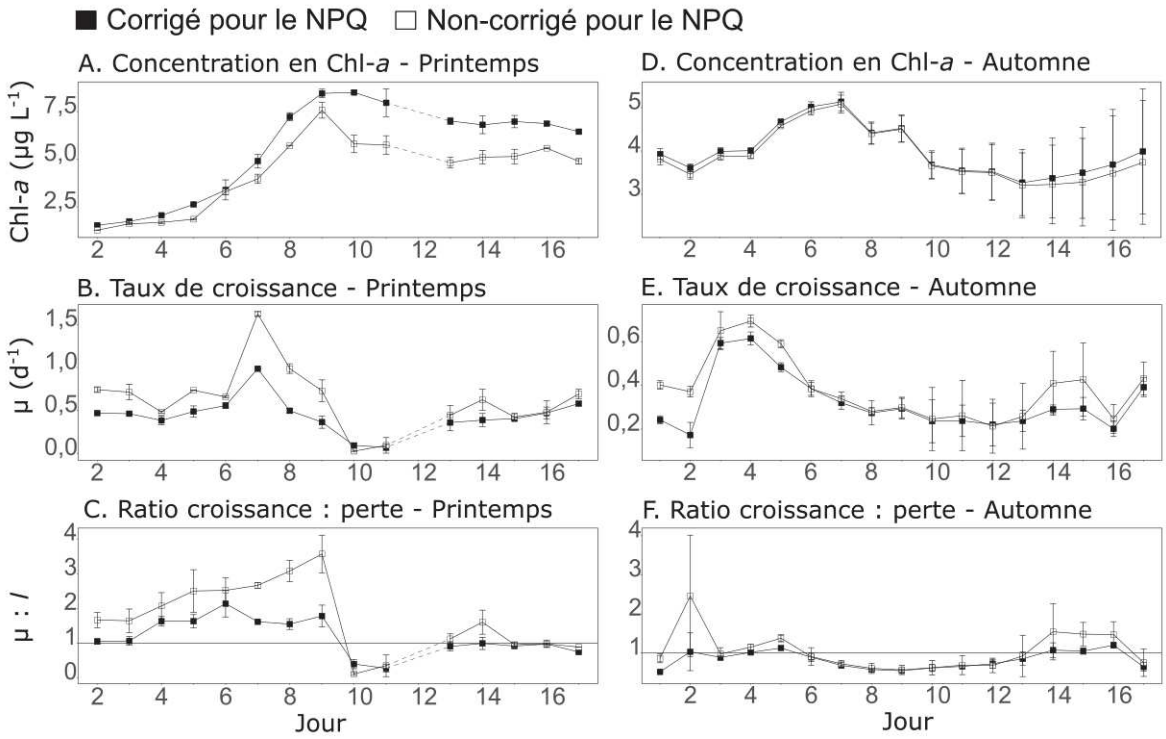

Figure A1. Fluorescence de la chlorophylle-*a* (Chl-*a*, A, D), taux de croissance (µ, B, E) et ratio entre croissance et perte (µ : *l*, C, F) pour l'expérience de Printemps (A, B, C) et d'Automne (D, E, F) obtenus avec les données de fluorescence corrigées pour le NPQ (noir) et non-corrigées pour le NPQ (blanc). Pour l'expérience de Printemps, les données sont la moyenne journalière ± l'étendue d'un duplicat de mésocosmes contrôles, pour l'expérience d'Automne, les données sont la moyenne journalière ± l'écart-type d'un triplicat de mésocosmes contrôles.

Tableau A1. Résultats de la comparaison statistique entre les paramètres obtenus à partir de données corrigées pour le NPQ et ceux à partir de données non-corrigées. Lorsque les hypothèses de la RM-ANOVA n'étaient pas réunies, même après transformation des données, un test non-paramétrique de Kruskal-Wallis (KW) a été utilisé à la place. Les valeurs *P* inférieures ou égales à 0,05 sont considérées significatives et représentées en gras.

Paramètre	Printemps	Automne
Fluorescence de la chl-*a*	**$<1{,}0 \times 10^{-4}$** ($F_{1,14}$=33,7)	0,38 (KW)
µ	**0,03** (KW)	**$3{,}4 \times 10^{-3}$** ($F_{1,16}$=11,8)
µ : *l*	**$2{,}8 \times 10^{-3}$** ($F_{1,14}$=13,1)	0,22 (KW)

Lors de l'expérience de Printemps, la fluorescence de la chl-*a* corrigée pour le NPQ était significativement plus élevée que celle non-corrigée d'en moyenne 30,2%. En revanche, les fluorescences corrigée et non-corrigée n'étaient pas significativement différentes lors de l'expérience d'Automne. Lors des deux expériences, µ obtenu avec la fluorescence corrigée était significativement plus faible que lorsqu'obtenu avec la fluorescence non-corrigée, d'en moyenne 24,3% et 8,2% pour les expériences de Printemps et d'Automne, respectivement. En conséquence, le ratio µ : *l* était significativement plus faible avec µ obtenu avec la fluorescence corrigée lors de l'expérience de

Printemps, d'en moyenne 25,9%, tandis qu'il n'était pas significativement différent pour l'expérience d'Automne. L'amplitude du quenching non-photochimique (NPQ) était significativement et linéairement reliée à l'amplitude de la quantité de lumière intégrée (DLI) pour les deux expériences (Fig. E3.3).

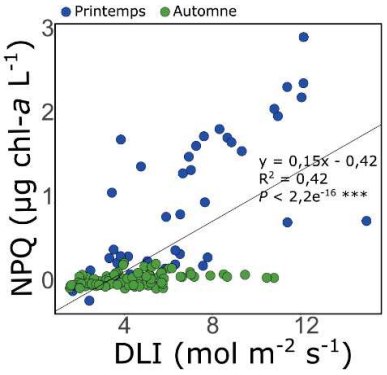

Figure E3.3. Amplitude du NPQ en fonction de la DLI. Les données de l'expérience de Printemps et d'Automne sont représentées en bleu et en vert, respectivement. La droite en noir représente la régression linéaire de type II.

Annexe II

Formations réalisées, enseignement et congrès scientifiques internationaux

----- Formations réalisées -----

Ethique de la recherche – Université de Montpellier - 15h

Environnement R, traitement de données et analyses statistiques – Université de Montpellier - 14h

R Markdown & fonction ggplot – Université de Montpellier - 6h

Bio-informatique : algorithmes et génomes – Inria, Paris - 10h

Writing your first paper step by step – Université de Montpellier - 20h

Dealing with scientific literature – Université de Montpellier - 21h

----- Enseignement -----

Introduction à l'écologie aquatique - Travaux Pratiques – Licence 3 Biologie des Organismes HLBE 609 – Station Méditerranéenne de l'Environnement Littoral, Université de Montpellier – 15h

----- Congrès scientifiques internationaux -----

2nd International Aquatic Mesocosm Research Symposium – From local processes to cross-domain interactions – AQUACOSM – 12 avril 2021 – 16 avril 2021 – En ligne

ePoster : « Brownification effects on the plankton community of a North Atlantic Bay during an *in situ* mesocosm experiment combined with high-frequency sensor measurements of oxygen metabolism », Soulié T., Stibor H., Mas S., Sommer U., Braun B., Knechtel J., Vidussi F. et Mostajir B.

ASLO 2021 Aquatic Sciences Meeting – ASLO – 22 juin 2021- 27 juin 2021 – En ligne

Présentation orale : « Effects of brownification on the plankton oxygen metabolism and community of a North Atlantic Bay : an *in situ* mesocosm experiment combined with high-frequency measurements », Soulié T., Stibor H., Mas S., Braun B., Knechtel J., Nejstgaard J.C., Sommer U., Vidussi F. et Mostajir B.

----- Publications scientifiques -----

Soulié, T., S. Mas., D. Parin, F. Vidussi and B. Mostajir. 2021. A new method to estimate planktonic oxygen metabolism using high-frequency sensor measurements in mesocosm experiments and considering daytime and nighttime respirations. *Limnology and Oceanography: Methods* **19**(5): 303-316. doi: 10.1002/lom3.10424

Courboulès, J., F. Vidussi, **T. Soulié**, S. Mas, D. Pecqueur, and B. Mostajir. 2021. Effects of experimental warming on small phytoplankton, bacteria and viruses in autumn in the Mediterranean coastal Thau Lagoon. *Aquatic Ecology* **55**: 647–666. doi:10.1007/s10452-021-09852-7

Soulié, T., H. Stibor, S. Mas., B. Braun, J. Knetchel, J. C. Nejstgaard, U. Sommer, F. Vidussi and B. Mostajir. In revision in Limnology and Oceanography 2021. Brownification reduces oxygen gross primary production and community respiration and changes the phytoplankton community: an *in situ* mesocosm experiment with high-frequency sensor measurements in a North Atlantic bay. *Limnology and Oceanography*.

Soulié, T., F. Vidussi, J. Courboulès, S. Mas and B. Mostajir. 2021. Warming enhanced phytoplankton growth and loss rates during two contrasted productive seasons in Mediterranean coastal waters: evidences from *in situ* mesocosm experiments and high-frequency sensor measurements. *En préparation*.

Soulié, T., F. Vidussi, S. Mas and B. Mostajir. 2021. Low functional stability of a coastal Mediterranean plankton community to an experimental marine heatwave unraveled by high-frequency measurements. *En préparation*.

Annexe III

Version publiée du Chapitre 1

Cette annexe contient la version publiée de l'article qui fait l'objet du Chapitre 1, ainsi que les données supplémentaires attachées à l'article.

Soulié, T., Mas, S., Parin, D., Vidussi, F. and Mostajir, B. (2021), A new method to estimate planktonic oxygen metabolism using high-frequency sensor measurements in mesocosm experiments and considering daytime and nighttime respirations. *Limnol Oceanogr Methods*, **19**: 303-316. https://doi.org/10.1002/lom3.10424

Check for updates

LIMNOLOGY
and
OCEANOGRAPHY: METHODS

ASLO

Limnol. Oceanogr.: Methods 2021
© 2021 The Authors. *Limnology and Oceanography: Methods* published by Wiley Periodicals LLC on behalf of Association for the Sciences of Limnology and Oceanography.
doi: 10.1002/lom3.10424

A new method to estimate planktonic oxygen metabolism using high-frequency sensor measurements in mesocosm experiments and considering daytime and nighttime respirations

Tanguy Soulié,[1]* **Sébastien Mas**,[2] **David Parin**,[2] **Francesca Vidussi**,[1] **Behzad Mostajir**[1]

[1]MARBEC (MARine Biodiversity, Exploitation and Conservation), Univ Montpellier, CNRS, Ifremer, IRD, Montpellier, France
[2]MEDIMEER (Mediterranean Platform for Marine Ecosystems Experimental Research), OSU OREME, CNRS, Univ Montpellier, IRD, IRSTEA, Sète, France

Abstract

Understanding how aquatic ecosystems respond to perturbations has emerged as a crucial way to predict the future of these ecosystems and to assess their capacity to produce oxygen and store atmospheric carbon. In this context, in situ mesocosm experiments are a useful approach for simulating disturbances and observing changes in planktonic communities over time and under controlled conditions. Within mesocosm experiments, the estimation of fundamental parameters such as gross primary production (GPP), net community production (NCP), and respiration (*R*) allows the evaluation of planktonic metabolic responses to a perturbation. The continuous estimation of these metabolic parameters in real time and at high frequency is made possible by employing noninvasive automated sensors in the water column. However, some uncertainties and methodological questions about the estimation of daytime respiration remain to be addressed for this method, and notably to address the fact that respiration could be significantly higher during the day than during the night. In this study, data from two in situ mesocosm experiments performed in fall and spring in a coastal Mediterranean area were used to develop a new method of estimating daytime respiration, and in turn daily GPP, *R*, and NCP, by considering the maximum instantaneous *R*, and that takes into account the variability of the coupling between day–night and dissolved oxygen cycles. This new method was compared with the Winkler incubation technique and with another existing method. Results showed that using this existing method, daytime *R* was significantly underestimated relative to estimates obtained with the newly proposed method.

Aquatic ecosystems undergo many perturbations at different temporal and spatial scales due to natural and anthropogenic factors. Understanding how these perturbations affect these ecosystems is crucial for predicting their future status. Due to their importance in global biogeochemical cycles and in aquatic ecosystem functioning, assessing the response of planktonic communities to various environmental disturbances is therefore of great importance and interest. To do so, mesocosm experiments are experimental units that can be used to simulate disturbances and observe changes in the studied community over time and under controlled conditions while ensuring the reproducibility of the tested perturbations (Stewart et al. 2013; Dzialowski et al. 2014). They closely simulate the natural environment and therefore constitute a link between laboratory and field observations (Odum 1984; Crossland and Point 1992).

Changes in the metabolic processes associated with planktonic communities indicate the response of these communities to disturbances; therefore, measuring metabolic parameters during mesocosm experiments is essential, and there is a need to obtain reliable estimates of these parameters. Some of these metabolic parameters that are related to oxygen, such as gross primary production (GPP), which is the autotrophic production of oxygen through the conversion of inorganic carbon to organic carbon, and aerobic respiration (R), which is the consumption of oxygen through the oxidation of organic carbon to inorganic carbon by both autotrophic and

*Correspondence: tanguy.soulie@gmail.com

Author Contribution Statement: B.M. and F.V. conceived the study. B.M., F.V., and S.M. designed and managed the mesocosm experiments. D.P. set up the sensor system and retrieved the sensor data. T.S. and S.M. calibrated the sensors. T.S. processed the sensor data, performed all the analyses, and wrote the original draft of the article, with the input of B.M., F.V., and S.M.

Additional Supporting Information may be found in the online version of this article.

This is an open access article under the terms of the Creative Commons Attribution-NonCommercial-NoDerivs License, which permits use and distribution in any medium, provided the original work is properly cited, the use is non-commercial and no modifications or adaptations are made.

heterotrophic organisms, are of great importance in understanding and managing aquatic ecosystems (Hanson et al. 2008). Indeed, the net community production (NCP), which is the difference between GPP and *R*, represents the balance between anabolic and catabolic processes and thus between autotrophy and heterotrophy (Staehr et al. 2012).

Due to their importance in understanding the functioning of aquatic ecosystems, these metabolic parameters have been estimated for more than half a century using various methods. The Winkler incubation method, which is the reference method, consists of light and dark incubations of natural samples in small glass bottles for a certain interval of time. The production of dissolved oxygen (DO) in the light bottles and its consumption in the dark bottles is determined by titration with the Winkler technique (Winkler 1888). Another technique used to estimate metabolic parameters is measuring the diel free-water changes in the DO concentration over a certain period of time (Odum 1956). Oviatt et al. (1986) proposed estimating the net production from dawn to dusk and the respiration from dusk to the following dawn. More recently, Kritzberg et al. (2014) obtained GPP, R, and NCP with four DO measurements over a 24 h period.

Additionally, submersible automated DO sensors, that provide high-frequency DO measurement data allowing for real-time observations at intervals of every minute to every hour, can be used to assess metabolic parameters. These sensors can be deployed for a long period and in remote locations and are traditionally used on buoys and gliders to monitor key environmental parameters, at various time scales and for different aquatic systems. They have enabled a better understanding of the trends in the physical and biological variables in these systems and have even provided new insights into ecosystem functioning (de Eyto et al. 2019; Trombetta et al. 2019). Within the framework of mesocosm experiment, using sensor data to estimate metabolic parameters has several advantages compared to the traditional incubation technique, as the sensors are noninvasive and their use does not introduce bottle or container effects into the measurement, thus avoiding the error propagation associated with incubations (Staehr et al. 2010*a*). Moreover, ecologically important short-timescale temporal changes in the DO can easily be monitored with sensors but are not detected by the Winkler incubation method.

Despite its advantages, only a few studies have used the free-water method of estimating metabolic parameters in mesocosm experiments, and even fewer studies have used high-frequency sensors to assess metabolic parameters in mesocosm experiments (Oviatt et al. 1984, 1986; Brinkman et al. 1995; Leclercq et al. 1999; Whitledge and Rabeni 2000; Mostajir et al. 2013; Reijo et al. 2018; Hensley and Cohen 2020). Because of the substantial technical constraints, estimating oxygen-related metabolic parameters using high-frequency sensors in mesocosm experiments is still not widespread in the scientific community. However, high-frequency sensors have been commonly used to estimate oxygen metabolic parameters in the field, especially in lake studies (Van de Bogert et al. 2007; Hanson et al. 2008; Staehr et al. 2010*b*; Alkire et al. 2012; Wikner et al. 2013; Briggs et al. 2018; Demars et al. 2018).

Due to the limited number of studies that have used high-frequency DO data to estimate metabolic parameters in mesocosm experiments, there are still some methodological questions regarding the use of this technique and the reliability of the metabolic estimates derived from it. The main uncertainty is related to the estimation of respiration occurring during the day (Rdaytime). For simplicity, Rdaytime has been assumed to be equal to the R that occurs at night (Rnight) in most field studies using sensor data to derive planktonic respiration rate (Hanson et al. 2003; Lauster et al. 2006; Staehr et al. 2010*a*), despite increasing evidence that Rdaytime is significantly greater than Rnight, for example, up to 640% higher at the beginning of the night than that at the end of it (Markager et al. 1992; Xue et al. 1996; Pringault et al. 2007; Carvalho and Eyre 2012). Indeed, previous studies have reported that respiration is enhanced by photosynthesis and the resultant photosynthetic products (Markager and Sand-Jensen 1989; Markager et al. 1992; Mantikci et al. 2017), with postillumination rates 50–340% higher than dark respiration levels (Beardall et al. 1994; Hotchkiss and Hall 2014). The calculation of Rdaytime has been proposed to be done just after sunset, when autotrophic respiration still relies on the photosynthetic products accumulated during the daylight period (Mostajir et al. 2013). Nevertheless, the method of Mostajir et al. (2013) does not consider the fact that the DO cycle does not strictly follow the day–night cycle. Indeed, this method assumes that the DO concentration starts to decrease at sunset; however, this decrease can start earlier if respiration is stronger than production even when there is still daylight. This mismatch can be caused by various environmental factors, including the amount of light available for photosynthesis and the water temperature, which affects metabolic processes. Hence, it seems clear that considering a period starting at sunset for the calculation of Rdaytime may yield very different estimates for days when the cycle of oxygen matches the light cycle and days when the cycles do not match. Therefore, there is a need to establish a method that considers this variability in the calculation of Rdaytime.

Accordingly, a new method to estimate Rdaytime using high-frequency DO data from enclosed mesocosm experiments that takes into account the potential variability between DO and day–night cycles is provided in this investigation. In addition, the metabolic estimates obtained with this new method were compared with those obtained with the method of Mostajir et al. (2013) and with the Winkler incubation technique. Moreover, a comparison was performed between two time periods used for the daily integration of daytime and night respiration estimates. Overall, this new method is based on data obtained during two in situ enclosed

mesocosm experiments conducted in a Mediterranean coastal shallow lagoon in fall 2018 and spring 2019.

Materials and procedures

Experimental setup

Mesocosm experiments

Two mesocosm experiments were carried out in Thau Lagoon, which is a productive shallow (4 m mean depth) coastal lagoon located in the western Mediterranean in southern France. The experiments lasted 15 d in October 2018 (Exp. 1) and 17 d in May and June 2019 (Exp. 2). In this article, data from three mesocosms in Exp. 1 (Oct 01, Oct 02, and Oct 03) and three mesocosms in Exp. 2 (Jun 01, Jun 02, and Jun 03) were used. As an example, Oct 01 refers to the data set obtained for one of the three replicates mesocosms of the Exp. 1 which took place in October 2018.

The mesocosms were established at the Mediterranean platform for Marine Ecosystem Experimental Research (MEDIMEER) pontoon (43°24′53″N, 3°41′16″E) located on the east side of the lagoon. The mesocosm bags were 280 cm high, with a diameter of 120 cm and an additional 50 cm long sediment trap located at the bottom of the bag. They were made of a transparent nylon-reinforced 200 µm thick vinyl acetate polyethylene film (Insinööritoimisto Haikonen Ky). The emerged part of each mesocosm was covered with a transparent plastic dome to avoid contamination by rain and waves (Fig. 1), making the total structure 300 cm high. The main use of the dome is to prevent precipitations and other external inputs into the mesocosm; however, it allows gas exchange with the atmosphere. The mesocosms were filled with 2200 L of lagoon water.

The water column was gently mixed with a pump (Rule, Model 360), leading to a turnover rate of approximately 3.5 d^{-1}. Each mesocosm unit was equipped with a set of high-frequency automated sensors positioned 1 m deep to measure the DO concentration with an oxygen optode (Oxygen optode 3835, Aanderaa), the conductivity with an electromagnetic induction conductivity sensor (Conductivity sensor 4319, Aanderaa), and the incident photosynthetically active radiation (PAR) with a spherical underwater quantum sensor (LI-193, Li-Cor). Additionally, the water temperature was measured by three temperature sensors (Campbell Scientific Thermistor probe 107) placed at three different depths (0.5, 1, and 1.5 m). For the present study, only the data measured by the oxygen optode and the conductivity, temperature, and incident PAR sensors were used.

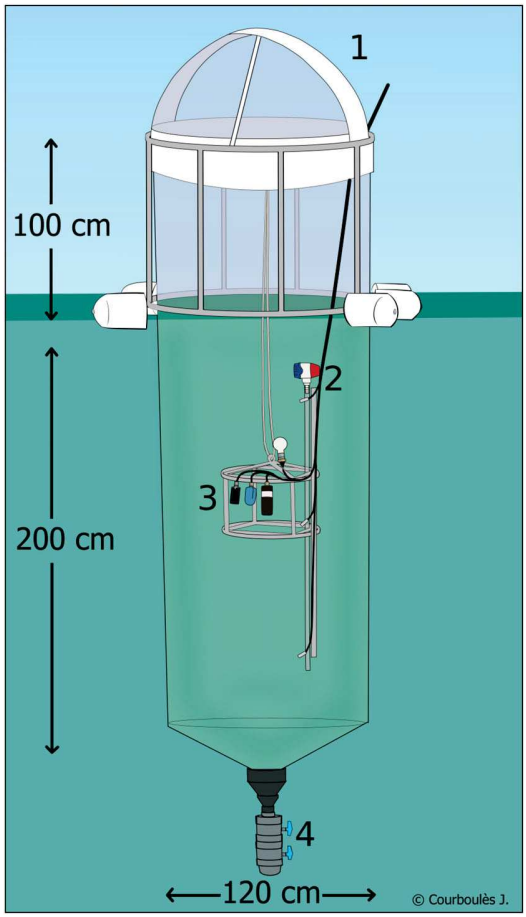

Fig 1. A single mesocosm unit equipped with a dome to cover the structure (1), a pump (2), a sensor system (3), and a sediment trap at the bottom (4) (illustration courtesy of Justine Courboulès).

Estimating metabolic parameters with light and dark incubations using the Winkler method

To compare the metabolic sensor data with data obtained with a classical reference method, Winkler incubations were performed every 2 d. To do so, mesocosm water was sampled using a 5-liter Niskin water sampler. Nine borosilicate bottles of 120 mL were directly filled with water from the Niskin bottle for each mesocosm. The DO contained in three bottles (the t0 bottles) was immediately fixed by adding Winkler reagents as described by Carrit (1966). Three other bottles were carefully wrapped in aluminum foil (the dark bottles) to prevent photosynthesis. These bottles were then incubated in incubation mesocosms along with the three remaining bottles (the light bottles) from 10:00 h to 18:00 h. The two incubation mesocosms were established to incubate light and dark incubation bottles following the Winkler technique as described above. Incubation mesocosms were used to avoid potential contamination and changes in the light environment of the main mesocosms. For the October and June experiments, the incubation mesocosms were located directly adjacent to the other mesocosms and were therefore subject to the same environmental conditions as the control mesocosms. After incubation, the DO in the incubated bottles was fixed as described above. The oxygen concentration in the bottles was measured by using an automated Winkler titrator with a potentiometric

titration method (Crisson titrator and Methrom 916-Ti-touch titrator in the October and June experiments, respectively) (Carpenter 1965).

NCP (in $gO_2\ m^{-3}\ d^{-1}$) was then calculated as in Eq. 1:

$$NCP = \left(\frac{\text{mean}\left(O_{2_{Light}}\right) - \text{mean}(O_{2_{t0}})}{\text{Incubation time}}\right) * \text{dayfraction} * 24 \quad (1)$$

where the mean (O_{2Light}) is the mean value from the triplicate bottles incubated in the light (in $gO_2\ m^{-3}$), the mean (O_{2t0}) is the mean value from the triplicate bottles directly fixed after sampling (in $gO_2\ m^{-3}$), and the day fraction is $\text{dayfraction} = {}^{\text{lightperiod}}/_{24}$, where the light period refers to the duration from sunrise to sunset in hours.

Respiration (R) (in $gO_2\ m^{-3}\ d^{-1}$) was then calculated as in Eq. 2:

$$R = \left(\frac{\text{mean}(O_{2_{t0}}) - \text{mean}\left(O_{2_{Dark}}\right)}{\text{Incubation time}}\right) * 24 \quad (2)$$

where the mean (O_{2Dark}) is the mean value from the triplicate dark bottles (in $gO_2\ m^{-3}$).

Then, GPP (in $gO_2\ m^{-3}\ d^{-1}$) was obtained as:

$$GPP = NCP + R. \quad (3)$$

Free-water diel oxygen method for metabolic parameter measurements using sensors

Sensor data acquisition and correction

Sensor data were acquired every 1 min in all the mesocosms. The choice of the sampling frequency is very important as useful information to get reliable metabolic estimates could be missed with a slow frequency while a rapid frequency could lead to high amount of data not necessarily needed. This question was addressed and a power analysis assessing the required duration of sensor deployment with sampling frequencies ranging from 1 to 60 min was performed, suggesting that sampling frequencies up to 10 min were sufficient for the 15 d lasting October experiment. This analysis is presented in Appendix 1 in Supporting Information).

Oxygen sensors were calibrated before and after each deployment using three saturation points (0%, 50%, and 100%) and at three different temperatures (17°C, 20°C, and 22°C), according to a calibration procedure described in Bittig et al. (2018). The 100% saturation point was reached by bubbling air into the water, and the 0% and 50% saturation points were reached by adding potassium metabisulfite. The raw DO data measured during the mesocosm experiments were then corrected with the obtained calibration coefficient. Then, the DO data were corrected with the salinity and water temperature data obtained from the conductivity sensors and the temperature probe positioned at 1 m deep, respectively; salinity and temperature correction is required for oxygen optodes in order to take into account variations in O_2 solubility (Bittig et al. 2018). The DO-corrected data were then smoothed using a 9-point moving average. To estimate planktonic metabolism, the smoothed data were then separated into different periods according to the minima and the maxima of the DO curve. Periods between a minimum and the following maximum, indicating that DO was increasing and thus the instantaneous NCP of O_2 was positive, were considered Positive NCP periods. Periods between a maximum and the following minimum, when DO was decreasing and thus the instantaneous NCP was negative, were considered Negative NCP periods. An example of the separation of the data into periods is given for the Oct 01 DO data set in Fig. 2A.

A five-parameter sigmoidal model was built to fit the DO data for each Positive NCP period and each Negative NCP period to reduce short-timescale noise (Mostajir et al. 2013) (SigmaPlot software version 12.3). The initial raw data calibrated and corrected for salinity and temperature, the data smoothed by a 9-point moving average followed by a locally estimated scatterplot smoothing (LOESS) regression, and the data modeled with the five-parameter sigmoidal model are presented in Fig. 2b–d. Outliers in the raw sensor data set were defined as values 20% higher or lower than their direct neighbors and were removed. Consequently, between 0% (Oct 01) and 1.49% (Oct 02) of the initial DO data was removed. Missing values were extrapolated using a linear regression in the local neighborhood of the missing value.

Metabolic parameter calculation

Instantaneous NCP

The governing equation comes from (Odum and Odum 1955), the first application of the method:

$$\frac{\Delta O_2}{\Delta t} = GPP - R - F - A \quad (4)$$

where $\frac{\Delta O_2}{\Delta t}$ is the change in DO concentration during a time interval Δt, GPP is the gross primary production, R is the respiration, F is the exchange of O_2 between the water and the atmosphere, and A is a combined parameter that includes all other phenomena responsible for changes in the DO concentration in the considered system. In this article, A was considered to be negligible.

The exchange between the water surface and the atmosphere, F, was calculated as:

$$F = (k * (O_2 - O_{2_{Sat}}))/Z_{mix} \quad (5)$$

where O_2 is the concentration in DO, O_{2sat} is the oxygen saturation, k is the piston velocity coefficient, and Z_{mix} is the mixing depth of the water column, that is, in the present study, the depth of the mesocosms. In this study, k was set to

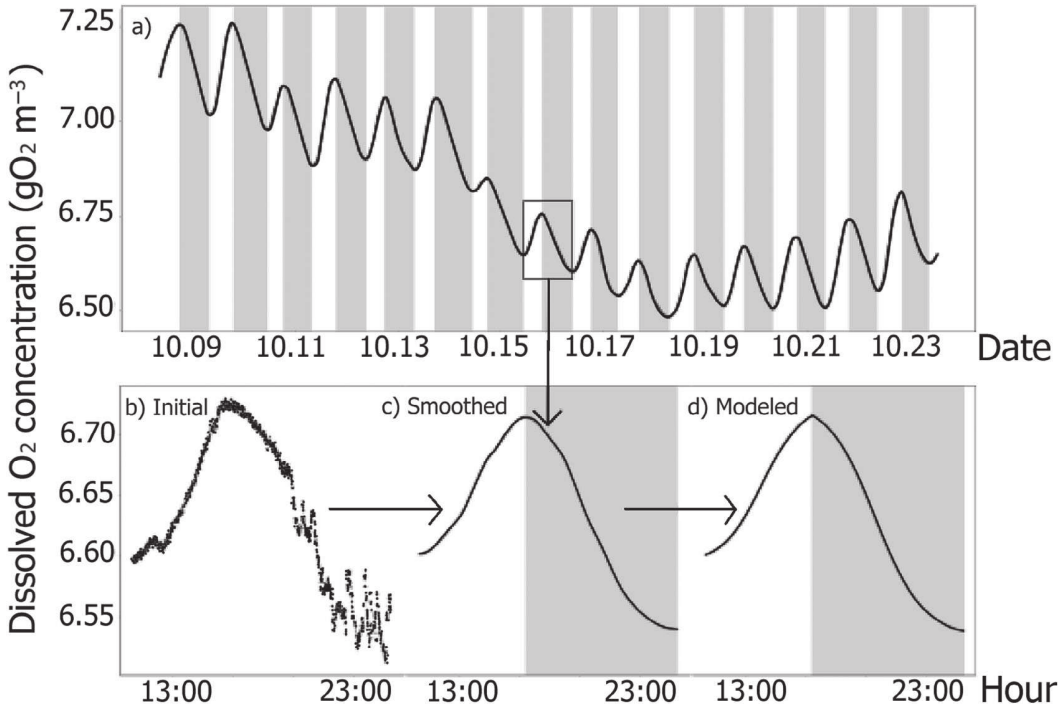

Fig 2. (**a**) Oct 01 smoothed DO data. Shading separates Positive NCP periods (white background) and Negative NCP periods (gray background). The parts in which DO is increasing are considered Positive NCP periods, and the parts in which DO is decreasing are considered Negative NCP periods. The same separation was applied to the data from all the mesocosms. The black rectangle shown in (**a**) is shown in the bottom figure as (**b**), (**c**), and (**d**), corresponding to the initial data (raw data calibrated and corrected for salinity and temperature) (**b**), the smoothed data with a 9-point moving average followed by a LOESS regression (**c**), and the data modeled using a five-parameter sigmoidal model (**d**).

0.000156 m min^{-1}. This value was chosen as it was experimentally measured in open-top laboratory microcosm (Alcaraz et al. 2001) in salinity and temperature conditions close to the conditions of both of the mesocosm experiments used in the present investigation. Moreover, this k value was chosen because it was the lowest value obtained with non-null conditions as our in situ mesocosms naturally experience turbulence due to marine waves. To test eventual differences on metabolic estimates induced by the choice of the k value, a sensitivity analysis using the lowest and the highest value of k measured in similar experimental conditions as in our in situ mesocosms (Alcaraz et al. 2001) was performed and is presented in Appendix 2 in Supporting Information. It appeared that GPP estimates were not significantly sensitive to the choice of the k value. In contrast, significantly higher estimates of R were obtained with the lower k, pointing out that the choice of the k value is more critical for the estimation of R.

For each time step of 1 min, the instantaneous NCP was calculated as:

$$\mathrm{NCP} = \Delta O_2 - F \quad (6)$$

where NCP is the instantaneous net community production of O_2 per minute, ΔO_2 is the difference between two successive DO concentration values, and F is the exchange between the water surface and the atmosphere as previously described.

Instantaneous metabolism values can be integrated over certain periods of the day and the night to obtain daily estimates of GPP, NCP, and R. However, it is still unclear how daily metabolic parameters, notably Rdaytime, should be calculated. Various methods are selected, compared, and presented in the following sections.

Statistical analyses

ANOVAs were used to assess the differences between sensor-based metabolic estimates such as Rdaytime, Rnight, and R24h and to test the effects of the sampling period and the piston velocity coefficient variations on these sensor-based metabolic estimates. A p value less than or equal to 0.05 was considered statistically significant. These analyses were also used to compare the sensor-based metabolic estimates with the estimates obtained with the Winkler method. When the assumptions of ANOVA could not be met even through data transformation (logarithmic, exponential or square-root transformation), a nonparametric Kruskal–Wallis test was used instead. Following the ANOVAs, Tukey honest significant difference (Tukey HSD) tests were used to perform multiple comparisons of means and to test the differences among estimates. Following the Kruskal–Wallis tests, a post hoc nonparametric

Table 1. Presentation of the two methods for estimating Rdaytime and Rnight compared in the present work using certain periods of the instantaneous NCP data.

Data and methods	Rdaytime calculation	Rnight calculation
Sensor data and "max" method (present study)	Mean of instantaneous NCP during a 1-h period centered on the maximum instantaneous negative NCP	Mean of instantaneous NCP for the entire negative NCP period
Sensor data and "Most" method (Mostajir et al. 2013)	Mean of instantaneous NCP during a 1-h period following sunset	Mean of instantaneous NCP for the entire negative NCP period, apart from the period considered in the Rdaytime calculation

Dunn test was performed. All statistical analyses were performed using the *R* software (version 3.4.2).

Estimation of *R* during the day (Rdaytime), at night (Rnight), and daily *R* (R24h), using sensor data

In the present study, as shown in Table 1, Rdaytime, Rnight, and R24h were estimated using sensor data and certain periods of the instantaneous NCP data and were integrated either from sunrise to sunset or only over the production period (e.g., only when the instantaneous NCP was positive). Means of instantaneous NCP over certain time periods were used as in previous studies, including Staehr et al. (2010*a*,*b*), Laas et al. (2012), Idrizag et al. (2016), Richardson et al. (2017), and Chiu et al. (2020). More precisely, Rdaytime was estimated either with the mean of the instantaneous NCP during a 1-h period centered on the maximum of the instantaneous Negative NCP (hereafter referred to as the "Max" method) or with the mean of the instantaneous NCP during a 1-h period following sunset, as in Mostajir et al. (2013) (hereafter referred to as the "Most" method). As the Winkler method is still considered the reference method for estimating planktonic metabolism, the R obtained from sensor data by applying the Max and Most methods were then compared with the R obtained using the Winkler method.

Once the instantaneous Rdaytime and Rnight were calculated as described in Table 1, they were integrated to provide daily values. Two methods of integration were compared. Rdaytime was integrated either over the whole day (e.g., from sunrise to sunset, hereafter referred to as SS) or over the production period (e.g., when instantaneous NCP was positive, hereafter referred to as PP).

When Rdaytime was integrated from sunrise to sunset, Rnight was integrated over the whole night (e.g., from sunset to the following sunrise). When Rdaytime was integrated over the production period, Rnight was integrated over the Negative NCP period.

Therefore, Rdaytime and Rnight were calculated with the following equation:

$$R = (\text{Mean of instantaneous NCP during the considered period}) * 60 * \text{integration period} \quad (7)$$

where R corresponds to either Rdaytime or Rnight ($gO_2\ m^{-3}\ d^{-1}$), the mean of instantaneous NCP is measured in $gO_2\ m^{-3}\ min^{-1}$, and the integration period either to the period from sunrise to sunset (hours) or to the production period (the Positive NCP period, in hours) for Rdaytime calculation, or to the period from sunset to the following sunrise (hours) or to the Negative NCP period (hours) for Rnight calculation. It should be noted that the units of Rdaytime (or Rnight) are indifferently $gO_2\ m^{-3}$ integration $period^{-1}$ or $gO_2\ m^{-3}\ d^{-1}$ because during a given 24 h period, Rdaytime (or Rnight) only occurs during the period in which it is integrated, so its value per 24 h is equal to its value per integration period.

Then, the daily R (R24h) was calculated as the sum of Rdaytime and Rnight. A summary of all the parameters compared in the present work and their designations is presented in Table 2. For the Winkler estimates, the instantaneous Winkler-R was integrated over the Positive NCP period (Rdaytime-Winkler-PP) or from sunrise to sunset (Rdaytime-Winkler-SS) to obtain the daytime R, and it was integrated over the Negative NCP period (Rnight-Winkler-PP) or from sunset to sunrise (Rnight-Winkler-SS) to obtain the night R.

Assessment

Comparison of Rdaytime, Rnight, and R24h estimations from the three different methods and two integration periods

For all mesocosms, the Rdaytime, Rnight, and R24h estimates integrated from sunrise to sunset (SS) and over the PP are presented in Fig. 3. Regardless of their integration period, the Rdaytime estimates were significantly different depending on the method used for their estimation (ANOVA, $p < 10^{-4}$ for all mesocosms and for the two integration periods, Supporting Information Table S1). Rnight estimates were significantly different for three mesocosms out of six (Oct 02, Jun 01, and Jun 03) (ANOVA or Kruskal–Wallis test, $p < 0.05$, Supporting Information Table S1). Consequently, R24h estimates were significantly different for all mesocosms when they were integrated from sunrise to sunset and over the production period. The only exception was in the Oct 01 mesocosm when the estimates were integrated over the production period; these estimates were not significantly different.

Post hoc tests were performed to assess multiple comparisons between estimates and to determine which estimates

Table 2. Presentation of all daily integrated parameters that are compared in the present study.

Parameter	Method	Integrated from sunrise to sunset (SS)	Integrated over the production period (PP)
Rdaytime	Max	Rdaytime-Max-SS	Rdaytime-Max-PP
	Most	Rdaytime-Most-SS	Rdaytime-Most-PP
	Winkler	Rdaytime-Winkler-SS	Rdaytime-Winkler-PP
Rnight	Max	Rnight-Max-SS	Rnight-Max-PP
	Most	Rnight-Most-SS	Rnight-Most-PP
	Winkler	Rnight-Winkler-SS	Rnight-Winkler-PP
R24h	Max	R24h-Max-SS	R24h-Max-PP
	Most	R24h-Most-SS	R24h-Most-PP
	Winkler	R24h-Winkler	R24h-Winkler

were significantly different. For all mesocosms, and regardless of the integration period considered, Rdaytime-Max was significantly higher than Rdaytime-Most (between 75% and 198% higher, depending on the period of integration and on the mesocosm). For both integration periods, Rdaytime-Winkler was significantly higher than Rdaytime-Most for the October mesocosms (on average 150.2%) and significantly lower than Rdaytime-Max for the June mesocosms (on average −61.6%). However, for Rnight, the Max, Most, and Winkler methods gave similar estimates, with only one exception (Rnight-Max-PP was significantly different from Rnight-Winkler-PP for Oct 02). As a result of the differences in Rdaytime and Rnight, R24h-Max was generally significantly higher than R24h-Most. The only exceptions were for Jun 03 integrated over the production period and for Oct 02 and Oct 03 integrated from sunrise to sunset. In contrast, R24h-Winkler was systematically lower than R24h-Max and R24h-Most for all June mesocosms, whereas it was significantly higher than R24h-Most for the Oct 02 and Oct 03 mesocosms. Notably, R24h-Most-PP was on average 1.43, 1.47, and 1.58 times higher than R24h-Winkler for Jun 01, Jun 02, and Jun 03, respectively.

The comparisons reported earlier were performed for the entire experiments. In addition, day-by-day comparisons were also performed and are presented in the Supporting Information Table S2. Generally, the day-by-day comparisons had the same results as reported for the entire experiment. However, occasionally, the difference between Rdaytime-Max and Rdaytime-Most was not significant, as the periods considered for the Max and the Most methods were almost the same. An example is given in Fig. 4: on day 11 in Jun 01, Rdaytime-Max was only 48.9% higher than Rdaytime-Most (Fig. 4b), unlike on day 4 in Oct 01, when Rdaytime-Max was 100.6% higher than Rdaytime-Most (Fig. 4a). The greatest discrepancy between Rdaytime-Max and Rdaytime-Most was found on day 14 of Oct 02 (485.4%), while the smallest difference was on day 14 of Jun 02 (34.8%).

To assess whether the integration period significantly affected the results for Rdaytime, Rnight, and R24h, comparisons were also performed between integration periods (e.g., from sunrise to sunset or over the production period) (Table 3). The ANOVA and Kruskal–Wallis test results showed nonsignificant differences in October, while the values of Rdaytime and Rnight were significantly different in June (Table 3). More precisely, Rdaytime-Max-SS was between 4% and 36% higher than Rdaytime-Max-PP. The observed differences were similar when the Most method was used.

A new method of estimating Rdaytime, Rnight, R24h, GPP, and NCP using sensor data

Regardless of the integration period, Rdaytime-Max was significantly higher than Rdaytime-Most, as demonstrated above. As numerous studies have shown that light respiration is substantially higher than dark respiration (Markager et al. 1992; Pringault et al. 2007; Tobias et al. 2007), we suggest using the new method presented in this investigation, called the "Max method," to estimate Rdaytime, Rnight, and therefore R24h.

Moreover, as demonstrated above, major discrepancies were introduced into the respiration estimates for the Jun experiment by the integration period (SS vs. PP). Thus, we also suggest integrating Rdaytime over the production period, as this method enables us to consider only the period in which production is higher than respiration and therefore is representative of the most productive period of the day. In the same way, we suggest that Rnight be integrated over the Negative NCP period (e.g., when the DO concentration is decreasing).

Hence, based on the sensor data, we suggest calculating Rdaytime, Rnight, R24h, GPP. and NCP as presented in Eqs. 8, 9, 10, 11, and 12 respectively:

$$\text{Rdaytime} = (\text{mean instantaneous NCP during Max period}) \text{ *60*duration of Production Period} \quad (8)$$

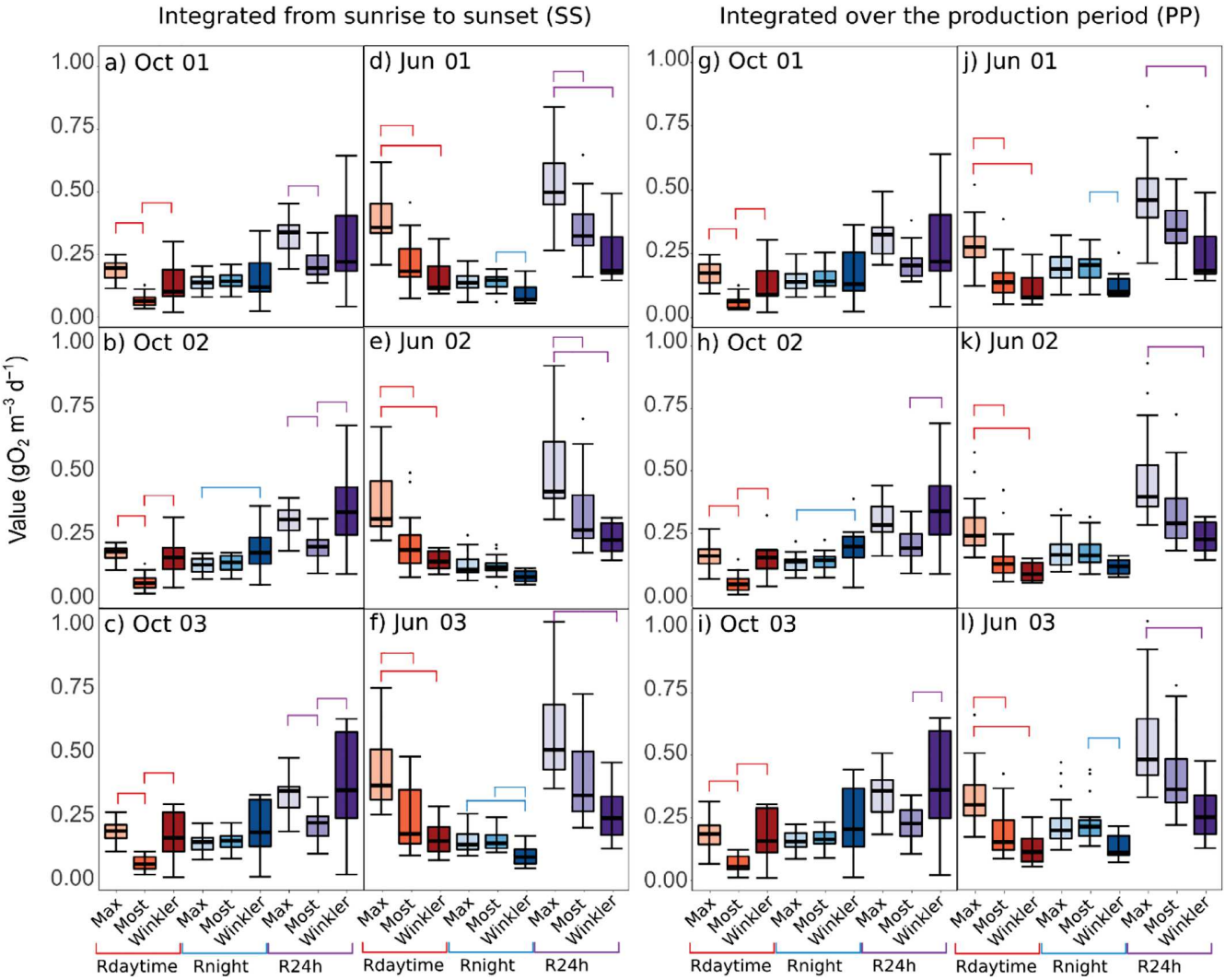

Fig 3. Estimates of Rdaytime (the three leftmost boxplots in orange), Rnight (the three boxplots in blue in the middle), and R (the three rightmost boxplots in purple) obtained from sensor data using the Max and Most methods and from Winkler incubation data integrated from sunrise to sunset or over the production period for Oct 01 (**a**, **g**), Oct 02 (**b**, **h**), Oct 03 (**c**, **i**), Jun 01 (**d**, **j**), Jun 02 (**e**, **k**), and Jun 03 (**f**, **l**). For each box, the lower quartile, median, and upper quartile values are displayed with horizontal lines. Whiskers show the range of the data, from the minimum to the maximum, excluding outliers. Brackets represent the comparisons between estimates that were found to be significantly different ($p < 0.05$, Tukey HSD or Dunn test). Oct 01, Oct 02, and Oct 03 refer to the mesocosms no.1, no.2, and no.3 of the October 2018 experiment, and similarly Jun 01 Jun 02, and Jun 03 refer to the mesocosms no.1, no.2, and no.3 of the May and June 2019 experiment.

where Rdaytime is measured in $gO_2\ m^{-3}\ d^{-1}$, the Max period is a 1-h period centered on the maximum instantaneous Negative NCP, the mean instantaneous NCP is measured in $gO_2\ m^{-3}\ min^{-1}$, and the duration of the production period is the duration of the Positive NCP period in hours.

$$\text{Rnight} = (\text{mean instantaneous NCP during Night period}) \text{*60*duration of Night Period} \quad (9)$$

where Rnight is measured in $gO_2\ m^{-3}\ d^{-1}$, the Night period refers to the Negative NCP period, the mean instantaneous NCP is measured in $gO_2\ m^{-3}\ min^{-1}$, and the duration of the night period is the duration of the Negative NCP period in hours.

R24h is calculated as:

$$\text{R24h} = \text{Rdaytime} + \text{Rnight} \quad (10)$$

Hence, GPP is calculated as follows:

$$\text{GPP} = \text{mean of instantaneous NCP during the Positive NCP period*60*duration of Production Period} + \text{Rdaytime} \quad (11)$$

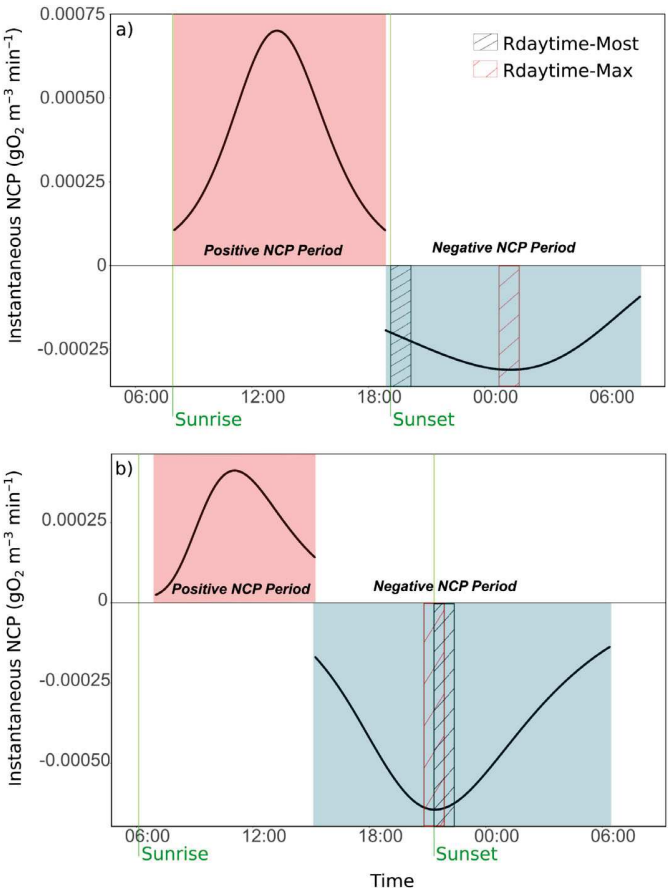

Fig 4. Instantaneous NCP during the Positive and the Negative NCP periods on (**a**) day 4 (11 October 2018) in Oct 01 and (**b**) day 11 (05 June 2019) in Jun 01. The sunrise and sunset times are shown as vertical green lines. The Positive NCP period is represented by a red rectangle, and the Negative NCP period is represented by a blue rectangle. The periods considered for the Rdaytime-Most and Rdaytime-Max calculations are shown as black and red striped rectangles, respectively. The gap between the instantaneous NCP during the Positive NCP period and during the Negative NCP period is a consequence of modeling the DO curve separately for each Positive NCP period and for each Negative NCP period.

where GPP and Rdaytime are measured in $gO_2\ m^{-3}\ d^{-1}$, and the duration of the production period is the duration of the Positive NCP period in hours.

Finally, NCP is calculated as follows:

$$NCP = GPP - R24h \quad (12)$$

Discussion

A computation of daytime respiration that takes into account variations in the coupling of the day–night and O_2 cycles

As discussed before, it has been shown that planktonic daytime respiration is significantly higher than night respiration. Therefore, in the present work, Rdaytime is proposed to be estimated with the maximum instantaneous respiration that can be measured at night. With this method, an average Rdaytime ranging from 23% to 58% higher than Rnight was obtained; this range is consistent those in with previous studies calculated using other methods, as previously noted.

In the present study, the Rdaytime estimated with this new method, using the maximal respiration at night (i.e., the Max method) was compared with the method proposed by Mostajir et al. (2013) (i.e., the Most method). For all mesocosms and regardless of the integration period considered, the Rdaytime obtained with the Max method was generally significantly higher than the Rdaytime obtained with the Most method. This means that respiration directly after sunset had not reached its maximum value yet in most cases. However, on some long, warm days (in the present work, in June, when days were more than 15 h long), the DO cycle does not perfectly match the day–night cycle (e.g., the DO concentration starts to increase sometime after sunrise and/or starts to decrease some time before sunset; Fig. 4b), resulting in Rdaytime-Most and Rdaytime-Max being equivalent. In these cases, the mismatch observed between the DO and the day–night cycles occurred because more DO was consumed

Table 3. Summary table of the *p* values obtained for the one-way ANOVA comparisons between Rdaytime, Rnight, and R24h obtained with the Max and Most methods integrated from sunrise to sunset or over the production period. When the assumptions for a parametric test were not met, a Kruskal–Wallis test was used instead. *p* values lower than 0.05 were considered significant and are presented in bold (*$p < 0.05$, **$p < 0.01$).

Estimate	Test	Oct 01	Oct 02	Oct 03	Jun 01	Jun 02	Jun 03
Rdaytime	Max-SS × Max-PP	0.43	0.51	0.76	**0.01***	**0.02***	**0.03***
	Most-SS × Most-PP	0.61	0.68	0.82	0.09	0.12	0.15
Rnight	Max-SS × Max-PP	0.53	0.64	0.70	**0.006****	**0.02***	**0.03***
	Most-SS × Most-PP	0.53	0.63	0.67	**0.001****	**0.009****	**0.008****
R24h	Max-SS × Max-PP	0.92	0.86	0.99	0.49	0.33	0.52
	Most-SS × Most-PP	0.81	0.87	0.78	0.92	0.88	0.71

through respiration than was produced through photosynthesis, even though the irradiance was still strong in the middle of the afternoon. This phenomenon can be explained by several factors, including a decrease in O_2 production from photosynthesis due to photoinhibition induced by the high irradiance level (Powles 1984) or an increase in bacterial and phytoplankton respiration due to warmer conditions (Jones 1977; Robinson 2008). These variations in the coupling of the day–night and O_2 cycles were not taken into account in previous methods of estimating Rdaytime, whereas the Max method proposed in this article considers them.

As Rdaytime is used to calculate GPP estimates, they were significantly different when estimated with the Max and the Most methods, and are presented in Supporting Information Table S4. The Max method resulted in GPP estimates between 32.6% and 50.5% higher in average than those estimated with the Most method, depending on the mesocosm and the integration period considered. As Rdaytime is also used for the R24h calculation (the total daily respiration), the R24h estimates obtained with the Max method were, similarly to GPP, between 48.2% and 55.8% compared to those obtained with the Most method. As a consequence, daily NCP estimates, which represent the balance between GPP and R24h, were not significantly different using the Max or the Most methods. Therefore, even if one method is underestimating both GPP and R24h comparing to the other, because it is to the same extent, the global oxygen balance is not significantly different.

Patterns in the nighttime data

Dark, or night, respiration by phytoplankton can be basically separated into three distinct phases (Markager and Sand-Jensen 1989; Markager et al. 1992; Mantikci et al. 2017). The first phase corresponds to the direct enhancement of respiration by photosynthesis and lasts for only a few minutes after the onset of darkness. This period is followed by a second phase in which respiration is still higher than basal maintenance respiration due to the intracellular substrate pool created during the previous light exposure (Mantikci et al. 2017, 2019) and lasts for several hours (from 2.5 to 3.6 h; Falkowski et al. 1985; Sadro et al. 2011). Moreover, the duration of this light-enhanced respiration period is season-dependent, with longer durations in the months with longer daylengths (Sadro et al. 2011). This phase is also dependent on the substrate pool available for phytoplankton and must be differentiated from the final phase, which represents basal maintenance respiration (Mantikci et al. 2017). However, in the present study, the durations of the second phase (e.g., between the start of the Negative NCP period, when respiration starts to be higher than O_2 production, and the point of maximum instantaneous respiration) in October and June were similar (Supporting Information Table S3). This phase includes a period in which production is still occurring but is lower than respiration (between the start of the Negative NCP period and sunset, see Fig. 4b). The latter phase was several hours longer in June than in October because the DO concentration started to decrease well before sunset in June. Consequently, the period in which only respiration occurs (e.g., from sunset to the point of maximum respiration) was longer in October than in June, and its duration is in line with those measured in previous studies (Falkowski et al. 1985; Markager and Sand-Jensen 1989; Sadro et al. 2011).

Moreover, the respiration pattern observed in the present investigation encompasses also heterotrophic respiration, and not only phytoplanktonic one. Bacterial respiration depends on other types of substrates, and does not necessarily vary throughout day and night the same way phytoplanktonic respiration does. An increasing respiration rate during dark conditions was found for a planktonic population dominated by bacteria (e.g., a planktonic community after a phytoplankton bloom). This increase in respiration during a dark period was proposed to be related to an increase in bacteria biomass and production (Briand et al. 2004). Overall, the nighttime respiration pattern gives information about the dominant respiratory processes in the studied system (Mantikci et al. 2019). Indeed, the nighttime respiration pattern varies accordingly to the quality and the quantity of organic substrates available, as well as the distribution of the global respiration between heterotrophic and autotrophic organisms. In a system with different characteristics than that of the present study, respiration patterns may be very different from the ones observed in the present investigation.

Comparison between sensor data and Winkler data

The values of Rdaytime, Rnight, and R24h estimated by the Winkler method, which were normalized on the same period as those obtained with the Max and the Most methods, were sometimes significantly different from those obtained using sensor data. These discrepancies are in accordance with Mostajir et al. (2013), who obtained Winkler respiration rates that were three times lower than sensor respiration rates. These discrepancies may be due to several fundamental differences between the two methods. First, the Winkler method requires the confinement of the plankton community in small, closed bottles (several hundred milliliters). As a result, the metabolism estimated in the glass bottles might not be representative of the mesocosm (several m^3). Additionally, the plankton community must acclimate to its new confined environment, leading to potential differences between the metabolism of the community in the incubation glass bottles and that of the natural or mesocosm waters. This so-called "bottle effect" has long been noted as a potential bias in metabolism estimation using the Winkler technique (Bender et al. 1987). Moreover, to measure respiration, Winkler incubations are typically performed during the day or under light exposure, with bottles covered to prevent light and thus photosynthesis (Smith and Kemp 1995; Liess et al. 2016; Mesa et al. 2017). Therefore, Winkler respiration values are obtained from a

community that is acclimated to natural light conditions and is suddenly put in the dark. Thus, the organisms must instantaneously change their metabolism without an acclimation period, which creates a source of bias in respiration measurements. In contrast, the sensors installed in the mesocosms allow us to measure the plankton community's metabolic parameters in a noninvasive way, directly in their quasi-natural environment, with natural light conditions during the day and at night.

Comparison of two integration periods for the sensor data

The discrepancies between the daily Rdaytime estimates integrated from sunrise to sunset and those integrated over the production period were greater when the daylength was longer (i.e., in June in the present study). This is because, even if the daylength varies, the production period is still comparable across seasons (Supporting Information Table S3). This characteristic of the production period may be explained by the fact that metabolic processes are controlled by various mechanisms, such as temperature variations, throughout the seasons and not only by the daylength and the amount of light received (Solomon et al. 2013; Alfonso et al. 2018; Lopez Sandoval et al. 2019). As a result, during long days, the actual production period is considerably shorter than the daylength, and hence Rdaytime integrated over the production period is in fact integrated over a significantly shorter period than that integrated from sunrise to sunset. Rnight estimates were also significantly different between the two integration periods but in the opposite way as Rdaytime estimates; the Rnight estimates integrated from sunset to the following sunrise are integrated over a shorter period than those integrated over the entire Negative NCP period. Consequently, R24h was not significantly affected by the integration period, as the differences induced in both Rdaytime and Rnight were equal to each other. Hence, when comparing Rdaytime estimates obtained in different seasons, the estimates should be integrated over comparable time periods, but the integration time period is less important in studies focusing only on R24h.

Comments and recommendations

In situ mesocosm experiments are a useful approach in aquatic ecology because they allow the assessment and quantification of the responses of planktonic and microbial communities to various perturbations within a controlled environment under in situ conditions. The ability of these experiments to effectively mirror in situ conditions has been investigated often; although there are some discrepancies between the biotic and abiotic parameters of mesocosms and those of the ecosystem they are deployed in, mesocosms still represent one of the best experimental ways to address certain fundamental questions in aquatic ecology (Dzialowski et al. 2014). However, mesocosm experiments often require a meticulous, time-consuming, and labor-intensive sampling effort to obtain enough data to be able to monitor several key parameters, such as oxygen concentrations. High-frequency automated sensors can be used to monitor these parameters in a more efficient and easier way, as they need only to be deployed at the beginning of the experiment and retrieved at the end. Data generated via these sensors can be used to obtain valuable insights into the responses of the system to the tested perturbation(s), notably by assessing the metabolism of the system. As mentioned before, this method has many advantages compared to classical methods; however, it also has a few limitations and uncertainties. One of the limitations is the dependence of the method on a reliable estimate of the air–water exchange coefficient. This is combined with the fact that physical phenomena and their contributions to DO variability may vary greatly depending on both the tested ecosystem and the mesocosm structure. These physical aspects should be the focus of future research. Nevertheless, the goal of mesocosm experiments is to compare control mesocosms with mesocosms in which one or more disturbance(s) were applied. In this context, an over- or underestimated piston velocity coefficient will not have a substantial impact on the measured responses of the treatment compared to control mesocosms as long as the same piston velocity coefficient is used for all mesocosms.

Another limitation of this method is that it relies on strong daily DO cycles in order to be applicable. Therefore, this method is fully applicable in locations with pronounced day–night cycles, and it might be challenging to apply in low-production systems, like turbid rivers and estuaries. However, this method becomes more challenging to apply at latitudes where the cycle is less marked and impossible to apply when DO does not have a daily cycle. This means that the method can be used to calculate instantaneous NCP during only certain months of the year in polar ecosystems, as it is not possible to estimate both GPP and R without DO cycles.

To conclude, in the present study, we presented a reliable method of estimating daytime respiration developed using automated sensors in in situ mesocosms. This method takes into account the variability of the coupling between day–night and O_2 cycles and therefore provides a better assessment of planktonic metabolic parameters than other methods. We also provide recommendations about various aspects of the technique, such as the measurement frequency to use and the physical air–water exchange of oxygen.

Mesocosm studies investigating the responses of aquatic communities to environmental stress should move toward the use of devices that are more autonomous and less costly in terms of time, work, and price than classical methods. The use of high-frequency sensors in mesocosms is one way to achieve this goal. By addressing certain methodological questions regarding the use of the free-water diel oxygen technique for in situ enclosed mesocosm experiments, this work improves our ability to assess high-frequency instantaneous metabolism and consequently the metabolic responses of communities to

disturbance and establishes a common protocol for data analysis.

References

Alcaraz, M., C. Marrasé, F. Peters, L. Arin, and A. Malits. 2001. Seawater–atmosphere O2 exchange rates in open-top laboratory microcosms: application for continuous estimates of planktonic primary production and respiration. J. Exp. Mar. Biol. Ecol. **257**: 1–12. doi:10.1016/S0022-0981(00)00328-2

Alfonso, M. B., A. S. Brendel, A. J. Vitale, C. Seitz, M. C. Piccolo, and G. M. E. Perillo. 2018. Drivers of ecosystem metabolism in two managed shallow lakes with different salinity and trophic conditions: The Sauce Grande and La Salada Lakes (Argentina). Water **10**: 1136. doi:10.3390/w10091136

Alkire, M. B., and others. 2012. Estimates of net community production and export using high-resolution, Lagrangian measurements of O_2, NO_3^-, and POC through the evolution of a spring diatom bloom in the North Atlantic. Deep-Sea Res. I Oceanogr. Res. Pap. **64**: 157–174. doi:10.1016/j.dsr.2012.01.012

Beardall, J., T. Burger-Wiersma, M. Rijkeboer, A. Sukenik, J. Lemoalle, Z. Dubinsky, and D. Fontvielle. 1994. Studies on enhanced post-illumination respiration in microalgae. J. Plankton Res. **16**: 1401–1410. doi:10.1093/plankt/16.10.1401

Bender, M., and others. 1987. A comparison of four methods for determining planktonic community production. Limnol. Oceanogr. **32**: 1085–1098. doi:10.4319/lo.1987.32.5.1085

Bittig, H. C., and others. 2018. Oxygen optode sensors: Principle, characterization, calibration, and application in the ocean. Front. Mar. Sci. **4**: 429. doi:10.3389/fmars.2017.00429

Briand, E., O. Pringault, S. Jacquet, and J. P. Torreton. 2004. The use of oxygen microprobes to measure bacterial respiration for determining bacterioplankton growth efficiency. Limnol. Oceanogr. **2**: 406–416. doi:10.4319/lom.2004.2.4066

Briggs, N., K. Guðmundsson, I. Cetinić, E. D'Asaro, E. Rehm, C. Lee, and M. J. Perry. 2018. A multi-method autonomous assessment of primary productivity and export efficiency in the springtime North Atlantic. Biogeosciences **15**: 4515–4532. doi:10.5194/bg-15-4515-2018

Brinkman, A. G., C. J. M. Philippart, and A. F. Zuur. 1995. Model methods for the analysis of mesocosm experimental studies. Helgoländer Meeresuntersuchungen **49**: 771–784. doi:10.1007/BF02368400

Carpenter, J. H. 1965. The accuracy of the Winkler method for dissolved oxygen analysis. Limnol. Oceanogr. **10**: 135–140. doi:10.4319/lo.1965.10.1.0135

Carrit, D. E. 1966. Comparison and evaluation of currently employed modifications of the Winkler method for determining oxygen in seawater. A NASCO report. J. Mar. Res. **24**: 286–318.

Carvalho, M. C., and B. D. Eyre. 2012. Measurement of planktonic CO_2 respiration in the light. Limnol. Oceanogr.: Methods **10**: 167–178. doi:10.4319/lom.2012.10.167

Chiu, C.-Y., and others. 2020. Terrestrial loads of dissolved organic matter drive inter-annual carbon flux in subtropical lakes during times of drought. Sci. Total Environ. **717**. doi:10.1016/j.scitotenv.2020.137052

Crossland, N. O., and T. W. L. Point. 1992. The design of mesocosm experiments. Environ. Toxicol. Chem. **11**: 1–4. doi:10.1002/etc.5620110101

de Eyto, E., and others. 2019. High frequency monitoring reveals fine scale spatial and temporal dynamics of the deep chlorophyll maximum of a stratified coastal lagoon. Estuar. Coast. Shelf Sci. **218**: 278–291. doi:10.1016/j.ecss.2018.12.010

Demars, B. O. L., J. Thompson, and J. R. Manson. 2018. Stream metabolism and the open diel oxygen method: Principles, practice, and perspectives. Limnol. Oceanogr.: Methods **13**: 356–374. doi:10.1002/lom3.10030

Dzialowski, A. R., M. Rzepecki, I. Kostrzewska-Szlakowska, K. Kalinowska, A. Palash, and J. T. Lennon. 2014. Are the abiotic and biotic characteristics of aquatic mesocosms representative of in situ conditions? J. Limnol. **73**: 603–612. doi:10.4081/jlimnol.2014.721

Falkowski, P. G., Z. Dubinsky, and G. Santostefano. 1985. Light-enhanced dark respiration in phytoplankton. SIL Proc. 1922-2010 **22**: 2830–2833. doi:10.1080/03680770.1983.11897784

Hanson, P. C., D. L. Bade, S. R. Carpenter, and T. K. Kratz. 2003. Lake metabolism: Relationships with dissolved organic carbon and phosphorus. Limnol. Oceanogr. **48**: 1112–1119. doi:10.4319/lo.2003.48.3.1112

Hanson, P. C., S. R. Carpenter, N. Kimura, C. Wu, S. P. Cornelius, and T. K. Kratz. 2008. Evaluation of metabolism models for free-water dissolved oxygen methods in lakes. Limnol. Oceanogr.: Methods **6**: 454–465. doi:10.4319/lom.2008.6.454

Hensley, R. T., and M. J. Cohen. 2020. Nitrate depletion dynamics and primary production in riverine benthic chambers. Freshw. Sci. **39**: 169–182. doi:10.1086/707650

Hotchkiss, E. R., and R. O. Hall Jr. 2014. High rates of daytime respiration in three streams: Use of $\delta^{18}O_{O2}$ and O_2 to model diel ecosystem metabolism. Limnol. Oceanogr. **59**: 798–810. doi:10.4319/lo.2014.59.3.0798

Idrizag, A., A. Laas, U. Anijalg, and P. Noges. 2016. Horizontal differences in ecosystem metabolism of a large shallow lake. J. Hydrol. **535**: 93–100. doi:10.1016/j.jhydrol.2016.01.037

Jones, R. I. 1977. The importance of temperature conditioning to the respiration of natural phytoplankton

communities. Br. Phycol. J. **12**: 277–285. doi:10.1080/00071617700650291

Kritzberg, E. S., W. Granéli, J. Björk, C. Brönmark, P. Hallgren, A. Nicolle, A. Persson, and L.-A. Hansson. 2014, Warming and browning of lakes: consequences for pelagic carbon metabolism and sediment delivery. Freshw Biol. **59**: 325–336. doi:10.1111/fwb.12267

Laas, A., Noges, P., Koiv, T., and Noges, T. 2012. High-frequency metabolism study in a large and shallow temperate lake reveals seasonal switching between net autotrophy and net heterotrophy. Hydrobiologia **694**: 57–74. doi:10.1007/s10750-012-1131-z

Lauster, G. H., P. C. Hanson, and T. K. Kratz. 2006. Gross primary production and respiration differences among littoral and pelagic habitats in northern Wisconsin lakes. Can. J. Fish. Aquat. Sci. **63**: 1130–1141.

Leclercq, N., J.-P. Gattuso, and J. Jaubert. 1999. Measurement of oxygen metabolism in open-top aquatic mesocosms: Application to a coral reef community. Mar. Ecol. Prog. Ser. **177**: 299–304. doi:10.3354/meps177299

Liess, A., and others. 2016. Terrestrial runoff boosts phytoplankton in a Mediterranean coastal lagoon, but these effects do not propagate to higher trophic levels. Hydrobiologia **766**: 275–291. doi:10.1007/s10750-015-2461-4

Lopez Sandoval, D., K. Rowe, P. Carillo-de-Albonoz, C. M. Duarte, and S. Agusti. 2019. Rates and drivers of Red Sea plankton community metabolism. Biogeosciences **16**: 2983–2995. doi:10.5194/bg-16-2983-2019

Mantikci, M., J. L. S. Hansen, and S. Markager. 2017. Photosynthesis enhanced dark respiration in three marine phytoplankton species. J. Exp. Mar. Biol. Ecol. **497**: 188–196. doi:10.1016/j.jembe.2017.09.015

Mantikci, M., P. A. Staerh, J. L. S. Hansen, and S. Markager. 2019. Patterns of dark respiration in aquatic systems. Mar. Freshw. Res. **71**: 432–442. doi:10.1071/MF18221

Markager, S., and K. Sand-Jensen. 1989. Patterns of night-time respiration in a dense phytoplankton community under a natural light regime. J. Ecol. **77**: 49. doi:10.2307/2260915

Markager, S., A.-M. Jespersen, T. V. Madsen, E. Berdalet, and R. Weisburd. 1992. Diel changes in dark respiration in a plankton community, p. 119–130.*In* T. Berman, H. J. Gons, and L. R. Mur [eds.], The daily growth cycle of phytoplankton: Proceedings of the fifth International Workshop of the Group for Aquatic Primary Productivity (GAP), held at Breukelen, The Netherlands 20–28 April 1990. Springer.

Mesa, E., and others. 2017. Continuous daylight in the high-Arctic summer supports high plankton respiration rates compared to those supported in the dark. Sci. Rep. **7**: 1247. doi:10.1038/s41598-017-01203-7

Mostajir, B., E. Le Floc'h, S. Mas, R. Pete, D. Parin, J. Nouguier, E. Fouilland, and F. Vidussi. 2013. A new transportable floating mesocosm platform with autonomous sensors for real-time data acquisition and transmission for studying the pelagic food web functioning. Limnol. Oceanogr.: Methods **11**: 394–409. doi:10.4319/lom.2013.11.394

Odum, E. P. 1984. The mesocosm. Bioscience **34**: 558–562. doi:10.2307/1309598

Odum, H. T. 1956. Primary production in flowing waters. Limnol. Oceanogr. **1**: 102–117. doi:10.4319/lo.1956.1.2.0102

Odum, H. T., and E. P. Odum. 1955. Trophic structure and productivity of a windward coral reef community on Eniwetok Atoll. Ecol. Monogr. **25**: 291–320. doi:10.2307/1943285

Oviatt, C., M. Pilson, S. Nixon, J. Frithsen, D. Rudnick, J. Kelly, J. Grassle, and J. Grassle. 1984. Recovery of a polluted estuarine system: A mesocosm experiment. Mar. Ecol. Prog. Ser. **16**: 203–217. doi:10.3354/meps016203

Oviatt, C., A. Keller, P. Sampou, and L. Beatty. 1986. Patterns of productivity during eutrophication: A mesocosm experiment. Mar. Ecol. Prog. Ser. **28**: 69–80. doi:10.3354/meps028069

Powles, S. B. 1984. Photoinhibition of photosynthesis induced by visible light. Annu. Rev. Plant Physiol. **35**: 15–44. doi:10.1146/annurev.pp.35.060184.000311

Pringault, O., V. Tassas, and E. Rochelle-Newall. 2007. Consequences of respiration in the light on the determination of production in pelagic systems. Biogeosciences **4**: 105–114.

Reijo, C. J., R. T. Hensley, and M. J. Cohen. 2018. Isolating stream metabolism and nitrate processing at point-scales, and controls on heterogeneity. Freshw. Sci. **37**: 238–250. doi:10.1086/697319

Richardson, D. C., C. C. Carey, D. A. Bruesewitz, and K. C. Weathers. 2017. Intra- and inter-annual variability in metabolism in an oligotrophic lake. Aquat. Sci. **79**: 319–333. doi:10.1007/s00027-016-0499-7

Robinson, C. 2008. Heterotrophic bacterial respiration, p. 299–334.*In* D. L. Kirchman [ed.], Microbial ecology of the oceans. Wiley.

Sadro, S., C. E. Nelson, and J. M. Melack. 2011. Linking diel patterns in community respiration to bacterioplankton in an oligotrophic high-elevation lake. Limnol. Oceanogr. **56**: 540–550. doi:10.4319/lo.2011.56.2.0540

Smith, E., and W. Kemp. 1995. Seasonal and regional variations in plankton community production and respiration for Chesapeake Bay. Mar. Ecol. Prog. Ser. **116**: 217–231. doi:10.3354/meps116217

Solomon, C. T., and others. 2013. Ecosystem respiration: Drivers of daily variability and background respiration in lakes around the globe. Limnol. Oceanogr. **58**: 849–866. doi:10.4319/lo.2013.58.3.0849

Staehr, P. A., D. Bade, M. C. V. de Bogert, G. R. Koch, C. Williamson, P. Hanson, J. J. Cole, and T. Kratz. 2010a. Lake metabolism and the diel oxygen technique: State of the science. Limnol. Oceanogr.: Methods **8**: 628–644. doi:10.4319/lom.2010.8.0628

Staehr, P. A., K. Sand-Jensen, A. L. Raun, B. Nilsson, and J. Kidmose. 2010b. Drivers of metabolism and net heterotrophy in contrasting lakes. Limnol. Oceanogr. **55**: 817–830. doi:10.4319/lo.2010.55.2.0817

Staehr, P. A., J. M. Testa, W. M. Kemp, J. J. Cole, K. Sand-Jensen, and S. V. Smith. 2012. The metabolism of aquatic ecosystems: History, applications, and future challenges. Aquat. Sci. **74**: 15–29. doi:10.1007/s00027-011-0199-2

Stewart, R. I. A., and others. 2013. Chapter two - Mesocosm experiments as a tool for ecological climate-change research, p. 71–181.*In* G. Woodward and E. J. O'Gorman [eds.], Advances in ecological research. Academic Press.

Tobias, C. R., J. K. Böhlke, and J. W. Harvey. 2007. The oxygen-18 isotope approach for measuring aquatic metabolism in high productivity waters. Limnol. Oceanogr. **52**: 1439–1453. doi:10.4319/lo.2007.52.4.1439

Trombetta, T., F. Vidussi, S. Mas, D. Parin, M. Simier, and B. Mostajir. 2019. Water temperature drives phytoplankton blooms in coastal waters. PLoS One **14**: e0214933. doi:10.1371/journal.pone.0214933

Van de Bogert, M. C., S. R. Carpenter, J. J. Cole, and M. L. Pace. 2007. Assessing pelagic and benthic metabolism using free water measurements. Limnol. Oceanogr.: Methods **5**: 145–155. doi:10.4319/lom.2007.5.145

Whitledge, G. W., and C. F. Rabeni. 2000. Benthic community metabolism in three habitats in an Ozark stream. Hydrobiologia **437**: 165–170.

Wikner, J., S. Panigrahi, A. Nydahl, E. Lundberg, U. Båmstedt, and A. Tengberg. 2013. Precise continuous measurements of pelagic respiration in coastal waters with oxygen optodes. Limnol. Oceanogr.: Methods **11**: 1–15. doi:10.4319/lom.2013.11.1

Winkler, L. W. 1888. Die Bestimmung des in Wasser gelösten Sauerstoffen. Berichte der Deutschen Chemischen Gesellschaft **21**: 2843–2855.

Xue, X., D. A. Gauthier, D. H. Turpin, and H. G. Weger. 1996. Interactions between photosynthesis and respiration in the green alga *Chlamydomonas reinhardtii* (characterization of light-enhanced dark respiration). Plant Physiol. **112**: 1005–1014. doi:10.1104/pp.112.3.1005

Acknowledgments

We would like to thank Rémi Valdès, Solenn Soriano, Kevin Mestre, and Camille Suarez-Bazille, the staff of the Sète Marine Station, for helping with setting up the mesocosms and with daily sampling. We also thank Thomas Trombetta, Emilie Eveque, and Jean-François Thevenot for assistance with the daily sampling and with the oxygen sample analyses. Furthermore, we would like to thank Emilie le Floc'h for commenting the model construction and Justine Courboulès for providing the illustration of the mesocosm system. The research leading to these results and a part of the PhD scholarship awarded to TS were funded under the European Union Horizon 2020 Program (H2020/2017-2020), grant agreement 731065-AQUACOSM: Network of Leading European AQUAtic MesoCOSM Facilities Connecting Mountains to Oceans from the Arctic to the Mediterranean. We would like to acknowledge Robert Ptacnik and Herwig Stibor for their helpful comments on the previous version of the manuscript, as well as other participants of the AQUACOSM European project for the constructive discussions during workshops and meetings.

Conflict of Interest

None declared.

Submitted 29 September 2020
Revised 28 January 2021
Accepted 18 February 2021

Associate editor: Scott Ensign

Supp. Table 1. Summary table of the p-values obtained for the one-way ANOVA or Kruskal-Wallis comparisons between Rdaytime, Rnight and R24h estimated with the Max and the Most methods. SS refers to the comparison of the estimates integrated from sunrise to sunset, and PP those integrated over the production period. The *p*-values smaller than 0.05 were considered as significant and are presented in bold.

Estimate	Integration	Oct-1	Oct-2	Oct-3	Jun-1	Jun-2	Jun-3
Rdaytime	SS	**6.7×10^{-6}**	**2.1×10^{-6}**	**9.4×10^{-6}**	**6.7×10^{-6}**	**1.4×10^{-4}**	**9.5×10^{-5}**
	PP	**4.9×10^{-5}**	**4.1×10^{-5}**	**1.7×10^{-4}**	**4.1×10^{-5}**	**4.0×10^{-4}**	**6.9×10^{-5}**
Rnight	SS	0.62	**0.03**	0.14	**0.03**	0.07	**0.01**
	PP	0.59	**0.03**	0.32	**0.04**	0.09	**0.01**
R24h	SS	**9.3×10^{-3}**	**3.7×10^{-3}**	**0.01**	**1.7×10^{-4}**	**3.1×10^{-4}**	**7.0×10^{-4}**
	PP	0.08	**0.01**	**0.02**	**2.2×10^{-3}**	**9.1×10^{-4}**	**1.1×10^{-3}**

Supp. Table 2. Day-by-day differences between estimates obtained with the Max method and with the Most method. Comparisons were done between each value obtained with the Max method and the corresponding value obtained with the Most method (obtained for the same mesocosm and for the same day). n.a.: value not available

Mesocosm	Day	$\frac{RdaytimeMax-RdaytimeMost}{RdaytimeMost} * 100$ (%)	$\frac{RnightMax-RnightMost}{RnightMost} * 100$ (%)
Jun-1	2	91.86	-10.96
Jun-1	3	255.55	-21.86
Jun-1	4	166.78	-16.94
Jun-1	5	168.50	-20.52
Jun-1	6	105.96	-11.11
Jun-1	7	127.17	-14.36
Jun-1	8	86.21	-10.58
Jun-1	9	96.33	-12.43
Jun-1	10	109.96	-15.94
Jun-1	11	48.95	7.46
Jun-1	12	81.92	-9.86
Jun-1	13	45.76	11.47
Jun-1	14	35.15	11.14
Jun-1	15	54.54	10.97
Jun-1	16	65.07	-2.31
Jun-1	17	104.72	-8.75
Oct-1	2	95.97	-5.08
Oct-1	3	267.52	-10.07
Oct-1	4	100.63	-5.80
Oct-1	5	173.96	-11.74
Oct-1	6	110.84	-6.53
Oct-1	7	149.83	-9.18

Oct-1	8	197.39	-5.91
Oct-1	9	378.59	-14.85
Oct-1	10	90.58	-6.94
Oct-1	11	107.32	-7.31
Oct-1	12	396.78	-14.76
Oct-1	13	167.79	-8.63
Oct-1	14	485.44	-5.23
Oct-1	15	212.18	-7.46
Jun-2	2	108.31	-15.83
Jun-2	3	207.13	-19.33
Jun-2	4	119.28	-11.91
Jun-2	5	218.74	-21.92
Jun-2	6	94.49	-12.20
Jun-2	7	68.23	-8.04
Jun-2	8	101.47	-16.25
Jun-2	9	66.79	-7.62
Jun-2	10	118.54	-19.20
Jun-2	11	n.a.	n.a.
Jun-2	12	59.13	-7.34
Jun-2	13	57.70	12.95
Jun-2	14	34.84	12.10
Jun-2	15	47.32	32.42
Jun-2	16	55.22	-2.09
Jun-2	17	74.94	36.07
Oct-2	2	94.88	-5.05
Oct-2	3	296.31	-10.08
Oct-2	4	105.92	-5.86
Oct-2	5	186.89	-11.86
Oct-2	6	113.24	-6.16
Oct-2	7	156.36	-9.43
Oct-2	8	436.17	-7.48
Oct-2	9	754.91	-15.35
Oct-2	10	190.30	-15.09
Oct-2	11	171.10	-12.03
Oct-2	12	437.40	-17.01
Oct-2	13	247.38	-13.45
Oct-2	14	465.52	-7.02
Oct-2	15	-12.66	0.74
Jun-3	2	109.54	-17.03
Jun-3	3	196.16	-19.31
Jun-3	4	119.06	-12.30
Jun-3	5	186.73	-23.23
Jun-3	6	129.94	-12.42
Jun-3	7	132.34	-14.68
Jun-3	8	87.04	-9.50
Jun-3	9	97.79	-14.54

Jun-3	10	108.25	-14.36
Jun-3	11	57.35	1.72
Jun-3	12	77.13	-11.17
Jun-3	13	48.71	-0.54
Jun-3	14	55.88	-0.19
Jun-3	15	38.21	19.86
Jun-3	16	59.91	-3.77
Jun-3	17	39.47	16.09
Oct-3	2	65.22	-4.18
Oct-3	3	140.75	-6.97
Oct-3	4	206.28	-9.65
Oct-3	5	205.15	-12.17
Oct-3	6	101.39	-5.93
Oct-3	7	469.64	-19.02
Oct-3	8	457.29	-8.84
Oct-3	9	230.56	-9.68
Oct-3	10	218.97	-13.64
Oct-3	11	104.12	-7.29
Oct-3	12	352.56	-14.90
Oct-3	13	149.94	-8.42
Oct-3	14	n.a.	-3.64
Oct-3	15	463.95	-8.07

Supp. Table 3. Average duration of the Positive NCP period and of the periods of light-enhanced respiration in hour.

Mesocosm	Positive NCP period	From the start of the Negative NCP period to the maximal respiration	From the sunset to the maximal respiration
Oct-1	10.22	5.65	5.22
Oct-2	10.15	5.37	4.81
Oct-3	10.29	5.28	4.82
Jun-1	11.13	5.61	2.16
Jun-2	11.14	5.67	1.94
Jun-3	11.44	5.41	2.10

Supp. Table 4. Mean GPP estimates with standard deviations ($gO_2\ m^{-3}\ d^{-1}$) obtained with the Max and the Most methods and integrated over the production period (PP) or from sunrise to sunset (SS).

Mesocosm	GPP-Max-PP ($gO_2\ m^{-3}\ d^{-1}$)	GPP-Most-PP ($gO_2\ m^{-3}\ d^{-1}$)	GPP-Max-SS ($gO_2\ m^{-3}\ d^{-1}$)	GPP-Most-SS ($gO_2\ m^{-3}\ d^{-1}$)
Oct-1	0.36 ± 0.11	0.25 ± 0.09	0.38 ± 0.08	0.26 ± 0.07
Oct-2	0.36 ± 0.14	0.26 ± 0.13	0.38 ± 0.09	0.26 ± 0.10
Oct-3	0.42 ± 0.18	0.28 ± 0.13	0.42 ± 0.13	0.29 ± 0.10
Jun-1	0.54 ± 0.19	0.41 ± 0.17	0.72 ± 0.19	0.54 ± 0.18
Jun-2	0.51 ± 0.21	0.38 ± 0.19	0.68 ± 0.24	0.51 ± 0.22
Jun-3	0.58 ± 0.21	0.43 ± 0.18	0.77 ± 0.25	0.58 ± 0.23

Appendix 1.

Sensor deployment duration and sampling frequency

In the present study, the data used wad obtained with a frequency of 1 measurement every minute. This measurement frequency or sampling frequency, which is the time period between two consecutive data acquisitions (Staehr et al. 2010a), has to be chosen wisely. Useful information from the DO data can be missed if the sampling frequency is too slow, leading to differences in metabolic estimates. On the other hand, a rapid sampling frequency might result in the generation of an extensive dataset, which is not necessary if it does not provide additional information. A sampling frequency of 30 min has been estimated to be sufficient to provide reliable daily metabolic estimates in field observations of lakes (Staehr et al. 2010a). In the same study, the required duration of sensor deployment to obtain powerful metabolic estimates (i.e., within 20% of the mean with a certainty of 80%) was calculated for various sampling frequencies (from 10 min to 4 hours).

As said before, in the present investigation, data were collected with a sampling frequency of 1min. To verify whether the duration of the experiments used in this work is sufficient to get powerful estimations of NCP using the new method described, the same power analysis was conducted with sampling frequency ranging from 1 to 60 min, using data from the Oct-1 mesocosm.

The Oct-1 data were collected with a 1-min SP (SP1) by the sensors. Data for SPs of 5, 10, 15, 30 and 60 min (SP5, SP10, SP15, SP30, SP60) were then obtained from the initial SP1 data. Then, the instantaneous and daily metabolic parameters were calculated with these 5 datasets. The results of the power analysis of the number of days that would be required for the Oct experiment with the tested sampling frequencies are presented in Supp. Table 5. The results showed that the 15 days of acquisition of data of Oct-1 obtained with a sampling frequency of 1 min greatly surpassed 0.8 days, which is the minimum required number of days to have powerful estimates of NCP in this case.

Supp. Table 5. Required duration of sensor deployment (in days) to obtain powerful NCP estimates (i.e. within 20% of the mean with a certainty of 80%) for the Oct-1 data at various sampling frequencies ranging from 1 to 60 min.

Sampling frequencies (minutes)	Required deployment time (days)
1	0.80
5	4.21
10	9.37
15	14.51
30	30.07
60	55.17

45

46 On a more general note, this power analysis highlights the fact that sampling frequency must be
47 considered when designing a mesocosm experiment and when using automated sensors that can
48 perform high-frequency measurements.

49 Appendix 2.

50 ***Sensitivity analyses of the method to the air-water exchange coefficient value***

51 The rate at which oxygen is exchanged with the atmosphere over time can be approximated as being
52 proportional to the oxygen deficit (e.g., the difference between DO and the oxygen saturation level)
53 (Cox 2003). The piston velocity coefficient k, a proportional constant, is needed to estimate the
54 transfer of oxygen between the atmosphere and the water surface. This parameter is related to surface
55 turbulence, internal mixing, water viscosity and temperature. In the field, k can be calculated with the
56 wind speed at 10 m above the water surface, but in enclosed mesocosms that are covered by a dome
57 and therefore not directly subject to wind-induced turbulence, this calculation is not possible.
58 However, despite the lack of direct wind effects, k cannot be considered equal to 0 in mesocosms
59 because of the water mass movement in the mesocosm caused by the external waves surrounding the
60 mesocosm and because of the mixing induced by the pump. An analysis of the sensitivity of the
61 calculation method to the value of k was performed in Staehr et al. (2010), with a k value of 0.4 m d^{-1}
62 (0.017 m h^{-1}). However, this analysis has never been done for an enclosed mesocosm situation, in
63 which estimating k can be very challenging.

Therefore, in the present investigation, metabolic parameters estimated with low and high piston velocity values were compared. More precisely, the instantaneous NCP and the daily metabolic parameters (Eq. 6 & Eq. 10-Eq. 12) obtained for the Oct-1 mesocosm with 2 piston velocity values from Alcaraz et al. (2001) were compared. The choice to compare the dataset obtained in October is justified because the experiment was carried out under similar temperature and salinity conditions as in Alcatraz et al. (2001). Thus, a low piston velocity value was used (klow = 0.00936 m h^{-1}) that corresponded to the lowest value obtained under nonnull turbulent conditions, as we considered that turbulence would not be zero in the mesocosms due to the external waves and pumping effects, and a high piston velocity value was also tested (khigh = 0.02322 m h^{-1}).

The instantaneous metabolism seemed to be affected by the value of k used for its calculation (Supp Fig. 1a). For example, the instantaneous NCP was the highest using khigh during the Positive NCP period. On the other hand, the instantaneous NCP was closer to 0 using khigh during the Negative NCP period (Supp. Fig. 1a). The daily GPP values obtained with khigh and with klow were not significantly different (Supp. Fig. 1b) (ANOVA, p = 0.98), while the R24h value obtained with khigh was significantly higher than that obtained using klow (ANOVA, p = 0.02*). Consequently, the daily NCP, which is the difference between GPP and R24h, was significantly greater when khigh was used (ANOVA, p = 0.01*).

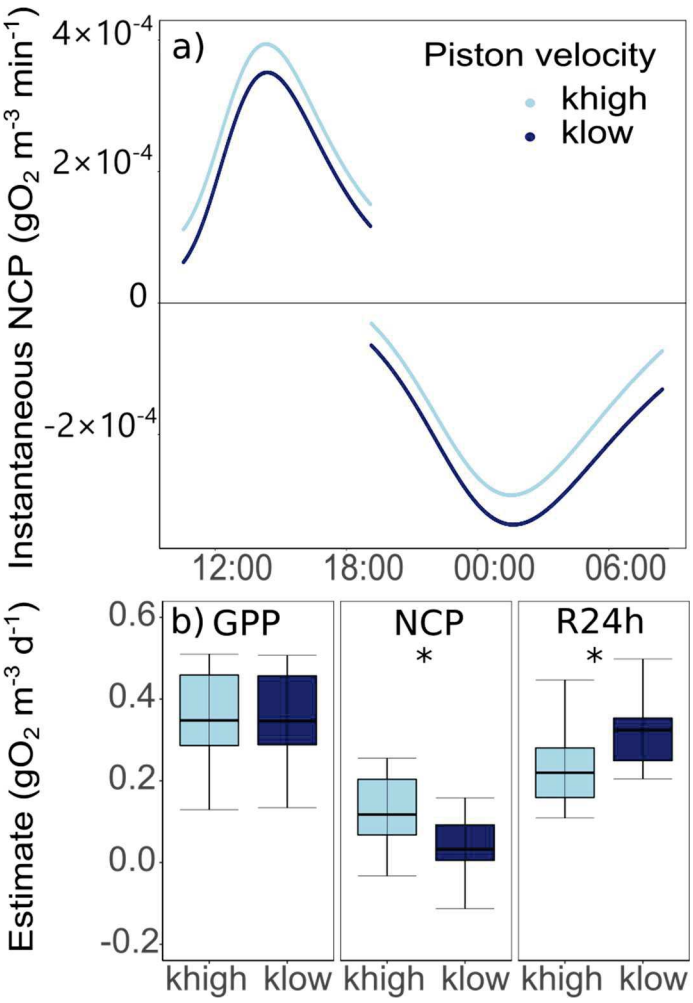

81

82 **Supp. Figure 1**. (a) Instantaneous positive and negative NCP on day 3 (C1-Oct) calculated with khigh
83 = 0.02322 m.h-1 (light blue) and klow = 0.009326 m h-1 (dark blue). (b) Daily estimates of GPP, NCP
84 and R calculated with khigh (dark blue) and klow (light blue). The levels of significance from
85 ANOVA are indicated with * ($p < 0.05$ *, $p < 0.01$ **, $p < 0.001$ ***). For each box, the lower
86 quartile, median, and upper quartile values are displayed with horizontal lines. Whiskers show the
87 range of the data, from the minimum to the maximum.

88

89 The instantaneous NCP value during Positive and Negative NCP periods was increased and decreased,
90 respectively, by a greater k value. This result explains why the daily GPP was not significantly
91 affected, as it is estimated using data from both the Positive and Negative NCP periods. The effects of
92 the piston velocity value on production were counterbalanced by its effects on daytime respiration,
93 resulting in an almost unaffected GPP estimate. However, R24h is calculated using only the

instantaneous NCP from the Negative NCP period. Hence, the magnitude of k affects R24h estimates in the same way that it affects instantaneous NCP estimates during Negative NCP periods.

To conclude, the present analysis highlights the fact that the method using high-frequency data to estimate metabolic parameter is sensitive to the air-water exchange coefficient value. This work underlines the need for a reliable estimation of the air-water exchange coefficient to obtain precise metabolic parameters. The dependence of the free-water method on an accurate estimation of the air-water exchange coefficient is one of the weaknesses of this method, and future research should focus on this topic. However, the aim of mesocosm experiments is to assess the effects of one or several simulated disturbance(s) on the studied system and therefore to compare control mesocosms with mesocosm(s) in which the disturbance(s) was applied. Hence, even if the air-water exchange is under- or overestimated, it will be estimated in the same way in all mesocosms. The comparison between the control and the other mesocosms will thus not be affected by the uncertainty related to the air-water exchange coefficient as long as the same coefficient is applied for all mesocosms and all mesocosms experience similar environmental conditions.

Annexe IV

Version publiée de l'article dont je suis co-auteur

Cette annexe contient la version publiée d'un article traitant de certaines données d'une expérience de mésocosmes présentée dans la thèse et dont je suis co-auteur.

Courboulès, J., F. Vidussi, **T. Soulié**, S. Mas, D. Pecqueur, and B. Mostajir. 2021. Effects of experimental warming on small phytoplankton, bacteria and viruses in autumn in the Mediterranean coastal Thau Lagoon. *Aquatic Ecology* **55**: 647–666. doi:10.1007/s10452-021-09852-7

Aquat Ecol
https://doi.org/10.1007/s10452-021-09852-7

Effects of experimental warming on small phytoplankton, bacteria and viruses in autumn in the Mediterranean coastal Thau Lagoon

Justine Courboulès · Francesca Vidussi · Tanguy Soulié · Sébastien Mas · David Pecqueur · Behzad Mostajir

Received: 16 October 2020 / Accepted: 9 March 2021
© The Author(s) 2021

Abstract To investigate the responses of a natural microbial plankton community of coastal Mediterranean waters to warming, which are still poorly known, an in situ mesocosm experiment was carried out in Thau Lagoon during autumn 2018. Several microorganisms, including virio-, bacterio-, and phytoplankton < 10 µm in size, were monitored daily and analysed using flow cytometry for 19 consecutive days in six mesocosms. Three mesocosms (control) had the same natural water temperature as the lagoon, and the other three were warmed by $+ 3$ °C in relation to the control temperature. The cytometric analyses revealed an unexpected community dominated by picophytoplanktonic cells, including *Prochlorococcus*-like and *Picochlorum*-like cells, which had not previously been found in Thau Lagoon. The experimental warming treatment increased the abundances of nanophytoplankton, cyanobacteria, bacteria and viruses during the experiment and triggered earlier blooms of cyanobacteria and picoeukaryotes. Only the abundance of *Picochlorum*-like cells was significantly reduced under warmer conditions. The growth and

Handling Editor: Télesphore Sime-Ngando.

J. Courboulès (✉) · F. Vidussi · T. Soulié · B. Mostajir
MARBEC (Marine Biodiversity, Exploitation and Conservation), Univ Montpellier, CNRS, Ifremer, IRD, Montpellier, France
e-mail: justine.courboules@hotmail.fr

F. Vidussi
e-mail: francesca.vidussi@cnrs.fr

T. Soulié
e-mail: tanguy.soulie@umontpellier.fr

B. Mostajir
e-mail: behzad.mostajir@umontpellier.fr

S. Mas
MEDIMEER (Mediterranean Platform for Marine Ecosystems Experimental Research), OSU OREME, CNRS, Univ Montpellier, IRD, IRSTEA, Sète, France
e-mail: sebastien.mas1@umontpellier.fr

D. Pecqueur
BioPIC Platform (Biology Platform of Imaging and Flow Cytometry) FR3724, Observatoire Océanologique de Banyuls-Sur-Mer Laboratoire Arago - SU/CNRS, Banyuls-sur-mer, France
e-mail: david.pecqueur@obs-banyuls.fr

Published online: 27 March 2021

grazing rates of phytoplankton and bacterioplankton estimated on days 2 and 8 showed that warming enhanced the growth rates of most phytoplankton groups, while it reduced those of bacteria. Surprisingly, warming decreased grazing on phytoplankton and bacteria at the beginning of the experiment, while during the middle of the experiment it decreased the grazing on prokaryote only but increased it for eukaryotes. These results reveal that warming affected the Thau Lagoon plankton community from viruses to nanophytoplankton in fall, inducing changes in both dynamics and metabolic rates.

Keywords Pico- and nanophytoplankton · Bacterioplankton · Virus · Warming · In situ mesocosm · Thau lagoon

Introduction

Small phytoplankton, such as picophytoplankton and nanophytoplankton, and nonphotosynthetic prokaryotes, such as heterotrophic bacteria and archaea (hereafter referred to as bacteria only), are key components of microbial food webs (Pomeroy 1974; Azam et al. 1983; Mostajir et al. 2015a). They play an important role in the production of biomass, which is transferred by microzooplankton to higher trophic levels through the marine food web. Planktonic microorganisms are known to rapidly respond to environmental change (Hays et al. 2005). Notably, the warming of surface waters in relation to global changes is expected to affect marine microorganisms (Hays et al. 2005; IPCC 2014).

For instance, an experimental increase in water temperature was reported to affect the relative abundance of phytoplankton, favouring small phytoplankton cells in the community, such as pico- and nanophytoplankton (Pulina et al. 2016). Additionally, using in situ mesocosms, Vidussi et al. (2011) reported a significant decrease in bacterial abundance, noting that trophic cascades led to this change. Changes in planktonic microorganism abundance are mainly shaped by individual growth and mortality rates (Calbet and Landry 2004). In general, predation by grazers is the main contributor to the plankton mortality rate (Calbet and Landry 2004); thus, grazing activity is a driver of plankton dynamics. This is particularly relevant during blooms, as strong phytoplankton growth is considered to be the main driver of bloom initiation, while intense grazing is responsible for ending the bloom (Trombetta et al. 2019). However, viruses are also considered to affect the plankton mortality rate because they infect and lyse both bacteria and small phytoplankton (Fuhrman 1999), thus partially regulating their populations. Both growth and grazing rates are dependent on the temperature (Brown et al. 2004) and are thus sensitive to thermal variation. Therefore, these two rates are of prime interest when investigating the effects of experimental warming on microbial communities and organisms.

Studies have reported that even a slight elevation of the water temperature could enhance metabolic rates, such as phytoplankton and bacterial growth (Eppley 1972; Rivkin et al. 1996; Savage et al. 2004; Lewandowska et al. 2014). Similarly, other studies reported a positive effect of warming on the abundances of their corresponding grazers such as herbivorous and bacterivorous protists (Aberle et al. 2007; Rose and Caron 2007; Rose et al. 2009), thus potentially increasing grazing pressure. However, in a natural environment, the plankton growth rate is also affected by factors other than just temperature, including physical, chemical or biological forcings (i.e. light, nutrients, biological interactions). Therefore, increasing temperature does not systematically result in higher growth rates and then abundances, especially considering that warming can also affect these other forcings. Similarly, the stimulation of grazer activity under warming can also result in complex interactions, such as trophic cascades (Vidussi et al. 2011), leading to nonintuitive changes in grazing and mortality rates (Lewandowska et al. 2014). Thus, it is essential to study the responses of natural plankton communities to warming from very sensitive regions such as the Mediterranean Sea (Giorgi 2006; Lejeusne et al. 2010) or coastal waters (Rabalais et al. 2009). In this context, as studies of experimental warming are scarcer during fall, the autumnal in situ plankton community of the coastal Mediterranean Thau Lagoon was investigated. Thau Lagoon is connected by channels to the Mediterranean sea, and has a salinity varying from 29.6 to 40.8 (Derolez et al. 2020b). This lagoon is rather shallow, with a mean depth of 4 m, and therefore is experiencing a great range of temperature variations through the

year (Trombetta et al. 2019). Phytoplankton of Thau Lagoon is numerically dominated by a picophytoplankton community usually represented by prasinophytes (Bec et al. 2005). Cyanobacteria are generally observed in lesser abundances and only represented by the *Synechococcus* genus (Bec et al. 2005). The nanophytoplankton, which can dominate the phytoplankton community in term of biomass (Trombetta et al. 2019), is characterised by cryptophytes, chrysophytes and prymnesiophytes (Bec et al. 2011; Trombetta et al. 2019). Microphytoplankton are mainly represented by diatoms and dinoflagellates are generally less abundant, excepted during exceptional blooms (Derolez et al. 2020b). Thus, the phytoplankton community of Thau Lagoon is generally dominated by small phytoplankton (Trombetta et al. 2020). Bacteria are also highly abundant in the lagoon, their abundances ranging from 2.0 to 10.0×10^6 cells cm^3 (Vidussi et al. 2011; Mostajir et al. 2015b). The grazers of these small phytoplankton and bacterial communities are mainly the heterotrophic flagellates and ciliates, as well as larger zooplankton such as rotifers, nauplii, and copepods (Lam-Hoai et al. 1997; Pecqueur et al. 2011).

To unravel how Thau Lagoon plankton community responds to warming, an in situ mesocosm study was conducted in this lagoon during the fall season. For this purpose, the water temperature of triplicate in situ mesocosms was increased by 3 °C (warmed mesocosms) compared to that of three other in situ mesocosms with natural lagoon water temperature (control mesocosms) to reproduce the predicted mean elevation in temperature expected for the Mediterranean region (IPCC 2007). To better reflect natural temperature changes over the course of the experiment, the warming procedure involved the continuous adjustment of the temperature of the warmed mesocosms by + 3 °C relative to that of the control mesocosms to follow natural nycthemeral and daily water temperature variations (Nouguier et al. 2007). The microbial community was sampled daily and analysed at fine cytometric resolution during the 19 days of the experiment, with the evaluation of viruses up to nanophytoplankton, including picoeukaryotes and cyanobacteria as well as bacteria. As a result, some unexpected picophytoplankton groups such as *Prochlorococcus*-like and *Picochlorum*-like cells were identified for the first time in Thau Lagoon. In addition, the growth and grazing rates of the phytoplanktonic and bacterial groups were estimated according to the 2-point dilution method two times during the experiment to determine the effect of an increase in water temperature on these specific rates. Finally, the biomass fluxes of the studied microbial components were estimated based on previous rate estimates to determine the effects of warming on biomass production and transfer through the system.

Material and methods

In situ mesocosm experiment

A mesocosm experiment was conducted from October 5 to 23, 2018, to assess the response of a natural autumnal plankton community to the mean warming expected to occur in the Mediterranean region by 2100 (IPCC 2007). Six mesocosms were immersed in the Mediterranean Thau Lagoon in southern France near the floating structure of the Mediterranean platform for Marine Ecosystems Experimental Research (MEDIMEER 43°24′00″ N, 3°36′00″ E). The mesocosms were all simultaneously filled on October 4th with 2200 dm^3 of lagoon subsurface water that was beforehand filtered through 1000 µm mesh and pooled in a tank on the MEDIMEER pontoon, before being distributed to the six mesocosms through 6 parallel pipes. The mesocosm bags were 1.2 m wide and 3 m long and installed on individual floating structures. Once filled, each mesocosm represented a 2-m water column immersed in the lagoon. The mesocosms were constructed with 200-µm-thick vinyl acetate mixed-polyethylene transparent film reinforced by nylon mesh (Insinööritoimisto Haikonen Ky). All bags were also covered by a transparent dome made of crystal-clear polyvinyl chloride to prevent external inputs and transmitting 73% of the photosynthetically active radiation (PAR). Finally, a pump (Rule 360) was installed in each mesocosm to provide gentle mixing of the water column with a turnover time of 3.5 d^{-1}.

Two treatments, each performed in triplicate, were applied in the present study: (1) the control, with a natural water temperature showing the same daily variations as the surrounding water in the lagoon, and (2) the warmed treatment, in which the temperature was elevated by 3 °C on the basis of model predictions generated by the Intergovernmental Panel on Climate Change (IPCC). On October 5th (day 0 of the

experiment), the water temperature in the mesocosms under the warmed treatment was raised, after the samples were collected for that day, to reach a target of + 3 °C on October 6th prior to sampling. This target temperature was then maintained until the end of the mesocosm experiment on October 23rd. The increase in water temperature was achieved by using a heating element (Galvatec) placed in each mesocosm in the warmed treatment to continuously adjust the temperature to 3 °C higher than that in the control to reflect natural water temperature conditions. Therefore, both the control and warmed mesocosms followed the same day/night and daily natural temperature fluctuations as the surrounding water in the lagoon but with a 3 °C increase in the warmed treatment (Nouguier et al. 2007).

To prevent accidental contamination and changes in the light conditions within the experimental mesocosms, two incubation mesocosms (1.2 m wide, 2 m long) were also immerged in the lagoon near the six experimental mesocosms to incubate the samples taken from the control and heated mesocosms for parallel experiments, such as dilution experiments and Winkler incubations.

Sampling and analyses of the physical and chemical properties of the experimental mesocosms

Daily sampling of all mesocosms was carried out every morning (09:00 h local time) from October 5th until October 23rd (representing day 0–18 of the experiment). Temperature and salinity in all the mesocosms were monitored at the surface and at 1 m and 2 m depth using an EC300 (VWR) probe. A Niskin bottle (5 dm^3) was deployed inside each mesocosm at 1 m depth to collect water for the assessment of chemical variables. Samples for nutrient analyses (50 cm^3) were carefully taken from the Niskin bottles with acid-washed polycarbonate bottles. The samples were then filtered on 0.45-µm filters (Gelman) and stored at − 20 °C. An automated colorimeter (Skalar Analytical) was used to determine the concentrations of nitrate (NO_3^-), nitrite (NO_2^-), orthophosphate (PO_4^{3-}), and silicate (SiO_2).

Sampling, Chl-*a* and flow cytometric plankton community analyses

All mesocosms were sampled daily (09:00 h) using two low-vacuum pumps connected in series (KNF-N035AN.18) placed at 1 m depth in each mesocosm to fill acid-washed polycarbonate carboys (20 dm^3) for biological analyses. This notably included the samples for cytometry and chlorophyll *a* (Chl-*a*) analyses. For Chl-*a* analyses, 0.5–1 dm^3 of the mesocosms water was daily filtered over Whatman glass-fibre filters (GF/F 25 mm diameter). Filters were frozen in liquid nitrogen and then stored at − 80 °C until analyses. Chl-*a* concentrations were determined by high-performance liquid chromatography (HPLC, waters), using the method of Zapata et al. (2000), following the protocol of Vidussi et al. (2011).

Daily abundances of small phytoplankton, bacteria and viruses, from day 1 to day 18 of the experiment (October 5 and 23, respectively) were determined through flow cytometry (FCM) analyses. For this purpose, three samples of 1.5 cm^3 were taken from the carboys to analyse separately the microorganisms. Phytoplankton and bacteria samples were fixed with 60 mm^3 of glutaraldehyde (Grade 1), and viruses samples were fixed with 30 mm^3 of glutaraldehyde (Grade 1 filtered over 0.02 µm), frozen in liquid nitrogen and stored at − 80 °C. All phytoplankton groups were analysed simultaneously with a CytoFLEX flow cytometer (Beckman Coulter) for 3 min at high speed. Cyanobacteria were identified and counted on the basis of their relative forward scatter (FSC) and phycoerythrin and phycocyanin fluorescence (Fig. 1). Picoeukaryotes and nanophytoplankton were enumerated according to their FSC and Chl-*a* fluorescence. All bacterial samples were analysed using a FACSCalibur flow cytometer (Becton–Dickinson) for 3 min at low speed after being stained with SYBR Green I (S7563, Invitrogen; 2% final dilution) (Marie et al. 1997). Bacterial groups were identified and counted on the basis of their relative side scatter (SSC) and green fluorescence at 530/30 nm. Viruses were analysed using a FACSCanto2 flow cytometer (Becton–Dickinson). Samples were stained with SYBR Green I (at a final dilution of 0.5×10^{-4}). Then, virus-like particles (hereafter referred to as viruses for simplification) were counted according to their SSC and green fluorescence at 530/30 nm (Brussaard 2004). Cytometry fluorescent beads (Polysciences, Inc.) of 1, 2, 6

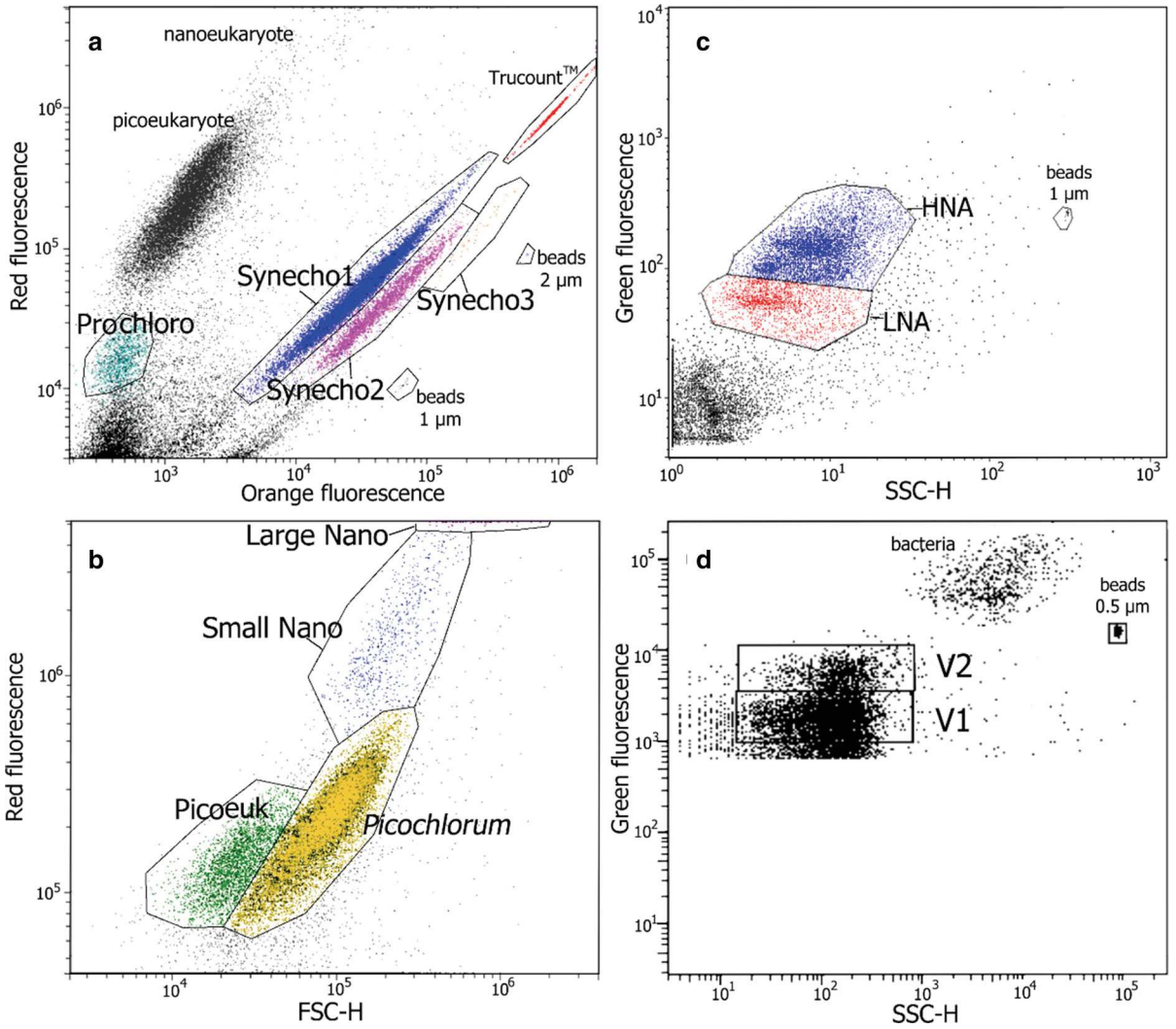

Fig. 1 The 12 different microbial groups (including viruses) identified by flow cytometry analyses. Among the cyanobacteria, there was one *Prochlorococcus*-like group, Prochloro, and three *Synechococcus*-like groups, Synecho1, Synecho2 and Synecho3 (**a**). There were also two picoeukaryote groups, Picoeuk and *Picochlorum*-like, (**b**) and two nanoeukaryote groups: Small Nano and Large Nano (**b**). Two bacterial groups, HNA and LNA (**c**), were identified, as well as two virus groups named V1 and V2 (**d**). FSC: forward scatter signal linked to size and SSC: side scatter, signal linked to the cell structure and granulosity

and 10 µm in diameter were used for phytoplankton sample analyses as internal cell size standards. This was also done for bacterial sample analyses with cytometry beads of 1 and 2 µm in diameter and for virus samples with beads of 0.5 µm in diameter (Polysciences, Inc.). In addition, Trucount™ beads were added to accurately estimate the volume of sample analysed (BD-Biosciences). On the basis of these FCM analyses, the concentration of each plankton group identified was estimated daily (cells cm^{-3}) from day 1 to day 18 of the experiment.

Analyses according to FCM revealed 8 phytoplanktonic, two bacterial and two viral groups. Three groups of phytoplankton had a similar fluorescence signature than *Synechococcus* cells. These *Synechococcus*-like cells were therefore called Synecho1, Synecho2 and Synecho3 (Fig. 1a). Another phytoplankton group had a fluorescence signature similar to *Prochlorococcus* cells (Chisholm 2017) and was thus

identified as *Prochlorococcus*-like cells and labelled Prochloro. Two groups of picoeukaryotes were also identified, one group usually found in Thau Lagoon named Picoeuk and another with a fluorescence signature similar to that of *Picochlorum* (Fig. 1b). Finally, two groups of nanophytoplankton with size ranges of approximately between 2 and 6 µm and between 6 and 10 µm were also present and were labelled Small Nano and Large Nano, respectively (Fig. 1b). Heterotrophic bacteria were distinguished in two groups: low nucleic acid (LNA) and high nucleic acid (HNA) according to their low and high amounts of nucleic acid, respectively (Fig. 1c). Finally, two groups of viruses were identified and labelled V1 and V2 (Fig. 1d).

To estimate the carbon biomass (µg C dm^{-3}) of each cytometric group, the phytoplankton and bacterial abundances were converted using previously published conversion factors: i.e. 20 fg C $cell^{-1}$ for bacteria (Sime-Ngando et al. 1995), 210 fg C $cell^{-1}$ for *Synechococcus* (Kemp et al. 1993), and 45 fg C $cell^{-1}$ for *Prochlorococcus* (Bertilsson et al. 2003). For the other phytoplankton groups, carbon biomass was estimated based on their relative volume by assuming a spherical shape for all groups and considering a conversion factor of 0.22 pg C μm^{-3} (Kemp et al. 1993). For this calculation, we estimated the approximate diameter of cells within a group by comparing their average forward scatter signal (approximate size) with that of the previously mentioned standard beads, assigning 1.0 and 1.5 µm diameter to Picoeuk and *Picochlorum*, respectively, and 4 and 8 µm to Small and Large Nano, respectively (Trombetta et al. 2019).

Growth and grazing rate estimation for phytoplankton and bacteria

The cell growth and grazing rates for each group in each mesocosm were estimated at the beginning (day 2) and halfway (day 8) through the experiment. For this purpose, a modified version of the original dilution method of Landry and Hassett (1982), using only 2 levels of dilution: 100% and 10%, was performed (Worden and Binder 2003; Strom and Fredrickson 2008; Menden-Deuer and Fredrickson 2010). After the daily sampling was performed, 20 dm^3 of water was gently collected from every mesocosm using a vacuum pump and filtered through 200 µm mesh. Triplicate Whirlpack bags (2 dm^3) were then filled with this filtered sample to constitute the level of 100%. To constitute the triplicate bags (2 dm^3) of the 10% sample dilution, some of the filtered sample was gravity filtered at 0.8 and 0.2 µm (Whatman Polycap TC Filter Capsule 0.8/0.2 µm) and used to dilute the previously filtered water to 10%. An additional set of triplicate of the undiluted (100%) filtered water was prepared and enriched with inorganic nutrients (final concentration of 4 µM N, 0.25 µM P, and 4 µM Si). This 100% + nutrient (NUT) addition allowed us to determine whether nutrients were limited during the dilution experiments. All bags were then placed in the incubation mesocosms for 24 h.

To determine the plankton abundances, two samples of 1.5 cm^3 were taken for FCM analyses from all 100% bags before incubation (T0) and from bags at all dilution levels (10%, 100%, 100% + NUT) after incubation (T24).

Instantaneous growth rates (k, d^{-1}) were then calculated for each group at every level of dilution following Eq. (1) (Landry and Hassett 1982):

$$k = \frac{1}{t} \times \ln\left(\frac{\mathrm{NT24}}{\mathrm{NT0}}\right) \quad (1)$$

where k is the instantaneous growth rate (d^{-1}) estimated from the initial and final plankton abundances, NT0 and NT24, respectively, during the incubation time, t (d). The initial (T0) plankton abundance at the 10% level was calculated from the plankton abundances quantified at the 100% level before incubation. The final growth rate was determined as the instantaneous growth rate at 10%, and the grazing rate was calculated as the difference in the instantaneous growth rate at 10 and 100% (Worden and Binder 2003; Strom and Fredrickson 2008; Menden-Deuer and Fredrickson 2010; Chen 2015).

In particular cases, negative growth and positive grazing rates (inverted slope) were considered as 0.01 d^{-1} growth and 0.00 d^{-1} grazing, respectively (Calbet and Landry 2004).

It should be noted that the growth rate estimated in the present study is not characterised as the maximal growth rate estimated according to the original method described by Landry and Hassett (1982). Indeed, the growth rates presently reported were not amended in the case of nutrient limitation; however, these specific cases are discussed, as they potentially occurred in the

mesocosms and were also under the effect of warming. Thus, the growth rates estimated in the present investigation represent a rate closer to what occurred in the mesocosms, encompassing the potential nutrient limitations that affected the natural plankton community.

Statistical analyses

To evaluate the effect of warming throughout the experiment, mean abundance time series were compared between the treatments using variance analyses of repeated measures (RM-ANOVA, p value < 0.05). More precisely, comparisons were performed when the warmed mesocosms reached the target temperature during the experiment (from day 1 to 18). Due to the observation of specific abundance trends, additional RM-ANOVAs were also performed over different periods for certain groups: from day 3 to 9 and 11 to 15 for Synecho1; from day 1 to 7 and 8 to 18 for Picoeuk; and from day 3 to 9 and 11 to 17 for HNA. Normality and homogeneity of variance were assessed, and data were occasionally log transformed to meet these assumptions. When the assumption of normality could not be met, a Kruskal–Wallis test was performed instead. Average growth and grazing rates were also compared between treatments. However, as the sample size was not sufficient to accurately verify normality and variance homogeneity, comparisons between treatments were performed using the Kruskal–Wallis test (p value < 0.05). Similarly, to determine whether inorganic nutrient addition had any significant effect on the various cytometric groups, instantaneous growth rates estimated for the 100% and 100% + NUT treatments were compared with the Kruskal–Wallis test. All data management and statistical analyses were performed using R software (R Project version 3.6).

Results

Temperature, nutrients and chlorophyll-a variability in the mesocosms

The average temperature across the triplicate control mesocosms decreased from 18.9 to 18.3 °C from day 1 to 4 and then increased, reaching 19.4 °C on day 9 (Fig. 2a). The average temperature then declined to

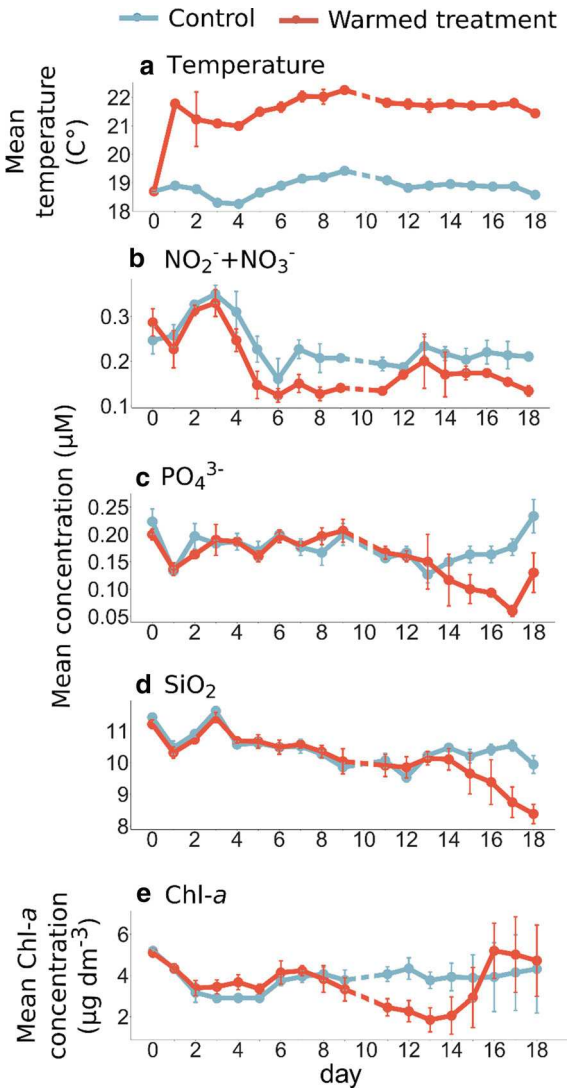

Fig. 2 Daily average temperature (**a**), and concentrations of nitrates + nitrites (**b**, NO_2^-, NO_3), orthophosphates (**c**, PO_4^{3-}), silicates (**d**, SiO_2) and chlorophyll-*a* (Chl-*a*, e) in the control (blue) and warmed mesocosms (red). Error bars represent the standard error of the mean. Dotted lines represent the missing data for day 10 due to bad meteorological conditions

18.6 °C by the end of the experiment (day 18). In the warmed treatment, the water temperature was successfully raised by an average of 2.8 °C (± 0.11 °C, $n = 54$) over the course of the experiment (from day 1 to 18).

The mean concentrations of nitrates + nitrites ($NO_2^- + NO_3^-$) and orthophosphate (PO_4^{3-}) were rather low during the experiment in the control mesocosms, reaching averages of 0.23 (± 0.02,

n = 57) and 0.18 (± 0.01, n = 57) µM, respectively (Fig. 2b, c). Silicates (SiO_2) occurred in relatively high concentrations, in contrast, reaching an average of 10.45 (± 0.15, n = 57) µM in the control (Fig. 2d). The nutrient concentrations were significantly lower under warming than in the control mesocosms. Notably, the mean $NO_2^- + NO_3^-$ concentration was 0.19 (± 0.02, n = 57) µM on average over the course of the experiment in the warmed treatment. The orthophosphate and silicate concentrations were rather similar within the treatments from day 0 to 13, and then they decreased in average under warming, reaching the lowest concentrations of 0.06 µM for orthophosphates on day 17 and 8.38 µM for silicates on day 18.

Chl-*a* concentrations were high during the whole experiment, attaining in average 3.84 (± 0.62, n = 57) µg dm^{-3} in the control (Fig. 2e). In the warmed treatment, Chl-*a* concentrations were similar to the control until day 7, after which it strongly decreased by 51% compared to the control, attaining 1.85 µg dm^{-3} on day 13. After day 13, concentrations in the warmed treatment increased, reaching 5.19 µg dm^{-3} on day 16, and even overcame concentrations in the control (Fig. 2e).

Phytoplankton, bacteria and virus dynamics in the control mesocosms

Among the different evaluated phytoplankton groups, Synecho1 and *Picochlorum* were the most abundant, reaching 2.1×10^5 (± 0.9×10^5, n = 57) and 7.8×10^4 (± 2.1×10^4, n = 57) cells cm^{-3} on average, respectively. Then, there were Synecho2, Prochloro and Picoeuk which abundances, ranging from 1.3×10^4 (± 0.8×10^4, n = 57) to 2.6×10^4 (± 4.4×10^4, n = 57) cells cm^{-3} on average. Other phytoplankton groups were the least abundant ranging from 230 (± 70, n = 57) to 5.8×10^3 (± 4.4×10^3, n = 57) cells cm^{-3} on average. The experiment began with high abundances of all phytoplanktonic groups in all mesocosms (Fig. 3). Then, the abundances generally decreased over time among all groups except for Synecho1 and Picoeuk, which abundances increased and then decreased, forming the bell-shape dynamic indicating a bloom, from day 3 to 11 and from day 6 to 8, respectively (Fig. 3a1, b1). In particular, Synecho1 reached a peak in abundance of 3.5×10^5 cells cm^{-3} on day 11, while Picoeuk reached a maximal abundance of 1.9×10^4 cells cm^{-3} on day 8.

Among the two bacterial groups, HNA had the highest abundance, with 3.0×10^6 (± 0.8×10^6, n = 57) cells cm^{-3} on average during the whole experiment, while LNA abundances were lower at 1.3×10^6 (± 0.9×10^6, n = 57) cells cm^{-3}. Bacteria followed the general trend of that of phytoplankton, with initial high abundances followed by a general decrease (Fig. 3c). However, HNA abundance also followed the same trend as the blooming Synecho1, with an increase from day 3, reaching a maximum abundance of 3.7×10^6 cells cm^{-3} on day 13, followed by a decrease. On the other hand, LNA abundances decreased at the beginning of the experiment and then remained at approximately 8.8×10^5 (± 1.2×10^5, n = 57) cells cm^{-3} on average until the end of the experiment.

In contrast, virus abundances generally increased from the beginning to the end of the experiment from 3.5×10^7 (day 0) to 5.9×10^7 viruses cm^{-3} (day 18) for V1, and from 7.8×10^6 (day 0) to 1.1×10^7 viruses cm^{-3} (day 18) for V2 (Fig. 3d).

Effects of warming on the dynamics and abundances of phytoplankton, bacteria and viruses in the heated mesocosms

In general, warming significantly increased the abundances of most cyanobacteria and nanophytoplankton groups by 21–264% on average (Fig. 4, Table 1). In addition, for Picoeuk and Synecho1, which bloomed, abundances were significantly higher in the warmed treatment than in the control prior to reaching their maximal abundances, which occurred 2–3 days earlier under warming than under control conditions. Afterward, the abundances of these two groups decreased sharply and were then significantly lower in the warmed treatment than in the control (Fig. 4, Table 1). A notable exception to these results was observed for *Picochlorum*, which was the only phytoplanktonic group showing a significant decrease in abundance with warming, with 25% lower abundances in the warmed treatment than in the control. More specifically, the abundances of *Picochlorum* were similar in the two treatments until day 5 but then decreased in the warmed mesocosms until the end of the experiment.

Bacteria showed a similar response to warming to that of the phytoplankton groups (Fig. 4, Table 1).

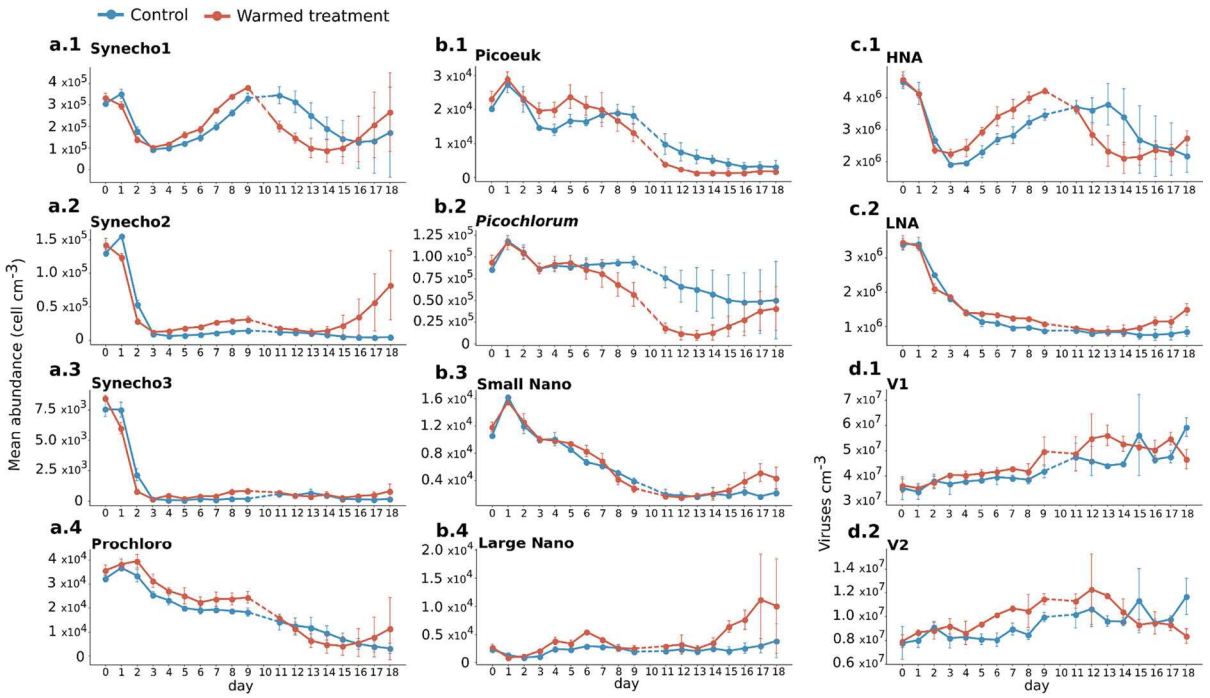

Fig. 3 Daily mean abundances of cyanobacteria (**a.1**, **4**), picophytoeukaryotes (**b.1**, **2**), nanophytoplankton (**b.3**, **4**), bacteria (**c.1**, **2**) expressed as cells cm^{-3}, ± standard deviations, and mean abundances of viruses (**d.1**, **2**) expressed as viruses cm^{-3}, ± standard deviations in the controls (blue) and warmed (red) treatments. Dotted lines represent the missing data from day 10 due to bad meteorological conditions

LNA abundances were consistently higher by 19% on average in the warmed treatment than in the control. Similar to those of Synecho1, HNA abundances were significantly higher in the warmed treatment than in the control from day 3 to 9, before reaching a maximal abundance of 15% higher 4 days earlier than in the control. Afterward, the HNA abundances also sharply decreased and were significantly lower in the warmed treatment than in the control from day 11 to 17.

Similar to the bacteria, the V1 and V2 groups were 7% more abundant on average in the warmed treatment than in the control (Fig. 4, Table 1).

Effects of warming on carbon biomass repartition

In the control mesocosms, the phytoplankton groups (< 10 µm) were the main contributors to the daily carbon biomass (derived from abundances), representing 60% of the estimated carbon biomass on average (phytoplankton < 10 µm + bacteria) and ranging from 78 to 287 µg C dm^{-3} (Fig. 4a). Bacteria represented 40% of the estimated carbon biomass, ranging from 61 to 158 µg C dm^{-3}. The total phytoplankton (< 10 µm) and bacterial carbon biomass estimated in the control mesocosms was the highest at the beginning of the experiment (day 1), reaching 438 µg C dm^{-3}. Then, the estimated carbon biomass decreased from day 1 to day 3 before increasing and reaching a second maximum of 240 µg C dm^{-3} on day 9. The carbon biomass then decreased to 142 µg C dm^{-3} on day 17 (the end of the experiment) (Fig. 4a).

In the warmed mesocosms, phytoplankton (< 10 µm) also represented 60% of the estimated carbon biomass, while bacteria represented 40%. However, after the initial high carbon biomass value in the warmed treatment, the maximal estimated carbon biomass was 13% higher than that in the control and occurred two days earlier, reaching 271 µg C dm^{-3} on day 7 (Fig. 4b). Finally, the summed daily phytoplankton and bacterial carbon biomass values were only 6 and 4% higher, respectively, in the warmed treatment than in the control treatment.

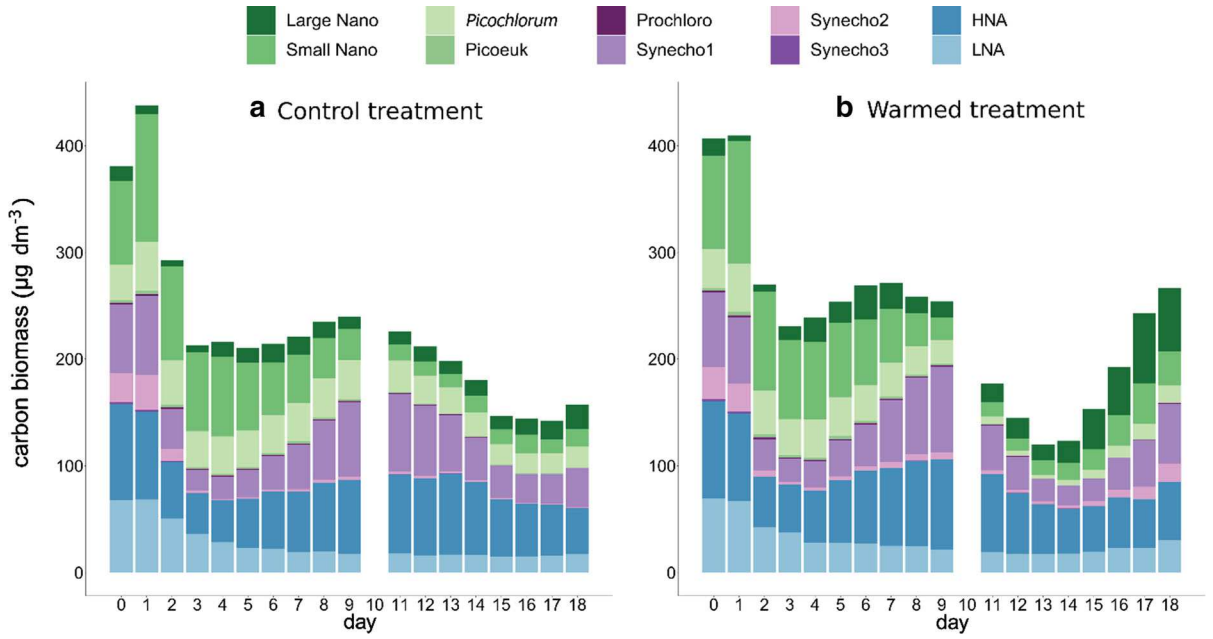

Fig. 4 Histograms of the cumulative daily average carbon biomass (µg C dm^{-3}) estimated for different phytoplankton (< 10 µm) and bacterial groups in the triplicate control (**a**) and triplicate warmed (**b**) mesocosms. Bacterial groups (LNA and HNA) are represented in shades of blue, cyanobacteria (Prochloro, Synecho1, Synecho2, Synecho3) are represented in purple, and phytoeukaryotes (Picoeuk, *Picochlorum*, Small Nano and Large Nano) are represented in green

Phytoplankton and bacterial growth and grazing rates

Growth and grazing rates were estimated for the phytoplankton and bacterial groups twice over the course of the experiment, at the beginning (day 2) and in the middle of the experiment (day 8) during the period when Synecho1 exhibited a bloom and the HNA bacterial group reached a high abundance. In the control on day 2, Large Nano had the highest growth rate of 1.16 d^{-1}, followed by bacterial groups, with growth rates ranging from 0.65 to 0.77 d^{-1}, and Small Nano, with a growth rate of 0.35 d^{-1} (Fig. 5a). In contrast, the other phytoplankton groups had relatively low growth rates, ranging from 0.01 to 0.07 d^{-1}. On day 8, the Large Nano and both the HNA and LNA bacterial groups still showed high growth rates of 0.61, 0.65 and 0.79 d^{-1}, respectively, and Synecho3 reached a high growth rate of 0.50 d^{-1} (Fig. 5b).

Warming generally enhanced the growth rates of the phytoplankton. Both picophytoplankton groups of Picoeuk and *Picochlorum,* in particular, showed growth rates significantly higher in the warmed treatment than in the control, with an increase of approximately 150%, on day 2 (Fig. 5a, Table 2). Similarly, on day 8, the growth rates of most phytoplankton groups were higher in the warmed treatment, especially among Prochloro, Picoeuk and Small Nano, whose growth rates were significantly higher by 150–750% than in the control (Fig. 5b, Table 2). In contrast to this general trend, warming appeared to have a negative effect on bacterial group growth rates, with consistently negative effects on LNA and HNA, showing a higher growth rate only once at the beginning of the experiment. In fact, on day 2, the HNA growth rate was significantly higher by 29% in the warmed treatment than in the control, while that of LNA was 14% lower. Afterwards, on day 8, both LNA and HNA growth rates were lower by 42 and 17%, respectively, under warmer conditions than in the control treatment (Fig. 5, Table 2).

To further analyse the growth rate response of the cytometric groups, nutrients were added to determine whether any nutrient limitation occurred during the dilution experiment (Fig. 6). However, among those of the 10 studied groups, only the instantaneous growth rate of Large Nano was consistently significantly enhanced by the addition of nutrients regardless of the treatment (control or warmed) on days 2 and 8, with

Table 1 Summary of the *p* values from the RM-ANOVA comparing Chl-*a* concentrations, nutrient concentrations and cell abundances in each group resolved by flow cytometry over different periods during the experiment

Variables		Periods	*p* values
Chl-*a* concentrations ($\mu g\ dm^{-3}$)		1–18	0.39
Nutrient concentrations (μM)	$NO_2^- + NO_3^-$	1–18	**8.5×10^{-5}**
	PO_4^{3-}	1–18	**3.9×10^{-4}**
	SiO_2	1–18	**2.1×10^{-4}**
Cell group abundance (cell cm^{-3})	Synecho1	1–18	0.56
	Synecho1	3–9	**4.1×10^{-3}**
	Synecho1	11–15	**5.5×10^{-3}**
	Synecho2	1–18	**7.5×10^{-8}**
	Synecho3	1–18	**6.5×10^{-3}**
	Prochloro	1–18	**2.2×10^{-2}**
	Picoeuk	1–18	0.59
	Picoeuk	1–7	**8.5×10^{-3}**
	Picoeuk	8–18	**2.0×10^{-4}**
	Picochlorum	1–18	**1.1×10^{-3}**
	Small Nano	1–18	0.1
	Large Nano	1–18	**3.0×10^{-4}**
	LNA	1–18	**0.01**
	HNA	1–18	0.89
	HNA	3–9	**7.5×10^{-5}**
	HNA	11–17	**0.03**
Viruses group abundance (viruses cm^{-3})	V1	1–18	**0.02**
	V2	1–18	0.11

p values smaller than or equal to 0.05 were considered significant and are highlighted in bold characters

instantaneous growth rates increasing by 101–224% upon nutrient addition depending on the treatment and the day. Additionally, only three other groups (Small Nano, Synecho3 and HNA) showed significantly higher rates under nutrient enrichment than without on day 8 and only in the warmed treatment.

The analyses of grazing mortality rates in the control revealed that on day 2, the grazing mortality rates were particularly high for the *Synechococcus*-like groups, with the rates for Synecho3 and Synecho2 reaching 1.40 and 1.26 d^{-1}, respectively (Fig. 5, Table 2). The grazing mortality rates for the other phytoplankton groups were lower, ranging from 0.18 to 0.62 d^{-1}. Bacterial grazing mortality rates were particularly high on day 2, reaching 1.19 and 1.09 d^{-1} for LNA and HNA, respectively (Fig. 5, Table 2). On day 8, the grazing mortality rates for Synecho3 and bacterial groups HNA and LNA decreased by approximately two times, although Synecho3 still showed the highest rates among the phytoplankton groups, with a value of 0.60 d^{-1}, while the rates of the other phytoplankton groups ranged between 0.05 and 0.44 d^{-1}.

In the warmed treatment, the grazing mortality rates for most phytoplanktonic groups were lower than those in the control on day 2, with values decreasing by 13–57% (Fig. 5c). This difference was significant for all *Synechococcus*-like groups (Synecho1, 2, and 3) and Picoeuk (Table 2). The grazing mortality rates for cyanobacteria (Synecho1, 2, and 3 and Prochloro) were still lower on day 8, with values that were 30–69% lower under warmer conditions than in the control and being significantly lower for Synecho1 and Synecho2 (Table 2). Additionally, the grazing mortality rates for both HNA and LNA cell groups were significantly lower by 11–55% in the warmed treatment than in the control on both day 2 and day 8 (Fig. 5c, Table 2). In contrast, on day 8, the grazing mortality rates for almost all eukaryotic phytoplanktonic groups studied showed an opposite trend, with values higher by 46–156% in the warmed treatment

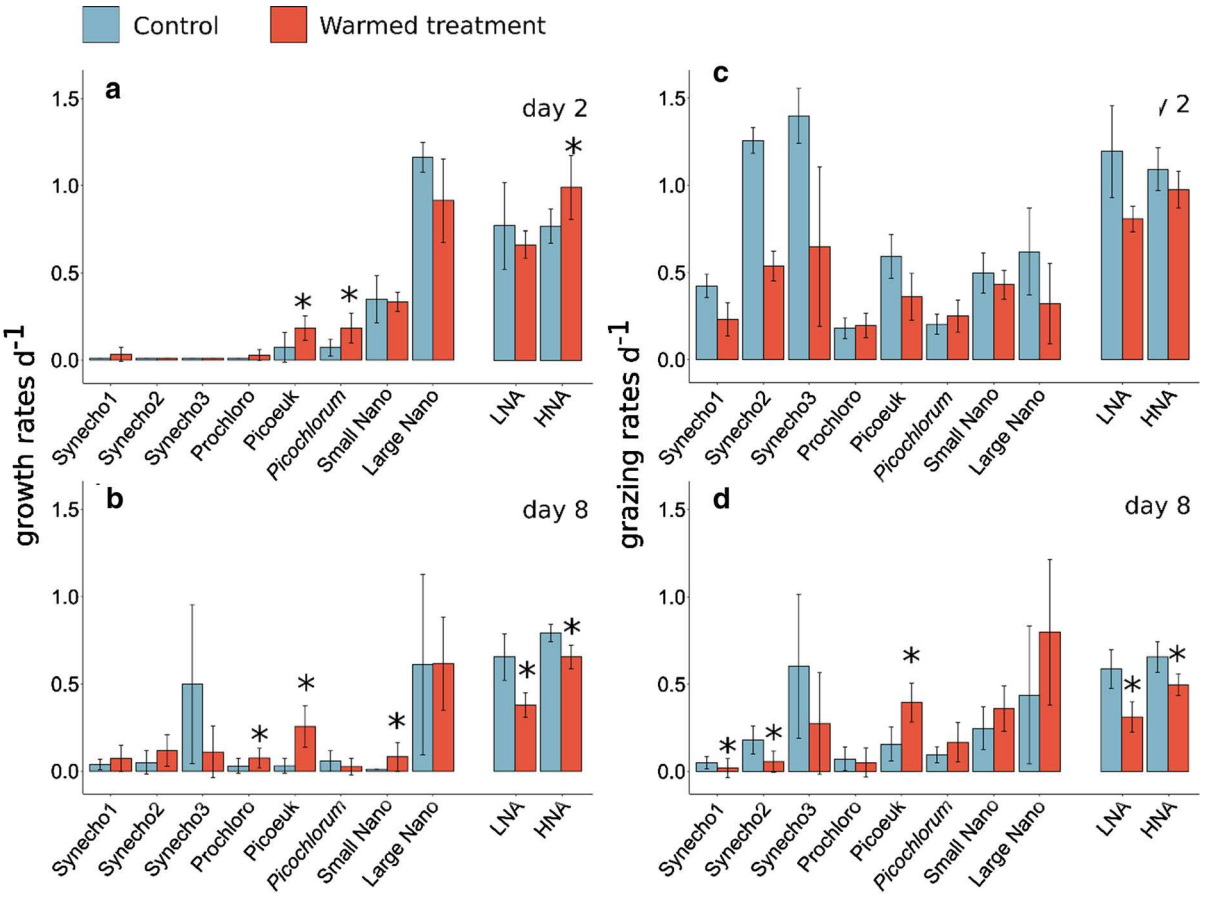

Fig. 5 Determination on day 2 and day 8 of the mean growth rates (d^{-1}; **a**, **b**) and grazing rates (d^{-1}; **c**, **d**) for phytoplankton and bacterial groups in the control (blue) and warmed treatment (red) according to the dilution method. The error bars represent standard deviations from the means. *When the mean rate estimated in the warmed treatment is significantly different from that in the control treatment (Kruskal–Wallis $p < 0.05$)

than in the control and this difference being significant for Picoeuk (Fig. 5d, Table 2).

Discussion

An unexpected autumnal plankton community in Thau Lagoon

This study shows that the phytoplankton community investigated in October 2018 was quite different from what is usually expected at this season in Thau Lagoon. For instance, in the present study, the Chl-*a* concentration, ranging from 2.90 to 5.19 µg dm^{-3}, was higher than what was previously reported in October in Thau Lagoon, ranging from 0.61 to 3.55 µg dm^{-3} (Pecqueur et al. 2011; Mostajir et al. 2015b; Trottet et al. 2016; Fouilland et al. 2017). These higher Chl-*a* concentrations were surprising considering the fact that the nutrient concentrations measured in the present investigation were within the range as those reported in previous works in October in Thau Lagoon (Pecqueur et al. 2011; Mostajir et al. 2015b; Trottet et al. 2016; Fouilland et al. 2017). Nonetheless, these high Chl-*a* concentrations observed during the present autumnal study were similar to what was recently reported during winter and spring phytoplankton blooms in Thau Lagoon (Trombetta et al. 2019). However, the fact that the dynamic of Chl-*a* concentration observed in the present study was flat despite high values was quite unusual for the study site, suggesting peculiar conditions more similar to a dysfunctional situation leading to Chl-*a* accumulation than to a seasonal bloom. The

Table 2 Summary of the growth and grazing rates and in parentheses the p values from the Kruskal–Wallis test for the comparison between the control and warmed treatments

	Cell group	Growth rates (d^{-1})			Grazing rates (d^{-1})		
		Control	Warmed treatment		Control	Warmed treatment	
Day 2	Synecho1	0.01	0.03	(0.07)	0.42	0.23	**(< 0.001)**
	Synecho2	0.01	0.01	(–)	1.3	0.54	**(< 0.001)**
	Synecho3	0.01	0.01	(–)	1.4	0.65	**(3.0×10^{-3})**
	Prochloro	0.01	0.03	(0.07)	0.18	0.2	(0.57)
	Picoeuk	0.07	0.18	**(0.01)**	0.59	0.36	**(3.0×10^{-3})**
	Picochlorum	0.07	0.18	**(5.0×10^{-3})**	0.2	0.25	(0.23)
	Small Nano	0.35	0.33	(0.90)	0.5	0.43	(0.10)
	Large Nano	1.16	0.91	(0.06)	0.62	0.32	(0.08)
	LNA	0.77	0.66	**(0.01)**	1.19	0.81	**(< 0.001)**
	HNA	0.77	0.99	(0.57)	1.09	0.97	(0.06)
Day 8	Synecho1	0.04	0.07	(0.40)	0.05	0.02	(0.02)
	Synecho2	0.05	0.12	(0.09)	0.18	0.06	**(4.0×10^{-3})**
	Synecho3	0.5	0.11	(0.08)	0.6	0.27	(0.08)
	Prochloro	0.03	0.08	**(0.05)**	0.07	0.05	(0.39)
	Picoeuk	0.03	0.26	**(1.0×10^{-3})**	0.16	0.39	**(2.0×10^{-3})**
	Picochlorum	0.06	0.03	(0.11)	0.10	0.17	(0.07)
	Small Nano	0.01	0.08	**(0.02)**	0.25	0.36	(0.10)
	Large Nano	0.61	0.62	(0.75)	0.44	0.8	(0.14)
	LNA	0.65	0.38	**(1.0×10^{-3})**	0.59	0.31	**(1.0×10^{-3})**
	HNA	0.79	0.65	**(< 0.001)**	0.65	0.5	**(1.0×10^{-3})**

p values ≤ 0.05 were considered significant and are highlighted in bold characters

The symbol (–) indicates undetermined p values, which were obtained when tests were not considered relevant or could not be computed

main potential reason that could explain these unusual Chl-*a* concentrations was related to the in situ pico-phytoplankton community which was unexpected for Thau Lagoon.

First, *Synechococcus*-like cells in this study reached exceptionally high abundances (2.4 (± 1.2) $\times$ 10^5 cells cm^{-3} on average), approximately 480 times higher than the average abundance reported in fall in a previous study (0.5 $\times$ 10^3 cells cm^{-3}, Bec et al. 2005) and were approximately 30 times higher than the maximal abundance of 8.0 $\times$ 10^3 cells cm^{-3} reported in the lagoon by Bec et al. (2005) and Collos et al. (2009). Such high abundances have only been reported three other times before in Thau Lagoon, as exceptional events in 2003, in 2006 and, more recently, in 2018 (Derolez et al. 2020a). It appears that these high

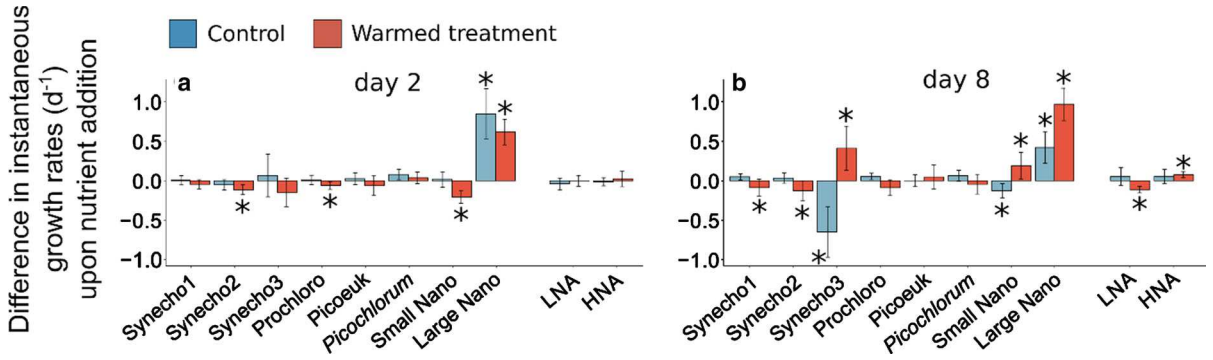

Fig. 6 Determination on day 2 and day 8 of the difference in phytoplankton and bacteria instantaneous growth rates upon nutrient addition, in the control (blue) and warmed treatment (red). The error bars represent standard deviations from the means. *Significant change in the instantaneous growth rate upon nutrient addition (Kruskal–Wallis $p < 0.05$)

abundances of picocyanobacteria were concurrent with relatively warm years, suggesting that warming in Thau Lagoon naturally favours picocyanobacteria (Trombetta et al. 2019; Derolez et al. 2020a). It should be noted that at the very beginning of the experiment, the *Synechococus*-like abundance declined accordingly to the low growth and high grazing rates estimated on day 2. The low growth of *Synechococcus*-like may appear contradictory with their high abundance observed in the present study. However, the sharp decrease in *Synechococcus*-like abundances followed by a bloom for Synecho1 might indicate that the balance between their growth and losses can change rapidly. In addition, these changes in the balance between growth and grazing rates over the course of the experiment were difficult to track due to the dilution experiment frequency applied.

Second, the cytometric analyses of cyanobacteria also revealed *Prochlorococcus*-like cells, a genus that, to our knowledge, had never been reported in Thau Lagoon during the past 20 years (Bec et al. 2005; Collos et al. 2009; Trombetta et al. 2019; Derolez et al. 2020a). Nevertheless, the *Prochlorococcus* genus present in the Mediterranean Sea could potentially drift into the lagoon via the channels connecting it to the sea. In the present investigation, cyanobacteria were the most abundant but also the most diverse phytoplankton group studied with FCM, as they account for three groups of *Synechococcus*-like and one group of *Prochlorococcus*-like genus.

Third, another picoeukaryote taxon that has never been reported in Thau Lagoon before was observed: the genus *Picochlorum* (Fig. 1), which belongs to the *Trebouxiophyceae* class (Foflonker et al. 2016). The abundance of *Picochlorum*, which we observed for the first time in our mesocosm experiment in October 2018, exponentially increased in the lagoon a few weeks later, leading to an ecological and socioeconomic crisis called the "Green Waters". While this "Green Waters" crisis related to *Picochlorum* in Thau Lagoon has not yet been described in the literature, a quite similar crisis due to an extensive bloom of nontoxic microalgae identified as *Nannochloris* was reported in the Salses-Leucate Lagoon in the same region and near Thau Lagoon in 1979–1980 (Boutière et al. 1982).

In the present study, nanophytoplankton were also more abundant (ranging from approximately 2.0–16.0 $\times$ 10^3 cells cm^{-3}) than what was previously reported by Bec et al. (2005) in October at the same location (50–100 cells cm^{-3}), but remains in the same range of nanophytoplankton abundances reported over the year (Vaquer et al. 1996; Trombetta et al. 2019).

The other plankton cytometric groups, namely, Picoeuk, HNA, LNA, as well as the two virus groups have been commonly reported in previous studies performed in Thau Lagoon and with a similar range of abundances in October (Bec et al. 2005; Mostajir et al. 2015b) as in the present study.

Nanophytoplankton, cyanobacteria, bacteria and virus abundances increased under warming in fall

There is growing evidence that the plankton community response to warming represents a complex combination of individual and common responses. One of the objectives of the present investigation was to experimentally elucidate how an increase in water temperature affects the metabolic rates and shapes the dynamics of the planktonic community in fall.

One of the main results of the present study was that warming slightly but significantly increased the abundances of most cyanobacteria. Moreover, numerous studies have similarly reported a positive correlation between cyanobacteria abundance and temperature (Maugendre et al. 2015; Chen and Laws 2017; Trombetta et al. 2019), even during a fall bloom in the St. Lawrence Estuary (Bénard et al. 2018). In addition, previous studies have reported higher abundances of pico- and nanophytoplankton under warmer temperatures (Pulina et al. 2016; Trombetta et al. 2019). In the present investigation, this trend was also observed for nanophytoplankton over the course of the experiment, but not for picoeukaryotes.

Higher cyanobacteria and nanophytoplankton abundances, especially towards the end of the experiment under warming, resulted in the assimilation of more nutrients, likely causing the lower nutrient concentrations observed in the warmed treatment relative to those in the control. This result highlights that both groups could experience growth even in low nutrient conditions in fall and under warming, suggesting a potential competitive advantage of these groups in warm and nutrient-poor waters (Agawin et al. 2000; Daufresne et al. 2009). In addition, the similarity between the trend of Chl-*a* concentrations under warming at the end of the experiment and those

of cyanobacteria and nanophytoplankon underlines that these two groups can be major contributors to the total phytoplankton biomass.

Among the phytoplankton groups, only the abundance of *Picochlorum* decreased under warming, coinciding with the trend observed for Chl-*a* concentrations at the middle of the experiment. This highlights the fact that the decrease in Chl-*a* concentration is likely due to the decrease in *Picochlorum* abundances. As *Picochlorum* was observed here for the first time in Thau Lagoon, it was not possible to compare the present results with previous studies from the same location. However, some studies investigating a cultured strain of *Picochlorum* identified its thermotolerance, which is up to 35 °C (de la Vega et al. 2011; Foflonker et al. 2016), exceeding by far the average of 25 °C reached in the warmed mesocosms in the present work. However, this high thermotolerance of *Picochlorum* was evaluated under optimal nutrient and light conditions. Within a natural plankton assemblage, on the other hand, biotic factors such as predation, infection and competition, which can be affected by an increase in the water temperature, could decrease *Picochlorum* abundance. For instance, stronger grazing triggered by warming, as reported in the literature (Rose et al. 2009; Vidussi et al. 2011), could depress *Picochlorum* abundances. Indeed, the grazing rates estimated for *Picochlorum* tended to increase under warming, suggesting that its predators, benefitting from warmer conditions directly or indirectly through trophic cascades, constituted a main driver of *Picochlorum* abundances under warming. Alternatively, the higher viral abundances in the warmed treatment, potentially accompanied by higher viral infection and mortality rates among plankton, suggest that viruses could also play a role in the decrease in *Picochlorum* abundance under warming. Finally, increased competition with other phytoplankton groups could also regulate its abundance under warming. In particular, the cyanobacteria that were found to increase in abundance under warming during the present study and are known to be strong competitors in warm and low-nutrient waters (Bec et al. 2011; Chen and Laws 2017) are potential competitors of *Picochlorum* under warmed conditions. In regard to the "Green Waters" ecological crisis provoked by *Picochlorum*, considering that its abundance began to rise in the lagoon at the end of October, *Picochlorum* potentially benefitted from the colder season to outcompete other phytoplankton. This corroborates the hypothesis that *Picochlorum* is under weaker control of its population in colder than warmer waters, at least in Thau Lagoon.

The elevation of water temperature in the warmed treatment also resulted in a bloom of picophytoplankton (Synecho1 and Picoeuk) a few days earlier than that in the control, as was also reported in previous studies describing earlier spring (Vidussi et al. 2011) and fall blooms (Bénard et al. 2018) under experimental warming. The significantly stronger increase in the Synecho1 and Picoeuk abundances during the bloom under warming, however, was followed by a significantly stronger decrease in abundance immediately after the bloom. This result indicates that warming also amplified the changes in picophytoplankton abundances and thus their dynamics over time.

The responses of HNA and LNA to elevated temperature were comparable to those of the phytoplankton groups. LNA abundance slightly but significantly increased under warming in the present study, similar to the results of previous studies indicating a positive correlation between LNA abundance and temperature (Morán et al. 2015). HNA abundance, on the other hand, displayed a dynamic comparable to that of the *Synechococcus*-like bloom (Synecho1), with an increase in abundance followed by a decrease, suggesting a tight coupling with this *Synechococcus*-like group dynamic. In addition, this increase in HNA abundance also occurred a few days earlier under warming than in the control, highlighting that temperature also drives changes in HNA abundance. However, these results contrast with those from a previous study performed during spring in Thau Lagoon with an identical experimental warming procedure (Vidussi et al. 2011), which reported that warming led to lower bacterial abundances. While these authors suggested that stronger grazing could explain these lower bacterial abundances, we found instead lower grazing rates on bacteria under warming, highlighting that the factor driving bacterial abundance under experimental warming differed from spring to fall in this lagoon, or because initial conditions were different.

Finally, viruses were also more abundant in the warmer treatment than in the control; thus, the possibility of an increase in viral lysis under warming cannot be excluded. Viral lysis has been reported to

contribute to 10–50% of bacterial mortality in some regions (Fuhrman 1999; Ory et al. 2010). However, considering the generally slightly higher microbial abundances reported in the current study, viral lysis was not a main driver of the phytoplankton (< 10 μm) and bacterial populations under warming, except potentially for *Picochlorum*. These results also contrast with those from the study by Vidussi et al. (2011), as they reported no significant effect of warming on virus abundance during the spring. This could suggest that viruses differently affect the plankton communities in Thau Lagoon in spring than in this study in fall.

Warming in fall promotes phytoplankton and depresses bacterial growth

Warming enhanced the growth rates of most phytoplankton groups according to the results of the two dilution experiments performed on days 2 and 8 of the mesocosm experiment. This trend was less pronounced at the beginning of the experiment, when the warming exposure time was too short to cause a strong effect. In contrast, higher growth rates of phytoplankton after a longer time of exposure to warming were observed on day 8, in accordance with the literature (Eppley 1972; Savage et al. 2004). The addition of inorganic nutrients revealed that Large Nano growth rates were potentially limited by inorganic nutrients in both treatments on days 2 and 8. However, on day 8, Small Nano and Synecho3 were also limited by nutrients, but only in the warmed treatment, indicating a potential stronger nutrient limitation effect under warming. These results suggest that the growth rates of some phytoplankton groups in the absence of nutrient limitation could be even more enhanced under warming. This corroborates the competitive advantage observed in some cyanobacteria and nanophytoplankton in terms of growth under warming despite low nutrient concentrations.

Several previous studies have reported a positive correlation between bacterial growth and temperature (White et al. 1991; Huete-Stauffer et al. 2016). However, and surprisingly, the warming in the present study had contrasting effects on bacterial growth rates. HNA growth under warming was significantly increased on day 2, but then both bacterial group growth rates were significantly reduced under warming on day 8. The former of these two results is in line with those from a study by Huete-Stauffer et al. (2015) describing some cases of bacterial growth decrease under warmed conditions, suggesting that temperature does not always enhance bacterial metabolic rates. The HNA growth rate was potentially limited by inorganic nutrients under warming, as the instantaneous growth rate of this group increased under nutrient addition on day 8 in the warmed treatment. While bacteria mainly use dissolved organic carbon (DOC) for growth, they also need inorganic nutrients (Kirchman 1994). Therefore, a lack of inorganic nutrients could also affect the bacterial growth rate. However, potential nutrient limitation could explain the decrease in the HNA growth rate under warming, but not that of LNA, as the instantaneous growth rate of the latter group did not increase as a result of nutrient addition. As DOC was not added in the dilution experiment, it was not possible to evaluate whether bacteria, especially LNA, were limited by organic carbon. However, the higher viral abundances observed under warming, which could induce more cell lysis, as well as the stronger grazing on eukaryotes observed in the middle of the experiment in the warmed treatment could provide DOC, as these processes have been described as a source of DOC (Danovaro et al. 2011). Therefore, it seems unlikely that bacteria were limited by DOC under warming. The simultaneous decrease in growth rates of both bacterial groups with the increase in those of some phytoplankton groups observed in the present study might suggest an accentuation in competition among these groups under warming. Competition for resources among bacteria and between bacteria and phytoplankton are commonly described in natural plankton communities (Løvdal et al. 2007; Trombetta et al. 2020), and it was shown that warming can accentuate competition for resources (Goldman and Ryther 1976; Kordas et al. 2011).

Warming decreases grazing on small phytoplankton and bacteria in fall

In the present study, elevating the water temperature by 3 °C surprisingly significantly decreased the microzooplankton grazing rates on most of the studied phytoplankton and bacteria groups at the beginning of the experiment (day 2). This result highlights the fast response of grazers to the warming treatment and was rather unexpected, as several previous studies reported a positive relationship between microzooplankton

grazers and temperature (Rose and Caron 2007; Chen et al. 2012). Experimentally elevating the temperature by a few degrees also enhanced grazing on both phytoplankton (Rose et al. 2009) and bacteria (Vázquez-Domínguez et al. 2012). Vidussi et al. (2011) investigated the spring Thau Lagoon plankton community and suggested also that warming enhances grazing on both phytoplankton and bacteria. This significant decrease in microzooplankton grazing on phytoplankton and bacteria under experimental warming suggests that warming had a negative effect on the corresponding grazer metabolism, activity or abundance. As previously mentioned, microzooplankton grazers are usually positively affected by an elevation in temperature (Rose and Caron 2007; Chen et al. 2012); thus, a direct negative effect on their metabolism seems unlikely. However, the lower nitrate concentrations under warming could have reduced the nutritional quality of the preys and thus indirectly decreased grazing rates, as prey quality is a criterion of predators selectivity (Burkill et al. 1987). An alternative possible hypothesis is that warming enhanced grazing by larger zooplankton on the grazers of small phytoplankton and bacteria. This could decrease the microzooplankton abundance and thus release their prey, specifically the cytometric groups, from predation pressure in a cascading manner under warming (Vidussi et al. 2011; Lewandowska et al. 2014). During the middle of the experiment (day 8), however, grazing on prokaryotes was still reduced under warming, but that on eukaryote cells increased. This suggests the occurrence of differences in sensitivity between the grazers of prokaryotes and those of eukaryotes, potentially due to changes in the communities of grazers or predators of eukaryotes in response to warming.

Conclusion

In the present investigation, several significant effects of warming were reported in relation to microbial community abundances, dynamics, and metabolic rates. Warming induced a change at the base of the microbial community, increasing the abundances of nanophytoplankton, cyanobacteria, bacteria and viruses but not those of the newly found *Picochlorum* in Thau Lagoon. Phytoplankton growth rates were enhanced under warming, while bacterial growth rates were declined, suggesting different mechanisms of their responses to warming. Grazing rates were generally reduced, suggesting that a trophic cascade was triggered under warming. Despite these changes, warming only had a minor effect on phytoplankton (< 10 μm) and bacterial carbon biomass, which only increased by 5% compared to that in the control. Phytoplankton (< 10 μm) and bacteria also accounted for similar percentages of carbon biomass, 60 and 40%, respectively, in both treatments. Therefore, the fall plankton community appeared to be rather resistant to warming in terms of the balance of biomass between phytoplankton (< 10 μm) and bacteria, while its functioning in terms of microbial abundance and metabolic rates were affected. These findings also highlight the need for more studies on specific plankton assemblages in different seasons and locations to better understand their response to warming.

Acknowledgements We would like to thank the MEDIMEER crew: David Parin for electronic management, Solenn Soriano and Remy Valdes for the daily sampling and setup of the mesocosms and Florian Voron for nutrient analyses. We also warmly thank Maria Protopapa for her help during the dilution experiments. The cytometric analyses of phytoplankton and bacterial samples was performed using the MARBEC MICROBEX platform. We would like to thank Christophe Salmeron from the SU/CNRS BioPIC Imaging and Cytometry platform of Banyuls-sur-mer Oceanologic Observatory for viral abundances analyses. The mesocosm experiment was part of the project AQUACOSM: Network of Leading European AQUAtic MesoCOSM Facilities Connecting Mountains to Oceans from the Arctic to the Mediterranean funded by the European Union Horizon 2020 Program (H2020/2017-2020), Grant Agreement No. 731065.

Authors' contributions BM and FV with SM conceived and designed the study and established and managed the in situ mesocosm experiment. DP analysed the virus data and TS participated to the sampling, and data processing of the Chl-*a* concentration. JC performed the dilution experiment, collected and analysed the data for phytoplankton and bacteria, and wrote the original draft of the manuscript. All authors participated to the redaction of the final manuscript.

Funding The mesocosm experiment was partly funded by the European Union Horizon 2020 Program (H2020/2017-2020), Grant Agreement N° 731065, through the project AQUACOSM: Network of Leading European AQUAtic MesoCOSM Facilities Connecting Mountains to Oceans from the Arctic to the Mediterranean.

Availability of data and materials The data and material used in this study can be provided by the authors after requested.

Code availability Not applicable.

Declaration

Conflict of interest There are no conflicts of interest to disclose for this study.

Open Access This article is licensed under a Creative Commons Attribution 4.0 International License, which permits use, sharing, adaptation, distribution and reproduction in any medium or format, as long as you give appropriate credit to the original author(s) and the source, provide a link to the Creative Commons licence, and indicate if changes were made. The images or other third party material in this article are included in the article's Creative Commons licence, unless indicated otherwise in a credit line to the material. If material is not included in the article's Creative Commons licence and your intended use is not permitted by statutory regulation or exceeds the permitted use, you will need to obtain permission directly from the copyright holder. To view a copy of this licence, visit http://creativecommons.org/licenses/by/4.0/.

References

Aberle N, Lengfellner K, Sommer U (2007) Spring bloom succession, grazing impact and herbivore selectivity of ciliate communities in response to winter warming. Oecologia 150:668–681. https://doi.org/10.1007/s00442-006-0540-y

Agawin NSR, Duarte CM, Agustí S (2000) Nutrient and temperature control of the contribution of picoplankton to phytoplankton biomass and production. Limnol Oceanogr 45:591–600. https://doi.org/10.4319/lo.2000.45.3.0591

Azam F, Fenchel T, Field JG et al (1983) The ecological role of water-column microbes in the sea. Mar Ecol Prog Ser 10:257–263

Bec B, Husseini-Ratrema J, Collos Y et al (2005) Phytoplankton seasonal dynamics in a Mediterranean coastal lagoon: emphasis on the picoeukaryote community. J Plankton Res 27:881–894. https://doi.org/10.1093/plankt/fbi061

Bec B, Collos Y, Souchu P et al (2011) Distribution of picophytoplankton and nanophytoplankton along an anthropogenic eutrophication gradient in French Mediterranean coastal lagoons. Aquat Microb Ecol 63:29–45. https://doi.org/10.3354/ame01480

Bénard R, Levasseur M, Scarratt M et al (2018) Experimental assessment of the sensitivity of an estuarine phytoplankton fall bloom to acidification and warming. Biogeosciences 15:4883–4904. https://doi.org/10.5194/bg-15-4883-2018

Bertilsson S, Berglund O, Karl DM, Chisholm SW (2003) Elemental composition of marine Prochlorococcus and Synechococcus: implications for the ecological stoichiometry of the sea. Limnol Oceanogr 48:1721–1731. https://doi.org/10.4319/lo.2003.48.5.1721

Boutière H, de Bovée F, Delille D et al (1982) Effet d'une crise dystrophique dans l'etang de Salses-Leucate. Oceanol Acta SP:231–242

Brown JH, Gillooly JF, Allen AP et al (2004) Toward a metabolic theory of ecology. Ecology 85:1771–1789. https://doi.org/10.1890/03-9000

Brussaard CPD (2004) Optimization of procedures for counting viruses by flow cytometry. Appl Environ Microbiol 70:1506–1513. https://doi.org/10.1128/AEM.70.3.1506-1513.2004

Burkill PH, Mantoura RFC, Llewellyn CA, Owens NJP (1987) Microzooplankton grazing and selectivity of phytoplankton in coastal waters. Mar Biol 93:581–590. https://doi.org/10.1007/BF00392796

Calbet A, Landry MR (2004) Phytoplankton growth, microzooplankton grazing, and carbon cycling in marine systems. Limnol Oceanogr 49:51–57. https://doi.org/10.4319/lo.2004.49.1.0051

Chen B (2015) Assessing the accuracy of the "two-point" dilution technique. Limnol Oceanogr Methods 13:521–526. https://doi.org/10.1002/lom3.10044

Chen B, Laws EA (2017) Is there a difference of temperature sensitivity between marine phytoplankton and heterotrophs? Limnol Oceanogr 62:806–817. https://doi.org/10.1002/lno.10462

Chen B, Landry MR, Huang B, Liu H (2012) Does warming enhance the effect of microzooplankton grazing on marine phytoplankton in the ocean? Limnol Oceanogr 57:519–526. https://doi.org/10.4319/lo.2012.57.2.0519

Chisholm SW (2017) Prochlorococcus. Curr Biol 27:R447–R448. https://doi.org/10.1016/j.cub.2017.02.043

Collos Y, Bec B, Jauzein C et al (2009) Oligotrophication and emergence of picocyanobacteria and a toxic dinoflagellate in Thau lagoon, southern France. J Sea Res 61:68–75. https://doi.org/10.1016/j.seares.2008.05.008

Danovaro R, Corinaldesi C, Dell'Anno A et al (2011) Marine viruses and global climate change. FEMS Microbiol Rev 35:993–1034. https://doi.org/10.1111/j.1574-6976.2010.00258.x

Daufresne M, Lengfellner K, Sommer U (2009) Global warming benefits the small in aquatic ecosystems. Proc Natl Acad Sci 106:12788–12793. https://doi.org/10.1073/pnas.0902080106

de la Vega M, Díaz E, Vila M, León R (2011) Isolation of a new strain of Picochlorum sp and characterization of its potential biotechnological applications. Biotechnol Prog 27:1535–1543. https://doi.org/10.1002/btpr.686

Derolez V, Malet N, Fiandrino A et al (2020a) Fifty years of ecological changes: Regime shifts and drivers in a coastal Mediterranean lagoon during oligotrophication. Sci Total Environ 732:139292. https://doi.org/10.1016/j.scitotenv.2020.139292

Derolez V, Soudant D, Malet N et al (2020b) Two decades of oligotrophication: evidence for a phytoplankton community shift in the coastal lagoon of Thau (Mediterranean Sea, France). Estuar Coast Shelf Sci 241:106810. https://doi.org/10.1016/j.ecss.2020.106810

Eppley RW (1972) Temperature and phytoplankton growth in the sea. Fish Bull 70:1063–1085

Foflonker F, Ananyev G, Qiu H et al (2016) The unexpected extremophile: tolerance to fluctuating salinity in the green alga Picochlorum. Algal Res 16:465–472. https://doi.org/10.1016/j.algal.2016.04.003

Fouilland E, Trottet A, Alves-de-Souza C et al (2017) Significant change in marine plankton structure and carbon production after the addition of river water in a mesocosm experiment. Microb Ecol 74:289–301. https://doi.org/10.1007/s00248-017-0962-6

Fuhrman JA (1999) Marine viruses and their biogeochemical and ecological effects. Nature 399:541–548. https://doi.org/10.1038/21119

Giorgi F (2006) Climate change hot-spots. Geophys Res Lett 33:L08707. https://doi.org/10.1029/2006GL025734

Goldman JC, Ryther JH (1976) Temperature-influenced species competition in mass cultures of marine phytoplankton. Biotechnol Bioeng 18:1125–1144. https://doi.org/10.1002/bit.260180809

Hays GC, Richardson AJ, Robinson C (2005) Climate change and marine plankton. Trends Ecol Evol 20:337–344. https://doi.org/10.1016/j.tree.2005.03.004

Huete-Stauffer TM, Arandia-Gorostidi N, Díaz-Pérez L, Morán XAG (2015) Temperature dependences of growth rates and carrying capacities of marine bacteria depart from metabolic theoretical predictions. FEMS Microbiol Ecol 91:fiv111. https://doi.org/10.1093/femsec/fiv111

Huete-Stauffer TM, Arandia-Gorostidi N, Alonso-Sáez L, Morán XAG (2016) Experimental warming decreases the average size and nucleic acid content of marine bacterial communities. Front Microbiol 7:1–13. https://doi.org/10.3389/fmicb.2016.00730

IPCC (2007) Climate Change 2007: Synthesis Report. Contribution of Working Groups I, II and III to the Fourth Assessment Report of the Intergovernmental Panel on Climate Change [Core Writing Team, Pachauri RK, Reisinger A (eds)]. IPCC, Geneva

IPCC (2014) Climate Change 2014: Synthesis Report. Contribution of Working Groups I, II and III to the Fifth Assessment Report of the Intergovernmental Panel on Climate Change [Core Writing Team, Pachauri RK, Meyer LA (eds)]. IPCC, Geneva

Kemp PF, Cole JJ, Sherr BF, Sherr EB (1993) Handbook of methods in aquatic microbial ecology. CRC Press, Boca Raton

Kirchman DL (1994) The uptake of inorganic nutrients by heterotrophic bacteria. Microb Ecol 28:255–271. https://doi.org/10.1007/BF00166816

Kordas RL, Harley CDG, O'Connor MI (2011) Community ecology in a warming world: the influence of temperature on interspecific interactions in marine systems. J Exp Mar Bio Ecol 400:218–226. https://doi.org/10.1016/j.jembe.2011.02.029

Lam-Hoai T, Rougier C, Lasserre G (1997) Tintinnids and rotifers in a northern Mediterranean coastal lagoon. Structural diversity and function through biomass estimations. Mar Ecol Prog Ser 152:13–25. https://doi.org/10.3354/meps152013

Landry MR, Hassett RP (1982) Estimating the grazing impact of marine micro-zooplankton. Mar Biol 67:283–288. https://doi.org/10.1007/BF00397668

Lejeusne C, Chevaldonné P, Pergent-Martini C et al (2010) Climate change effects on a miniature ocean: the highly diverse, highly impacted Mediterranean Sea. Trends Ecol Evol 25:250–260. https://doi.org/10.1016/j.tree.2009.10.009

Lewandowska AM, Boyce DG, Hofmann M et al (2014) Effects of sea surface warming on marine plankton. Ecol Lett 17:614–623. https://doi.org/10.1111/ele.12265

Løvdal T, Eichner C, Grossart H-P et al (2007) Competition for inorganic and organic forms of nitrogen and phosphorous between phytoplankton and bacteria during an *Emiliania huxleyi* spring bloom (PeECE II). Biogeosci Discuss 4:3343–3375. https://doi.org/10.5194/bgd-4-3343-2007

Marie D, Partensky F, Jacquet S, Vaulot D (1997) Enumeration and cell cycle analysis of natural populations of marine picoplankton by flow cytometry using the nucleic acid stain SYBR green I. Appl Environ Microbiol 63:186–193. https://doi.org/10.1128/AEM.63.1.186-193.1997

Maugendre L, Gattuso J-P, Louis J et al (2015) Effect of ocean warming and acidification on a plankton community in the NW Mediterranean Sea. ICES J Mar Sci 72:1744–1755. https://doi.org/10.1093/icesjms/fsu161

Menden-Deuer S, Fredrickson K (2010) Structure-dependent, protistan grazing and its implication for the formation, maintenance and decline of plankton patches. Mar Ecol Prog Ser 420:57–71. https://doi.org/10.3354/meps08855

Morán XAG, Alonso-Sáez L, Nogueira E et al (2015) More, smaller bacteria in response to ocean's warming? Proc R Soc B Biol Sci 282:20150371. https://doi.org/10.1098/rspb.2015.0371

Mostajir B, Amblard C, Buffan-Dubau E et al (2015a) Microbial food webs in aquatic and terrestrial ecosystems. In: Bertrand J-C, Caumette P, Lebaron P et al (eds) Environmental microbiology: fundamentals and applications. Springer, Dordrecht, pp 485–509

Mostajir B, Roques C, Bouvier C et al (2015b) Microbial food web structural and functional responses to oyster and fish as top predators. Mar Ecol Prog Ser 535:11–27. https://doi.org/10.3354/meps11429

Nouguier J, Mostajir B, Le Floc'h E, Vidussi F (2007) An automatically operated system for simulating global change temperature and ultraviolet B radiation increases: application to the study of aquatic ecosystem responses in mesocosm experiments. Limnol Oceanogr Methods 5:269–279. https://doi.org/10.4319/lom.2007.5.269

Ory P, Hartmann HJ, Jude F et al (2010) Pelagic food web patterns: do they modulate virus and nanoflagellate effects on picoplankton during the phytoplankton spring bloom? Environ Microbiol 12:2755–2772. https://doi.org/10.1111/j.1462-2920.2010.02243.x

Pecqueur D, Vidussi F, Fouilland E et al (2011) Dynamics of microbial planktonic food web components during a river flash flood in a Mediterranean coastal lagoon. Hydrobiologia 673:13–27. https://doi.org/10.1007/s10750-011-0745-x

Pomeroy LR (1974) The ocean's food web, a changing paradigm. Bioscience 24:499–504. https://doi.org/10.2307/1296885

Pulina S, Brutemark A, Suikkanen S et al (2016) Effects of warming on a Mediterranean phytoplankton community. Web Ecol 16:89–92. https://doi.org/10.5194/we-16-89-2016

Rabalais NN, Turner RE, Díaz RJ, Justić D (2009) Global change and eutrophication of coastal waters. ICES J Mar Sci 66:1528–1537. https://doi.org/10.1093/icesjms/fsp047

Rivkin R, Anderson M, Lajzerowicz C (1996) Microbial processes in cold oceans. I. Relationship between temperature and bacterial growth rate. Aquat Microb Ecol 10:243–254. https://doi.org/10.3354/ame010243

Rose JM, Caron DA (2007) Does low temperature constrain the growth rates of heterotrophic protists? Evidence and implications for algal blooms in cold waters. Limnol Oceanogr 52:886–895. https://doi.org/10.4319/lo.2007.52.2.0886

Rose JM, Feng Y, Gobler CJ et al (2009) Effects of increased pCO2 and temperature on the North Atlantic spring bloom. II. Microzooplankton abundance and grazing. Mar Ecol Prog Ser 388:27–40. https://doi.org/10.3354/meps08134

Savage VM, Gillooly JF, Brown JH et al (2004) Effects of body size and temperature on population growth. Am Nat 163:429–441. https://doi.org/10.1086/381872

Sime-Ngando T, Gosselin M, Roy S, Chanut J (1995) Significance of planktonic ciliated protozoa in the Lower St. Lawrence Estuary: comparison with bacterial, phytoplankton, and particulate organic carbon. Aquat Microb Ecol 9:243–258. https://doi.org/10.3354/ame009243

Strom SL, Fredrickson KA (2008) Intense stratification leads to phytoplankton nutrient limitation and reduced microzooplankton grazing in the southeastern Bering Sea. Deep Res Part II Top Stud Oceanogr 55:1761–1774. https://doi.org/10.1016/j.dsr2.2008.04.008

Trombetta T, Vidussi F, Mas S et al (2019) Water temperature drives phytoplankton blooms in coastal waters. PLoS ONE 14:e0214933. https://doi.org/10.1371/journal.pone.0214933

Trombetta T, Vidussi F, Roques C et al (2020) Marine microbial food web networks during phytoplankton bloom and non-bloom periods: warming favors smaller organism interactions and intensifies trophic cascade. Front Microbiol 11:1–19. https://doi.org/10.3389/fmicb.2020.502336

Trottet A, Leboulanger C, Vidussi F et al (2016) Heterotrophic bacteria show weak competition for nitrogen in Mediterranean coastal waters (Thau Lagoon) in autumn. Microb Ecol 71:304–314. https://doi.org/10.1007/s00248-015-0658-8

Vaquer A, Troussellier M, Courties C, Bibent B (1996) Standing stock and dynamics of picophytoplankton in the Thau Lagoon (northwest Mediterranean coast). Limnol Oceanogr 41:1821–1828. https://doi.org/10.4319/lo.1996.41.8.1821

Vázquez-Domínguez E, Vaqué D, Gasol J (2012) Temperature effects on the heterotrophic bacteria, heterotrophic nanoflagellates, and microbial top predators of the NW Mediterranean. Aquat Microb Ecol 67:107–121. https://doi.org/10.3354/ame01583

Vidussi F, Mostajir B, Fouilland E et al (2011) Effects of experimental warming and increased ultraviolet B radiation on the Mediterranean plankton food web. Limnol Oceanogr 56:206–218. https://doi.org/10.4319/lo.2011.56.1.0206

White PA, Kalff J, Rasmussen JB, Gasol JM (1991) The effect of temperature and algal biomass on bacterial production and specific growth rate in freshwater and marine habitats. Microb Ecol 21:99–118

Worden AZ, Binder BJ (2003) Application of dilution experiments for measuring growth and mortality rates among Prochlorococcus and Synechococcus populations in oligotrophic environments. Aquat Microb Ecol 30:159–174. https://doi.org/10.3354/ame030159

Zapata M, Rodríguez F, Garrido J (2000) Separation of chlorophylls and carotenoids from marine phytoplankton:a new HPLC method using a reversed phase C8 column and pyridine-containing mobile phases. Mar Ecol Prog Ser 195:29–45. https://doi.org/10.3354/meps195029

Publisher's Note Springer Nature remains neutral with regard to jurisdictional claims in published maps and institutional affiliations.

Résumé

Les processus planctoniques jouant un rôle primordial dans le devenir de la matière et les cycles biogéochimiques globaux, la production primaire brute (PPB), la production communautaire nette (PCN), la respiration (R) et les taux de croissance (μ) et de pertes (*l*) du phytoplancton ont été quantifiés via l'utilisation de données à haute-fréquence (HF) acquises par des capteurs immergés dans des mésocosmes *in situ* lors d'expériences simulant le réchauffement (lagune de Thau) et le brunissement (baie d'Hopavågen, Norvège). Une nouvelle méthode pour estimer la PPB, la R et la PCN a été établie à partir des données de capteurs mesurant la concentration en O_2 dissout issues d'expériences dans la lagune de Thau. Elle a été comparée avec une méthode utilisant des données HF déjà existante ainsi qu'avec la technique classique des incubations (Winkler). Elle présente l'avantage de prendre en compte la variabilité dans le couplage entre cycles jour-nuit et de l'O_2 dissout et a permis d'estimer une respiration la journée en moyenne 41% plus élevée que celle de la nuit, en accord avec l'effet théorique positif de la lumière sur la respiration. L'application de cette nouvelle méthode lors d'une expérience testant les effets du brunissement sur le fonctionnement des communautés planctoniques de la baie d'Hopavågen a révélé un effet négatif du brunissement d'environ 30% sur la PPB et la R, associé à d'importants changements dans la concentration des pigments phytoplanctoniques liés à une acclimatation physiologique aux faibles conditions de lumières. Le réchauffement simulant les scénarios pour 2100 en Méditerranée a été testée lors de deux expériences de mésocosmes *in situ* au printemps et à l'automne 2018 à Thau. Ainsi, le réchauffement a augmenté μ et *l* du phytoplancton, estimés avec les données de fluorescence HF. Les estimations de μ et de *l* ont été comparées aux taux de croissance et de prédation obtenus via la technique des dilutions, mettant en évidence une bonne concordance entre les résultats obtenus, confirmant la robustesse des estimations obtenues avec les données HF, ceci malgré certaines différences entre les résultats de deux méthodes employées du fait que *l*, estimé avec les données HF, prend en compte la sédimentation, la mortalité par le broutage du mésozooplancton et par la lyse virale alors que les dilutions ne permettent d'estimer que le broutage du microzooplancton. Une expérience simulant une vague de chaleur a également été réalisée à Thau au printemps 2019. Les données HF ont mis en lumière un effet positif de la vague de chaleur sur la PPB, la R, μ et *l* qui s'est prolongé plusieurs jours après l'arrêt de la vague de chaleur, sauf pour μ. La vague de chaleur a basculé l'état trophique du système vers l'hétérotrophie et a favorisé les cyanobactéries au détriment des dinoflagellés, cependant la majorité des processus étudiés ont montré de bonnes résistance et récupération face à la vague de chaleur. Le réchauffement a induit des réponses contrastées du plancton de la lagune de Thau, basculant le système vers l'autotrophie ou l'hétérotrophie en fonction de la saison investiguée. La communauté de Thau a été plus résistante et a mieux récupéré face à un événement ponctuel du changement climatique que la communauté d'Hopavågen, potentiellement parce que la communauté planctonique de Thau a évolué au sein d'un environnement naturellement soumis aux fortes variations de température et/ou parce que le réchauffement est une perturbation moins drastique que le brunissement. Les méthodes établies dans la thèse représentent une approche novatrice afin d'obtenir des estimations fiables de processus planctoniques mettant en évidence sur les effets du changement climatique sur le fonctionnement des écosystèmes côtiers. De nombreuses perspectives s'ouvrent quant à la poursuite de ces travaux, en utilisant ces nouvelles méthodes pour étudier d'autres perturbations dans d'autres écosystèmes.

Mots-clés : Données à haute-fréquence, capteurs, mésocosmes *in situ*, perturbation, changement global, processus planctoniques, production primaire brute, respiration, taux de croissance, taux de perte

Abstract

Planktonic processes playing a key role in the fate of matter and global biogeochemical cycles, gross primary production (GPP), net community production (NCP) respiration (R), growth (μ) and loss (*l*) rates of phytoplankton were quantified using high-frequency (HF) data acquired by sensors immersed in *in situ* mesocosms during experiments simulating warming (Thau Lagoon) and brownification (Hopavågen Bay, Norway). A new method for estimating GPP, R and NCP was established using sensor data measuring dissolved O_2 concentration from experiments in Thau lagoon. It was compared with an existing method using HF data and with the classical incubation technique (Winkler). It has the advantage of considering the variability in the coupling between day-night and dissolved O_2 cycles and allowed to estimate a daytime respiration on average 41% higher than the nighttime one, in agreement with the positive theoretical effect of light on respiration. Application of this new method in an experiment testing the effects of brownification on planktonic community functioning in Hopavågen Bay revealed a negative effect of brownification of about 30% on GPP and R, associated with significant changes in phytoplankton pigment concentration related to physiological acclimation to low light conditions. The warming scenario for 2100 in the Mediterranean was tested in two *in situ* mesocosm experiments in spring and autumn 2018 in Thau lagoon. Warming increased phytoplankton's μ and *l*, estimated with HF fluorescence data. The estimates of μ and *l* were compared to the growth and grazing rates obtained via the dilution technique, highlighting a good agreement between the two methods, confirming the robustness of the estimates obtained with the HF data, despite some differences between results due to the fact that *l*, estimated with the HF data, considers sedimentation, mesozooplankton grazing mortality and viral lysis while the dilutions only allow the estimation of microzooplankton grazing. An experiment simulating a heatwave was also carried out in Thau in spring 2019. The HF data showed a positive effect of the heat wave on GPP, R, μ and *l* that lasted for several days after the end of the heatwave, except for μ. The heatwave shifted the trophic state of the system towards heterotrophy and favored cyanobacteria at the expense of dinoflagellates, however most of the studied processes showed good resistance and recovery from the heatwave. Warming induced contrasting responses in Thau lagoon planktonic community, shifting the system towards autotrophy or heterotrophy depending on the investigated season. The community from Thau lagoon was more resilient and recovered better from a punctual climate change event than the community from Hopavågen, potentially because the planktonic community from Thau evolved in an environment naturally subject to strong temperature variations and/or because warming is a less drastic disturbance than brownification. The methods established in the thesis represent a novel approach to obtain reliable estimates of planktonic processes highlighting the effects of climate change on the functioning of coastal ecosystems. There are many perspectives to continue this work, using these new methods to study other disturbances in other ecosystems.
.

Key-words: High-frequency data, sensors, in situ mesocosms, disturbance, global change, planktonic processes, gross primary production, respiration, growth rate, loss rate